DOCTOR OF PHILOSOPHY

Single cell analysis of Keap1-Nrf2 dynamics

Baird, Liam

Award date:
2013

DOCTOR OF PHILOSOPHY

Single cell analysis of Keap1-Nrf2 dynamics

Liam Baird

2013

University of Dundee

Single Cell Analysis of Keap1-Nrf2 Dynamics

Liam Baird

A thesis submitted for the degree of Doctor of Philosophy, October 2012

Acknowledgements

Firstly, and most importantly, I would like to thank Lulu and Sophia Baird for all of their valuable support during the three years in which I have been working towards my PhD. I am particularly indebted to Sophia, who has been, and will always be, a constant source of inspiration to me.

I would like to thank my supervisor Dr Albena Dinkova-Kostova for all of the help and guidance she has given me during my 3 years in Dundee. I am extremely grateful of the opportunity that Albena gave me, particularly given the "unconventional" route that I had taken once I completed my undergraduate degree. I would also like to acknowledge Dr David Lleres and Dr Sam Swift for both their time spent teaching me the FLIM technique, and their patience in answering all of my questions. Finally, I would like to thank Prof. Kevin Park and Prof. Ron Hay for agreeing to act as my examiners during my *viva voce* exam.

Contents

List of Figures

List of Tables

Abbreviations

ARE	–	Antioxidant response element
cDNA	–	Complementary deoxyribonucleic acid
Co-IP	–	Co-immunoprecipitation
Cul3	–	Cullin-3
Cys	–	Cysteine
EGFP	–	Enhance green fluorescent protein
FLIM	–	Fluorescence lifetime imaging microscopy
FRAP	–	Fluorescence recovery after photobleaching
FRET	–	Fluorescence resonance energy transfer
GCL	–	γ-Glutamyl-cysteine ligase
GSH	–	Glutathione
GSTs	–	Glutathione *S*-transferases
H_2O_2	–	Hydrogen peroxide
IRES	–	Internal ribosome entry site
IVR	–	Intervening region
mRNA	–	Messenger ribonucleic acid
NQO1	–	NAD(P)H:quinone acceptor oxidoreductase 1
PCR	–	Polymerase chain reaction
SFN	–	Sulforaphane
tBHQ	–	*tert*-Butylhydroquinone
UTR	–	Untranslated region

Abstract

The transcription factor Nrf2 is a master regulator of cytoprotective gene expression. Nrf2 is negatively controlled by Keap1, a sensor protein which allows Nrf2 to respond to changing cellular conditions. In the basal state, Nrf2 binds to two sites of a Keap1 dimer allowing its ubiquitination in a Cullin-3/Rbx1-dependent manner. In response to electrophiles and oxidants (termed inducers, which bind directly to Keap1) ubiquitination of Nrf2 is inhibited; consequently, Nrf2 accumulates and activates transcription.

We have developed aFLIM-based assay to study the dynamic interaction between Keap1 and Nrf2 in single live cells. Combinations of wild type and mutant proteins revealed that under basal conditions the Keap1-Nrf2 complex exists in two conformations, one in which Nrf2 is bound to both members or the Keap1 dimer ('closed' conformation), and a second in which Nrf2 interacts with a single Keap1 monomer ('open' conformation). We found that following exposure to a range of inducers the Cul3-Keap1-Nrf2 complex does not dissociate, but remains intact. Furthermore, we found that inducers lead to the accumulation of the Keap1-Nrf2 complex in the 'closed' conformation. Interestingly, blockage of the proteasome also leads to the accumulation of the complex in the closed conformation, suggesting that the binding of Nrf2 and its subsequent Keap1-dependent ubiquitination follows a cyclical pattern. We believe that the existence of a Keap1-Nrf2 binding cycle benefits the cell, as it allows other signaling pathways, such as those mediated by p21 and p62, to regulate Nrf2 activity in the absence of inducers.

Together our results show that the interaction between Keap1 and Nrf2 is more dynamic than previously anticipated and that inducers function to modulate this dynamism, leading to Nrf2 stabilisation and cytoprotective gene expression.

Chapter 1

Introduction

In the late 1980s, Paul Talalay and his colleagues predicted the existence of a protein endowed with highly reactive cysteine residue(s) that serves as the sensor for small-molecule inducers of cytoprotective enzymes, such as NAD(P)H:quinone acceptor oxidoreductase 1 (NQO1) and glutathione *S*-transferases (GSTs). In a seminal study (Talalay et al. 1988) aiming to obtain mechanistic insights into the perplexing question of how numerous structurally diverse small molecules induce these proteins, a common chemical signature was identified, leading the investigators to conclude: "*…it is gratifying that the capacity of an extraordinary variety of seemingly unrelated anticarcinogens to induce protective enzymes can be attributed to the presence, or acquisition by metabolism, of a simple and hitherto unrecognized chemical property: that of a Michael reaction acceptor*." Following the discovery of Keap1 by Masayuki Yamamoto and his colleagues (Itoh et al. 1999) as the repressor of transcription factor Nrf2 that regulates the expression of these cytoprotective genes, the first question was: "*Does Keap1 have any (reactive) cysteine residues?*" In the ensuing years, several different laboratories have demonstrated cysteine modifications of Keap1 by inducers (see Sekhar et al. 2010; Holland and Fishbein, 2010; Hayes et al. 2010 for recent reviews), and it is now widely accepted that cysteine residues of Keap1 function as sensors of a chemical signal ultimately leading to enhanced expression of Nrf2-dependent cytoprotective genes.

Nrf2

Nrf2 (*N*F-E2 p45-*r*elated *F*actor *2*) is a bZip transcription factor and a member of the Cap 'n' Collar family of regulatory proteins which also includes NF-E2, Nrf1, Nrf3, Bach1 and Bach2 (Motohashi et al. 2002). Nrf2 is conserved in bilaterans with homologues found in nematodes, flies, fish and mammals, and was identified due to its ability to bind to NF-E2/ AP-1 enhancer elements in cDNA library screens (Moi et al. 1994; Itoh et al. 1995; Kobayashi et al 2002; An and Blackwell, 2003; Sykiotis and Bohmann 2008). Nrf2 was later shown to

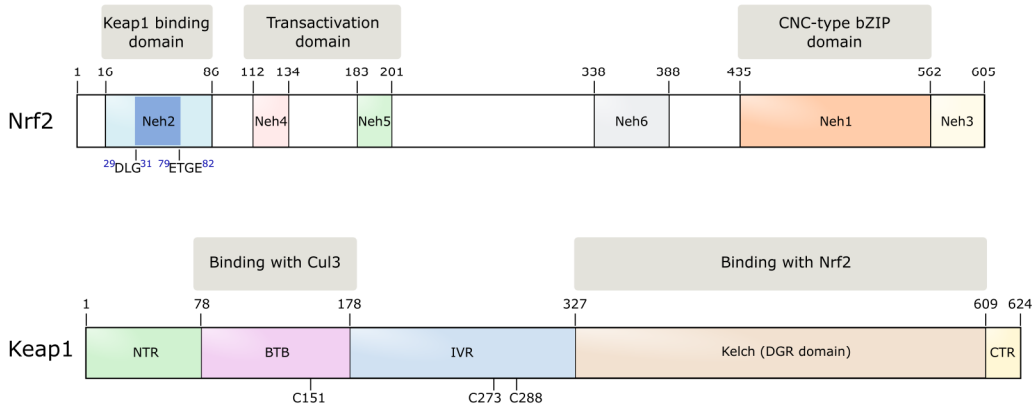

Figure 1.1. Domain structures of Nrf2 and Keap1. (A) In Nrf2, shown are the positions of the Neh2, Neh4, Neh5, Neh6, Neh1, and Neh3 domains, and the location of the DLG and ETGE motifs within the Neh2 domain through which Nrf2 binds to Keap1. Neh1 contains the bZip DNA binding and heterodimerisation domain through which Nrf2 interacts with the small Mafs, and binds to DNA as a heterodimer. The Neh4 and Neh5 domains act synergistically to bind the transcriptional co-activator, CBP. The Keap1-independent negative regulation of Nrf2 is controlled by the Neh6 domain.**(B)** In Keap1,shown are the positions of the N-terminal region (NTR), the BTB domain, the intervening region (IVR), the Kelch (DGR) domain, and the C-terminal region (CTR), and the location of C151, C273, and C288. Keap1 dimerises through the BTB domain that is also the domain through which Keap1 binds to Cullin 3 (Cul 3). The Kelch domain formsa 6-bladed β-propeller structure through which Keap1 interacts with the Neh2 domain of Nrf2.

mediate the cellular response to electrophiles and oxidants (collectively referred to as inducers) by binding to an enhancer element inthe promoter regions of cytoprotective genes (Itoh et al. 1997). Thus Nrf2 is activated by changes in the redox state of the cell, and functions to restore homeostasis by upregulating antioxidant, xenobiotic-metabolising, and other cytoprotective enzymes (see below). The critical importance of Nrf2 in the cellular stress response is highlighted by the phenotype of the Nrf2 null mice. In the absence of Nrf2, mice are viable and fertile but show increased sensitivity to numerous xenobiotics including benzo(*a*)pyrene, butylated hydroxytoluene, acetaminophen, diesel exhaust fumes, dimethylbenz(*a*)anthracene, cigarette smoke, dextran sulfate, 3-nitropropionic acid and malonate (Chan and Kan 1999; Enomoto et al. 2001; Aoki et al. 2001; Ramos-Gomez et al 2002; Xu et al. 2006; Rangasamy et al. 2004; Calkins et al. 2005; Khor et al. 2006; 2008).

The Nrf2 protein contains 605 amino acids which form 6 functional domains (**Figure 1.1A**) named Neh1-6 (*N*rf2-*E*CH *h*omology) (Itoh et al 1999).

Neh1 contains the bZip DNA binding and heterodimerisation domain through which Nrf2 interacts with its transcriptional partners, the small Mafs, and binds to DNA as a heterodimer (Itoh et al. 1995; 1997; Marini et al. 1997; Katsuoka et al. 2005). Domain deletion analysis identified the Neh2 domain as the negative regulatory domain of Nrf2. A yeast two-hybrid screen using Neh2 as bait identified Keap1 as the negative regulator of Nrf2 activity (Itoh et al 1999). The Neh3 domain binds to the chromo-ATPase/ helicase DNA binding protein family member CHD6, which functions as a transcriptional co-activator to promote transcription of ARE-dependent genes (Nioi et al. 1995). The Neh4 and Neh5 domains act synergistically to bind another transcriptional co-activator, CBP (Katoh et al 2001). Finally, the Keap1-independent negative regulation of Nrf2 is controlled via the Neh6 domain (McMahon et al. 2004).

ARE

The upstream regulatory regions of cytoprotective genes to which Nrf2-small Maf heterodimers bind are called antioxidant response elements or electrophile response elements (ARE or EpRE). They were identified by the laboratories of Cecil Pickett and Violet Daniel in the promoter of the gene encoding glutathione transferase Ya subunit, before the discovery of Nrf2 (Rushmore and Pickett 1990; Friling et al. 1990). The ARE consensus sequence is TGACnnnGC and was named due to its requirement in phenolic antioxidant-induced gene regulation (Rushmore and Pickett 1990; Rushmore et al. 1991). Following the discovery of the ARE, multiple proteins were shown to bind to it (Wasserman and Fahl 1997). Thus, in addition to small Mafs, numerous other transcription factors have also been implicated in the regulation of ARE-dependent gene expression and/ or binding to Nrf2, including; the Cap 'n' Collar proteins Nrf1, Nrf3, Bach1 and Bach2; ATF1, ATF2, ATF3, ATF4, JunD, c-Jun, c-Fos and Fra1, which are all members of the AP-1 transcription factor super family; the nuclear receptors RARα, PPARγ, ERα and ERRβ; the chromarin remodelling factor BRG1 and the transcriptional co-repressor SMRT (Venugopal and Jaiswal, 1996; Johnsen et al. 1998; Ikeda et al. 2000; He at al. 2001; Kim et al

2001; Muto et al. 2002; Gong et al. 2002; Sankaranarayanan and Jaiswal, 2004; Ansell et al. 2005; Dhakshinamoorthy et a. 2005; Ki et al. 2005; Tsuji 2005; Zhang et al. 2006; Iwasaki et al. 2007; Wang et al. 2007; Zhou et al 2007; Brown et al. 2008; Levy et al. 2009).

Keap1

Keap1 (*K*elch-like *E*CH *a*ssociated *p*rotein *1*) is a 624 amino acid protein which contains three main domains: a BTB dimerisation domain (*B*road-Complex, *T*ramtrack, and *B*ric à brac); a cysteine-rich IVR domain (*I*nter*v*ening *r*egion); and a Kelch domain consisting of 6 Kelch repeats through which Keap1 binds to Nrf2 (**Figure 1.1B**). Keap1 is a cysteine-rich protein, containing 25 and 27 cysteine residues within the mouse and the human homologues, respectively. Furthermore, 10 of these cysteines are predicted to be reactive due to the presence of adjacent positively-charged amino acids. This positive charge reduces the pK_a of the neighbouring cysteine thiol group, stabilising the thiolate anion, and therefore maintains the cysteines in a reactive state (Snyder et al. 1981). Together, the facts that Keap1 negatively regulates Nrf2 and contains a number of reactive cysteine residues made it the perfect candidate for the inducer sensor. This idea was supported by experimental evidence when it was shown that Keap1 binds directly to inducers of three different types, i.e., the isothiocyanate sulforaphane, the double Michael acceptor bis(2-hydroxybenzylidene)acetone, and the steroid dexamethasone 21-mesylate (Dex-mes); four cysteine residues (C257, C273, C288 and C297), all within the IVR domain of Keap1, and C613 in the C-terminal region, were modified when purified recombinant murine Keap1 was incubated with Dex-mes (Dinkova-Kostova et al. 2002). It was also found that recombinant Keap1 binds Zn^{2+} stoichiometrically with an association constant of 10^{11} M^{-1}, and that Co^{2+}substitution for Zn^{2+} yields an optical spectrum consistent with tertrahedral metal coordination (Dinkova-Kostova et al. 2005a).

Once Keap1 had been identified as the chemical sensor responsible for Nrf2 activation, it was then asked which cysteine residue(s) were important for

its activity. Mutation analysis of the IVR domain showed that substitution of C273 or C288 with either serine or alanine rendered Keap1 unable to repress Nrf2 activity under basal conditions (Zhang and Hannink 2003; Levonen et al. 2004; Wakabayashi et al. 2004). In contrast, mutation of C257 or C297, which had also been shown to bind inducers *in vitro*, had no effect on Nrf2 basal activity. The increased activity of Nrf2 in the presence of C273S/A or C288S/A mutant Keap1 was caused by reduced ubiquitination of Nrf2, and not by the dissociation of Keap1 from Nrf2 or Cullin 3 (Cul3) (Kobayashi et al. 2004; 2006; Zhang et al. 2004). Together these data suggest that C273 and C288 are important for the repression of Nrf2 by Keap1 under basal conditions, and that their modification by inducers may reduce the rate of ubiquitination and degradation of Nrf2. *In vivo* experiments using transgenic mice expressing either C273A or C288A Keap1 mutants confirmed that these residues are required for repression of Nrf2 under basal conditions (Yamamoto et al. 2008).

Interestingly, mutation of C151 in the BTB domain had a different effect on Keap1, by turning it into a constitutive repressor of Nrf2 in both basal and induced states (Zhang and Hannink, 2003). It was suggested that C151 is important for binding of Keap1 to Cul3, and that when inducers bind to Keap1, they may cause a dissociation of Keap1 from Cul3, and therefore stabilise Nrf2. In the absence of C151, inducers are unable to dissociate Keap1 and Cul3, making the C151 mutant Keap1 a constitutive repressor of Nrf2 (Zhang et al. 2004). *In vivo* data confirmed that the C151S mutant is a functional repressor of Nrf2; however experiments with embryonic fibroblasts isolated form these mice did not support the idea that the C151S mutant was a constitutive repressor of Nrf2, as Nrf2 was both stabilised and able to induce reporter gene expression in response to *tert*-butylhydroquinone (tBHQ) (Yamamoto et al. 2008).

Together, the analysis of Keap1 cysteines suggested that C151, C273 and C288 were all important for the function of Keap1. Subsequent work showed that although C151 is indispensable for Nrf2 stabilisation in response to inducers like tBHQ, is was not required for arsenite-mediated Nrf2 activation, suggesting that different classes of inducers may react with Keap1 in different ways (Wang et al. 2008a). Following on from this, a study in zebrafish found that inducers can be divided into two categories: those which react with C151 (e.g., sulforaphane,

tBHQ), and those which are independent of C151 and dependent on C273 (e.g., 15-deoxy-$\Delta^{12,14}$-prostaglandin J_2). This suggested that Keap1 contains multiple sensors (Kobayashi et al. 2009). Using murine Keap1 that was ectopically-expressed in mammalian cells, McMahon et al. (2010) found that C151 and C288 each comprise discrete sensors, whilst a third sensor is formed by H225, C226 and C613. Each of the three sensors was shown to be specific for certain types of inducers, with C151 required for nitric oxide, sulforaphane and tBHQ reactivity, C288 responding to alkenals, and H225, C226 and C613 comprising a sensor for zinc (McMahon et al. 2010). The idea that Keap1 may sense different inducers in different ways is not without precedent. In yeast, the transcriptional master regulator of oxidative stress Yap1 responds differently to the oxidants H_2O_2 and diamide, and like Keap1, different inducers of Yap1 depend on different cysteine residues to activate the signalling pathway (Delaunay et al. 2000; Kuge et al. 1997; 2001).

Whilst the crystal structure of full-length Keap1 is not available, several groups have analysed the Nrf2-binding Kelch domain of Keap1 using X-ray crystallography (Li et al. 2004; Padmanabhan et al. 2005; 2006; 2008; Lo et al. 2006). Crystallisation of the Kelch domain (residues 321-609) of human Keap1 found that it forms a 6-bladed β-propeller. Each of the blades is comprised of four anti-parallel β-strands which together form a twisted β-sheet. Blade I consists of strands from both the N- and C-terminus of the domain and this arrangement stabilises the closure of the ring-shaped β-propeller. Although each blade consists of variable number of amino acids (from 44 to 51), they all contain 7 conserved residues which are required for forming interactions between the blades and for further stabilisation of the β-propeller (Li et al. 2004).

Each β-strand is connected to the next by loops of varying lengths which extend both above and below the β-propeller. Co-crystallisation of the Kelch domain with a peptide of Nrf2 showed that the interaction between Keap1 and Nrf2 takes place in a shallow pocket formed by these loops, specifically the loops which connect β-strands A-D and B-C (Padmanabhan et al. 2006; Lo et al. 2006). Nrf2 interacts with Keap1 through its ETGE motif, which in humans consists of residues 77-82 (Kobayashi et al. 2002). The ETGE motif forms β-hairpin conformation and only the side-chains of residues E79 and E82 in Nrf2 interact

with the Kelch domain. In Keap1, all 6 blades of the β-propeller form bonds with Nrf2, either with E79/E82 side chains, or with the Nrf2 peptide backbone. In total, 13 intermolecular interactions are formed between Keap1 and Nrf2 (Padmanabhan et al. 2006; Lo et al. 2006).

Single particle electron microscopy has been used to generate a 3-dimensional reconstruction model of full length Keap1 dimer (Ogura et al. 2010). This model revealed that Keap1 forms a spherical body joined by a thin linker to the dimersation interface. The spherical structure consists of the entire Kelch and IVR domains and includes part of the BTB domain. The remainder of the BTB domain forms the linker and dimerisation surface. Interestingly, this reconstruction model suggests that the Kelch and BTB domains do not form distinct structures separated by the IVR or 'linker' domain as previously assumed. In addition, the structural proximity of the IVR and the Kelch domains provides a possible explanation of how covalent modifications of the IVR-residing C273 and C288 by inducers, or their substitution with other amino acids, may affect the Nrf2-binding affinity of the Kelch domain. In contrast, the assigned position of C151 is far away from the Kelch domain, suggesting that its modification by inducers is more likely to affect the interaction between Keap1 and Cul3, rather than Nrf2.

In addition to Nrf2, Keap1 has also been shown to bind to other proteins, including IKKβ, p62, and PGAM5 (Lo and Hannink, 2006a; Lo et al. 2008; Lee et al. 2009; Komatsu et al. 2010; Lau et al. 2010; Jain et al. 2010; Kim et al. 2010). The binding of Keap1 to p62 is significant as it suggests that Nrf2 can be activated by a deficiency in autophagy, whilst the interaction with IKKβ shows that Keap1 could regulate other signalling pathways (in this case NF-κB) independently of Nrf2.

Models of regulation of the Keap1-Nrf2 pathway

Sequester and release

The first model of the Keap1-Nrf2 interaction was heavily influenced by its similarities with other signalling pathways. Sub-cellular localisation studies using GFP-fusion proteins and immunocytochemistry showed that Keap1 was a cytoplasmic protein, whereas Nrf2 could be found in both the nucleus and cytoplasm (Itoh et al. 1999). In the absence of co-expressed Keap1, Nrf2 had a mostly nuclear localisation; however, when Keap1 was co-expressed, it appeared to sequester Nrf2 from the nucleus into the cytoplasm. As Keap1 was named after the *Drosophila* actin-binding protein Kelch (Xue et al. 1993), it was logically asked whether Keap1 was also able to bind to actin, and whether this was important for the repression of Nrf2 activity. This was found to be the case, as was the fact that similarly to Kelch, Keap1 dimerisation through the BTB domain was necessary for its function as a repressor of Nrf2 (Robinson et al. 1997; Zipper and Mulcahy 2002; Kang et al. 2004). The sub-cellular localisation studies also showed that in response to inducers, Nrf2 was able to migrate to the nucleus, even in the presence of co-expressed Keap1 (Itoh et al. 1999). Together, these data led to a model in which under basal conditions, Keap1 formed a dimer and sequestered Nrf2 in the cytoplasm by binding to actin (**Figure 1.2**). Inducers reacted with cysteine(s) in Keap1, leading to the release of Nrf2, and potentially to a loss of Keap1 dimerisation, allowing Nrf2 to translocate to the nucleus and turn on the expression of cytoprotective genes. This model found further support when it was shown that *in vitro*, Keap1-Neh2 (molar ratio of 2:1) complexes could be dissociated by the inducers sulforaphane and bis(2-hydroxybenzylidene)acetone in a concentration-dependent manner (Dinkova-Kostova et al. 2002).

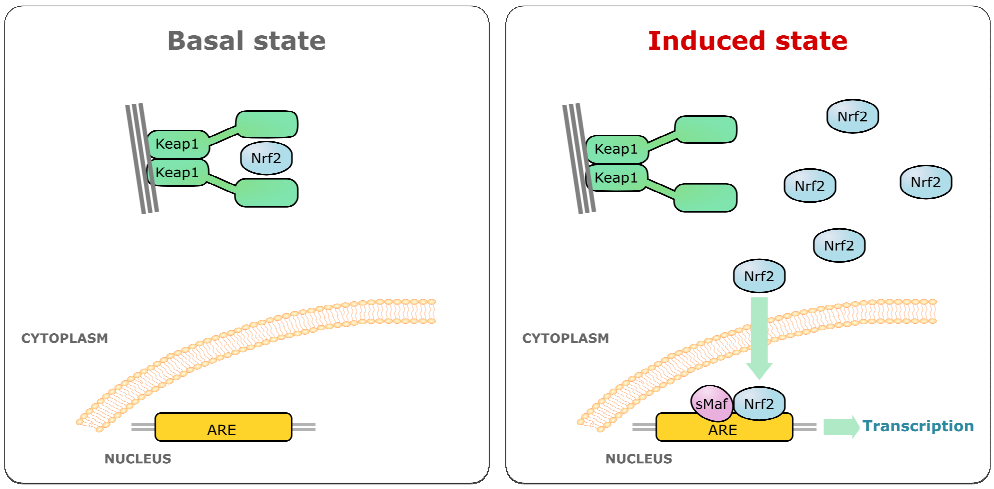

Figure 1.2. Sequester and release model of regulation of the Keap1-Nrf2 pathway. Dimeric Keap1 sequesters Nrf2 in the cytoplasm by binding to the actin cytoskeleton. Inducers react with specific cysteine residues in Keap1, leading to release of Nrf2, allowing the transcription factor to translocate to the nucleus and turn on the expression of cytoprotective genes.

This logical model was supported not only by the data available, but also by the similarity in function of Keap1 and Nrf2 with the *Drosophila* proteins Costal2 (Cos2) and Cubitus Interruptus (Ci) which function as the cytoplsmic repressor and transcription factor, respectively, in the hedgehog pathway (Sisson et al. 1997; Robbins et al. 1997). A similar sequester and release model had been proposed for Ci activation, which in turn was based on the precedent set by signalling in the NF-κB pathway (Baeuerle and Baltimore 1988; Siebenlist et al. 1994). In *Streptomyces coelicolor*, transcription factor σ^R controls induction of the thioredoxin reductase/thioredoxin operon in response to oxidants (Paget et al. 1998; Kang et al. 1999). Under basal conditions, σ^R is bound to a repressor protein, RsrA. Oxidants react with specific cysteine residues of RsrA leading to a disulfide bond formation within the repressor, loss of its ability to bind σ^R, and ultimately enhanced transcription of σ^R-dependent genes. Thus it appeared that the Keap1-Nrf2 pathway followed a well-used pattern in biology, that a cytoplamic repressor holds onto a transcription factor until it is "told" to release it by a pathway-specific signal.

Subsequent work using human recombinant proteins showed that in contrast to previous reports with the murine proteins, inducers were unable to dissociate the Keap1-Nrf2 complex (Eggler et al. 2005) and that upon the

addition of inducers more, not less Nrf2 was bound to Keap1. Together these data suggested that the sequester and release model may need to be modified (Zhang et al. 2004).

Protein stability

The idea that Nrf2 may be controlled at the level of protein stability was first suggested in 2000, when it was found that inhibition of the proteasome produced a rapid and robust increase in mRNA of the Nrf2 target gene GCLC (Sekhar et al. 2000). GCLC is the catalytic subunit of γ-glutamylcysteine ligase (GCL), the enzyme which catalyses the rate limiting step in glutathione synthesis. This increase in GCLC mRNA was functionally relevant, as it resulted in a 2-fold increase in the cellular glutathione level. Gel shift mobility assays and a transcriptional reporter demonstrated that the underlying mechanism involved Nrf2 and the ARE sequence within the promoter of GCLC.

Subsequent work showed that in response to cadmium, the amount of Nrf2 within the cell increased in a time-dependent manner, beginning after 30 min, and reaching 20 times the basal level after 4 hours (Stewart et al. 2003). The inducer-mediated accumulation of Nrf2 was coupled with an increase in Nrf2 protein half-life which extended from 13 to almost 100 min. Interestingly, the effect of cadmium on Nrf2 accumulation could be mimicked using proteasome inhibitors, and furthermore, overexpression of Nrf2 showed that it was a target of ubiquitination (Stewart et al. 2003). Together these data strongly suggested that Nrf2 was regulated at the level of protein stability. Similar results were obtained using the inducers tBHQ, sulforaphane and diethyl maleate (DEM), and each time the inducer was shown to stabilize Nrf2 (Nguyen et al. 2003; McMahon et al 2003; Itoh et al. 2003), whereas the level of Nrf2 mRNA was unaffected by the addition of inducers (Stewart et al. 2003; Nguyen et al. 2003; McMahon et al 2003; Itoh et al. 2003). Notably, the absence of Keap1 was sufficient for maximal Nrf2 accumulation, and neither DEM nor sulforaphane were able to significantly increase the Nrf2 levels any further (McMahon et al 2003; Itoh et al. 2003).

Although by then it was well established that Nrf2 activity was regulated by its stability, and that inactivation of Keap1 by inducers was required for the stabilisation, it was unknown exactly how Keap1 targeted Nrf2 for degradation. It was known that other BTB containing proteins were able to act as substrate adaptors for Cullin 3-based E3 ubiquitin ligases (Furukawa et al. 2003; Geyer et al. 2003; Pintard et al. 2003; Xu et al. 2003). As Keap1 contains a BTB domain, Cullin 3 (Cul3) was the perfect candidate for a Keap1-interacting protein which could mediate the degradation of Nrf2. Four groups independently reported that Keap1 was able to bind to Cul3 and ubiquitinate Nrf2 both *in vivo* and *in vitro* (Kobayashi et al. 2004; Cullinan et al. 2004; Zhang et al. 2004; Furukawa et al. 2005). Overexpression of Cul3 or Keap1 decreased the level of Nrf2, and conversely, the use of a dominant negative Cul3 or siRNA against Cul3 lead to the accumulation of Nrf2 and increased transcription from an ARE transcriptional reporter (Cullinan et al. 2004). Indeed, further work looking at the role of CAND1 suggests that the Keap1-Cul3-Rbx1 complex uses the same mechanism of ubiquitination as other Cullin-dependent E3 ubiquitin ligases (Lo and Hannink, 2006b).

These results complemented work which firmly established that Keap1 is the long-sought sensor for inducers (Dinkova-Kostova et al. 2002; Wakabayashi et al. 2004; Levonen et al. 2004), and together the available experimental evidence suggested that inducers may directly alter the activity of Keap1. Together these data were used to form the model of Nrf2 control which has received the most experimental support. Under basal conditions, Nrf2 is bound to Keap1 and targeted for ubiquitination and proteasomal degradation by the Cullin3-Rbx1 E3 ubiquitin ligase (**Figures 1.3 and 1.4**). Inducers chemically react with specific cysteine residues in Keap1, leading to stabilisation of Nrf2 and its translocation to the nucleus where it activates transcription of ARE-dependent genes. Stress responses mediated by other transcription factors such as HIF-1α and NF-κB are also regulated by the ubiquitin-proteasome system (UPS), suggesting that the UPS represents a conserved pathway of cellular adaptation to changing environmental conditions (Maxwell et al. 1999; Pause et al. 1997; Yaron et al. 1998; Kamura et al. 1999).

If Nrf2 is regulated by its stabilisation in response to inducers, how does this occur mechanistically? A number of models have been proposed to solve this problem: the dissociation of Keap1 and Cul3; the hinge and latch model; nucleocytoplasmic shuttling of Keap1; the ubiquitination of Keap1; and, Nrf2 directly sensing inducers.

Dissociation of Keap1 and Cul3

One of the first experiments to identify the role of Cul3 in the Keap1-Nrf2 pathway found that Keap1 and Cul3 were dissociated by the inducers tBHQ and sulforaphane (Zhang et al. 2004). This work was extended using eicosapentaenoic acid (EPA) and N-iodoacetyl-N-biotinylhexylenediamine (IAB), and in all cases dissociation of Cul3 from Keap1 was observed (Niture and Jaiswal 2009; Gao et al. 2007; Rachakonda et al. 2008). *In vitro* assays using purified recombinant proteins showed that IAB could both prevent Keap1 from binding to Cul3, and dissociate pre-formed Keap1-Cul3 complexes (Rachakonda et al. 2008). Together these data suggest that inducers function to stabilise Nrf2 by dissociating the Keap1-Cul3 complex, leading to the inhibition of Nrf2 ubiquitination and its stabilisation (**Figure 1.3**). Importantly, C151 in the BTB domain of Keap1 was found to be necessary for this effect (Zhang et al. 2004; Rachakonda et al. 2008).

Thus multiple groups have shown that inducers are able to affect the binding between Keap1 and Cul3, and have demonstrated the importance of C151 of Keap1. Although the BTB domain of Keap1 has not been crystallised, models of the Keap1-Cul3 interaction have been proposed based on the known structure of Cul1-Rbx1-Skp1-F box^{Skp2} complex (Zheng et al. 2002). One of the models shows that C151 is not located near either the BTB dimerisation interface or the Cul3 binding surface of Keap1, but instead is buried within the domain by four positively charged amino acids, i.e., K131, R135, and K150, and H154 (Fourquet et al. 2010). This positioning suggests that: firstly, the surrounding positively charged amino acids may contribute to the reactivity of C151 by stabilising the thiol anion; and secondly, because of the buried nature of

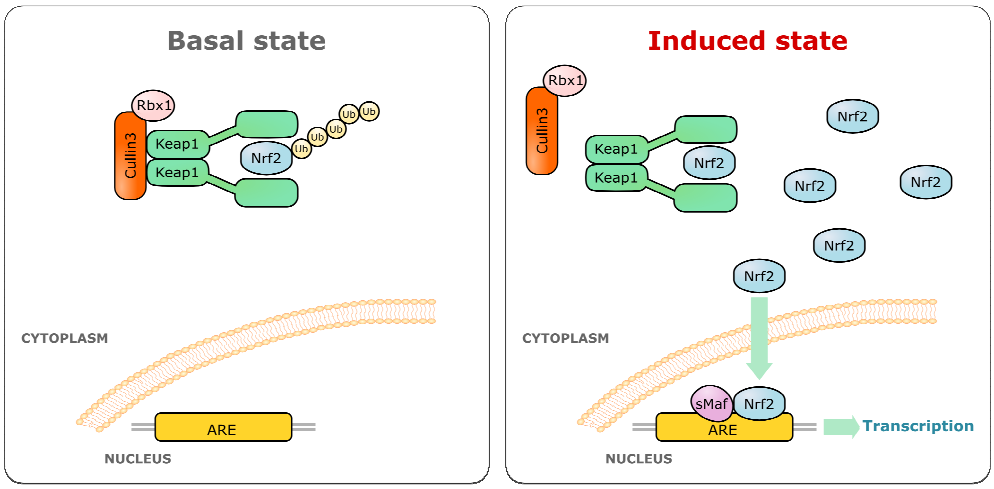

Figure 1.3. Dissociation of Keap1 and Cullin 3 model of regulation of the Keap1-Nrf2 pathway. Dimeric Keap1 binds Nrf2 and serves as a substrate adaptor for Cullin 3 (Cul3)-based ubiquitin ligase to target Nrf2 for ubiquitination and proteasomal degradation. Inducers react with specific cysteine residues in Keap1, leading to dissociation of the Keap1-Cul3 complex, inhibition of Nrf2 ubiquitination, and stabilisation of the transcription factor.

the residue, binding of inducers may alter the structure of the BTB domain. Indeed, mutant Keap1 in which K131, R135, and K150, were substituted with methionine residues had substantially reduced ability to sense sulforaphane or tBHQ (McMahon et al., 2010). Another model of the BTB domain proposes that binding of inducers to C151 leads to a steric clash with residues in the adjacent α-helix, which may in turn alter the position ofthe Cul3 binding site and thus lead to Keap1-Cul3 dissociation (Eggler et al. 2009). This model is supported by *in vitro* data which showed the binding of IAB caused a change in the secondary structure of Keap1 (Rachakonda et al. 2008). Thus it appears that at least in response to certain inducers, stabilisation of Nrf2 may be brought about by a change in interaction between Keap1 and Cul3.

Hinge and latch model

The interacting surface of Nrf2 and Keap1 was identified as the ETGE motif in the Neh2 domain of Nrf2 and the Kelch domain of Keap1 (Kobayashi et al. 2002). X-ray crystallography confirmed that the ETGE motif was able to bind

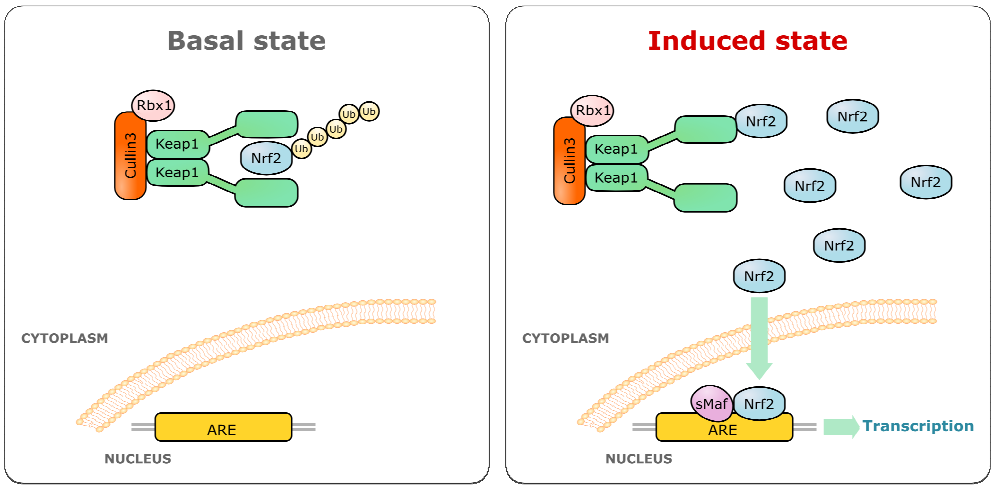

Figure 1.4. Hinge and latch model of regulation of the Keap1-Nrf2 pathway. Under basal conditions, monomeric Nrf2 binds to Keap1 homodimer. Each Keap1 subunit binds to Nrf2 through the ETGE and DLG motifs, respectively, allowing ubiquitination of the lysine residues in the a-helix of the Neh2 domain. Inducers react with cysteine residues within Keap1, leading to a conformational change in Keap1 and release of the weaker interaction with the DLG motif. As a result, the orientation of Nrf2 is not fixed and it is no longer efficiently targeted for ubiquitination and degradation. As Nrf2 is still bound to Keap1, any newly translated Nrf2 will not be able to bind Keap1 and will accumulate, translocate to the nucleus, dimerise with small Mafs, and activate ARE-dependent transcription. The mode of binding of Nrf2 to Keap1 gives the model its name, with the ETGE motif being the hinge, and the DLG, the latch.

to the beta propeller formed by the Kelch repeats (Padmanabhan et al. 2006; Lo et al. 2006). In the absence of this motif, Nrf2 is still able to bind Keap1 (McMahon et al. 2006); however it becomes insensitive to Keap1-mediated degradation allowing it to accumulate under basal conditions and to become insensitive to further stabilisation by inducers (McMahon et al. 2004). Together these data suggest a number of points. Firstly, that binding of Nrf2 to Keap1 is insufficient to target Nrf2 for degradation. Secondly, that for efficient degradation Nrf2 must bind to Keap1 through an additional motif, and finally, that because inducers were unable to additionally stabilise the ETGE mutant Nrf2, they may function by altering the binding of Nrf2 to Keap1 without leading to the release of Nrf2.

Subsequent work identified the second binding site of Nrf2 to Keap1 to be within the Neh2 domain (McMahon et al. 2004). This motif, consisting of residues 17-32, was originally named the DIDLID element but was renamed the DLG motif after further work found two distinct functions for residues 17-32 of

Nrf2 (Katoh et al. 2005; McMahon et al. 2006). In the absence of the DLG motif, the Nrf2 phenotype is the same as in the absence of the ETGE motif: it is able to bind to Keap1, however this binding to Keap1 does not lead to the ubiquitination and degradation of Nrf2. This allows Nrf2 to accumulate under basal conditions and it is not further stabilised by the addition of inducers (Katoh et al. 2005; McMahon et al. 2004; 2006). Crucially, in the absence of both the ETGE and DLG motifs, Nrf2 is no longer able to bind to Keap1 (McMahon et al. 2006).

Further analysis showed that the ETGE and DLG motifs bind to Keap1 with different affinities, with DLG binding to Keap1 with an affinity approximately 2 orders of magnitude lower than ETGE (Tong et al. 2006). This difference in affinity is caused by a difference in the number of electrostatic interactions between each motif and Keap1, with the ETGE motif forming 13 compared with 8 for the DLG (Tong et al. 2007; Padmanabhan et al. 2008). Structural analysis of the Neh2 domain showed that in the region between the DLG and ETGE motifs, Nrf2 forms an alpha helix containing 6 lysine residues on one side of the helix (Tong et al. 2006), and deletion of these lysines greatly increases the half-life of the resultant mutant Nrf2 (Zhang et al 2004). Together, these data were reconciled into a model of Nrf2 activation called "two-site substrate recognition" model, "fixed-ends" model, or "hinge and latch" model (**Figure 1.4**) (McMahon et al. 2006; Tong et al. 2006; 2007; Padmanabhan et al. 2008).

Under basal conditions, monomeric Nrf2 binds to a Keap1 dimer. One of the Keap1 monomers binds to Nrf2 through the ETGE motif, whilst the other monomer binds the DLG. This double binding of Nrf2 stabilises its orientation, allowing efficient ubiquitination of the lysine residues in the □-helix of the Neh2 domain. When inducers enter the cell, they bind to the reactive cysteine residues within Keap1, leading to a conformational change in Keap1 and the release of the weaker interaction with the DLG motif. Under these conditions the orientation of Nrf2 is not fixed and it is no longer efficiently targeted for ubiquitination by Keap1. The reduced rate of Nrf2 ubiquitination leads to a reduced rate of Nrf2 degradation. As Nrf2 is still bound to Keap1, any newly translated Nrf2 will not be able to bind Keap1, and can therefore bypass the "Keap1 gate", allowing it to accumulate in the cell, translocate to the nucleus, dimerise with small Mafs, and

activate the transcription of ARE-dependent genes. The specific mode of binding of Nrf2 to Keap1 gives the model its name, with the ETGE motif forming the hinge, and the DLG the latch. When inducers bind to Keap1, the hinge is maintained but the latch is released, leading to the accumulation of Nrf2.

This model is well supported by *in vitro* data, but its physiological relevance has yet to be determined. In addition, it is not clear from this model whether inducers cause a reduced rate of Keap1-mediated ubiquitination of Nrf2, or completely abolish it. As expected, when the half-life of Nrf2 was measured in the presence of inducers, it was unaffected by the presence or absence of Keap1; however, even under those conditions Nrf2 is a relatively short-lived protein, suggesting the existence of other factor(s) that regulate Nrf2 degradation (McMahon et al. 2004). Whilst this model postulates that Keap1 binds to Nrf2 at a 2:1 ratio, there is also evidence to suggest that Keap1 and Nrf2 bind at a 2:2 ratio (Tong et al. 2006; Lo et al. 2006). In addition, the hinge and latch model predicts that Nrf2 is not released by Keap1 in response to inducers, however whilst tBHQ does not dissociate Nrf2 from Keap1, the heavy metals cadmium and chromium, and arsenic have all been shown to dissociate the complex, suggesting that the mechanism of control of Nrf2 by Keap1 may be inducer-specific (He et al. 2006; 2007; 2008).

Keap1 nucleocytoplasmic shuttling

An alternate model of Nrf2 control by Keap1 involves the nucleocytoplasmic shuttling of Keap1 (**Figure 1.5**). By studying the Nrf2-knockout mouse it became clear that Nrf2 was required for both basal and inducible activity of ARE-dependent genes (McMahon et al 2001; Chanas et al. 2002), and therefore that under basal conditions some of the cellular pool of Nrf2 must be nuclear. Sequence analysis of Keap1 identified a putative nuclear export signal in the IVR domain (Velichkova et al. 2005; Nguyen et al. 2005; Karapetian et al. 2005), and chemical inhibition of the nuclear exporter Crm1 led to the nuclear accumulation of Keap1 (Velichkova et al. 2005; Nguyen et al. 2005; Karapetian et al. 2005; Sun et al. 2007; Niture et al. 2009). Together these data

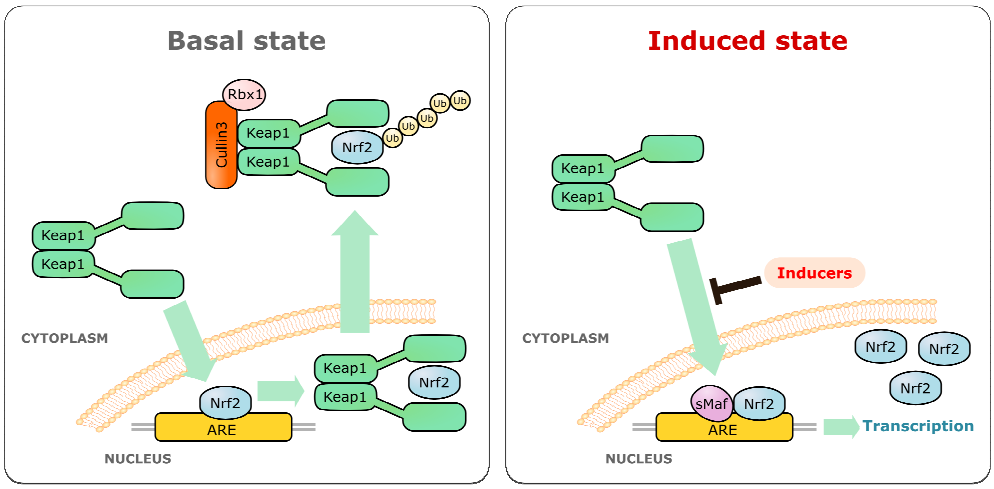

Figure 1.5. Keap1 nucleocytoplasmic shuttling model of regulation of the Keap1-Nrf2 pathway. Keap1 enters the nucleus and removes Nrf2 under both basal and induced conditions. Inducers inhibit the nuclear entry of Keap1 allowing transcription of Nrf2-dependent genes.

suggested that Keap1 may be able to enter the nucleus and remove Nrf2 under either basal or stressed conditions, and that the addition of inducers may affect the efficiency of this process. The problem with this model is that although all of the studies agree that Keap1 accumulates in the nucleus after blocking the nuclear transporter Crm1, they disagree about almost everything else. For example, the reports conflict as to whether Keap1 enters the nucleus in response to inducers (Velichkova et al. 2005; Nguyen et al. 2005), whether Nrf2 is predominantly localised in the cytoplasm or the nucleus under basal conditions (Nguyen et al. 2005; Sun et al. 2007), whether Cul3 can translocate to the nucleus (Sun et al. 2007; Niture et al. 2009), whether nuclear Keap1 activates or represses ARE-dependent genes (Velichkova et al. 2005; Nguyen et al. 2005), or which domain of Keap1 is required for nuclear localisation (Velichkova et al. 2005; Niture et al. 2009).

It had also been shown that Keap1 can bind to the nuclear protein prothymosin-α (Karapetian et al. 2005; Padmanabhan et al. 2008; Niture et al. 2009) in a similar way to the binding of the ETGE motif of Nrf2 (Padmanabhan et al. 2008). Two groups then proposed alternate models to explain how nuclear Keap1, Nrf2 and prothymosin-α interact, with either prothymosin-α dissociating the Keap-Nrf2 complex in response to inducers, or Nrf2 dissociating the Keap1-prothymosin-α interaction (Karapetian et al. 2005, Niture et al. 2009). It was

proposed that the Keap1-prothymosin-α complex forms in the cytoplasm in response to inducers, but this first requires the release of Nrf2 from Keap1, something which has been refuted elsewhere (Zhang et al. 2004; Eggler et al. 2005; Niture et al. 2009).

Finally, the use of a highly specific antibody against Keap1 revealed that endogenous Keap1 is predominantly cytoplasmic, and does not translocate to the nucleus in response to either inducers or Crm1 inhibition (Watai et al. 2007). This study did find that a small percentage of Keap1 (5%) was present in the nucleus under both basal and induced conditions. Together all these data agree that at least a fraction of Keap1 can enter the nucleus, however they do not present a clear coherent model for the physiological function of nuclear Keap1.

Ubiquitination of Keap1

A further model has been proposed whereby in response to inducers, Keap1 and not Nrf2 becomes the target of Cul3-mediated ubiquitination (**Figure 1.6**) (Zhang et al. 2005; Hong et al. 2005). It was shown that both ectopic and endogenous Keap1 could be ubiquitinated in response to tBHQ, but not sulforaphane (Zhang et al. 2005). By use of mass spectrometry it was found that the ubiquitination of Keap1 took place on lysine-298 in response to the inducer IAB, in agreement with work showing that the IVR domain of Keap1 was required its ubiquitination (Zhang et al. 2005; Hong et al. 2005).

Together these data raise a number of different points. They suggest not only an alternate mechanism of Nrf2 control, but also show that all inducers may not function in the same way, as tBHQ, IAB but not sulforaphane were able to target Keap1 for ubiquitination. Interestingly, Hong et al. also found that the electrophile 1-biotinamido-4-(4'-[maleimidoethylcyclohexane]-carboxamido)butane (BMCC)was able to bind to Keap1 but this did not lead to the stabilisation of Nrf2, suggesting that simply binding of an electrophile to the reactive cysteines of Keap1 is insufficient for Nrf2 stabilisation.

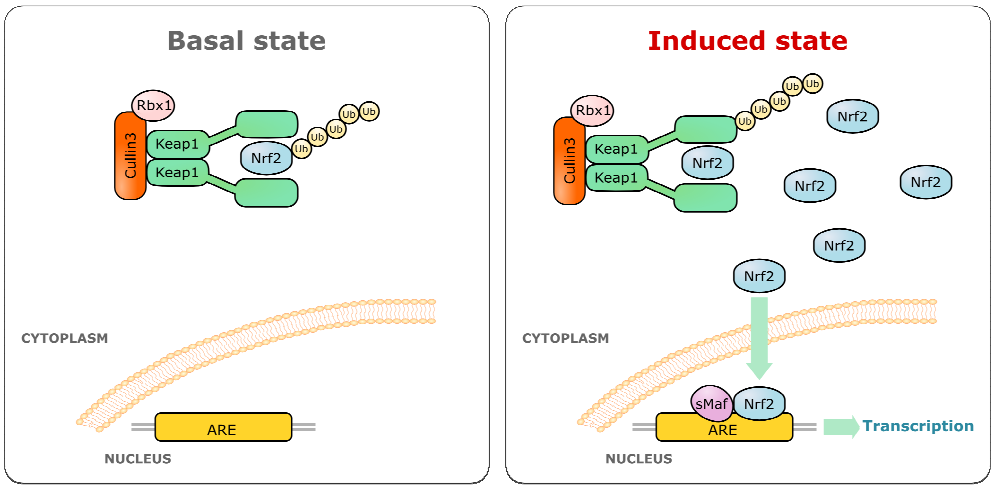

Figure 1.6. Ubiquitination of Keap1 model of regulation of the Keap1-Nrf2 pathway. Dimeric Keap1 binds and targets Nrf2 for ubiquitination and proteasomal degradation. Inducers cause a switch in ubiquitination from Nrf2 to Keap1 which becomes the target of Cul3-mediated ubiquitination and degradation, allowing the transcription factor to stabilise, translocate to the nucleus and turn on the expression of cytoprotective genes.

Such a model of auto-ubiquitination of a substrate adaptor protein is not without precedent. In yeast, multiple E3 ubiquitin ligase substrate adaptors are ubiquitinated by the same machinery which normally targets their substrates for degradation; in mammals, the F-box E3 ligases Skp2 and β-TrCP are also ubiquitinated (Zhou and Howley 1998; Galan and Peter 1999; Li et al. 2004; Bashir et al. 2004; Wei et al. 2004).

Nrf2 senses inducers directly

Nrf2 contains seven cysteine residues, four of which are conserved in human, mouse, rat and chicken, suggesting that Nrf2 itself may be able to react with inducers. This possibility was tested experimentally using arsenic-based inducers with both purified recombinant and cell lysate derived Nrf2 (He et al. 2009). The idea that Nrf2 may directly sense and react with inducers led to the formation of a Keap1-independent model of Nrf2 control. Nrf2 contains a number of putative nuclear import (NLS) and export (NES) signals (Li et al. 2005; 2008; Jain et al. 2005). One such NES located within the Neh5

transactivation domain was shown to be redox-sensitive, and led the authors to propose a model whereby Nrf2 activity is regulated by its cellular localisation (Li et al. 2006). Under basal conditions, the combined NES signals overcome the NLS resulting in a mostly cytoplasmic distribution of Nrf2 (**Figure 1.7**). Inducers cause an inactivation of this export signal, shifting the balance from nuclear export to nuclear entry of Nrf2, allowing it to accumulate in the nucleus and turn on cytoprotective genes (Li et al. 2006). Mutation of C183 to A within one of the NES motifs attenuated nuclear accumulation and ARE-dependent reporter gene expression following exposure to inducers.

This model accounts for both the low basal Nrf2-dependent gene expression and the increased expression caused by inducers, but it also conflicts with some previously published data. Firstly, in cells derived from Keap1-knockout mice, the levels of Nrf2 target genes such as *gclc*, *nqo1* and *prdx1* are all constitutively upregulated, and cannot be further increased by inducers, suggesting that Keap1 and not Nrf2 is responsible for inducer sensitivity (Wakabayashi et al. 2003). In addition, the redox sensitivity of the Nrf2 NES requires much higher concentrations of inducers than those that inactivate Keap1, which questions the physiological relevance of these results (Nguyen et al. 2003; McMahon et al. 2003). However, the idea that the sub-cellular localisation of a redox-sensitive transcription factor is controlled by cellular stress is not without precedent. In yeast, transcription factor Yap1 contains a redox-sensitive NES similar to that described for Nrf2 (Yan et al. 1998); in mammals, Bach2 contains a cytoplasmic localisation signal which is overridden in response to oxidative stressors (Hoshino et al. 2000).

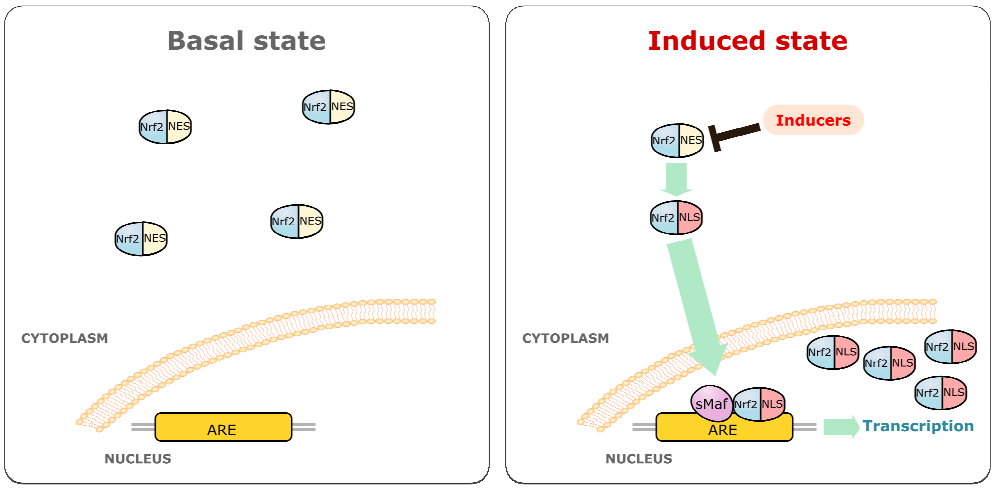

Figure 1.7. Nrf2 senses inducers directly. Under basal conditions, the nuclear export signal (NES) dominates over the nuclear localization signal (NLS), resulting in a cytoplasmic distribution of Nrf2. Inducers react with cysteine residues within Nrf2 causing inactivation of the nuclear export signal, which shifts the balance from nuclear export to nuclear entry of Nrf2, allowing it to accumulate in the nucleus and turn on cytoprotective genes.

Transcriptional and translational control of Nrf2

The majority of the data used to formulate the models already described come from experiments using overexpressed Nrf2 and Keap1 in cultured cells. Analysis of the endogenous action of inducers in mice showed an additional mechanism of ARE control, the increased transcription of Nrf2. When given to mice, the inducers 3*H*-1,2-dithiole-3-thione (D3T), β-naphthoflavone (β-NF), ethoxyquin(EQ) and oltipraz all increased the amount of Nrf2 mRNA relative to basal levels (Kwak et al. 2001; Ramos-Gomez et al. 2001). These results are in stark contrast to most cell culture data which show no increased transcription of Nrf2 in response to inducers (Nguyen et al. 2003; McMahon et al. 2003; Stewart et al. 2003; Itoh et al. 2003). This conflict between *in vivo* and cell culture-derived data suggests that Nrf2 control may be complex and regulated at different levels simultaneously. If Nrf2 is regulated at the level of transcription, how is this transcription induced? A putative ARE was found in the promoter of Nrf2, suggesting Nrf2 may regulate its own transcription in a positive feedback loop (Kwak et al. 2002). This idea is supported by microarray data from mouse lung and liver (Li et al. 2004; Cho et al 2005).

Beyond the transcriptional control of Nrf2, work using rat cardiomyocytes suggested that Nrf2 may also be regulated at the level of translation (Purdom-Dickinson et al. 2007). This work was extended to shown that Nrf2 mRNA contains a redox-sensitive internal ribosomal entry site (IRES) in the 5'-UTR (Li et al. 2010). Reporter assays showed that in response to sulforaphane or H_2O_2, translation was increased from the IRES in the Nrf2 transcript. Sequence analysis of the IRES show it contains a putative 18*S* rRNA binding site which is conserved in the human, mouse and rat mRNA (Li et al. 2010).

The idea of a redox-sensitive IRES is not without precedent (MacCallum et al. 2006); indeed the master regulator of the oxidative stress response in yeast Yap1 has been shown to contain a functional IRES within the 5'-UTR of its mRNA (Zhou et al. 2001). Although these data suggest that Nrf2 activity is also regulated at the level of transcription, it is unlikely that this type of regulation is responsible for the rapid increase in Nrf2 protein level after 30 min treatment with inducers (Stewart et al. 2003; Nguyen et al. 2003), suggesting that it may function in concert with increased Nrf2 stability to provide a robust long-term response to inducers.

Keap1-independent control of Nrf2

Under basal conditions Nrf2 has a short half life (7-15 min), however, all studies which showed an increase in Nrf2 stability in response to inducers found that even in the presence of these chemicals, Nrf2 still has a half life between 30 and 100 minutes, suggesting it is still rapidly turned over (Stewart et al. 2003; Nguyen et al. 2003; McMahon et al. 2004). Analysis of mutant Nrf2 proteins suggested that the Neh6 domain may contain a redox-insensitive degron. Under basal conditions, the deletion of this degron had no effect on Nrf2 stability, and it was degraded in a Keap1-dependent manner. However, after addition of sulforaphane, the half-life of the Neh6-mutant Nrf2 increased by more than 2-fold in comparison with the wild-type counterpart, suggesting that Neh6 may be important for regulating Nrf2 in the presence of inducers, or in the absence of

functional Keap1 (McMahon et al. 2004). Furthermore, recent work suggests that the Neh6 domain is regulated through a β-TRcP-GSK3-dependent pathway (Rada et al. 2011, Rada et al. 2012, Chowdhry et al. 2012). Similarly, work carried out in Keap1-knockout cells suggested that the DIDLID element in the Neh2 domain may be required for Nrf2 regulation in redox-stressed cells (McMahon et al. 2006). How the Neh6 degron or the DIDLID element control Nrf2 stability in the presence of inducers is currently unknown.

Phosphorylation

The fact that Keap1 is the major regulator of the protein stability of Nrf2 does not preclude any other signalling pathway involvement in Nrf2 regulation. Indeed, Nrf2 is activated by chemicals which have a number of different effects in the cell, in addition to modifying Keap1. For example, hydrogen peroxide activates many signalling pathways, including the kinase ATM (Guo et al. 2010), sulforaphane has been shown to inhibit HDAC6 activity (Myzak et al. 2004; 2006; Gibbs et al. 2009). Recently, proteomics analysis using a sulfoxythiocarbamate analogue of sulforaphane found that it bound to over 100 proteins (Ahn et al. 2010). Thus it is clear that compounds which modify Keap1 could also affect the cellular phenotype in many other ways, and some of these effects may converge to affect Nrf2 activity in a Keap1-independent manner.

Many signalling pathways are controlled post-translationally by the activity of protein kinases (Karin and Hunter 1995). Thus it has been shown that the hypoxia stress response is activated by phosphorylation from the PI3K and MAPK pathways, demonstrating that stress responses can be activated by diverse mechanisms (Semenza, 2003). In light of this idea, it is not surprising that a number of protein kinases have been implicated in the regulation of Nrf2 activity.

One such kinase proposed to play a role in Nrf2 regulation is protein kinase C. Activation of PKC increased ARE-dependent gene expression, whereas inhibition of PKC reduced tBHQ-mediated Nrf2 accumulation (Huang et al. 2000). The target of PKC phosphorylation was later shown to be S40 of Nrf2, and

whilst mutation of this residue reduced ARE-dependent gene expression, the reduction was only by 50%, suggesting that PKC acts in concert with Keap1 in response to inducers (Huang et al. 2002; Bloom and Jaiswal 2003). Mechanistically, it has been suggested that phosphorylation of S40 by the PKCδ isoform promotes the release of Nrf2 from Keap1, leading to increased ARE-dependent gene expression (Huang et al. 2002; Niture et al. 2009). A role for phosphorylation in the control of Nrf2 activation is not surprising, and is in keeping with many other signalling pathways (Karin 1995; DiDonato et al. 1997). Indeed, it has been shown that the activity of PKCδ is increased by oxidative stress, and that this increase is mediated by the Src family kinases (Konishi et al. 1997; 2001; Rybin et al. 2004) and ATM (Li et al. 2004; Guo et al. 2010). Furthermore, PKCδ-knockout cells show a reduced accumulation of Nrf2 in response to inducers, providing support that this kinase may be required for full activation of Nrf2 (Li et al. 2004).

Another signalling cascade which is activated by oxidative stress and has been implicated in Nrf2 control is the mitogen activated protein kinase (MAPK) pathway. The Nrf2 inducers tBHQ, sulforaphane and cadmium have also been shown to modulate MAPK activity (Yu et al. 1999; 2000; Alam et al. 2000). In addition, inhibition of ERK, MEK or p38 leads to a decrease in ARE-dependent gene expression, suggesting that these kinases play a positive role in Nrf2 activation (Yu et al. 1999; Alam et al. 2000). In contrast, it has also been shown that p38 negatively regulates Nrf2, suggesting that MAPK control of ARE-dependent gene expression may be complex, and both inducer- and cell type-specific (Yu et al. 2000). The effect of MAPK activity on ARE-dependent gene expression could be due to either the direct phosphorylation of Keap1 and/or Nrf2, or through an indirect, less specific mechanism. By use of mass spectroscopy, it was shown that Nrf2 is phosphorylated at several serine and threonine residues in cells (S215, S408, S558, T559, S577), with three out of these five sites fitting the MAPK consensus sequence (Sun et al. 2009). Interestingly, phosphorylation of S40 was not identified in this study. Mutation of individual phosphorylation sites had no effect on Nrf2 activity, whereas mutation of all 5 sites caused only a modest decrease in ARE-dependent gene

expression, suggesting that MAPK plays only a limited role in the activation of Nrf2.

An alternate role of protein kinase-mediated control of Nrf2 has been proposed to solve the problem of how the increased Nrf2 levels are brought down to basal levels when the inducers are removed. It has been proposed that the return of elevated Nrf2 back to basal levels is controlled by GSK3β and the Src family member, Fyn kinase (Jain et al. 2006; 2007). The authors propose that in response to inducers such as H_2O_2, Nrf2 accumulates in the nucleus, whilst Fyn is depleted from the nucleus, and GSK3β is inactivated. After a few hours, a delayed response to H_2O_2 is initiated, and GSK3β is phosphorylated, leading to phosphorylation and nuclear accumulation of Fyn which in turn phosphorylates Nrf2 at Y568. The phosphorylation of Nrf2 leads to its nuclear export, allowing it to be degraded by Keap1 (Jain et al. 2006; 2007). However, there are currently no data showing how GSK3β is either repressed or activated by inducers.

The inducer tBHQ has also been shown to activate PI3K, inhibition of which caused a significant decrease in ARE-dependent gene expression (Lee et al. 2001; Kang et al. 2001). Significantly, in the absence of inducers, constitutively active PI3K has also been shown to increase the activity of the Nrf2 target gene NQO1, and the levels of glutathione (Healy et al. 2005). It is interesting to note that in Nrf2-knockout cells both Akt and ERK1/2 show decreased responsiveness to PDGF and/ or insulin, suggesting the existence of a reciprocal interaction between Nrf2 and PI3K signalling (Reddy et al. 2008). In addition, Nrf2 has also been shown to be phosphorylated by GSK3β, PERK and CK2, suggesting that the regulation of Nrf2 has the potential to be very complex, and could be fine-tuned by a number of different mechanisms (Salazar et al. 2006; Cullinan et al 2003; Cullinan and Diehl 2004; Pi et al. 2007).

In light of the data suggesting that Nrf2 is controlled by protein kinases, it is important to note that, as previously mentioned, in cells derived from Keap1-knockout mice or following knockdown of Keap1 by siRNA, Nrf2 target genes are constitutively activated, and their expression cannot be further increased by inducers (Wakabayashi et al. 2003; Devling et al. 2005; MacLeod et al. 2009). This implies that Keap1 plays by far the greatest role in regulating Nrf2 activity.

Any role of other pathways may simply fine-tune ARE-dependent gene expression and become important only in the absence of functional Keap1.

The cytoprotective functions of Nrf2-target gene products

Based on numerous individual biochemical studies and global gene expression profiling, it is now evident that the Keap1-Nrf2 pathway controls the gene expression of a family of cytoprotective proteins that is characterized by extraordinary diversity. The available microarray data describing Nrf2-target genes in rodent liver, lung, small intestine, and mouse embryonic fibroblasts (MEFs), as well as in human cell lines and tissues were recently summarised (Hayes et al. 2010). Below is a brief outline of the cytoprotective roles of two major groups of Nrf2 target gene products that: (i) are involved in the metabolism and transport of a wide array of endo- and xenobiotics; and (ii) have antioxidant functions. Notably, the distinction between these two groups is not unequivocal, and some enzymes that are listed in the first category also could be classified under the second. Thus, specific glutathione *S*-transferases exhibit glutathione peroxidase activity towards hydroperoxides (Hurst et al. 1998). NQO1 protects against generation of reactive oxygen intermediates that are formed during oxidative cycling of quinones (Prochaska et al. 1987), and it has also been shown to scavenge superoxide directly (Siegel et al. 2004).

Proteins involved in the metabolism and transport of endo- and xenobiotics

Historically, this group represents the earliest recognized class of Nrf2-dependent genes. NQO1 is one of the most robust responders to both pharmacological (by small-molecule inducers) and genetic (deletion of Keap1) activation of Nrf2 (Benson et al. 1980; Yates et al. 2009). NQO1 is a widely-distributed FAD-dependent flavoprotein that catalyses the obligatory 2-electron reductions of quinones, quinoneimines, nitroaromatics, and azo dyes, using either NADH or NADPH equally efficiently as the hydride donor (for recent reviews see Ross and Zhou, 2010; Dinkova-Kostova and Talalay, 2010). In doing

so, NQO1 reduces the opportunities for generation of reactive oxygen intermediates mediated by redox cycling, and for depletion of intracellular sulfhydryl pools. Induction of NQO1 levels decreases, whereas depletion increases the susceptibility to oxidative stress. Human polymorphisms that lead to low NQO1 activity are associated with increased predisposition to disease, especially childhood leukemia (Smith et al. 2002), and represent a strong prognostic factor in breast cancer survival and metastasis (Fagerholm et al. 2008). In addition, NQO1 binds and protects the tumor suppressor p53 against proteasomal degradation (Asher et al. 2001, 2002), and thus has even broader cytoprotective roles, beyond its enzymatic functions.

The aldo-keto reductases (AKRs) are some of the most inducible Nrf2-target genes in human cells and tissues (Burczynski et al 1999; Devling et al. 2005; Gasper et al. 2007; Chambers et al. 2009; MacLeod et al. 2009). The AKRs catalyse the NAD(P)H-dependent reductions of the carbonyl groups of numerous aliphatic and aromatic aldehydes and ketones, retinals, ketoprostaglandins, and ketosteroids, leading to either their detoxification or activation (see Jin and Penning, 2007 for a comprehensive review). In doing so, the AKRs prepare the carbonyl group for subsequent conjugation, such as glucuronidation and sulfation, and ultimately for excretion. The sulfated and glucuronidated conjugates then become substrates for sulfotransferases (SULTs) and uridine diphosphoglucuronosyltransferases (UGTs), respectively, two other classes of Nrf2-target genes. In addition to products of the reactions catalysed by the AKRs, the SULTs catalyse the sulfation of various other xenobiotics, as well as endogenous hormones and neurotransmitters using 3'-phosphoadenosine 5'-phosphosulfate (PAPS) as the sulfuryl donor (reviewed by Coughtrie, 2002). Interestingly, in humans the SULTs are highly expressed in the developing fetus at levels equivalent to or exceeding those in the adult, and may represent its primary detoxification system (Stanley et al. 2005). Also characterized by very broad substrate specificity, the members of the UGT family catalyse the glucuronidation of numerous endogenous and exogenous lipophilic molecules, such as steroids, bile acids, bilirubin, dietary substances, environmental pollutants, increasing their water solubility and facilitating their subsequent excretion (see Tukey and Strassburg, 2000 for a comprehensive review). Specific

human polymorphisms in the UGTs are responsible for the clinical manifestation of Crigler-Najjar's and Gilbert's syndromes, illustrating the critical role of these enzymes in the glucuronidation of bilirubin.

In rodents, the glutathione *S*-transferases (GSTs) are among the most inducible Nrf2-dependent genes. Whereas in humans the gene expression of the GSTs might be regulated differently (Hayes et al. 2010), their cytoprotective functions are undebatable. The vital importance of the GSTs is evidenced by their wide distribution, with specific isoforms abundant in the cytoplasm, endoplasmic reticulum, and the mitochondria (for comprehensive reviews see Hayes et al. 2005; Mannervik et al. 2005). The GSTs catalyse the conjugation of a wide variety of substrates with glutathione, thereby playing critical roles in the detoxification of xenobiotic electrophiles, such as environmental pollutants, chemical carcinogens, chemotherapeutic agents, as well as endogenous α,β-unsaturated aldehydes, epoxides, and hydroperoxides. In addition to their detoxification roles, the GSTs also participate in the biosynthesis of leukotrienes, prostaglandins, testosterone, and progesterone, and in the degradation of tyrosine.

The conjugation products of the GSTs, the SULTs, and the UGTs are exported out of the cell by members of the multidrug resistance-associated protein (MRP) family. The MRPs are ATP-dependent membrane-associated organic anion transporters; MRP4 is also involved in the export of nucleosides and prostaglandins (Borst et al. 2000; Reid et al. 2003). MRP2 is the major transporter responsible for the export of bilirubin glucuronides into bile; its deficiency in humans leads to Dubin-Johnson syndrome. Pharmacological or genetic (liver-specific Keap1-knockout) activation of Nrf2 causes upregulation of several MRPs; especially striking is the effect of Keap1 deletion on MRP4 (~80-fold) and MRP5 (~40-fold) (Yates et al. 2009). Interestingly, the same genetic model revealed that the absence of Keap1 (and therefore the constitutive activation of Nrf2) in the liver also leads to increases in the levels of several members of the cytochrome P450 family of drug metabolizing enzymes; such increases have been observed with some (e.g., 3*H*-1,2-dithiole-3-thione), but not other (e.g., CDDO-Im) pharmacological activators of Nrf2 (Kwak et al. 2003; Osburn et al. 2008; Yates et al. 2009).

Proteins with antioxidant functions

Both the catalytic and the regulatory subunits of γ-glutamylcysteine ligase (GCL), the enzyme that catalyses the rate-limiting step in the biosynthesis of glutathione, the principal endogenous small-molecule antioxidant, are regulated by Nrf2 (Wild et al. 1999). In addition, χ-CT, the core subunit of the cystine/glutamate membrane transporter, which is responsible for the uptake of cystine that in turn is rapidly reduced to cysteine and used for the synthesis of glutathione (Bennai and Ishii, 1982), is also an Nrf2 target (Ishii et al. 2000). In addition to its essential role for the conjugation of electrophiles catalysed by the GSTs, glutathione is used by glutathione peroxidases to enzymatically reduce hydrogen peroxide to water. Glutathione reductase, which catalyses the reduction of oxidized glutathione and the regeneration of reduced glutathione, is also Nrf2-dependent, as is glucose 6-phosphate dehydrogenase, which provides NADPH to glutathione reductase (Kwak et al. 2003). The transcriptional regulation of glutathione peroxidase 2 (and possibly also glutathione peroxidase 1) is Nrf2-dependent (Lubos et al. 2010). Nrf2 also regulates the gene expression of other NADPH-generating enzymes, i.e., malic enzyme and phosphogluconate dehydrogenase (Thimmulappa et al. 2002). NADPH is used as a source of reducing equivalents for the selenocysteine-containing thioredoxin reductases, which are also Nrf2-target genes, as are the thioredoxins themselves. In addition to being direct antioxidants in quenching of reactive oxygen intermediates, the thioredoxins undergo reversible oxidation of their conserved cysteine residues through the transfer of reducing equivalents to disulfide substrates. In doing so, the thioredoxins modulate the activities of many cellular proteins, including those involved in signaling cascades (Powis and Montford, 2001). Reduction of oxidized thioredoxins is then catalysed by thioredoxin reductases (Mustacich and Powis, 2000; Holmgren and Lu, 2010).

Thioredoxin (together with NADPH) also plays a critical role in the completion of the catalytic cycle of the peroxiredoxins (Prxs). The Prxs are ubiquitous peroxidases that use a conserved Cys residue (called the peroxidatic Cys) to reduce peroxide substrates, such as H_2O_2. Their high catalytic efficiencies (on the order of $\sim 10^7$ $M^{-1}s^{-1}$) are achieved by activation not only of the

peroxidatic Cys thiolate, but also of the peroxide substrate, and by a hydrogen bonding network created by four residues (Pro, Thr, Arg and the peroxidatic Cys) that are conserved in the active sites of all Prxs, which stabilizes the transition state of the peroxidatic S_N2 displacement reaction (Hall et al. 2010). During the catalytic cycle of a eukaryotic dimeric Prx, the peroxidatic Cys of one subunit is oxidized by the substrate to sulfenic acid (-SOH), which then reacts with a second conserved Cys residue (called the resolving Cys) of the other subunit to form an intermolecular disulfide bond. It is the reduction of this disulfide bond that is carried out by thioredoxin/NADPH to complete the cycle. Intriguingly, during the reduction of their substrates, the peroxidatic Cys of the Prxs can be overoxidized to sulfinic acid (-SOOH) that, in turn is reduced back to Cys by the ATP-dependent sulfinic acid reductase sulfiredoxin (Srx) (Biteau et al 2003; Woo et al. 2003). Srx is the only known enzyme that catalyses the reduction of sulfinic acid in mammals, and the Prxs are its only identified substrates (Woo et al. 2005). Both have been reported to be Nrf2-target genes (Ishii et al. 2000; Osburn et al. 2008; Singh et al. 2009).

Nrf2 participates in the regulation of the gene expression of heme oxygenase 1, which, in concert with bilirubin reductase, generates the antioxidants carbon monoxide and bilirubin (Ryter and Choi, 2010). The upstream regulatory regions of the gene encoding heme oxygenase 1 contain multiple AREs, which are responsible for its quick and robust inducibility by various small-molecule Nrf2 activators (Prestera et al. 1995). Free iron, also a product of the heme oxygenase 1 catalysis, is then efficiently sequestered by another Nrf2-regulated gene product, i.e., ferritin (Pietsch et al. 2003), that has the remarkable capacity to store 4500 (Fe^{3+}) ions in a bioavailable and nontoxic form (Harrison and Arosio, 1996). Nrf2 also takes part in the transcriptional regulation of another class of metal-binding-proteins, the metallothioneins (Katsuoka et al. 2005). The metallothioneins are small cysteine-rich (20 cysteine residues out of a total of 61 or 62 amino acids) proteins that have an exceedingly high metal and sulfur content, up to 10% w/w (Henkel and Krebs, 2004). These highly conserved multifunctional proteins protect against the toxicity of heavy metals and oxidative damage, and in addition, limit inflammation, modulate immune responses, and contribute to tissue repair.

Thus the large and functionally diverse family of Nrf2-dependent cytoprotective proteins bestows the cell with multiple layers of protection by providing: (i) antioxidant enzymes (e.g., heme oxygenase 1, NAD(P)H:quinone oxidoreductase 1); (ii) conjugating enzymes (e.g. glutathione *S*-transferases and uridine diphosphoglucuronosyltransferases); (iii) proteins that enhance export of xenobiotics and/or their metabolites (e.g., solute carrier- and ATP-binding cassette transporters); (iv) enzymes that participate in the synthesis and regeneration of glutathione (e.g., γ-glutamylcysteine synthetase, glutathione reductase); (v) enzymes that promote the synthesis of reducing equivalents, i.e., NADPH (e.g., glucose 6-phosphate dehydrogenase, 6-phosphogluconate dehydrogenase); (vi) enzymes that inhibit inflammation (e.g., leukotriene B_4 dehydrogenase); (vii) proteins that do not have enzymatic activities, but are nevertheless essential for cytoprotection (e.g., ferritin which has an enormous capacity to protect against iron overload, metallothioneins); (viii) proteins that participate in the repair and removal of damaged proteins (e.g., subunits of the 26S proteosome); and (ix) proteins that regulate the expression of other transcription factors and growth factors. A recent study that used a high-throughput chromatin-immunoprecipitation with parallel sequencing methodology identified more than 600 Nrf2-target genes, further confirming the essential role of Nrf2 as a central regulator of cell protective and survival responses (Malhotra et al. 2010). In addition, genetic versus chemoprotective activation of Nrf2 has been shown to result in overlapping, yet distinct gene expression profiles (Yates et al. 2009). It is also becoming increasingly evident that a portion of the protective effects of Nrf2 activation is mediated indirectly through cross-talks with other pathways, such as the aryl hydrocarbon receptor (AhR), NF-kB, p53, and Notch1 (Wakabayashi et al. 2010a).

Chemistry of inducers

The Keap1-Nrf2 pathway can be upregulated by various cellular stresses (e.g., oxidative stress, shear stress, endoplasmic reticulum stress) and structurally diverse small molecules (inducers) of endogenous (e.g., 15-deoxy-$\Delta^{12,14}$-prostaglandin J_2, nitro oleic acid, nitric oxide, hydrogen peroxide, hydrogen sulfide) as well as exogenous origin. The development and use of a quantitative bioassay which evaluates the ability of small molecules to induce the prototypic Nrf2-target NQO1 in Hepa1c1c7 murine hepatoma cells (Prochaska and Santamaria 1988; Fahey et al. 2004) led to the classification of inducers into ten distinct chemical classes: (i) oxidizable diphenols, phenylenediamines, and quinones, (ii) Michael reaction acceptors (olefins or acetylenes conjugated with electron-withdrawing groups), (iii) isothiocyanates and sulfoxythiocarbamates, (iv) thiocarbamates, (v) dithiolethiones, (vi) conjugated polyenes, (vii) hydroperoxides, (viii) trivalent arsenicals, (ix) heavy metals, and (x) vicinal dimercaptans. Remarkably, more than 20 years following its first application, at time long before Keap1 or Nrf2 had been discovered, this assay remains a major screening tool for potential inducers, and arguably, allows the most reliable comparisons of inducer potencies. Specific examples of molecules that belong to three of the most prominent classes of inducers are given below.

Oxidizable diphenols, phenylenediamines, and quinones

Some of the first compounds for which inducer activity was demonstrated belong to this class. Experiments conducted in the late 1970s found that dietary administration of the phenolic antioxidant BHA [2(3)-*tert*-butyl-4-hydroxyanisole] (**Figure 1.8**) to mice reduced the formation of mutagenic metabolites of benzo[*a*]pyrene, and induced the cytoprotective enzymes GST, epoxide hydrolase, and NQO1 in many tissues (Benson et al. 1978; 1979; 1980). Structure-activity studies with the demethylation product of BHA, *tert*-butylhydroquinone (tBHQ), and a series of mono- and dialkyl ethers of tBHQ showed that the free phenol was more potent than the alkyl ethers (Prochaska et

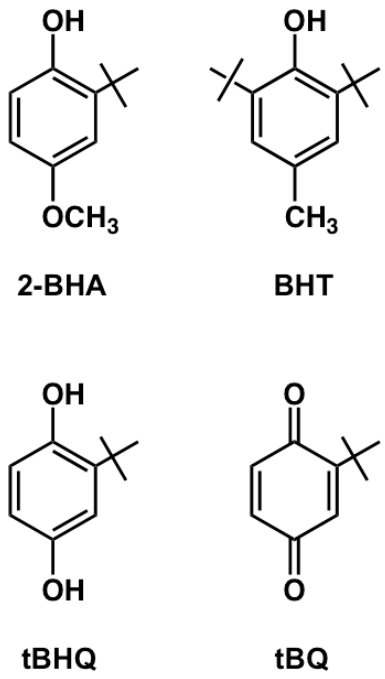

Figure 1.8. Chemical structures of the phenolic antioxidant BHA [2(3)-*tert*-butyl-4-hydroxyanisole] and BHT [3,5-di-*tert*-butyl-4-hydroxytoluene], and the metabolites tBHQ (*tert*-butylhydroquinone), and tBQ (*tert*-butylquinone).

al. 1985a,b; De Long et al. 1985). Furthermore, when simpler diphenols and phenylenediamines were evaluated, it became clear that the criticalfeature for inducer activity was the oxidative lability of these compounds (Prochaska et al. 1985b). Following the discovery of the Michael acceptor class of inducers, taken together the two findings led to the hypothesis that the diphenols need to be oxidized first to their corresponding quinones, which are the ultimate inducers. Further support to this hypothesis was provided by molecular orbital calculations which showed linear correlations between inducer potency for NQO1, and: (i) the ability of diphenols to release electrons, and (ii) the electron affinity of their corresponding quinones (Bensasson et al. 2008). A two-step mechanism in the upregulation of the Keap1-Nrf2 pathway was proposed which involves oxidation of the diphenols to their corresponding quinone derivatives, followed by modification of specific highly reactive cysteine residues of Keap1. This theoretical conclusion was recently tested experimentally. By use of UV spectroscopy, it was found that in the presence of oxygen and transition metals, tBHQ is rapidly oxidized to its corresponding quinone, tBQ. In addition, tBQ, but

not tBHQ, reacts with cysteine residues of purified recombinant murine Keap1. The cellular response to tBHQ or tBQ in terms of ARE-dependent transcription was then examined using the AREc32 reporter cell line. This reporter is derived from the human breast cancer cell line MCF7 that has been stably transfected with a luciferase reporter gene under thetranscriptional control of eight tandemly arrayed copiesof the ARE (Wang et al. 2006). Exposure of these cells to the hydroquinone tBHQ for 30 min induced ARE-luciferase (measured 24 hours later) only in the presence of transition metals, whereas induction by the quinone tBQ occurred in the absence of metals (Wang et al. 2010). Endogenous *para*- and *ortho*-hydroquinones, such as catechol estrogens, dopamine, and L-DOPA, also induce ARE-dependent gene expression, and induction is substantially potentiated by the presence of transition metals. Taken together, the available data strongly suggest that oxidizable diphenols are not inducers themselves, but their oxidation to the corresponding electrophilic quinones (the ultimate inducers) is a requisite step for the activation of the Keap1-Nrf2 pathway.

Michael reaction acceptors

The discovery that many compounds that induce cytoprotective enzymes are molecules bearing Michael acceptor group(s) and that inducer potency correlates with reactivity in the Michael reaction (Talalay et al. 1988) was a critical milestone in the understanding of the mechanism of action of inducers. The Michael acceptor functionality is essential for the inducer activity of many natural products such as cinnamates, curcuminoids, chalcones, avicins, and withanolides (Talalay et al. 1988; Spencer et al. 1991; Dinkova-Kostova et al. 1998; 1999; 2001; Chang et al. 1997; Misico et al. 2002; Gu et al. 2002; 2003; Su et al. 2003) (**Figure 1.9**). Furthermore, the introduction of highly activated Michael acceptor groups (by simultaneous conjugation to both cyano- and carbonyl moieties) in the molecules of oleanolic- and betulinic acid-derived semisynthetic triterpenoids (**Figure 1.10**) has led in the identification of the most potent inducers known to date that are active at sub- to low-nanomolar

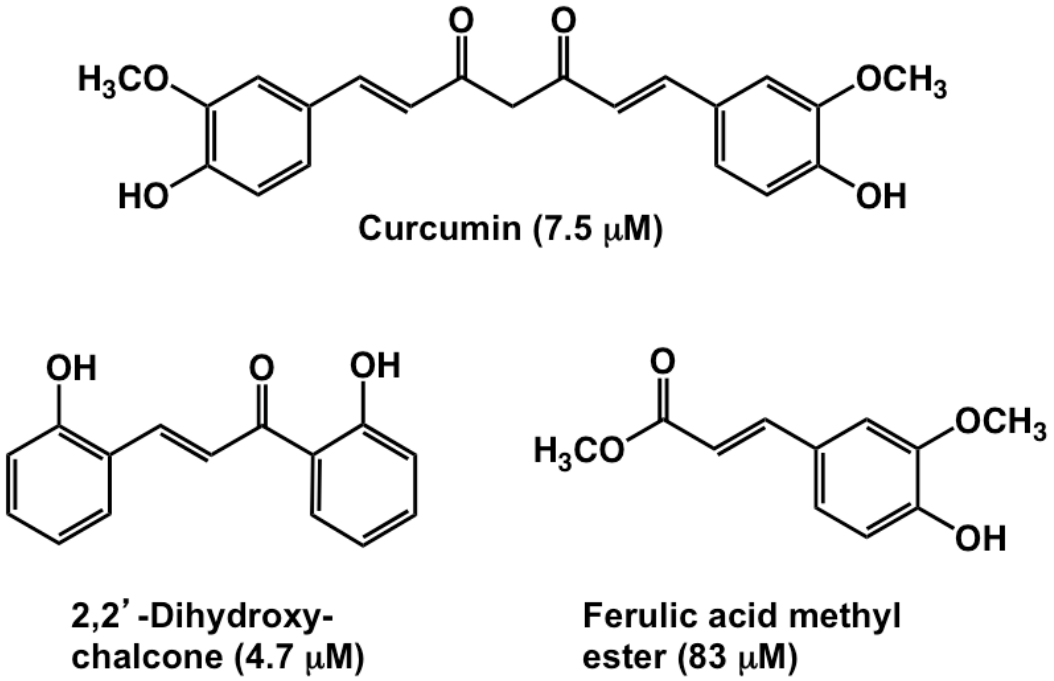

Figure 1.9. Chemical structures of the phenolic Michael acceptor-containing curcumin, 2,2'-dihydroxychalcone, and ferulic acid methyl ester. The CD (Concentration that Doubles the NQO1 enzyme activity) values are shown in parentheses.

concentrations (Dinkova-Kostova et al. 2005b; Liby et al. 2007a). Recently, simpler tricyclic derivatives bearing highly activated Michael acceptor moieties on rings A and C were developed which retain the inducer potency of the pentacyclic analogues, and the tricyclic molecule TBE-31 [(±)-(4a□,8a□,10aβ)-1,2,4a,6,8a,9,10,10a-octahydro-8a-ethynyl-1,1,4a-trimethyl-2,6-dioxophenanthrene-3,7-dicarbonitrile] (**Figure 1.11**) was found to be the most potent compound in this series both *in vitro* and *in vivo* (Liby et al. 2008a). Evaluation of its monocyclic "building blocks" representing ring A [MCE-5 (3,3,5,5-tetramethyl-6-oxocyclohex-1-enecarbonitrile)] and ring C [MCE-1 ((±)-3-ethynyl-3-methyl-6-oxocyclohexa-1,4-dienecarbonitrile)], respectively revealed that the contribution to inducer potency of ring C is 100-fold greater than that of ring A, and that potency is further enhanced by spatial proximity to an acetylenic group (Dinkova-Kostova et al. 2010).

Critically, the simultaneous presence of rings A and C within a contiguous three-ring system results in exceptionally high inducer potency, much higher than would have been expected based on the additive effect of the two monocyclic Michael acceptors. Thus, TBE-31 is ~30-fold more potent than the

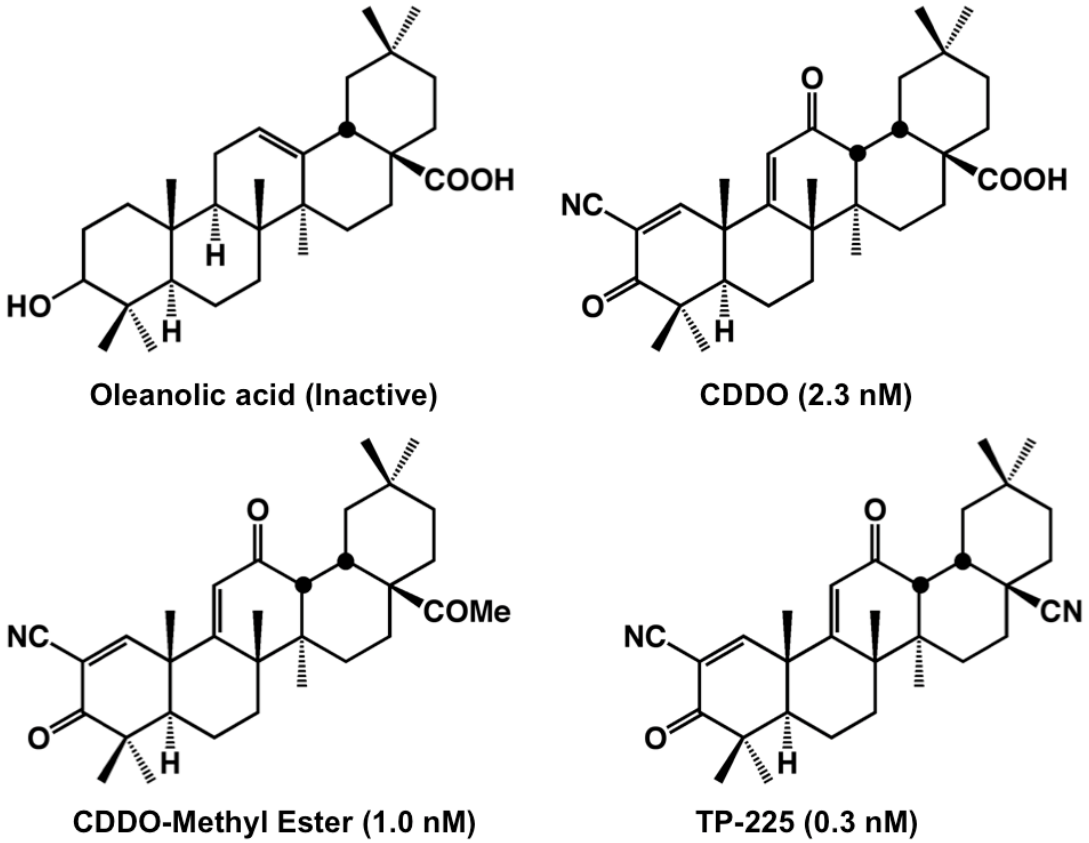

Figure 1.10. Chemical structures of the naturally-occurring triterpenoid oleanolic acid and its cyano enone-containing semisynthetic derivatives CDDO, CDDO-methyl ester, and TP-225. The CD values are shown in parentheses.

monocyclic ring-C compound MCE-1, and ~1000-fold more potent than the monocyclic ring-A compound MCE-5 (Dinkova-Kostova et al. 2010). Curiously, the synergistic effect on inducer potency resulting from the presence of two Michael acceptors on a single molecule is not restricted to the tricyclic cyanoenones. Thus bis(2-hydroxybenzylide)acetone is ~30-fold more potent than *trans*-4-(2-hydroxyphenyl)-3-buten-2-one (Dinkova-Kostova et al. 1998; 2001). Curcumin is ~10-fold more potent than ferulic acid methyl ester (Dinkova-Kostova et al. 1999). This finding strongly suggests that both electrophilic carbons react simultaneously with two cysteine residues within Keap1 that are in close spatial proximity to each other.

Isothiocyanates and sulfoxythiocarbamates

The isothiocyanates occur naturally as inert glucosinolate precursors that are abundant in cruciferous vegetables (Fahey et al. 2001; Halkier and Gershenzon, 2006). Upon injury of the plant, the glucosinolates come into contact with the otherwise compartmentalised enzyme myrosinase which catalyses their conversion to a range of hydrolytic products, including isothiocyanates. The central carbon atom of the isothiocyanate (–N=C=S) group (**Figure 1.12A**) is highly electrophilic and reacts avidly with sulfhydryl groups to give dithiocarbamate products. The isothiocyanate sulforaphane [1-isothiocyanato-4-(methylsulfinyl)butane] was isolated as the principal NQO1 inducer from broccoli extracts in an activity-guided fractionation using the Hepa1c1c7 bioassay (Zhang et al. 1992). Systematic examination of the levels of inducer activity at specific developmental stages of the plant revealedthat the seeds are the richest source of glucoraphanin, the glucosinolate of sulforaphane, and 3-day-old broccoli sprouts contain 20 to 50 times higher levels than the mature plant (Fahey et al. 1997). Inducer potency among isothiocyanates correlates with their intracellular accumulation (Ye and Zhang, 2001), for which conjugation with cellular glutathione provides a major driving source (Zhang and Talalay, 1998; Zhang, 2000; 2001); export of the conjugates then occurs by a transporter-mediated mechanism (Zhang and Callaway, 2002).

Following the discovery of sulforaphane, a series of naturally-occurring and synthetic isothiocyanates were evaluated for inducer activity (Posner et al. 1994). It was found that an analogue of sulforaphane, in which the sulfoxide (S=O) group was replaced by a keto (C=O) group, retained the same inducer activity (**Figure 1.12A**). This finding was recently revisited, and two new series of analogues were synthesized, containing either a sulfoxide or a keto moiety, respectively, in which the strongly electrophilic isothiocyanate group was replaced with the weaker electrophilic sulfoxythiocarbamate group (Ahn et al. 2010). Unlike isothiocyanates which form reversible conjugates with sulfhydryl groups, the reaction with sulfoxythiocarbamates is essentially irreversible (**Figure 1.12B**). Using this property, combined with a click chemistry approach with one of theanalogues, S-ethyl (4-hex-5-ynyloxy-benzyl)-(5-oxo-hexyl)-

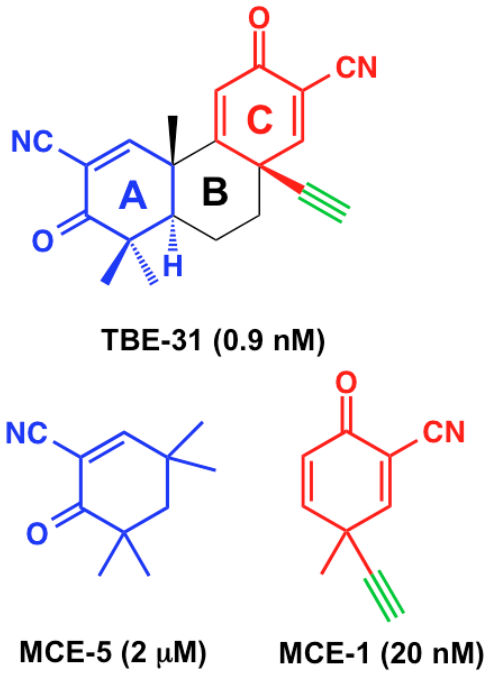

Figure 1.11. Chemical structures of the tricyclic bis(cyano enone) TBE-31 [(±)-(4b*S*,8a*R*,10a*S*)-10a-ethynyl-4b,8,8-trimethyl-3,7-dioxo-3,4b,7,8,8a,9,10,10a-octahydrophenanthrene-2,6-dicarbonitrile] and its monocyclic derivatives MCE-5 [(3,3,5,5-tetramethyl-6-oxocyclohex-1-enecarbonitrile)] and MCE-1 [(±)-3-ethynyl-3-methyl-6-oxocyclohexa-1,4-dienecarbonitrile]. The CD values are shown in parentheses.

thiocarbamate sulfoxide, that contains an alkynyl end group, it was found that C273, C288, and C613 of Keap1 were modified when cells were exposed to this compound (Ahn et al. 2010).

Inducers as chemoprotective agents

Many inducers that belong to different chemical classes have been shown to protect against chronic degenerative diseases in various animal models of carcinogenesis, cardiovascular disease, and neurodegeneration. The phenolic antioxidants BHA [2(3)-*tert*-butyl-4-hydroxyanisole] and BHT [3,5-di-*tert*-butyl-4-hydroxytoluene] inhibit experimental carcinogenesis caused by a wide range of chemical carcinogens (Frankfurt et al. 1967; Wattenberg et al. 1979). Related hydroquinone- and catechol-containing molecules, which could be viewed as "pro-drugs" that are converted to the ultimate inducers by oxidation reactions, are being developed as neuroprotective agents, with the interesting idea of their

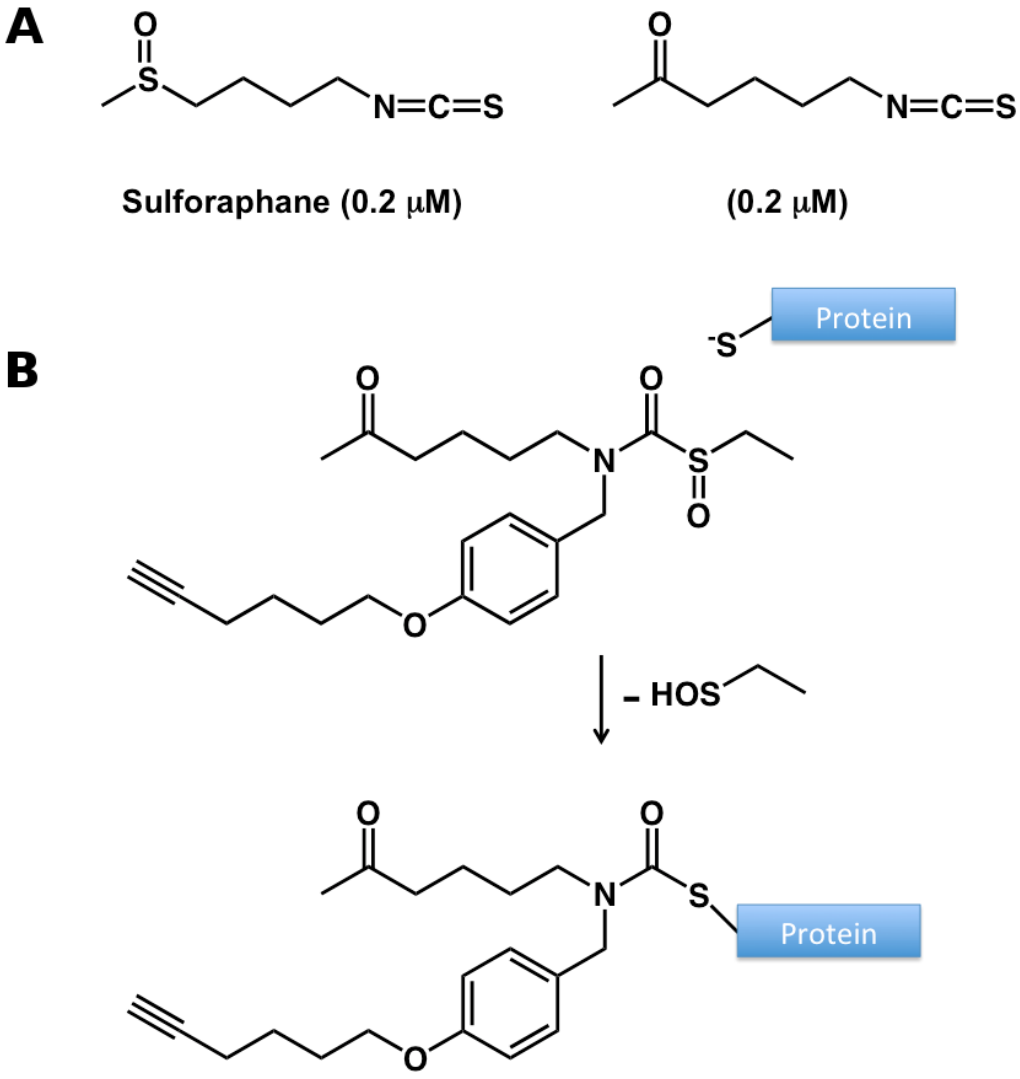

Figure 1.12. **(A)** Chemical structures of the isothiocyanate sulforaphane [1-isothiocyanato-4*R*-(methylsulfinyl)butane] and its carbonyl derivative 1-isothiocyanato-4*R*-(methylcarbonyl)butane. The CD values are shown in parentheses. **(B)** Reaction of S-ethyl (4-hex-5-ynyloxy-benzyl)-(5-oxo-hexyl)-thiocarbamate sulfoxide with a cysteine residue of a protein target showing the formation of a relatively stable thiocarbamate product.

activation occurring via the pathological activity that they are intended to combat (Lipton, 2007). The double Michael acceptor curcumin inhibits tumour development in animal models of oral, gastric, intestinal, colonic, hepatic, and cutaneous carcinogenesis (reviewed in Surh and Chun, 2007; Hatcher et al. 2008). Fumaric acid, another Michael acceptor-containing inducer, is protective against hepatic (Kuroda et al. 1983; 1987; 1989; Akao and Kuroda, 1990), gastric, and pulmonary (Kuroda et al 1982) carcinogenesis in rodents. In

humans, orally administered dimethyl fumarate reduces the appearance of new inflammatory lesions in patients with relapsing-remitting multiple sclerosis (Schimrigk et al. 2006; Kappos et al. 2008). Michael-acceptor-bearing semisynthetic triterpenoids inhibit the development of hepatic (Yates et al. 2006), pulmonary (Liby et al. 2007b; 2008b; 2009), mammary (Liby et al. 2008c), pancreatic (Liby et al. 2010), and cutaneous (Dinkova-Kostova et al. 2008) tumours. CDDO (bardoxolone) and CDDO-Me are currently in clinical trials with patients with chronic kidney disease, diabetic nephropathy, hepatic dysfunction, lymphoid tumours, and advanced metastatic or unresectable solid tumours. In addition to protection against carcinogenesis, neuroprotective effects have also been reported for CDDO-methylamide in mouse model of Alzheimer's disease (Yang et al. 2009; Dumont et al. 2009) and for CDDO-ethyl amide and CDDO-trifluoroethyl amide in a mouse model of Huntington's disease (Stack et al 2010).

The early studies demonstrating the chemoprotective effects of isothiocayantes date from the 1960s. Thus, feeding of α-naphthyl isothiocyanate to rats, dose-dependently reduced chemically-induced hepatocarcinogenesis (Sasaki 1963; Sidransky et al. 1966; Lacassagne et al. 1970). Benzyl-, phenyl-, and phenethyl isothiocyanate suppressed the carcinogenic effects of polycyclic aromatic hydrocarbons in a rat mammary carcinogenesis model, and benzyl isothiocyanate effectively inhibited the formation of gastric and pulmonary tumours in mice (Wattenberg 1977; 1983; 1985; 1987; Kuroiwa et al. 2006). Orally administered isothiocyanates also inhibited chemically-induced lung (Morse et al. 1989a,b; 1991; 1992; Hecht et al. 1991) and esophageal (Siglin e al. 1995; Stoner et al. 1998) carcinogenesis. In an orthotopic rat bladder cancer model, feeding of mustard seed preparation as a source of sinigrin, the glucosinolate precursor of allyl isothiocyanate, inhibited bladder cancer growth and completely blocked muscle invasion (Bhattacharya et al. 2010). Sulforaphane or sulforaphane-rich broccoli extracts have been shown to protect rodents against mammary (Zhang et al. 1994), gastric (Fahey et al. 1997), pulmonary (Conaway et al. 2005), pancreatic (Kuroiwa et al., 2006), cutaneous (Gills et al. 2006; Xu et al. 2006; Dinkova-Kostova et al. 2006), colonic (Chung et al. 2005; Myzak et al. 2006; Hu et al. 2006; Shen et al. 2007) and bladder

(Munday et al. 2008) carcinogenesis. Sulforaphane has neuroprotective effects in rodent models of brain ischemia/reperfusion (Zhao et al 2006; Ping et al 2010), traumatic brain injury (Zhao et al. 2005; 2007a; Dash et al. 2009), stroke (Zhao et al 2007b), and endotoxin exposure (Innamorato et al 2008). Chemoprotective effects of sulforaphane-containing broccoli extracts have been observed in rat models of hypertension (Wu et al. 2004; Noyan-Ashraf et al. 2006) and heart ischemia/reperfusion (Mukherjee et al. 2008; 2010).

Because 3-day-old broccoli sprouts are a rich source of glucoraphanin, the glucosinolate precursor of sulforaphane, extracts of this vegetable have been used in human studies as delivery vehicles of either sulforaphane or glucoraphanin. In six healthy human subjects, the susceptibility to erythema caused by ultraviolet (UVB) radiation was reduced by ~40% (compared to vehicle-treated skin) at sites that received topical treatment with broccoli sprout extract delivering a daily dose of 200 nmol of sulforaphane on three successive days before the day of radiation (Talalay et al., 2007). A randomized, placebo-controlled, double-blind clinical Phase 1 study of safety, tolerance, and pharmacokinetics of an extract delivering either: (i) 25 □mol of glucoraphanin, (ii) 100 □mol of glucoraphanin, or (iii) 25 □mol of sulforaphane, p.o. at 8-h intervals, for seven days, found no evidence of systematic, clinically significant, adverse events that could be attributed to ingestion of the extract (Shapiro et al. 2006). A randomized, placebo-controlled, double-blind chemoprevention trial in 200 healthy human subjects was conducted in Qidong Province in the People's Republic of China (Kensler et al. 2005). The study examined the effect of a broccoli sprout extract delivering 400 □mol of glucoraphanin that was given p.o. once a day for two weeks, on the metabolic disposition of aflatoxin and the combustion product phenanthrene. The study found an inverse association for excretion of dithiocarbamates (the metabolic products of isothiocyanates) and aflatoxin-DNA adducts, as well as for excretion of dithiocarbamates and phenanthrene tetraols. A 12-month dietary intervention study in human volunteers diagnosed with high-grade prostatic intraepithelial neoplasia was conducted in which subjects were randomly assigned to either a broccoli-rich- (400 g per week) or a pea-rich (400 g per week) diet, in addition to their usual diet (Traka et al. 2008). Needle biopsy tissues were obtained before and after the

intervention, and global gene expression profiles were compared. Pathway analyses showed that consumption of broccoli-rich-, but not pea-rich diet, resulted in perturbations of pathways associated with carcinogenesis and inflammation, i.e., TGF receptor-β, EGF receptor-, and insulin signaling pathways. Another curious property of sulforaphane is its bactericidal activity against *Helicobacter pylori* infections, which are strongly associated with gastric cancer (Fahey et al. 2002). In a randomized placebo-controlled intervention study, 48 *Helicobacter pylori*-infected patients were assigned to diets containing daily doses of 70 grams of either broccoli (delivering 420 □mol of glucoraphanin) or alfalfa sprouts for eight weeks (Yanaka et al. 2009). Intervention with broccoli, but not with alfalfa sprouts, decreased bacterial colonization (evaluated by the levels of urease and *Helicobacter pylori* stool antigen), and reduced gastric inflammation (indicated by the levels of serum pepsinogens I and II). Taken together, the human studies strongly suggest that sulforaphane has promise as a chemoprotective agent against various pathologies that have both oxidative stress and inflammatory components.

Indeed, Nrf2 inducers also have anti-inflammatory effects, and furthermore, there is a linear correlation between these two activities over a very broad range (six orders of magnitude) of concentrations (Dinkova-Kostova et al. 2005b; Liu et al. 2008). In contrast to the NQO1 inducer activity which is fully dependent on Nrf2, the anti-inflammatory properties of these molecules are only partially Nrf2-dependent. In addition, global gene expression and proteomics studies have revealed that such molecules have multiple targets. Whereas it is not presently clear how exactly the anti-inflammatory and Nrf2-inducer activities are mechanistically related, there is no doubt that both properties contribute to the observed chemoprotective effects of these compounds.

The dual role of the Keap1-Nrf2 pathway in carcinogenesis

Due to the ability of the Keap1-Nrf2 pathway to protect cells from the harmful effects of electrophiles and oxidants by regulating both the basal and inducible levels of cytoprotective proteins, it has been considered a chemopreventive pathway. Indeed, studies involving chemical carcinogenesis in knockout mice show that Nrf2 protects against tumour formation in the stomach, bladder and skin (Ramos-Gomez et al. 2001; Fahey et al. 2002; Iida et al. 2004; 2007; Xu et al. 2006). Nrf2 has also been shown to be downregulated in skin tumours in mice, and multiple studies of prostate cancer in humans (Xu et al. 2006, Frohlich et al. 2008). The mechanism by which Nrf2 is protective against tumourigenesis may in part be due to its ability to reduce the amount of reactive oxygen intermediates and DNA damage in cells (Frohlich et al. 2008; Aoki et al. 2001; Li et al. 2004; Reddy et al. 2008). Loss of Nrf2 activity in tumours could be caused by either inactivating mutation(s) in Nrf2, or by increased degradation mediated by Keap1. However, a large-scale analysis of many cancer-associated genes found that additional copies of the *KEAP1* gene were found in over 10% of tumours analysed, whereas it was lost in just 3% (Kan et al. 2010). This copy number variation analysis clustered *KEAP1* with known oncogenes like *KRAS* and *BRAF*, suggesting that *KEAP1* may be a putative oncogene. In addition, in breast cancer the low expression of Nrf2 was associated with increased Cul3, suggesting an alternate mechanism by which tumours may be able to reduce the expression of cytoprotective genes (Loignon et al. 2009).

Mutations have also been found in Nrf2. Interestingly these mutations are exclusively in the ETGE and DLG motifs of Neh2 domain, and lead to a reduction of Nrf2 degradation and an increase in ARE-dependent gene expression in both lung and head and neck tumours (Shibata et al. 2008a). Further work found Nrf2 to be overexpressed in 91.5% of head and neck squamous cell carcinomas, and that high Nrf2 expression is correlated with aggressiveness and chemoresistance of endometrial tumours (Stacy et al. 2006; Jiang et al. 2010). In addition, inactivating mutations of Keap1 have been identified in tumours of the lung, breast and gallbladder (Padmanabhan et al. 2006; Singh et al. 2006; Ohta et al. 2008; Sjöblom et al. 2006; Nioi and Nguyen 2007; Shibata et al. 2008b). Together

these data suggest that constitutive activation of the Nrf2 pathway can be beneficial for tumour survival. Indeed in breast cancer patients, the Kaplan-Meier survival curves show that low Keap1 levels, and presumably active Nrf2, are associated with poor survival (Lee et al. 2009). Moreover, a mutant Nrf2 gene expression signature is associated with poor prognosis in head and neck cancer (Shibata et al. 2010).

It has been suggested that the beneficial activity of Nrf2 which protects normal cells from oxidative stress can be subverted by cancer cells to protect them from the stress-inducing conditions found in the tumour microenvironment. Active Nrf2 may promote tumorigenesis by maintaining the redox balance and generating antioxidants in cancerous cells through upregulation of ARE-dependent genes. In addition, it has also been shown experimentally that Nrf2 can protect tumours and cell lines from chemotherapeutic drugs, desensitising them to etoposide, carboplatin, cisplatin, doxorubicin, 5-fluorouracil and Paclitaxel (Singh et al. 2006; Wang et al. 2008b; Ohta et al. 2008; Shibata et al. 2008a; 2008b; Loignon et al. 2009; Jiang et al. 2010). The ability of Nrf2 to protect cells from chemotherapeutics may in part be due to its ability to upregulate drug efflux pumps (Hayashi et al. 2003; Maher et al. 2007; Mahaffey et al. 2009). This tumour protective role of Nrf2 has been referred to as its 'dark side' (Wang et al. 2008b), and the cancer preventing/ cancer protecting dichotomy suggests that the role of Nrf2 in cancer in not straightforward and may be context-dependent. Furthermore, in Keap1-knockdown mice, which have constitutively high Nrf2 levels, the activated Nrf2 did not promote tumourigenesis, reinforcing the idea that the Keap1-Nrf2 pathway plays a complex role in cancer (Taguchi et al. 2010). In this way parallels can be drawn between the action of the Keap1-Nrf2 pathway and TGF-β or NF-κB signalling in cancer, as all three pathways have pleiotropic effects on the tumour phenotype (Derynck et al. 2001; Perkins, 2004).

In addition to the well-documented role that Nrf2-mediated cytoprotective gene expression plays in cancer, emerging data suggests that the Keap1-Nrf2 pathway may play a larger role in tumourigenesis. A number of reports have suggested that Nrf2 may play a role in cell cycle regulation. For example, the knockdown of Nrf2 reduces the rate of proliferation in both the

mouse liver and in cells lines, whilst the loss of Keap1 increases proliferation (Beyer et al. 2008; Ohta et al. 2008; Homma et al. 2009). The loss of Nrf2 has been shown to induce cell cycle arrest at the G1-S checkpoint. This was caused by reduced phosphorylation of pRB and increased p21 expression. Interestingly, co-treatment of Nrf2 knockdown cells with the antioxidant NAC reduced p21 expression, but had no effect on pRb status, suggesting that Nrf2 may regulate the cell cycle by both redox-dependent and redox-independent mechanisms (Homma et al. 2009). In reciprocal experiments carried out in pRB null cells, both Nrf2 and its target genes were expressed at lower levels, suggesting the existence of a co-regulatory mechanism between Nrf2 and pRB (Frohlich et al. 2008). In alveolar epithelial cells, loss of Nrf2 causes cell cycle arrest at the G2/ M checkpoint, which could not be rescued by GSH supplementation, again pointing to a redox independent effect of Nrf2 on the cell cycle (Reddy et al. 2008). In the same study loss of Nrf2 was shown to impair Akt, ERK1/2 and Stat3 signaling in response to PDGF and/ or insulin. In a hepatectomy model, loss of Nrf2 led to decreased IGF-1 and insulin receptor (IR) signalling resulting in reduced PI3K and Akt activation (Beyer et al. 2008). This reduction in IGF-1/ IR-PI3K-Akt signalling in Nrf2 null livers was thought to be a result of increased oxidative stress. In addition, activation of Nrf2 signalling has been shown to positively regulate mTOR signalling, via the transcriptional control of the mTOR activator RagD, and the Notch pathway through an ARE element in the Notch1 promoter (Shibata et al. 2010; Wakabayashi et al. 2010b). Thus Nrf2 is able to regulate multiple pathways involved in cancer proliferation and cell cycle progression. Together these data may also indicate why inactivating somatic mutations of Nrf2 are rare in tumours. If in the absence of Nrf2 p21 and pRB are activated, whilst PI3K, Akt, ERK, p38 and Stat3 signalling are all reduced, it may be beneficial for tumour development to maintain functional or hyperactive Nrf2 activity in order to aid cell proliferation.

Although Nrf2 may play a role in promoting cell proliferation, this activity may be balanced by the up-regulation of negative regulators of the cell cycle. ChIP-PCR and qRT-PCR assays found the cell cycle inhibitors p21 and p15 to be direct targets of induced Nrf2-mediated transcription (Malhotra et al. 2010). In addition to promoting cell cycle arrest, p21 is also involved in other cellular

processes including sensescence, apoptosis and the response to oxidative stress (Esposito et al. 1998; Gartel and Tyner 2002; Abbas and Dutta 2009). Recently it has also been shown that p21 plays a role in regulating Nrf2 activity. p21 binds to the ETGE and DLG motifs in Nrf2 and thus competes with the binding of Keap1, leading to Nrf2 stabilisation due to reduced ubiquination (Chen et al. 2009). In p21-null mice and cell lines, the level of Nrf2 and its target genes is significantly reduced under both basal and induced conditions, confirming the importance of p21 in ARE-mediated gene expression (Chen et al. 2009). p21 has been shown to be regulated by both p53-dependent and independent mechanisms. Interestingly, the activation of p53 suppresses Nrf2-dependent transcription by directly binding to the promoters of ARE-dependent genes suggesting alternate regulation of Nrf2 by the p21-p53 axis (Faraonio et al. 2006). Together these data have been combined to form a model whereby the interaction between p53, p21 and Nrf2 form a dynamic response to cellular stress (Wakabayashi et al. 2010a). Wakabayashi et al. (2010a) proposed that in the case of mild stress, p21-induced cell cycle arrest and Nrf2-mediated upregulation of ARE-dependent genes may be sufficient to protect cells from damage. In contrast, if the level of damage is severe, p53 may suppress cytoprotective protein expression and promote apoptosis.

In addition to the upregulation of cytoprotective genes, Nrf2 may also protect cells from tumourigenesis by inhibiting cell migration. The knockdown of Nrf2 leads to anchorage-independent growth, a change in cell morphology, and significantly increased migrating capacity in A549 cells (Rachakonda et al. 2010). This phenotype is caused by a loss of E-cadherin and an increase in the expression of the E-cadherin repressor Slug. Slug in turn is induced by Smad-dependent signalling. Endogenous Nrf2 was shown to interact with Smad3 and Smad4 in cells, leading to a reduction in Smad-mediated transcription (Rachakonda et al. 2010). Smads are the downstream effectors of the TGF-β signalling pathway which has previously been shown to negatively regulate Nrf2 (Bakin et al. 2005; Coulouarn et al. 2008). Indeed, a TGF-β expression signature, which included down regulation of Nrf2, was associated with the invasive form of hepatocellular carcinoma (Coulouarn et al. 2008). Together these data show that Nrf2 and TGF-β negatively regulate each other, and add a significant new

twist to the role of Nrf2 in cancer. The loss of E-cadherin is a rate-limiting step in the progression of invasive carcinoma and a fundamental event in the epithelial to mesenchymal transition which is associated with metastasis (Perl et al. 1998; Gupta and Massagué 2006). The idea that Nrf2 indirectly regulates the transcription of E-cadherin suggests that this transcription factor plays a far wider role in the cell than that of redox regulator, or conversely that the redox state regulates multiple diverse aspects of the cellular phenotype.

In addition, in both BRCA1 and ATM deficient cells, Nrf2 and its target genes are repressed, suggesting that the activity of the Keap1-Nrf2 pathway can be further regulated by other pathways, specifically those commonly mutated in the inherited forms of breast cancer (Bae et al. 2004; Li et al. 2004). Moreover, a number of Nrf2 target genes have been implicated in either preventing or promoting tumorigenesis. For example, NQO1 has been shown to stabilise p53 (Asher et al. 2001; 2002), thioredoxin-1 has been implicated in HIF-1 transcriptional activity (Huang et al. 1996; Welsh et al. 2002), and HO-1 has anti-apoptotic effects in leukemia cells (Rushworth and MacEwan 2008).

Concluding remarks

The Keap1-Nrf2 pathway allows adaptation and survival following various conditions of chemical and physical stress by controlling the gene expression of a large and diverse family of cytoprotective proteins. These proteins orchestrate a network of reactions that, in almost all cases, collectively result in protection against electrophiles and oxidants, and in enhanced cell survival. The role of this pathway in cancer prevention and chemoresistance to the toxic and neoplastic effects of many agents is well established. In addition, it is becoming increasingly clear that the Keap1-Nrf2 pathway plays a much broader role in determining the fate of the cell through its context-dependent effects on proliferation, apoptosis, angiogenesis and metastasis.

Aims

The primary aim of the thesis is to establish a FRET (fluorescence resonance energy transfer) system in which to study the interaction between Keap1 and Nrf2. In order to achieve this, we will ectopically express Keap1 and Nrf2 proteins cloned in frame with either EGFP or mCherry. We will clone the fluorophores both N- and C-terminally to Keap1 and Nrf2 in order to find a combination of fusion proteins that generate a FRET signal.

Once a pair of fusion proteins has been produced which generate a FRET signal, we will carry out a number of experiments to determine whether or not they behave like the endogenous system at the population level. This will include making sure that the Keap1 fusion protein is able to target the Nrf2 fusion protein for proteasomal degradation in the basal state; that the function of the Keap1 fusion protein is inhibited by inducers; and that the Nrf2 fusion protein can promote the transcription of ARE-dependent genes.

When the FRET system has been established, we will use it to test the hypothesis that inducers activate Nrf2 by either promoting its dissociating from Keap1 or by an alternative mechanism which does not require release of Nrf2 from Keap1. To do this we will study the FRET interaction between Keap1 and Nrf2 in the basal state, and in the presence of inducers that differ in potency and target different cysteine residues of Keap1. If inducers lead to the release of Nrf2 from Keap1 we will see a reduction, or a complete loss, of the FRET signal in the induced state relative to the basal state.

The second aim of the thesis is to establish an ectopic system in which to study the interaction between Keap1 and Cullin-3 using FRAP (fluorescence recovery after photobleaching). This will allow us to test the hypothesis that Keap1 is released from Cullin-3 in response to inducers that directly bind to Cys-151 located in the BTB domain of Keap1, the site of interaction with Cullin-3. To test this hypothesis, we will carry out FRAP experiments in the basal state and in the presence of inducers which target different cysteine residues of Keap1. If Keap1 is released from Cullin-3 in response to certain inducers, we will observe an increase in its mobility in the induced state which can be measured using FRAP.

Chapter 2

Materials and methods

Chemicals and inducers

All chemicals used to make buffers and other solutions were from Sigma unless specified. Inducers and compounds added to cells for the microscopy experiments were sourced as follows: sulforaphane (LKT laboratories Inc., St. Paul, MN, USA), STCA (gift from Dr. Young-Hoon Ahn, Johns Hopkins University, USA), CDDO (gift from Dr Michael B. Sporn, Dartmouth College, USA), H_2O_2 (Sigma), MG132 (InSolution, Merck).

Cell lines

HEK293 cells were grown in α-MEM supplemented with 10% fetal bovine serum (both from Gibco) and seeded onto gelatin-coated plastic dishes (0.1% gelatin dissolved in water for 30 min). They were allowed to grow until they were confluent, and were split using a $^1/_5$ dilution factor twice a week. For experiments using cell lysates, 200,000 cells were added per well of a 6-well plate. For microscopy experiments, 200,000 cells were seeded onto Willco glass bottom dishes.

RL34 cells were grown in DMEM supplemented with 10% fetal bovine serum (both Gibco).They were allowed to grow until they were confluent, and were split using a $^1/_{10}$ dilution factor twice a week. For experiments using cell lysates, 150,000 cells were added per well of a 6-well plate.

Transfection

For each 6-well-plate well or Willco dish to be transfected, 100 µl of opti-MEM was added to two Eppendorf tubes, one labeled “A”, one labeled “B”. To the tube labeled “A”, the DNA was added (see table below for quantities). To the tube labeled “B”, 3.75µl Lipofectamine 2000 (Invitrogen) was added. These were incubated for 12 min at room temperature, after which the contents of the two tubes were mixed and incubated for a further 15 min at room temperature. After this final incubation, 200 µl of the final solution was added to each well of cells. The cells to be transfected were first washed with 2 ml PBS, and then 1.5 ml

Opti-MEM (Invitrogen) was added to each well. The cells were incubated with the DNA + lipofectamine solution for 4.5 hours, after which the Opti-MEM was replaced with complete media.

Plasmid	Amount of DNA (ug) per well
EGFP-Nrf2	0.75
mCherry	0.5
Keap1-mCherry	0.5
Keap1-EGFP	0.5
Cul3-mCherry	0.5

Cell handling during microscopy-based experiments

For FLIM, FRAP and time-lapse experiments, HEK293 cells were washed with PBS, and imaged in 2 ml phenol red free CO_2-independent DMEM supplemented with 10% fetal bovine serum (both from Gibco). For experiments carried out in the presence of inducers, 1 ml of media was removed from the dish, and transferred to an Eppendorf tube. To this tube 2 µl of a 1000x stock of inducer was added. This media solution was thoroughly mixed before being added back to the cells.

FLIM/ FRET imaging

FLIM/ FRET imaging was carried out using an inverted multiphoton laser-scanning microscope (Bio-Rad Radiance 2100MP) with a 60x oil immersion NA 1.4 Plan-Apochromat objective (Nikon). Lasersharp 2000 software was used to run the microscope. The microscope was equipped with a Solent Scientific incubation chamber to maintain the cells at 37^0C. Two-photon excitation of EGFP was achieved using a Chameleon laser at 900 nm. The FLIM capability was provided by Time Correlated Single Photon Counting (TCSPC) electronics (SPC-830, Becker & Hickl). The laser power was adjusted to give a mean photon count rate of 10^5-10^6 photons/ s, with the gain set at 33.3%. FLIM measurements were carried out over a 256 x 256 pixel area for 90 s.

FLIM Lifetime calculation

The .sdt file was imported into the SPCImage software (Becker & Hickl) and a region of interest was drawn around the area of the cell to be analysed

(corresponding to either the nucleus or the cytoplasm). The "bin" parameter was increased to 3, the "shift" was fixed at 0, and all other parameters were left at the default unchecked positions (Threshold = 5, Scatter = unfixed, Offset = unfixed). The image was then analysed using a single component exponential decay model. The region in which the lifetime data was to be presented was fixed between 1900 and 2600 ps for all cells.

FLIM FRET efficiency calculation

The FRET efficiency was also calculated in the SPCImage software (Becker & Hickl), using the same region of interest defined to calculate the lifetime. The "bin" parameter was increased to 3, the "shift" was fixed at 0, and all other parameters were left at the default unchecked positions (Threshold = 5, Scatter = unfixed, Offset = unfixed). The image was then analysed using a two-component exponential decay model. To do this, the t2 value was fixed at 2375 ps, whilst the t1 value was left unchecked. The region in which the FRET efficiency was to be presented was fixed between 0 and 30% for all cells.

FRAP

FRAP was carried out using a DeltaVision Spectris wide-field fluorescence microscope with a 60x oil immersion NA 1.4 Plan-Apochromat objective (Olympus), using the photokinetic experiment function of the SoftWoRx software. A small region in the cell was photobleached with a 488 nm laser (100% laser power for 0.1 s), and a time-lapse sequence of EGFP images were taken (exposure time 0.05 s, bin 2x2) to record the fluorescence recovery. The image data were analysed using SoftWoRx software to calculate the T½ recovery time for each cell.

Time-lapse

The time-lapse experiment was carried out using a DeltaVision Spectris wide-field fluorescence microscope with a 60x oil immersion NA 1.4 Plan-Apochromat objective (Olympus), using SoftWoRx software. Images of EGFP and mCherry were taken every 10 min for 6 hours.

Generation of cell lysates

The dish of cells was placed on ice, where the media was removed, and each well was washed three times with 2 ml PBS. The PBS was aspirated, and 200 µl of RIPA buffer was added to the cells. The cells were then scraped from the dish manually, transferred to an Eppendorf tube, and lysed on an orbital rotator at 4^0C for 30 min. The debris was then removed by centrifugation at 13,000 rpm for 5 min at 4^0C, and the supernatant was collected and transferred to a new tube. From the supernantant, 10 µl was aliquoted for use in the BCA protein assay, and to the remainder, protein loading buffer (5x solution: 100mM Tris-Cl pH 6.8, 4% (w/v) SDS, 20% (v/v) glycerol, 3.6 Mβ-mercaptoethanol, 0.05% bromo-phenol blue)was added. The tubes were then heated to 90^0C for 3 min, after which the samples were ready to be loaded onto SDS-page gels.

Protein concentration determination

A 10-µl sample of the protein lysates was diluted $^1/_5$ with lysis buffer. BSA protein standards were generated through serial two-fold dilutions of a 2 mg/ml standard soluntion, and loaded onto a 96-well plate. 10 µl of each diluted sample was loaded in triplicate onto the 96-well plate. The BCA reagent was mixed and added to the standards and samples according to the manufacturers instructions. After 30 min incubation at room temperature with gentle shaking, the absorbance was measured on a spectrophotometer at 562 nm. A standard curve of protein concentration versus absorbance was generated using the data from the standards, and from this, the concentration of each sample was calculated.

Co-immunoprecipitation lysis and pull-down

Cell lysates were generated according to the protocol above, with the following exception. The cells were lysed in 400 µl of modified RIPA buffer, which did not contain SDS or NP-40. To create the bait, 150 ng of GFP antibody was incubated with 40 µl Dynabeads Protein G (Invitrogen) in 300 µl of PBS-T. This solution was mixed for 90 min at room temperature on an orbital rotator, after which the antibody-conjugated beads were purified using a MagnaRack (Invitrogen). 350 µl of cell lysate was incubated with the antibody-conjugated dynabeads for 1 hour at room temperature on an orbital rotator. The cell lysate

was then removed, and the bound proteins were eluted from the dynabeads by incubating them in 50 µl of 2.5x protein loading buffer for 20 min at room temperature, followed by heating the samples to 70^0C for 10 min.

Sodium dodecyl sulfate-polyacrylamide gel electrophoresis (SDS-PAGE)

An equal amount of each protein sample (usually 5 µg) was loaded into each lane of an SDS-PAGE gel, which consisted of a stacking gel formed on top of a resolving gel. The gel was run at 100V for 2 hours in Tris-glycine electrophoresis buffer (25mM Tris base, 250mM glycine 0.1% SDS) to allow the proteins to separate according to size. The progress of the electrophoresis was monitored using a protein ladder.

The gel composition is shown in the table below.

8% Resolving Gel	**Volume (ml)**
Water	2.3
30% acrylamide mix	1.3
1.5 M Tris (pH 8.8)	1.3
10% SDS	0.05
10% ammonium persulphate	0.05
TEMED	0.003
Total	5

5% Stacking Gel	**Volume (ml)**
Water	1.4
30% acrylamide mix	0.33
1.0 M Tris (pH 6.8)	0.25
10% SDS	0.02
10% ammonium persulphate	0.02
TEMED	0.002
Total	2

Transfer to membrane

The protein samples were transferred from the SDS-PAGE gel to PVDF membrane (Immobilon-P, Millipore) using an electrophoresis chamber run at 60V for 1 hour in Tris-glycine transfer buffer (25mM Tris base, 250mM glycine 20% methanol), cooled with an ice pack.

Antibody incubation

The membranes were washed with PBS-T (PBS + 0.1% Tween), blocked in 5% milk for 2 hours at room temperature, and incubated overnight with 5 ml of the antibody solution at 4^0C. The membranes were then incubated with the appropriate secondary antibody (conjugated to HRP) for 1 hour at room temperature. The signal was then visualized using an HRP-dependent chemiluminescence reaction, and was developed on photographic film

The table below shows the antibodies used in this thesis:

Antibody	Source	Concentration
Anti-Nrf2	McMahon et al. 2003	1/1000
Anti-Keap1	McMahon et al. 2006	1/2000
Anti-GFP	Abcam (6556)	1/1000
Anti-mCherry	Clontech (632543)	1/1000

NQO1 assay

Cells were lysed in 200 µl digitonin (0.8 g/l in 2 mM EDTA, pH 7.8) and incubated at room temperature for 1 hour with constant agitation. The cell lysate was centrifuged at 3,000 rpm for 4 min, after which the supernatant was collected to be used in the assay. 25 and 50 µl of the supernatant was loaded onto a 96-well plate. The assay buffer was constructed according to the established protocol (Prochaska and Santamaria, 1988) and added to the cells. The enzyme activity of NQO1 was determined by using menadione as a substrate in the presence or absence of the potent inhibitor dicumarol. The absorbance at 610 nm was measured on a spectrophotometer over a 5 minute period using the "kinetic" program.

Cloning

The general cloning strategy used to generate the fusion proteins was the same for all of the constructs. Firstly, the cDNA encoding the gene of interest was amplified using PCR to introduce the restriction enzyme consensus sequences required for cloning. The product of this PCR reaction was then purified by running it on an agarose gel. The band corresponding to the PCR product was then cut from the gel, and the DNA was purified from this agarose slice. The

extracted DNA was then digested with the correct pair of restriction enzymes, along with the destination vector. The digested vector and PCR product were then purified again from an agarose gel, before being ligated together and transformed into competent bacteria. Transformed bacterial colonies were then picked and grown over night. From these 5 ml mini-cultures, the plasmids were purified, and the success of the ligation was determined by restriction digests and sequencing.

Sources of vector and gene of interest cDNA

The pEGFP-N1, pEGFP-C1, pmCherry-N1 and pmCherry-C1 (all from Clontech) were kind gifts from Dr. David Lleres (University of Dundee). The mouse Keap1, Nrf2, Cul3, Nrf2ΔDLG and Nrf2-doubleETGE cDNA vectors, and the EGFP-Keap1 vector were all kind gifts from Dr. Mike McMahon (University of Dundee). The Nrf2 mutantvectors contain the following mutations: Nrf2ΔDLG (D29A:L30G:G31E), Nrf2-doubleETGE (I28E:D29E:L30T:V32E) (McMahon et al. 2006). The Keap1-mono plasmid was a kind gift from Prof. Masi Yamamoto (Tohoku University, Japan). This plasmid encodes full-length Keap1 with the following mutations (H96A:K97A:V98A:V99A:L100A) (Suzuki et al. 2011).

Bacterial transformation

An Eppendorf tube containing 50 µlDH5α compenent cells was thawed on ice. Once liquid, 10-100 ng of DNA were added to the compentent cells and incubated on ice for 30 min. The bacteria were then subjected to a heat shock of 45 seconds at 42^0C, followed by 2 min on ice. Finally, 450 ul of SOC media was added to the cells, which were then incubated at 37^0C in a shaking incubator for 1 hour. From this bacterial culture, 20-200 µl was taken and plated on antibiotic plates (200 µl if the transformed plasmid was the product of a ligation reaction, 20-50 µl for other plasmids).

Plasmid preparation

For small quantities of plasmid DNA, the Macherey-Nagel NucleoSpin Plasmid kit was used. A single transformed bacterial colony was selected and grown overnight at 37^0C in 5 ml LB media plus the appropriate antibiotic. This

culture was then centrifuged at 3,500 rpm for 10 min on a benchtop centrifuge. The pellet was then resuspended, and the DNA was extracted from the bacteria according to the manufacturers instructions.

For large quantities of plasmid DNA, the Invitrogen PureLink HiPure Maxi Plasmid DNA purification kit was used. A single transformed bacterial colony was selected and grown for 8 hrs at 37^0C in 5 ml LB media plus the appropriate antibiotic. After 8 hours, this 5 ml culture was added to 195ml of LB media plus antibiotic and grown overnight at 37^0C. The cells were then harvested by centrifugation at 4,000g for 10 min in an angle rotor. The pellet was then resuspended, and the DNA was extracted from the bacteria according to the manufacturers instructions.

Polymerase chain reaction (PCR)

All PCR reactions were carried out using Pfx DNA polymerase (Invitrogen). The reaction mixtures were prepared on ice, and an example is shown in the table below.

	Volume (µl)
10 x PCR buffer	5
10 mM dNTPs	1.5
Forward Primer (10 µM)	1.5
Reverse Primer (10 µM)	1.5
DNA template (1ng/ µl)	1
Pfx DNA polymerase	1
Water	38.5
Total	50

A sample PCR amplification protocol for a 2-kb target sequence is shown below. The length of time required for the extension phase was calculated based on the target length (where each 1 kb requires 1 minute extension). The primer annealing temperature was determined by the Tm of the primers specific to each reaction, where Tm - 3^0C was used as the annealing temperature.

	Temperature (^{0}C)	Time
Stage 1	94	2 min
Stage 2 (35 cycles) - Denaturation	94	15 sec
- Primer annealing	60	30 sec
- Extension	68	2 min
Stage 3	68	5 min

A list of primers used to clone the plasmids used in this thesis is shown in the table below.

Primer	Sequence
Nrf2 into pEGFP-C1 FORWARD	TCCGCTCGAGCAATGATGGACTTGGAGTTGCCACCGCCAG
Nrf2 into pEGFP-C1 REVERSE	TCCTCGTCGACCTAGTTTTTCTTTGTATCTGGCTTCTTG
Nrf2 into pmCherry-N1 FORWARD	CCGCCGCTACCATGATGGACTTGGAGTTGCCACCGCCAG
Nrf2 into pmCherry-N1 REVERSE	ATCCTCCACCGGTTTGTTTTTCTTTGTATCTGGCTTCTTG
Keap1 into pmCherry-N1 FORWARD	ATTGGTACCATGCAGCCCGAACCCAAGCTTAG
Keap1 into pmCherry-N1 REVERSE	ATGAAGACCGGTGCTTTTGCTGCTGCCTCTTTAGCGGCTGCTTCTGCGCAGGTACAGTTTTGTTGATC
Cul3 into pmCherry-C1 FORWARD	GCCGCTCGAGCTATGTCGAATCTGAGCAAAGGC
Cul3 into pmCherry-C1 REVERSE	GAAGGTACCTTATGCTCACTATGTGTATAC

Purification of DNA from agarose gel

The DNA sample was run on low melting agarose gel for 1 hour at 60V to enable good band separation. The correct size bands were then cut with a clean scalpel blade, and collected in an Eppendorf tube. The DNA from the agarose slice was purified using the QIAquick Gel extraction kit. In the final step, the DNA was eluted into 50 µl Buffer EB.

Restriction digestion

All restriction digests were prepared on ice. A sample reaction is given below. Once prepared, the reaction was incubated at 37^{0}C for 2 hours. The reaction products were directly run on an agarose gel, either to extract the DNA for use in a ligation, or to determine the size and identity of the plasmid or plasmid inserts.

	Volume (µl)
Plasmid DNA (1 µg/ µl)	2
XhoI (10 units / µl)	0.5
KpnI (10 units / µl)	0.5
10 x Buffer	5
Water	42
Total	50

The table below shows the vector backbone and restriction enzymes used to construct the plasmids in this thesis. The mutant Nrf2 and Keap1 vectors were cloned in the same way as the wild type proteins, thus for simplicity only the wild type vectors are shown below.

Plasmid	Vector	Restriction enzymes
EGFP-Nrf2	pEGFP-C1	XhoI and KpnI
Nrf2-mCherry	pmCherry-N1	KpnI and AgeI
Keap1-mCherry	pmCherry-N1	KpnI and AgeI
Keap1-EGFP	pEGFP-N1	KpnI and AgeI
mCherry-Cul3	pmCherry-C1	XhoI and KpnI

Ligation

Prior to the ligation, the concentrations of insert and vector DNA were quantified using a spectrophotometer. In the ligation reaction, the total amount of DNA used was 10-100 ng. Two parallel ligation reactions were run, one in which there were the same number of insert and vector molecules (1:1), and one in which there were 10 times more insert than vector molecules in the reaction (10:1). The ligation was carried out at 20^0C for 1 hour, after which 1 µl was used directly to transform competent bacteria.

The table below shows a sample ligation reaction, where the vector was 1.8 times larger than the insert.

	1:1 insert:vector (µl)	10:1 insert:vector (ul)	No insert control (µl)	No ligase control (µl)
Insert	1	5.6	0	1
Vector	1.8	1	1.8	1.8
5 x Buffer	4	4	4	4
Ligase 1/10 Unit	1	1	1	0
Water	12.2	8.4	13.2	13.2
Total	20	20	20	20

Statistical analysis

Averages, standard deviation and p-values were all calculated using Excel (Microsoft). In chapters 3, 4 and 6, the p-values of the EGFP lifetime data and the NQO1 assay were calculated using two-tailed Student's T-tests. In chapter 5, where the lifetime of EGFP was calculated before and after the addition of inducers, all p-values were calculate using two-tailed paired T-tests.

Evaluation of methodology

Analysing the Keap1-Nrf2 pathway using FRET provides a number of advantages over other methods which have been previously reported in the literature, as well as a number of limitations which are inherent to the technique.

The principle advantage of studying protein interactions using FRET is that it allows the experimenter to study protein complexes in individual live cells. The consequence of this is that protein interactions can be studied in the correct physiological environment. This contrasts with *in vitro* techniques such as co-immunoprecipitation which show that proteins *can* interact, but not necessarily that they *do* interact in living cells. In addition, as FRET can be quantified in individual cells, it can be used to uncover cellular heterogeneity which may be masked when studying interactions at the cell population level.

These advantages of using FRET are coupled with a number of limitations. For example, in the majority of cases, FRET experiments involve the overexpression of the proteins which are being studied. This may result in a level of expression which is non-physiological and would not be seen in the

endogenous system. This is of particular concern when studying Keap1 and Nrf2, as both proteins are normally present at very low levels in the endogenous system. In order to measure the protein interaction using FRET, the fluorescent signal must be visible, and thus Keap1 and Nrf2 must be overexpressed beyond physiological levels. This has a number of knock-on effects. For example, whilst Keap1 and Nrf2 are both being overexpressed in our model, other factors required for the degradation of Nrf2, such as Cullin-3, are not. This may mean that some of the ectopic Keap1-Nrf2 complexes are unbound by Cullin-3 and thus may not be involved in the ubiquitination pathway. In addition, FRET requires an excess of the acceptor (in this case Keap1-mCherry) and thus in the majority of cells Keap1 is present at a much higher level than Nrf2. This, coupled with the transient transfection of the expression plasmids, means that the relative levels of the fusion proteins will be different in different cells, and most likely will differ from those found in the endogenous system. If the relative levels of Keap1 and Nrf2 are important for the regulation of the pathway *in vivo*, this property will not be observed using FRET, as the acceptor, Keap1-mCherry, must be in excess in order to optimise the quality of the data being collected. In addition, in order to study protein-protein interactions using FRET, large fluorescent tags must be added to the proteins that are being studied (26.9 kDa for EGFP, and 28.8 kDa for mCherry). These bulky tags may interfere with the function of the proteins in a number of ways. They may directly alter the function of the protein to which they are attached by inhibiting the correct folding of the protein, or alternatively, their size may restrict the access of other factors to binding domains on the protein of interest. Both of these possibilities would lead to an alteration in the behaviour of the proteins which are being studied, and may lead to the incorrect conclusions. Despite of these limitations, the facts that: the fusion proteins interact in the cell at basal state, Keap1 is able to efficiently target Nrf2 for degradation and to respond appropriately to inducers of several different types, strongly indicate that the ectopically-expressed proteins represent a good functional model for their endogenous counterparts.

Selection of inducers

It has previously been shown that Keap1 contains multiple cysteine residues which can be modified by inducers, and that inducers themselves can be divided into 10 different classes (Baird and Dinkova-Kostova, 2012). For this reason we will use a variety of different inducers which target different cysteine residues of Keap1 in order to gain a thorough understanding of the mechanism of Nrf2 activation. Thus, sulforaphane will be used as an inducer specific to the Cys-151 sensor of Keap1, and STCA will be used to specifically target the Cys-273 and Cys-288 sensors (McMahon et al. 2010, Ahn et al. 2010). In addition, the concentration of inducer required to stabilise Nrf2 is highly variable, which could reflect the mechanism through which it functions, and for this reason we will also use inducers with a wide range of potencies. Thus CDDO (which may target Cys-226 of Keap1, Kaidery et al. 2012) has been selected as a highly potent inducer, used at 0.1 μM, which contrasts sharply with the weak inducer H_2O_2, which will be used at 400 μM (Dinkova-Kostova et al. 2005b, Fourguet et al. 2010).

Chapter 3: Establishment of a FLIM-based assay to study the Keap1-Nrf2 pathway

Introduction

The current models describing the spatio-temporal regulation of Nrf2 by Keap1 suggest that the interaction is dynamic, and that inducers either lead to a change in the binding characteristics of the proteins, or to a change in localisation, or both. The data to support these models are either obtained from whole cell populations that had been analysed by western blotting, or through the use of recombinant proteins *in vitro*. Microscopy is ideally suited to overcome the limitations of these approaches and to examine dynamic cellular processes, as it can be used to study individual cells and thus can capture cellular heterogeneity which may be lost by analysing large populations of cells at the same time (Spiller et al. 2010). In addition, there are a number of microscopy-based techniques which enable the user to study protein-protein interactions in live cells, and thus in the correct physiological environment.

The use of microscopy to study protein-protein interactions is due in large part to the discovery of green fluorescent protein (GFP) from the bioluminescent jellyfish *Aequorea victoria* by Shimomura and colleagues (Shimomura et al. 1962). GFP is a barrel-shaped protein formed from 11 β-strands which is able to fluoresce, that is, when exposed to blue light the protein absorbs the blue photons and in turn emits green light. The chromophore responsible for the fluorescence is composed of 3 amino acid residues (Ser-Tyr-Gly) that are found in an α-helix which is threaded through the centre of the protective barrel (Tsien 1998). The F64L mutation within the GFP sequence allows the protein to efficiently fold at 37^0C (producing the GFP variant enhanced GFP, or EGFP) and importantly, it means that GFP can be expressed in mammalian cells where, along with its differently coloured mutants, it has been used to study protein localisation in live cells and in real time (Tsien 1998).

In addition to its use in visualising protein localisation, GFP has also been used to study protein-protein interactions in cells through the process of fluorescence resonance energy transfer (FRET). FRET is defined as the radiationless transfer of energy from an excited donor fluorophore to an acceptor (Miyawaki 2011). In practical terms, in order to use FRET to determine whether two proteins interact in cells they must first be cloned into expression vectors as fusion proteins in frame with fluorescent proteins whose excitation

and emission spectra overlap (like GFP and mCherry). When these expression vectors are co-expressed in cells it is possible to determine whether the proteins interact due to the presence or absence of FRET. If the proteins interact, then the two fluorphores may come sufficiently close together (1-10 nm) that the excitation of GFP leads to the emission of red light from mCherry. Alternatively, if the proteins do not interact, then excitation of GFP will lead to emission of only green light, and thus no FRET (Miyawaki 2011). There are three commonly used approaches to study protein-protein interations using FRET: sensitised emission, acceptor photobleaching, and fluorescence lifetime imaging (FLIM).

Sensitised emission involves the stimulation of the donor fluorphore (eg. GFP) and the measurement of fluorescence from the acceptor (eg. mCherry). The disadvantage of using this method is that it has a lower sensitivity compared with the other approaches. The reason for this is that the fluorophores have wide absorbtion and emission spectra, and thus when exciting GFP at its optimal frequency, mCherry will also be excited at a low level, and equally when measuring the emission from mCherry a small amount of the signal will be due to GFP emission at the longer wavelengths. This cross-contamination of fluorescence in both the excitation and emission channels leads to a "noisy" signal and low resolution data.

The second method by which FRET can be studied is acceptor photobleaching. As a FRET interaction consists in the transfer of energy from the green to red fluorophores, it results in a decrease in the intensity of the green signal within the cell. This decreased intensity can be measured by bleaching and therefore destroying the acceptor fluorophore with a laser. This leads to the loss of FRET (due to the destruction of the acceptor) and a concomitant increase in the intensity of the donor fluorescence. The disadvantages of this method are that it only collects data from a small region of the cell (the area which is bleached) and also that the photobleaching is destructive and therefore the cell can only be imaged once

The third method which can be used to measure FRET is FLIM. In this method, it is not the intensity of the GFP signal which is measured but the amount of time which the fluophore spends in the excited state (Miyawaki 2011, Lleres et al. 2007). When a fluophore is stimulated by a photon of light, it is

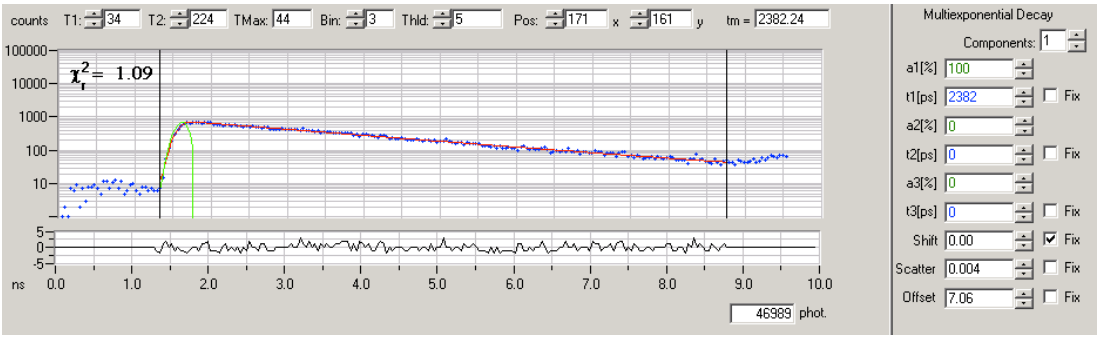

Figure 3.1. Exponential decay of EGFP lifetime. The image above is a screen shot taken from the SPCImage software, which was used to measure the lifetime of EGFP fluorescence in a HEK293 cell transfected with EGFP-Nrf2 and mCherry. The graph show the lifetime data for one pixel within the cell, with frequency plotted on the y-axis on a log scale, and the lifetime plotted on the y-axis.

raised to an excited state in which it spends a short period of time before emitting a photon of different coloured light and returning to the ground state. For a population of fluophores (like a population of GFP molecules in a cell) the combined time spent in the excited state follows an exponential decay pattern (**Figure 3.1**). FRET is a biased process which preferentially takes place between fluorophores with a longer lifetime, and thus, when FRET occurs, the longer lifetime fluorophores are removed from the GFP population (as their energy is transferred to mCherry and thus emitted as red light), which means that overall the remaining GFP population has a reduced lifetime. The advantage of this method is that it is independent of intensity and thus of any differences in levels of fluorophore expression among cells, is both highly sensitive and quantitative, and gives FRET data across the entire cell. FLIM has been used to study a wide variety of cellular processes, including signal transduction through the PKCα and Ras pathways, and DNA damage (Ng et al. 1999, Rocks et al. 2005, Morris et al. 2009). For these reasons, I have chosen to study the interaction between Keap1 and Nrf2 primarily using FLIM.

Other microscopy-based techniques which have been used to study protein-protein interactions include: fluorescence recovery after photobleaching (FRAP, see Chapter 6) and, bimolecular fluorescence complementation (BiFC). BiFC is a method in which a fluorescent protein is expressed in two complementary parts, one fused to each protein of interest. On their own, the halves of the fluorophore cannot fluoresce, however, if the proteins of interest

interact then the two complementary parts of the fluorophore may come sufficiently close together so that they bind to form a complete protein which can fluoresce (Kerppola 2006). The disadvantage of this system if that once formed from its complementary components, the fluorescent protein cannot dissociate and therefore this method cannot be used to study dynamic protein interactions, and for this reason it has not been used in my studies.

Aim

The aim of this part of the project was to generate Keap1 and Nrf2 fusion proteins which together produce a FRET interaction that could be studied using FLIM, and importantly, functioned in the same way as the endogenous system.

Results

In order to study the interaction between Keap1 and Nrf2 using FRET, we first needed to generate fusion proteins in which the EGFP and mCherry fluorophores were at the appropriate distance and orientation to allow FRET. As it is not possible to determine the relative positions of the EGFP and mCherry fluorophores within the Keap1-Nrf2 complex *a priori*, due to a lack of structural information, we generated a number of different fusion proteins in which both fluorophores were added N- or C-terminally to Keap1 and Nrf2, and a process of trial and error was used to test which combination would give rise to FRET.

Despite the fact that the fusion proteins accurately modelled the endogenous system, evidenced by the localisation of Nrf2 and Keap1 in the basal state and the stabilisation of Nrf2 in response to the inducer CDDO (**Figure 3.2**), the majority of these combinations produced no FRET interaction, and an example of this is shown in **Figure 3.3**. In this experiment, we transiently transfected expression plasmids for EGFP-Keap1 along with either free mCherry (**Figure 3.3A-B**) or Nrf2-mCherry (**Figure 3.3C-D**). The cells in which free mCherry was co-transfected are the negative controls, as in these cells there will be no expected interaction between EGFP and mCherry and thus no FRET. When Nrf2-mCherry was co-transfected along with EGFP-Keap1 we would have the potential to see FRET, as Nrf2 will interact with Keap1, bringing the EGFP and mCherry into a single protein complex.

In the first column of **Figure 3.3** the EGFP images of the cells are presented, showing the localisation and the fluorescence intensity of EGFP-Keap1. From this image the lifetime of EGFP is derived, and this is shown in pictorial form in the second column. The colour of the cell in the lifetime image corresponds to the EGFP lifetime depicted in the legend directly below the image, with the shortest lifetime of 1.9 ns in red, progressing to the longest lifetime of 2.6 ns in blue. The third column of **Figure 3.3** shows a graphical representation of the lifetime data. In the graphs, the lifetime value in picoseconds from each pixel of the image is plotted on the x-axis, and the frequency is plotted on the y-axis.

Figure 3.3 clearly shows that the lifetime of EGFP-Keap1 is unaffected by the presence of Nrf2-mCherry, and thus there is no FRET between this

A.

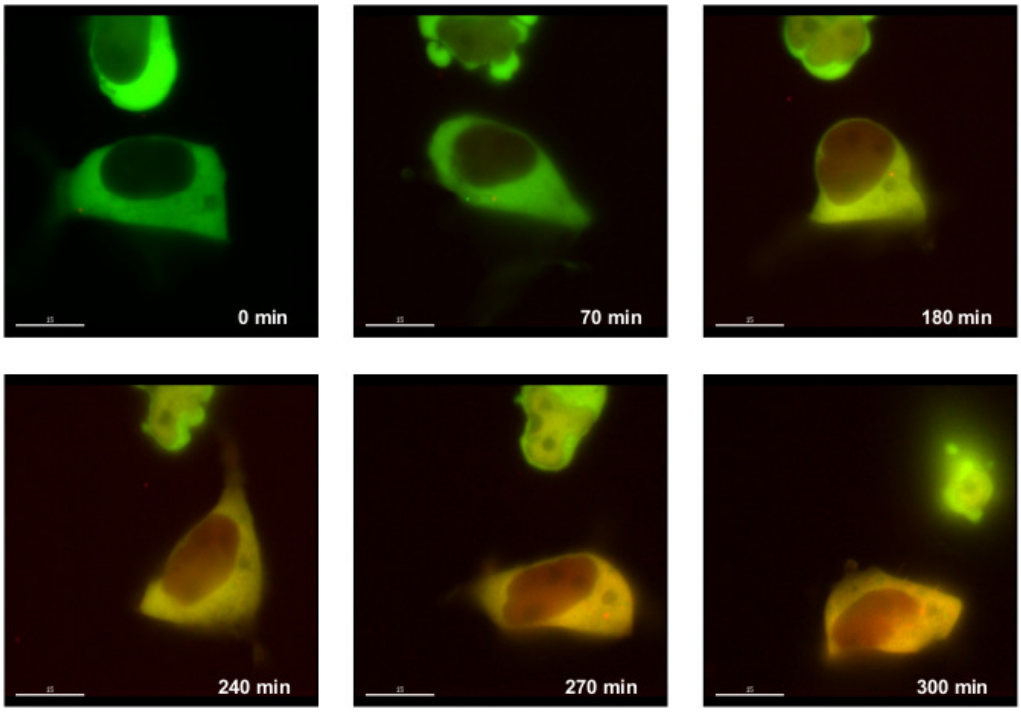

B.

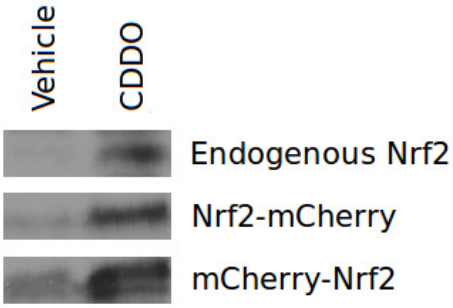

Figure 3.2. The ectopic expression of Nrf2 and Keap1 fusion proteins accurately models the endogenous system. A. Nrf2-mCherry and EGFP-Keap1 constructs were transfected into HEK293 cells, which were subsequently imaged in a time-lapse experiment where a single cell was imaged every 10 minutes for 5 hours. At 0 minutes, EGFP-Keap1 is localised in the cytoplasm and Nrf2 is undetectable. After the addition of 0.1 μM of the inducer CDDO, Nrf2 becomes stabilised as shown by the increase in red fluorescence from 70 minutes. After 300 minutes of CDDO treatment Nrf2-mCherry fluorescence is found in both the cytoplasm and nucleus. **B.** Western blot showing the stabilisation of endogenous Nrf2 in HEK293 cells in response to 2 hours of treatment with 0.1 μM CDDO. Similarly, in HEK293 cells co-transfected with expression plasmids for mCherry-tagged Nrf2 (either N- or C-terminally) and EGFP-Keap1, treatment with 0.1 μM CDDO also leads to the stabilisation of the ectopically expressed Nrf2 fusion proteins.

combination of fusion proteins. In both the presence and absence of Nrf2-mCherry, the lifetime image has a blue colour, corresponding to a lifetime of

2336 ps for the EGFP-Keap1 + free mCherry control, and 2346 ps in the presence of Nrf2-mCherry (**Table 3.1**).

Whilst these early experiments did not provide us with any FRET data, they were useful in providing us with guidance for future experiments. For example, as Keap1 targets Nrf2 for degradation it is always present at a much higher level when Keap1 and Nrf2 are co-expressed. In order to detect FRET, an excess of the acceptor (mCherry) has to be present, so that all of the EGFP donor proteins upon excitation have an opportunity to transfer energy to the acceptor. If the opposite is true, then the excess of EGFP will mean that only a fraction of the donor molecules can transfer their energy to mCherry, and thus any reduction in lifetime will become difficult to detect as many of the EGFP proteins within the cell will show no reduction in lifetime due to their inability to find free acceptor molecules. This means that the system could be optimised if Keap1 is fused to mCherry (and thus will be in excess), and EGFP is fused to Nrf2.

Deciding whether the fluorophores should be located at the N- or C-terminus of Keap1 and Nrf2 required a trial and error approach because the structure of the complex of the Keap1 dimer bound to Nrf2 is currently unknown. The availability of this structure would guide the design of FRET pairs of proteins as it would allow us to determine the distance between the N- and C-termini of each protein. This is important as FRET is a distance-dependent process, and only takes place when the fluorophores are between 10-100 Å from each other (Miyawaki 2011, Lleres et al. 2007). The availability of an accurate structure of the Keap1-Nrf2 complex may have allowed us to exclude certain fusion protein combinations, for example, if the N-terminus of Keap1 was 300 Å away from the C-terminus of Nrf2, then this FRET pair could be ruled out due to the insurmountable distance between the fluorophores.

	Lifetime (ps)	N	SD	T-test
EGFP-Keap1 + mCherry	2336	3	17	
EGFP-Keap1 + Nrf2-mCherry	2349	5	10	p = 0.225

Table 3.1. FLIM data for EGFP-Keap1 transfected cells. The table shows the lifetime, number of cells imaged and standard deviation of the lifetime for both EGFP-Keap1 + mCherry, and EGFP-Keap1 + Nrf2-mCherry co-transfected cells. The lifetime of EGFP-Keap1 is unaffected by the presence of Nrf2-mCherry (p = 0.225) showing that this combination of fusion proteins does not generate a FRET interaction.

EGFP Image	EGFP Lifetime	EGFP Lifetime
A. EGFP-Keap1 + mCherry	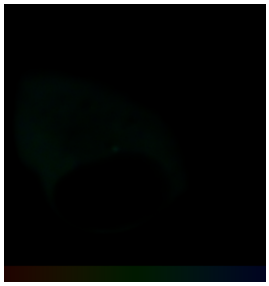 1.9 ns 2.6 ns	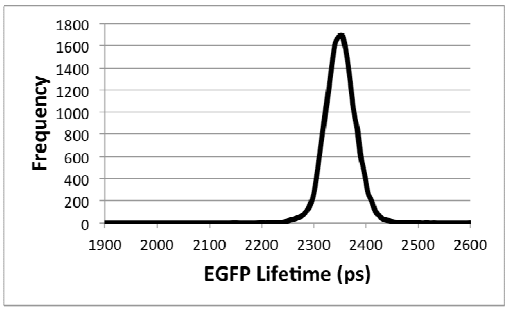
B. EGFP-Keap1 + mCherry	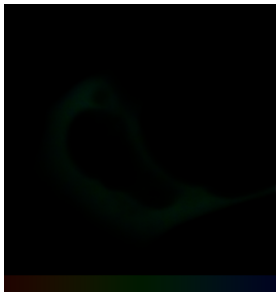 1.9 ns 2.6 ns	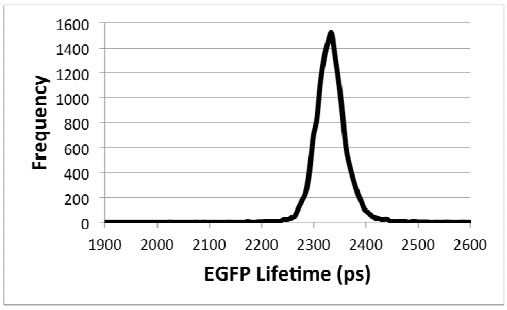
C. EGFP-Keap1 + Nrf2-mCherry	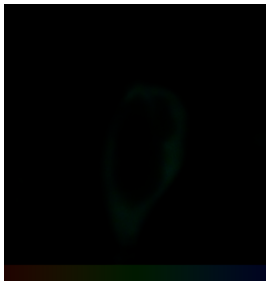 1.9 ns 2.6 ns	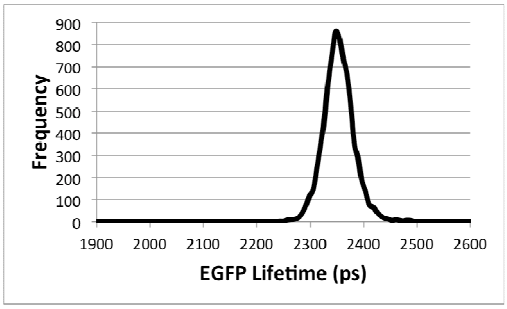
D. EGFP-Keap1 + Nrf2-mCherry	 1.9 ns 2.6 ns	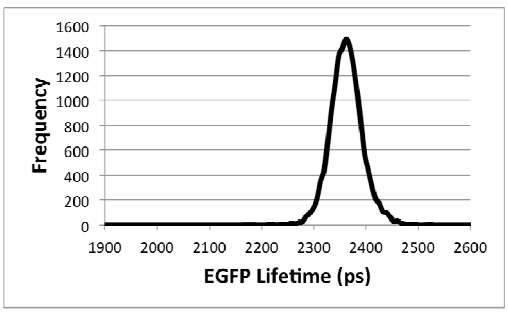

Figure 3.3. Fluorescence lifetime imaging of EGFP-Keap1. HEK293 cells were transfected with either EGFP-Keap1 + mCherry (A, B) or EGFP-Keap1 + Nrf2-mCherry (C, D). The left column shown the EGFP image from which the lifetime data are derived. The middle column shows a pictorial representation of the EGFP lifetime where the colour of the cell corresponds to the lifetime of EGFP, ranging from 1.9 ns to 2.6 ns as indicated on the legend below the image. The right column shows the lifetime data from

each pixel of the image plotted on a graph, with lifetime on the x-axis and frequency on the y-axis. Graphs A-D show the lifetime of EGFP-Keap1 is the same in the absence (A, B) and presence of Nrf2-mCherry (C, D) implying that there is no FRET interaction between the two fusion proteins.

At the beginning of 2010, a paper was published by Ogura et al. presenting the first structure of a full length Keap1 dimer. This single particle electron microscopy generated structure suggested that the C-terminus of Keap1 was significantly closer to the Nrf2 binding site than the N-terminus. Although there is currently no structure available for Nrf2, it binds to Keap1 through its Neh2 domain at the N-terminus, suggesting that EGFP fused here may be in close proximity to the C-terminus of Keap1. Together, these data suggested that the fusion of mCherry to the C-terminus of Keap1, and EGFP fused to the N-terminus of Nrf2 would give the best chance of producing a FRET-generating interaction.

The one caveat to this approach is that previous work in our laboratory has suggested that the fusion of peptides to the C-terminus of Keap1 interferes with the function of the protein. In order to prevent producing a non-functional fusion protein, we cloned mCherry to the C-terminus of Keap1 together with a specifically designed linker domain. It has previously been shown by Arai et al. that use of the helix-forming peptide linker $A(EAAAK)_nA$ can separate two functional domains (Arai et al. 2001). Thus we added between the C-terminus of Keap1 and the mCherry peptide the sequence AEAAAKEAAAKA, which will form an alpha-helix with two twists, to separate the mCherry peptide from Keap1, and allow both proteins to maintain their function.

In order to verify that Keap1-mCherry and EGFP-Nrf2 expression plasmids are in-frame and correctly translated in cells, we transfected the plasmids into HEK293 cells and generated cell lysates. These lysates were then analysed by western blot with antibodies targeting Keap1 and mCherry, and also against Nrf2 and EGFP. As shown in **Figure 3.4**, the pairs of antibodies correctly bind to the fusion proteins demonstrating that Keap1-mCherry and EGFP-Nrf2 are both correctly expressed in cells.

Next, we wanted to determine whether the addition of the fluorophores interfered with the function of Keap1 or Nrf2. Firstly, we wanted to check that

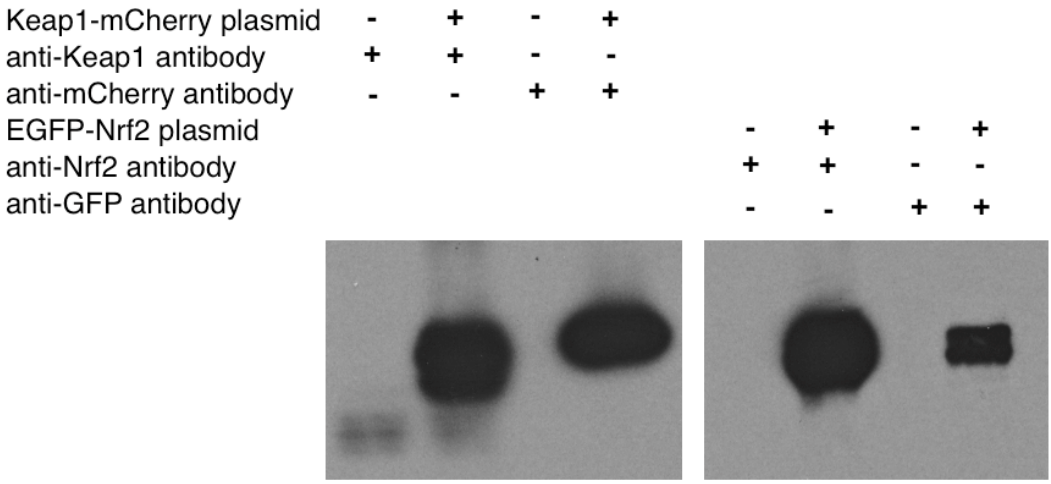

Figure 3.4. Identification of Keap1-mCherry and EGFP-Nrf2 fusion proteins. HEK293 cells were transfected with the indicated combination of plasmids, and cell lysates were generated 24 hours after transfection. An equal amount of protein was loaded on each lane, and the proteins were resolved on SDS-PAGE gels and probed with the antibodies specified above. The blots show that the Keap1-mCherry plasmid encodes a protein consisting of both Keap1 and mCherry, whilst the EGFP-Nrf2 plasmid encodes Nrf2 in-frame with EGFP. The images shown are representative of three independent experiments.

the proteins folded correctly and were able to interact. In order to do this we carried out a co-immunoprecipitation (co-IP) experiment in which cells were transfected with either EGFP-Nrf2 of Keap1-mCherry or both, and were then lysed and immunoprecipitated with an anti-GFP antibody. The input and IP samples were then probed with antibodies against mCherry and GFP, and the results show that Keap1-mCherry and EGFP-Nrf2 are able to interact with one another in the same way as the native proteins (**Figure 3.5**).

Once it had been established that the fluorophores did not inhibit the interaction between Keap1 and Nrf2, it was then necessary to ascertain whether their presence preserved the function of the proteins, namely the ability of Nrf2 to promote transcription of target genes and the ability of Keap1 to target Nrf2 for degradation, and to respond to inducers. In order to assay the transcriptional activity of EGFP-Nrf2, we transiently transfected it into RL34 cells and measured the ability of the ectopic fusion protein to promote the transcription of one of the best-characterised Nrf2 target genes, NQO1 (**Figure 3.6**). The level of NQO1

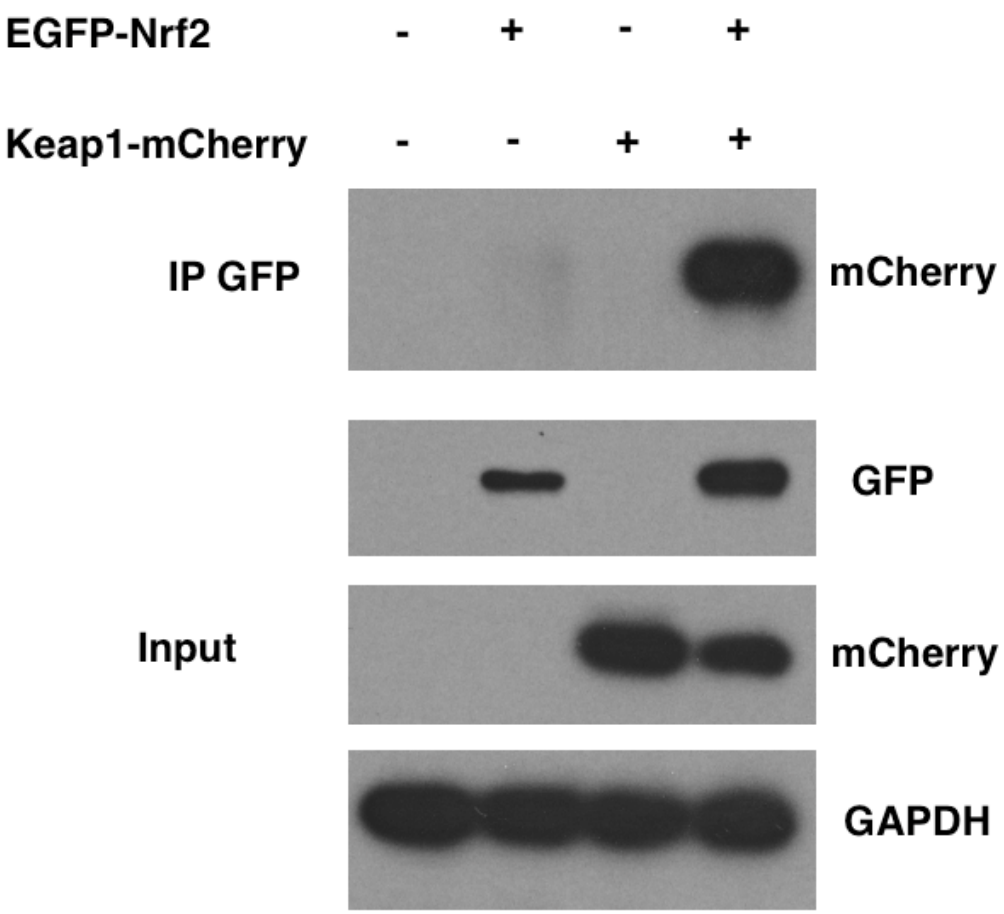

Figure 3.5. Co-immunoprecipitation of EGFP-Nrf2 with Keap1-mCherry. HEK293 cells were transfected with the indicated plasmids, and cell lysates were generated 24 hours after transfection. The lysate was split into two parts, one for the IP and one for the input. The IP sample was generated by treating the lysates with anti-GFP conjugated dynabeads to pull-down any proteins which interact with EGFP-Nrf2. The pulled-down lysates and untreated input samples were loaded onto SDS-PAGE gels which were probed with the specified antibodies. The images shown are representative of three independent experiments.

activity was 2.46 times higher when EGFP-Nrf2 was co-transfected along with mCherry, compared with the mCherry control ($p = 2.67E-11$), demonstrating that the fusion protein is transcriptionally active. The co-expression of Keap1-mCherry reduced the level of NQO1 activity down to the control level, showing that Keap1-mCherry is able to inhibit the transcriptional activity of EGFP-Nrf2 (**Figure 3.6**).

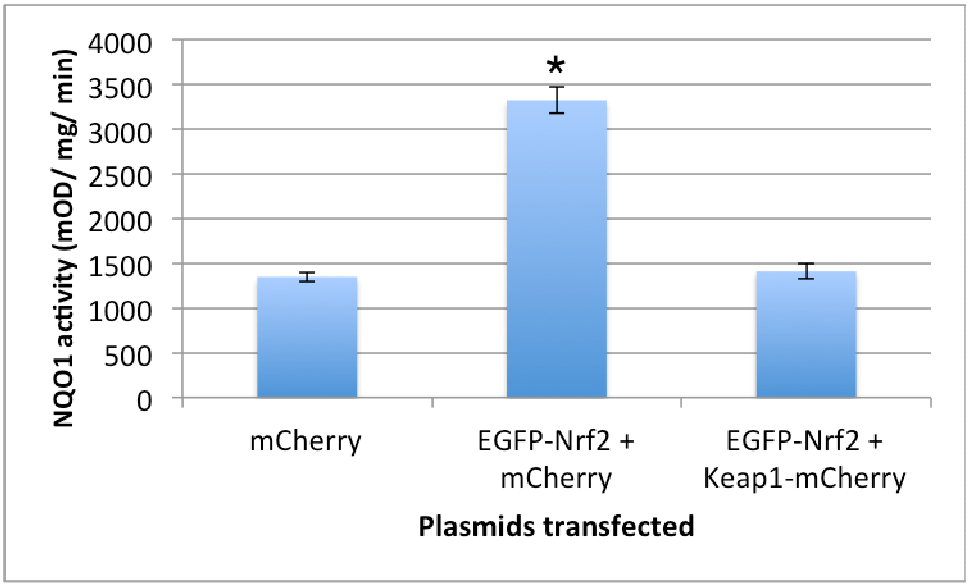

Figure 3.6. The transcriptional activity of EGFP-Nrf2. RL34 cells were transfected with the specified plasmids, and 48 hrs later cell lysates were generated. From these lysates the activity of the Nrf2 target gene quinone reductase 1 (NQO1) was determined. The samples (n=6 per plasmid combination) were normalised for total protein content, and show that expression of EGFP-Nrf2 increases NQO1 activity 2.5-fold, and that co-expression of Keap1-mCherry represses this increase (* $p = 2.67x10^{-11}$ when comparing mCherry to EGFP-Nrf2 + mCherry; $p = 7.82x10^{-11}$ when comparing EGFP-Nrf2 + mCherry to EGFP-Nrf2 + Keap1-mCherry).

The primary function of Keap1 is to target Nrf2 for ubiquitination in the basal state, and this activity is inhibited by inducers. In order to determine whether Keap1-mCherry is able to target Nrf2 for degradation, we co-expressed both expression plasmids in cells, and measured the level of Nrf2-EGFP by western blot in both the basal and induced state (**Figure 3.7**). In the basal state, the co-expression of Keap1-mCherry maintained EGFP-Nrf2 at a very low level (lane 4). However, after 4 hours of treatment with the inducer STCA or the proteasome inhibitor MG132, Nrf2 was stabilised (lanes 5 and 6), showing that in the basal state EGFP-Nrf2 is targeted for proteasomal degradation by Keap1-mCherry, and that both an inducer which directly targets Keap1, and an inhibitor which blocks the proteasomal degradation of Nrf2 lead to the stabilisation of EGFP-Nrf2.

Next, it was important to determine whether the localisation of the fusion proteins was correct. In order to do this we ectopically expressed EGFP-Nrf2 and Keap1-mCherry and imaged the cells using confocal microscopy (**Figure 3.8**). In

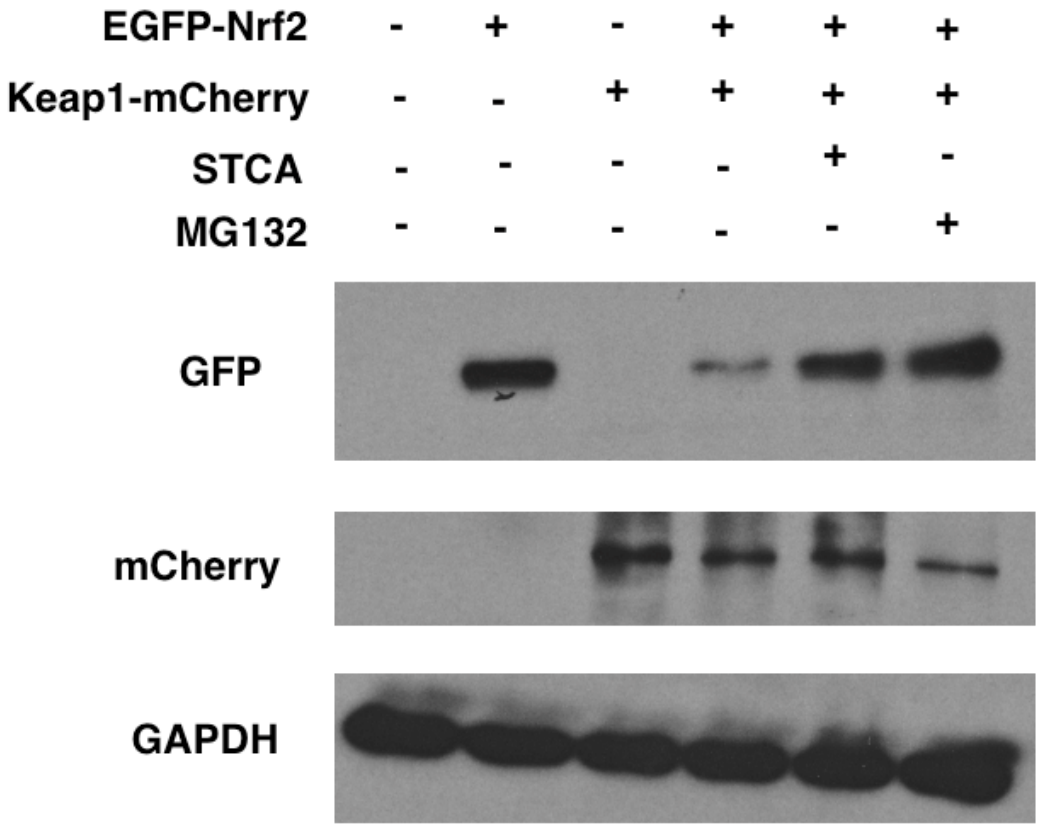

Figure 3.7. Stabilisation of EGFP-Nrf2 by inducers and inhibition of the proteasome. HEK293 cells were transfected with the indicated combination of plasmids, and then treated with either 10 μM of the inducer STCA or 10 μM of the proteasomal inhibitor MG132. After 4 hours of treatment with either STCA or MG132, cell lysates were generated. The samples were run on SDS-PAGE gels and probed with the antibodies specified above. In the absence of Keap1-mCherry, EGFP-Nrf2 is not degraded and is present in the cells (lane 2). When Keap1-mCherry is co-expressed along with EGFP-Nrf2, the level of EGFP-Nrf2 within the cell is low (lane 4), but can be increased through either the addition of the inducer STCA (lane 5) or inhibition of the proteasome (lane 6). Together these data show that the Keap1 and Nrf2 fusion proteins function in the same way as the endogenous system. The images shown are representative of three independent experiments.

the absence of Keap1-mCherry, EGFP-Nrf2 is predominantly localised in the nucleus as would be expected (**Figure 3.8A, B**). However, upon the addition of Keap1-mCherry, the localisation of EGFP-Nrf2 changes to mirror that of Keap1-mCherry, namely it is mainly cytoplasmic (**Figure 3.8C, D**). Together these data suggest that the normal localisation of Nrf2 and Keap1 is unaffected by the presence of the fluorescent proteins.

Finally we wanted to show that when EGFP-Nrf2 is stabilised it translocates to the nucleus in a similar fashion to endogenous Nrf2. Confocal

EGFP channel	mCherry channel
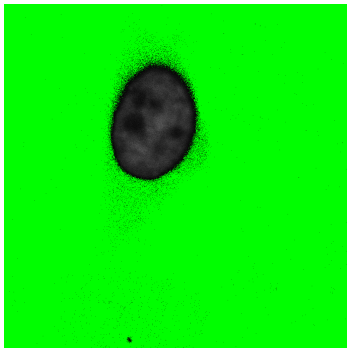 A. EGFP-Nrf2 + mCherry	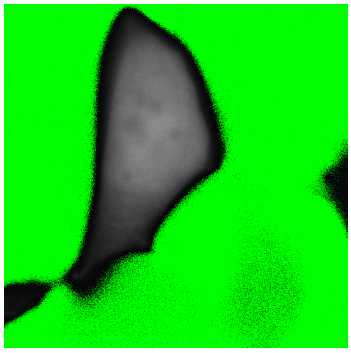 EGFP-Nrf2 + mCherry
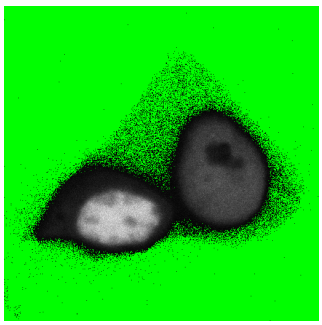 B. EGFP-Nrf2 + mCherry	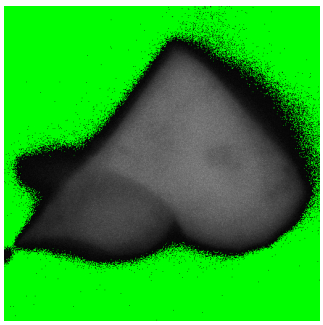 EGFP-Nrf2 + mCherry
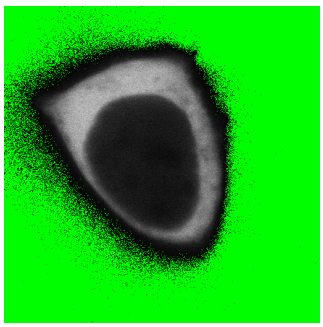 C. EGFP-Nrf2 + Keap1-mCherry	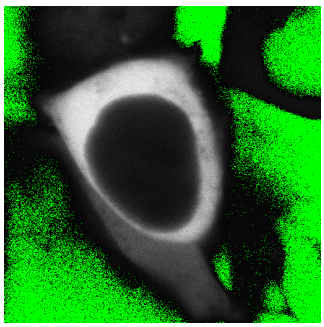 EGFP-Nrf2 + Keap1-mCherry
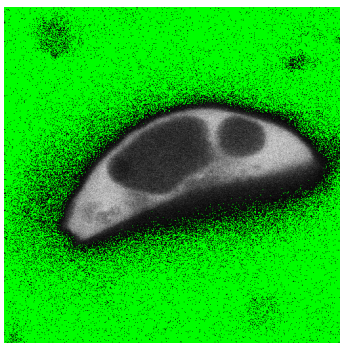 D. EGFP-Nrf2 + Keap1-mCherry	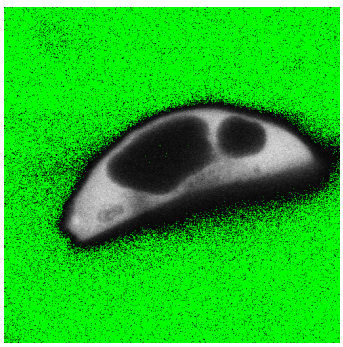 EGFP-Nrf2 + Keap1-mCherry

Figure 3.8. Cellular localisation of Nrf2 and Keap1 fusion proteins. HEK293 cells were transfected with the specified expression plasmids and the localisation of the resulting fluorescence was monitored using confocal microscopy. The EGFP channel is shown in the left column, and the mCherry channel in the right column **A, B.** In the

absence of Keap1, EGFP-Nrf2 is localised mainly in the nucleus, with mCherry dispersed throughout the cell. **C, D.** When Keap1-mCherry is co-expressed, it alters the localisation of the mCherry fluorescence to the cytoplasm, and also sequesters EGFP-Nrf2, changing its localisation from nuclear to mainly cytoplasmic.

microscopy was used to image a cell cluster which had been transfected with EGFP-Nrf2 and Keap1-mCherry. In the basal state, Nrf2 is mostly cytoplasmic, however when the same cells were imaged after 2 hours of treatment with MG132, Nrf2 is clearly localised throughout the entire cell, including the nucleus, whilst the localisation of Keap1 is unaffected (**Figure 3.9**).

Taken together, these data show that even with the addition of the EGFP and mCherry tags, Nrf2 and Keap1 behave like the endogenous proteins when analysed at the whole cell population level. Keap1 is able to bind to Nrf2, target it for proteasomal degradation, and respond to inducers. Nrf2 is able to migrate to the nucleus and activate target gene transcription, suggesting that Keap1-mCherry and EGFP-Nrf2 replicate a number of the important features of the endogenous signalling pathway and provide a useful model system in which to study the interactions between these proteins.

We were then able to transfect the Keap1-mCherry and EGFP-Nrf2 expression vectors into HEK293 cells and look for a FRET interaction. **Table 3.2** and **Figure 3.10 A-B** show that in control cells, in which Keap1-mCherry is not present, the lifetime of EGFP fluorescence is 2375 ps. When Keap1-mCherry is co-expressed, the lifetime graphs are clearly shifted to the left, corresponding to a reduction in the EGFP lifetime to 2155 ps (**Figure 3.10C-D**). This reduction in lifetime is statistically significant ($p = 2.09E-22$), and an indication of a FRET interaction. This means that when EGFP is fused to the N-terminus of Nrf2 and mCherry is fused onto the C-terminus of Keap1, the fluorophores are sufficiently close and in the correct orientation for FRET to occur. Thus we have established a single cell system in which to study how the interaction between Keap1 and Nrf2 changes, if at all, in response to inducers.

It has previously been shown that ten distinct classes of chemicals can act as inducers of the Keap1-Nrf2 pathway, and that these inducers target 3 different sensors in Keap1 (McMahon et al. 2010). For this reason we wanted to test a

Basal state EGFP-Nrf2 + Keap1-mCherry	Induced state EGFP-Nrf2 + Keap1-mCherry
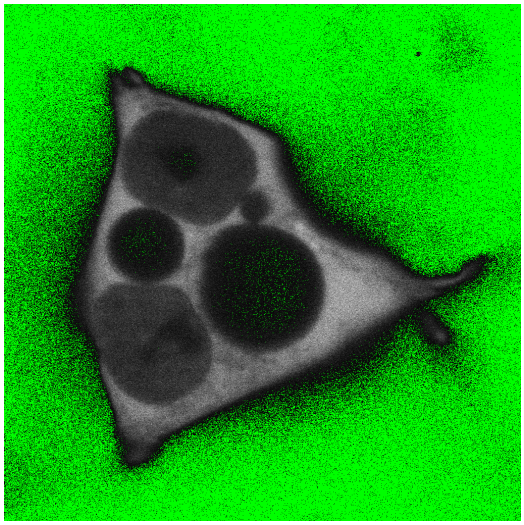 EGFP channel	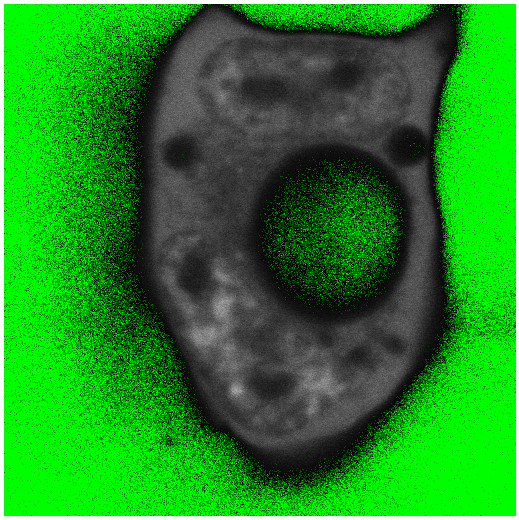 EGFP channel
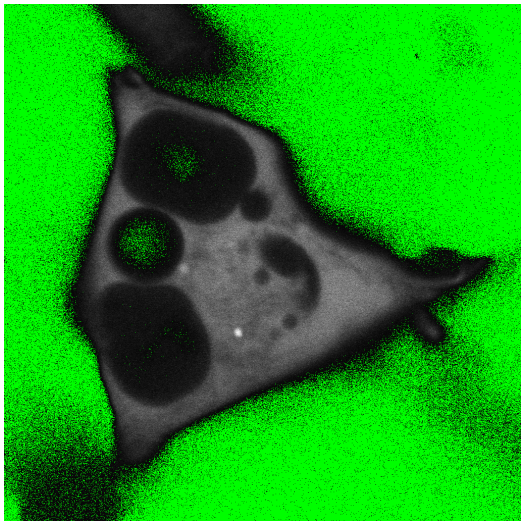 mCherry channel	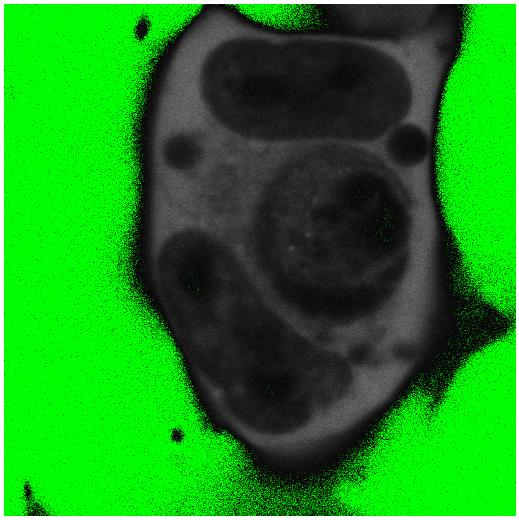 mCherry channel

Figure 3.9.Cellular localisation of Nrf2 and Keap1 fusion proteins in response to MG132. HEK293 cells were transfected with the specified expression plasmids and the localisation of the resulting fluorescence was monitored in the same cluster of cells both in the basal and induced state using confocal microscopy. In the basal state, EGFP-Nrf2 (top left) and Keap1-mCherry (bottom left) are both localised predominantly in the cytoplasm. After 2 hrs treatment with 10μM of the proteasomal inhibitor MG132 the cellular distribution of EGFP-Nrf2 changes, as it becomes localised throughout both the cytoplasm and nucleus (top right), whilst the Keap1-mCherry localisation is unaffected (bottom right).

EGFP Image	EGFP Lifetime	EGFP Lifetime
A. EGFP-Nrf2 + mCherry	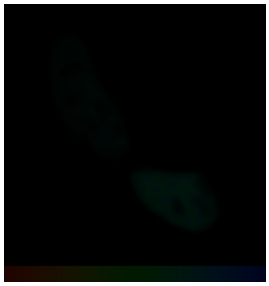 1.9 ns 2.6 ns	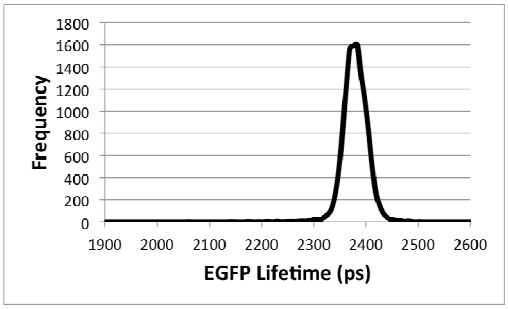
B. EGFP-Nrf2 + mCherry	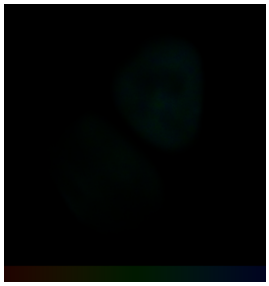 1.9 ns 2.6 ns	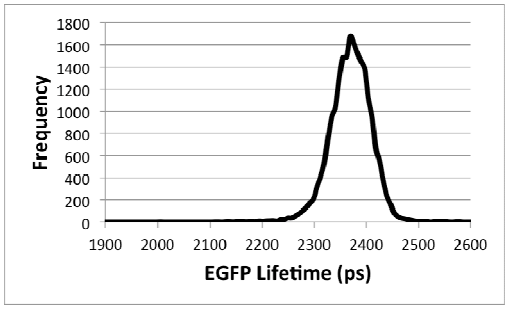
C. EGFP-Nrf2 + Keap1-mCherry	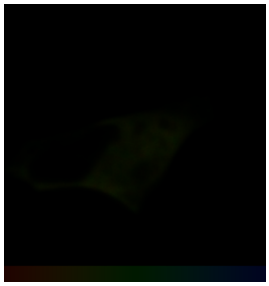 1.9 ns 2.6 ns	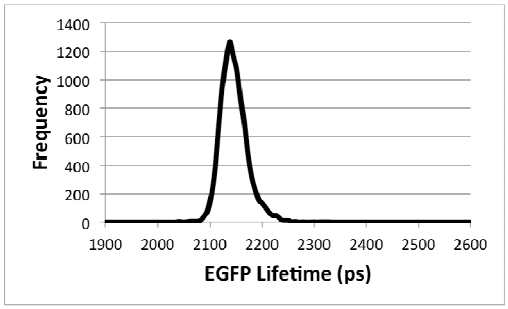
D. EGFP-Nrf2 + Keap1-mCherry	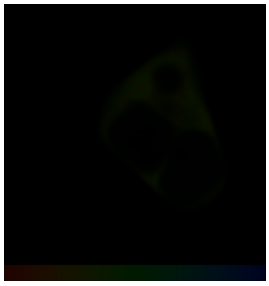 1.9 ns 2.6 ns	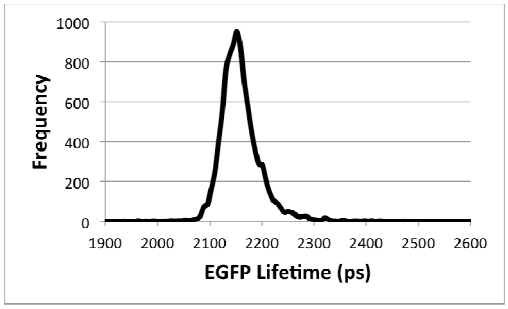

Figure 3.10. Fluorescence lifetime imaging of EGFP-Nrf2. HEK293 cells were transfected with either EGFP-Nrf2 + mCherry (A, B) or EGFP-Nrf2 + Keap1-mCherry (C, D). The left column shows the EGFP image from which the lifetime data are derived. The middle column shows a pictorial representation of the EGFP lifetime where the colour of the cell corresponds to the lifetime of EGFP, ranging from 1.9 ns to 2.6 ns as indicated on

the legend below the image. The right column shows the lifetime data from each pixel of the image plotted on a graph, with lifetime on the x-axis and frequency on the y-axis. Graphs A-D clearly show that the lifetime of EGFP-Nrf2 in the presence of mCherry alone (A, B) is significantly longer than in the presence of Keap1-mCherry (C, D) indicating that there is a FRET interaction between the two fusion proteins. This lifetime change is shown in the images in the second column, in which A and B are blue and C and D are yellow, corresponding to a reduced lifetime of EGFP-Nrf2 in the presence of Keap1-mCherry.

range of inducers in our FRET system to determine whether the inducer type affects the mechanism by which they activate the pathway (**Figure 3.11**).

The first inducer tested was the isothiocyanate sulforaphane (SFN), which reacts with Cys-151 of Keap1 (McMahon et al. 2010). The cells were treated with 5 μM SFN for 1 hour before being imaged. This gave time for the SFN to enter the cell and react with Keap1. The addition of SFN had no effect on the control

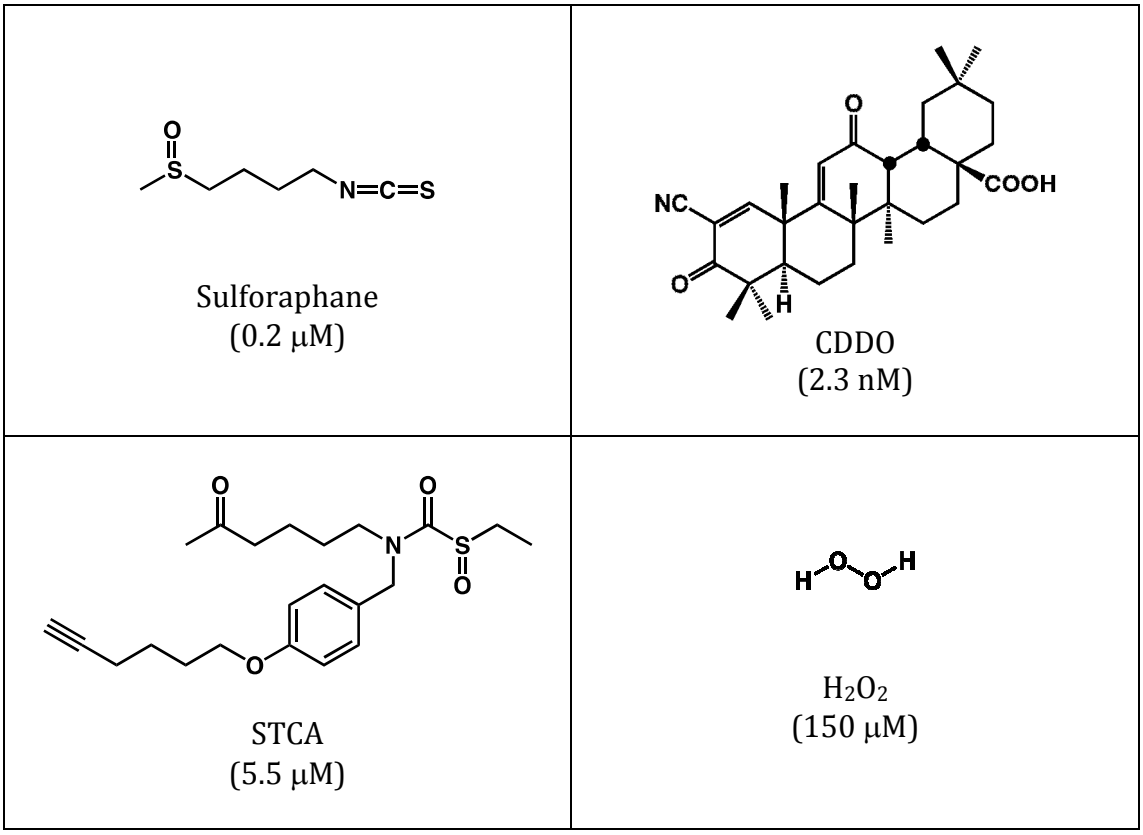

Figure 3.11. Structures and potencies of the Nrf2 inducers used throughout this study. The CD values (Concentration that Doubles the specific acidity of NQO1 in Hepa1c1c7 cells) are shown in parentheses illustrating the broad range of inducer potencies.

EGFP Image	EGFP Lifetime	EGFP Lifetime

A. EGFP-Nrf2 + mCherry	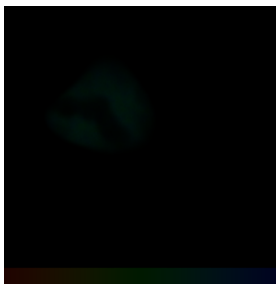 1.9 ns 2.6 ns	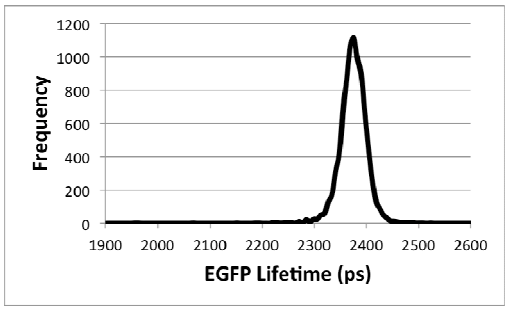
B. EGFP-Nrf2 + mCherry	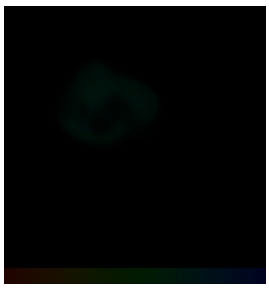 1.9 ns 2.6 ns	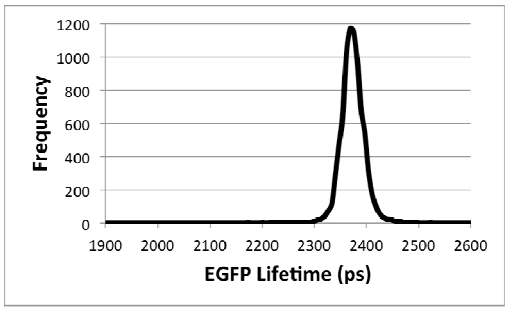
C. EGFP-Nrf2 + Keap1-mCherry	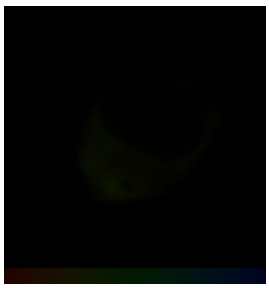 1.9 ns 2.6 ns	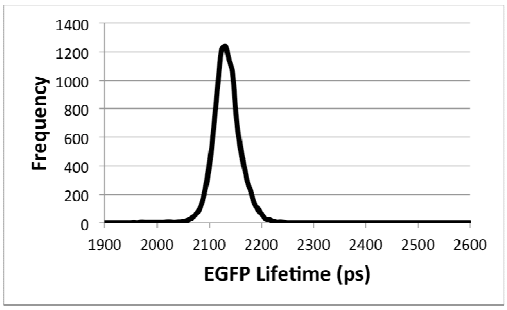
D. EGFP-Nrf2 + Keap1-mCherry	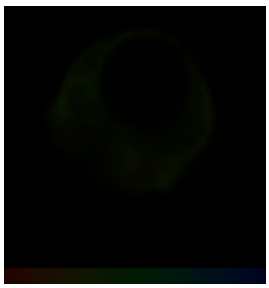 1.9 ns 2.6 ns	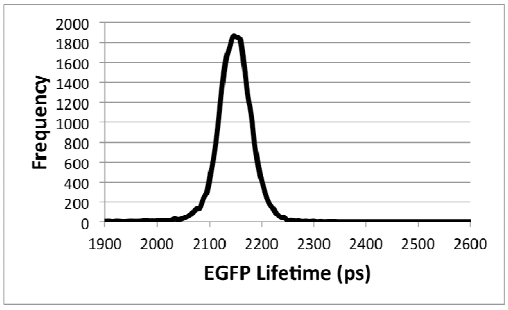

Figure 3.12. Fluorescence lifetime imaging of EGFP-Nrf2 in the presence of the inducer sulforaphane. HEK293 cells were transfected with either EGFP-Nrf2 + mCherry (A, B) or EGFP-Nrf2 + Keap1-mCherry (C, D) and treated with 5μM of the inducer sulforaphane for 1 hour before being imaged. The left column shows the EGFP image from which the lifetime data are derived. The middle column shows a pictorial representation of the EGFP lifetime where the colour of the cell corresponds to the lifetime of EGFP, ranging from 1.9 ns to 2.6 ns as indicated on the legend below the image. The right column shows the lifetime data from each pixel of the image plotted on

a graph, with lifetime on the x-axis and frequency on the y-axis. Graphs A-D clearly show that the lifetime of EGFP-Nrf2 in the presence of mCherry alone (A, B) is significantly longer than in the presence of Keap1-mCherry (C, D) indicating that there is a FRET interaction between the two fusion proteins 1 hour after sulforaphane treatment. This lifetime change is shown in the images in the second column, in which A and B are blue and C and D are yellow, corresponding to a reduced lifetime of EGFP-Nrf2 in the presence of Keap1-mCherry.

lifetime of EGFP-Nrf2 (**Figure 3.12A-B**). This means that any changes in lifetime found in the EGFP-Nrf2 and Keap1-mCherry co-transfected cells will be due to a change in FRET, and not due to a non-specific change in lifetime caused by the inducer itself. In the absence of SFN, the lifetime of EGFP-Nrf2 was 2375 ps, and upon the addition of SFN, it was 2385 ps (**Tables 3.1, 3.2**). When SFN was added to EGFP-Nrf2 and Keap1-mCherry co-transfected cells, the lifetime of EGFP fluorescence was again significantly reduced compared to the control (**Figure 3.12C-D, Table 3.3**), showing that in response to SFN, Nrf2 is not released from Keap1.

	Lifetime (ps)	N	SD	T-test
EGFP-Nrf2 + mCherry	2375	13	12	
EGFP-Nrf2 + Keap1-mCherry	2155	14	20	p = 2.09E-22

Table 3.2. FLIM data for EGFP-Nrf2 transfected cells. The table shows the lifetime, number of cells imaged and standard deviation of the lifetime for both EGFP-Nrf2 + mCherry, and EGFP-Nrf2 + Keap1-mCherry co-transfected cells. The lifetime of EGFP-Nrf2 is significantly reduced by the presence of Keap1-mCherry (p = 2.09E-22) showing that this combination of fusion proteins generates a FRET interaction.

We then studied the effect of the SFN analogue STCA, which activates Keap1 through a different sensor to SFN, as STCA binds directly to Cys-273 and -288 of Keap1 (Ahn et al. 2010). As with SFN, the addition of 10 μM STCA for 1 hour had no effect on the control lifetime of EGFP (**Figure 3.13A-B**). Similarly, in EGFP-Nrf2 and Keap1-mCherry co-transfected cells, the lifetime of EGFP fluorescence was still significantly reduced in the presence of STCA (**Figure 3.13C-D**). This is interesting as it suggests that inducers which target different sensors of Keap1 function through a similar mechanism, and that this mechanism does not involve the release of Nrf2 by Keap1.

EGFP Image	EGFP Lifetime	EGFP Lifetime
A. EGFP-Nrf2 + mCherry	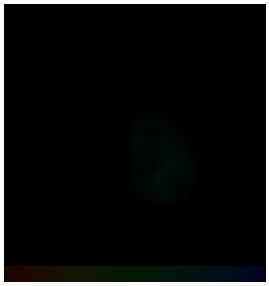 1.9 ns 2.6 ns	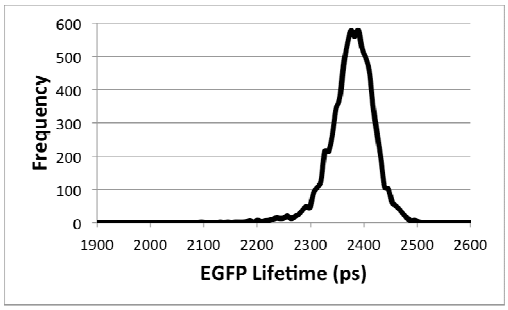
B. EGFP-Nrf2 + mCherry	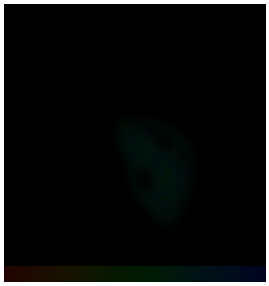 1.9 ns 2.6 ns	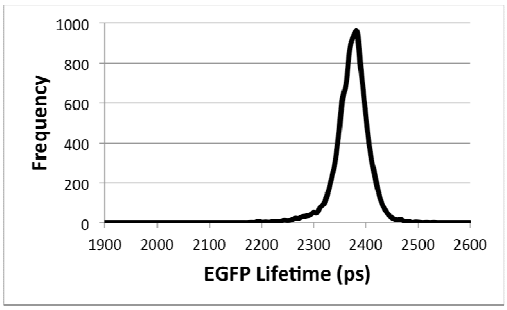
C. EGFP-Nrf2 + Keap1-mCherry	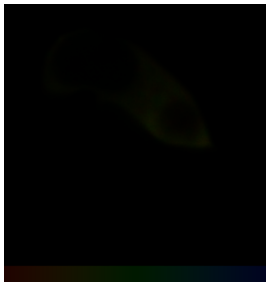 1.9 ns 2.6 ns	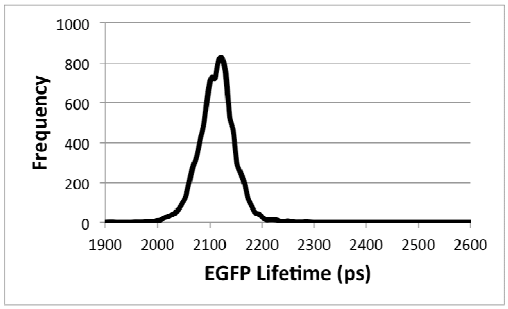
D. EGFP-Nrf2 + Keap1-mCherry	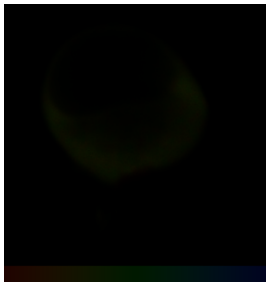 1.9 ns 2.6 ns	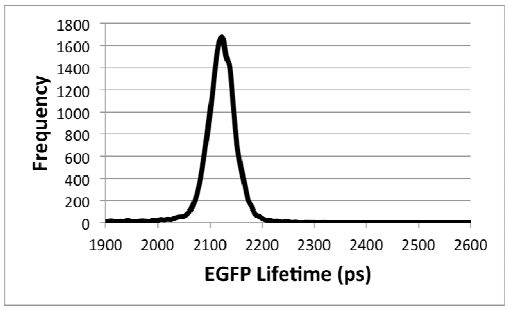

Figure 3.13. Fluorescence lifetime imaging of EGFP-Nrf2 in the presence of the inducer STCA. HEK293 cells were transfected with either EGFP-Nrf2 + mCherry (A, B) or EGFP-Nrf2 + Keap1-mCherry (C, D) and treated with 10μM of the inducer STCA for 1 hour before being imaged. The left column shows the EGFP image from which the lifetime data are derived. The middle column shows a pictorial representation of the EGFP lifetime where the colour of the cell corresponds to the lifetime of EGFP, ranging

from 1.9 ns to 2.6 ns as indicated on the legend below the image. The right column shows the lifetime data from each pixel of the image plotted on a graph, with lifetime on the x-axis and frequency on the y-axis. Graphs A-D clearly show that the lifetime of EGFP-Nrf2 in the presence of mCherry alone (A, B) is significantly longer than in the presence of Keap1-mCherry (C, D) indicating that there is a FRET interaction between the two fusion proteins 1 hour after STCA treatment. This lifetime change is shown in the images in the second column, in which A and B are blue and C and D are yellow, corresponding to a reduced lifetime of EGFP-Nrf2 in the presence of Keap1-mCherry.

In addition to assaying the effects of inducers which target different cysteine residues of Keap1, we also wanted to see whether the size of the inducer altered the mechanism by which Keap1 regulates Nrf2. In order to do this, we chose the bulky inducer CDDO, a triterpinoid with a 5-ringed structure and contrasted this with the small molecule hydrogen peroxide. Like SFN and STCA, neither 0.1 μM CDDO nor 400 μM H_2O_2 had any effect on the lifetime of EGFP-Nrf2 in control cells (**Table 3.3, Figure 3.14A-B, Figure 3.15A-B**). Interestingly, the mechanism by which inducers stabilise Nrf2 is also independent of the size of the inducer, as for both the bulky CDDO and the small H_2O_2, the lifetime of EGFP fluorescence in Nrf2 and Keap1 co-transfected cells was still reduced relative to the control, showing that the two proteins maintain their interaction in response to these inducers (**Table 3.3, Figure 3.14C-D, Figure 3.15C-D**).

	Inducer	Lifetime (ps)	N	SD	T-test
EGFP-Nrf2 + mCherry	5 μM SFN	2385	7	30	
EGFP-Nrf2 + Keap1-mCherry		2149	5	27	p=7.12E-8
EGFP-Nrf2 + mCherry	10 μM STCA	2370	7	18	
EGFP-Nrf2 + Keap1-mCherry		2130	9	28	p=1.62E-11
EGFP-Nrf2 + mCherry	0.1 μM CDDO	2371	7	20	
EGFP-Nrf2 + Keap1-mCherry		2151	8	32	p=1.01E-9
EGFP-Nrf2 + mCherry	400 μM H2O2	2382	12	25	
EGFP-Nrf2 + Keap1-mCherry		2117	10	44	p=1.21E-13

Table 3.3. FLIM data for EGFP-Nrf2 transfected cells treated with inducers. The table shows the lifetime, number of cells imaged and standard deviation of the lifetime for both EGFP-Nrf2 + mCherry, and EGFP-Nrf2 + Keap1-mCherry co-transfected cells treated with 4 different inducers. The lifetime of EGFP-Nrf2 is significantly reduced by the presence of Keap1-mCherry in all cases, showing that this combination of fusion proteins generates a FRET interaction in the presence of each of the 4 inducers.

EGFP Image	EGFP Lifetime	EGFP Lifetime
A. EGFP-Nrf2 + mCherry	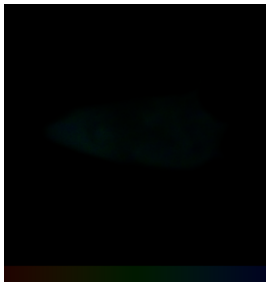 1.9 ns 2.6 ns	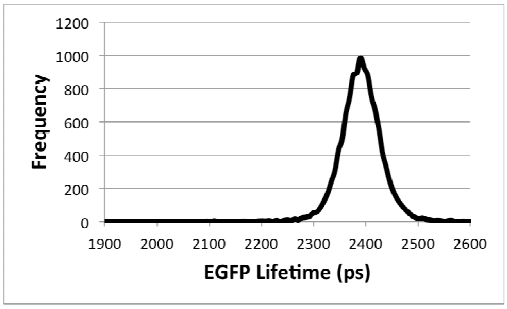
B. EGFP-Nrf2 + mCherry	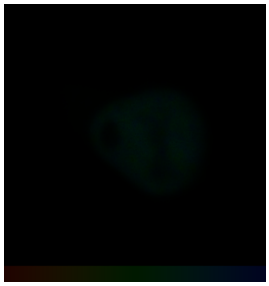 1.9 ns 2.6 ns	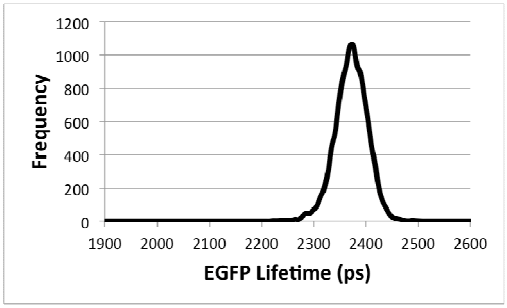
C. EGFP-Nrf2 + Keap1-mCherry	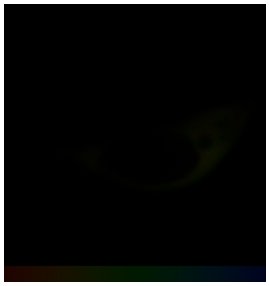 1.9 ns 2.6 ns	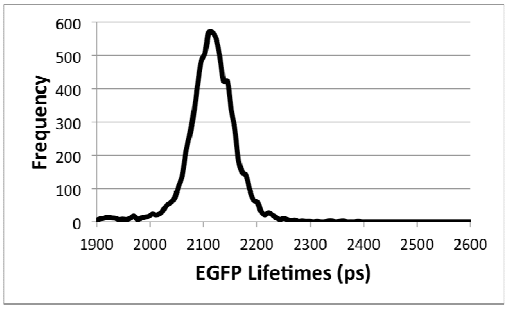
D. EGFP-Nrf2 + Keap1-mCherry	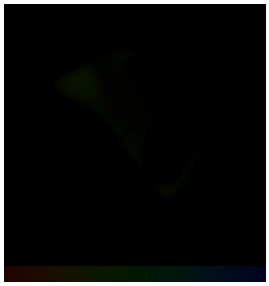 1.9 ns 2.6 ns	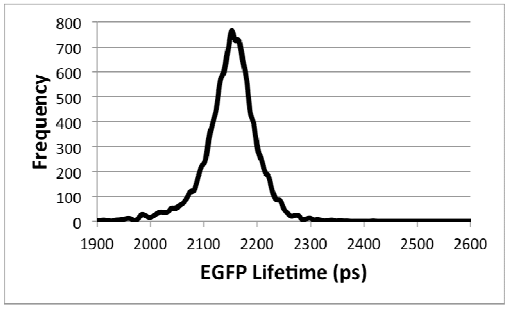

Figure 3.14. Fluorescence lifetime imaging of EGFP-Nrf2 in the presence of the inducer CDDO. HEK293 cells were transfected with either EGFP-Nrf2 + mCherry (A, B) or EGFP-Nrf2 + Keap1-mCherry (C, D) and treated with 0.1μM of the inducer CDDO for 1 hour before being imaged. The left column shows the EGFP image from which the lifetime data are derived. The middle column shows a pictorial representation of the EGFP lifetime where the colour of the cell corresponds to the lifetime of EGFP, ranging

from 1.9 ns to 2.6 ns as indicated on the legend below the image. The right column shows the lifetime data from each pixel of the image plotted on a graph, with lifetime on the x-axis and frequency on the y-axis. Graphs A-D clearly show that the lifetime of EGFP-Nrf2 in the presence of mCherry alone (A, B) is significantly longer than in the presence of Keap1-mCherry (C, D) indicating that there is a FRET interaction between the two fusion proteins 1 hour after CDDO treatment. This lifetime change is shown in the images in the second column, in which A and B are blue and C and D are yellow, corresponding to a reduced lifetime of EGFP-Nrf2 in the presence of Keap1-mCherry.

One caveat to the data presented so far is that the concentration of inducers used has been derived from data using the endogenous Keap1-Nrf2 system. Because out FRET system is an over-expression system, it is possible that higher concentrations of inducer may be required to simulate the endogenous system. Therefore, we used two of the inducers tested previously, SFN and STCA, at a 10 times higher concentration (**Figures 3.16, 3.17, Table 3.4**). Interestingly, the addition of inducers at these high concentrations had a small effect on the control lifetime, reducing it from 2375 ps to 2355 ps for SFN and 2343 ps for STCA treated cells. This reduced lifetime is not unexpected as it has previously been shown that changes in the intracellular environment (such as a change in level of cations) can lead to changes in fluorescence lifetimes (Jung et al. 2005). That notwithstanding, in EGFP-Nrf2 and Keap1-mCherry co-transfected cells we still see a significant decrease in the EGFP lifetime, showing that even when the cells are treated with extremely high concentrations of inducers, Nrf2 and Keap1 do not dissociate (**Table 3.4**).

	Inducer	Lifetime (ps)	N	SD	T-test
EGFP-Nrf2 + mCherry	50µM SFN	2355	3	7	
EGFP-Nrf2 + Keap1-mCherry		2106	5	43	p=6.85E-5
EGFP-Nrf2 + mCherry	100 µM STCA	2343	3	23	
EGFP-Nrf2 + Keap1-mCherry		2115	6	21	p=1.24E-6

Table 3.4. FLIM data for EGFP-Nrf2 transfected cells in the presence of inducers. The table shows the lifetime, number of cells imaged and standard deviation of the lifetime for both EGFP-Nrf2 + mCherry, and EGFP-Nrf2 + Keap1-mCherry co-transfected cells treated with high concentrations of the inducers sulforaphane (SFN) and STCA. The lifetime of EGFP-Nrf2 is significantly reduced by the presence of Keap1-mCherry in both cases, showing that this combination of fusion protein generates a FRET interaction in the presence of a high concentration of either SFN or STCA.

EGFP Image	EGFP Lifetime	EGFP Lifetime
A. EGFP-Nrf2 + mCherry	 1.9 ns 2.6 ns	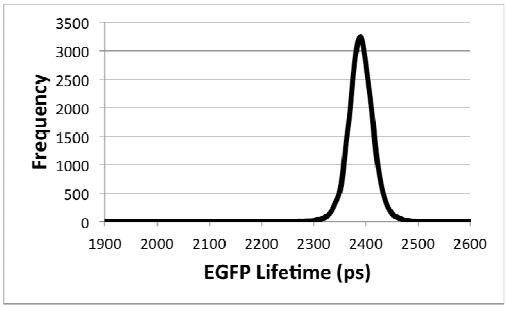
B. EGFP-Nrf2 + mCherry	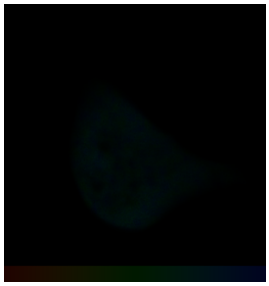 1.9 ns 2.6 ns	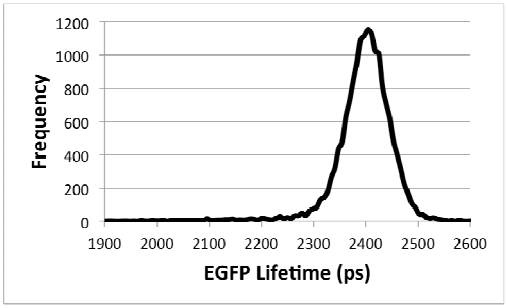
C. EGFP-Nrf2 + Keap1-mCherry	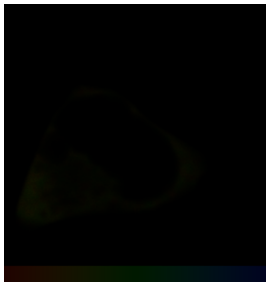 1.9 ns 2.6 ns	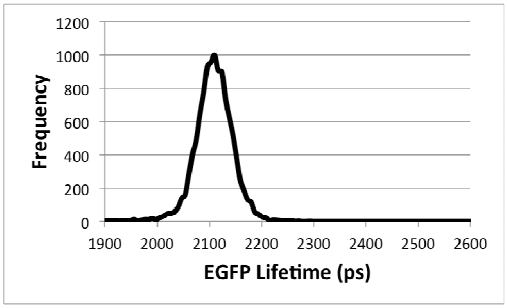
D. EGFP-Nrf2 + Keap1-mCherry	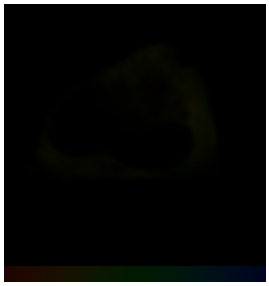 1.9 ns 2.6 ns	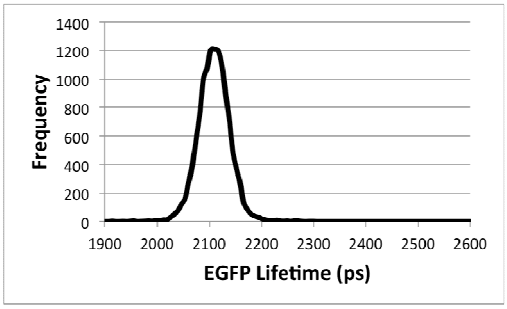

Figure 3.15. Fluorescence lifetime imaging of EGFP-Nrf2 in the presence of the inducer H_2O_2. HEK293 cells were transfected with either EGFP-Nrf2 + mCherry (A, B) or EGFP-Nrf2 + Keap1-mCherry (C, D) and treated with 400μM of the inducer H_2O_2 and imaged immediately for 1 hour. The left column shows the EGFP image from which the lifetime data are derived. The middle column shows a pictorial representation of the EGFP lifetime where the colour of the cell corresponds to the lifetime of EGFP, ranging

from 1.9 ns to 2.6 ns as indicated on the legend below the image. The right column shows the lifetime data from each pixel of the image plotted on a graph, with lifetime on the x-axis and frequency on the y-axis. Graphs A-D clearly show that the lifetime of EGFP-Nrf2 in the presence of mCherry alone (A, B) is significantly longer than in the presence of Keap1-mCherry (C, D) indicating that there is a FRET interaction between the two fusion proteins after H_2O_2 treatment. This lifetime change is shown in the images in the second column, in which A and B are blue and C and D are yellow, corresponding to a reduced lifetime of EGFP-Nrf2 in the presence of Keap1-mCherry.

Discussion

We have developed a system for studying the Keap1-Nrf2 pathway in live cells which accurately models the activity of the endogenous proteins. In the basal state, EGFP-Nrf2 is expressed at a low level, and is localised in the cytoplasm due to its interaction with Keap1-mCherry (**Figures 3.7, 3.8**). In response to inducers, EGFP-Nrf2 becomes stabilised allowing it to accumulate and translocate to the nucleus (**Figures 3.7, 3.8**).

Interestingly, we found that in response to inducers, the Keap1-Nrf2 interaction is maintained, as shown by the reduced lifetime in response to SFN, STCA, H_2O_2 and CDDO (**Table 3.3**). These data complements previously published reports where numerous biochemical techniques have been used to study the effect of inducers on the Keap1-Nrf2 complex. Isothermal titration calorimetry, native electrophoretic mobility shift assay (EMSA) and co-immunoprecipitation experiments have all shown that Keap1 and Nrf2 do not dissociate in response to inducers (Zhang et al. 2004, Eggler et al. 2005). However, all of these studies rely on the use of either recombinant proteins or the use of cell lysates derived from populations of cells as their experimental samples. To our knowledge our FRET/ FLIM data are the first to show the interaction between full length Keap1 and Nrf2 in single live cells and thus in the physiological cellular environment. Importantly, our data confirm that inducers do not lead to the release of Nrf2 from Keap1.

We chose to study the effects of inducers after 1 hour of treatment as it has previously been shown that Nrf2 is stabilised by multiple inducers within an hour (McMahon et al. 2003, Nguyen et al. 2003). In addition, it is known that after 1 hour of treatment, sulforaphane accumulates massively within the cell (with its peak intracellular concentration reaching ~200 μM), suggesting that this is a good time point at which to study its effects on Keap1 (Zhang and Talalay 1998). Interestingly, current data suggest that H_2O_2 is detoxified by the cell within 1 hour, and also that the intramolecular disulphide bonds formed within Keap1 by H_2O_2 may be resolved within 1 hour of treatment (Desaint et al. 2004, Fourquet et al. 2010). For these reasons, we imaged H_2O_2-treated cells only during the first hour following treatment, and not after 1 hour as we did for

EGFP Image	EGFP Lifetime	EGFP Lifetime
A. EGFP-Nrf2 + mCherry	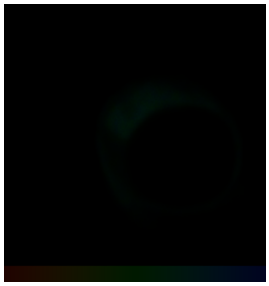 1.9 ns 2.6 ns	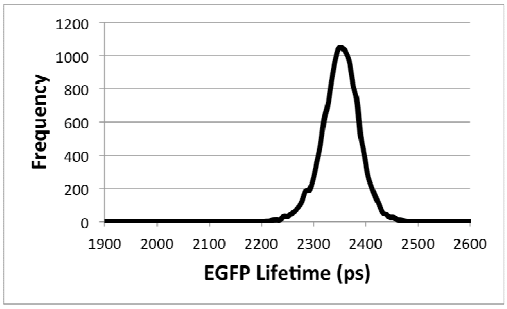
B. EGFP-Nrf2 + mCherry	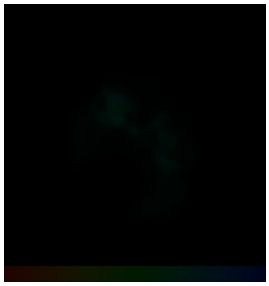 1.9 ns 2.6 ns	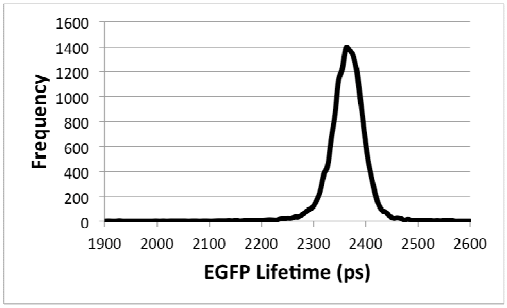
C. EGFP-Nrf2 + Keap1-mCherry	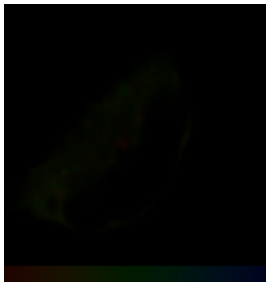 1.9 ns 2.6 ns	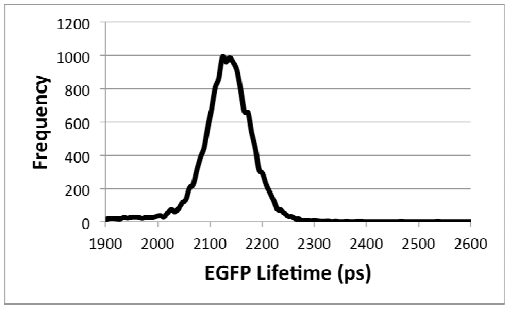
D. EGFP-Nrf2 + Keap1-mCherry	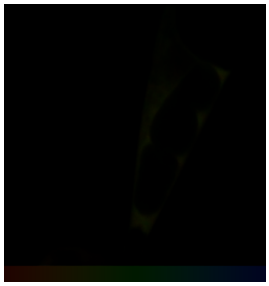 1.9 ns 2.6 ns	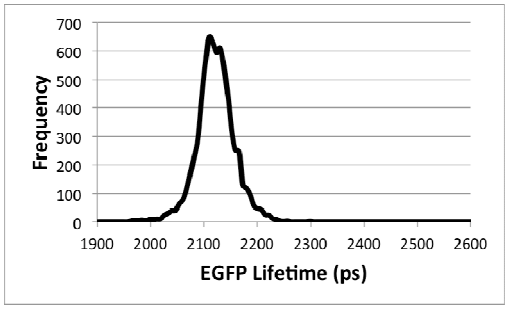

Figure 3.16. Fluorescence lifetime imaging of EGFP-Nrf2 in the presence of the inducer sulforaphane. HEK293 cells were transfected with either EGFP-Nrf2 + mCherry (A, B) or EGFP-Nrf2 + Keap1-mCherry (C, D) and treated with 50μM of the inducer sulforaphane for 1 hour before being imaged. The left column shows the EGFP image from which the lifetime data are derived. The middle column shows a pictorial representation of the EGFP lifetime where the colour of the cell corresponds to the

lifetime of EGFP, ranging from 1.9 ns to 2.6 ns as indicated on the legend below the image. The right column shows the lifetime data from each pixel of the image plotted on a graph, with lifetime on the x-axis and frequency on the y-axis. Graphs A-D clearly show that the lifetime of EGFP-Nrf2 in the presence of mCherry alone (A, B) is significantly longer than in the presence of Keap1-mCherry (C, D) indicating that there is a FRET interaction between the two fusion proteins 1 hour after sulforaphane treatment. This lifetime change is shown in the images in the second column, in which A and B are blue and C and D are yellow, corresponding to a reduced lifetime of EGFP-Nrf2 in the presence of Keap1-mCherry.

sulforaphane, STCA and CDDO, in order to accurately study the effect of H_2O_2 on the Keap1-Nrf2 interaction.

It has previously been shown that Keap1 contains multiple cysteine residues which can be modified by inducers, and that inducers themselves can be divided into 10 different classes. For this reason we wanted to use a variety of different inducers which target different cysteine residues of Keap1 in order to gain a thorough understanding of the mechanism of Nrf2 activation. Thus, sulforaphane was used as an induced specific to the Cys-151 sensor of Keap1, whilst STCA was chosen as an inducer which specifically targets the Cys-273 and Cys-288 sensor (Kobayashi et al. 2009, McMahon et al. 2010, Ahn et al. 2010). In addition, the concentration of inducer required to stabilise Nrf2 is highly variable, which could reflect the mechanism through which it functions, and for this reason we wanted to use inducers with a wide range of potencies. Thus CDDO (which may target Cys-226, Kaidery et al. 2012) was chosen as a highly potent inducer, used at 0.1 μM, which contrasts sharply with the weak inducer H_2O_2, which was used at 400 μM (Dinkova-Kostova et al. 2005b, Fourguet et al. 2010). Interestingly, our data suggest that inducers which target different cysteines of Keap1 and with differing potencies share one important property: they stabilise Nrf2 by inhibiting its Keap1-dependent ubiquitination, and not through the dissociation of the Keap1-Nrf2 complex.

EGFP Image	EGFP Lifetime	EGFP Lifetime
A. EGFP-Nrf2 + mCherry	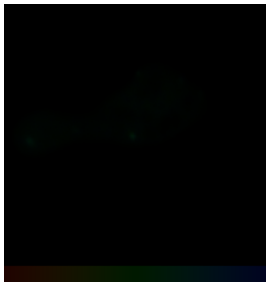 1.9 ns 2.6 ns	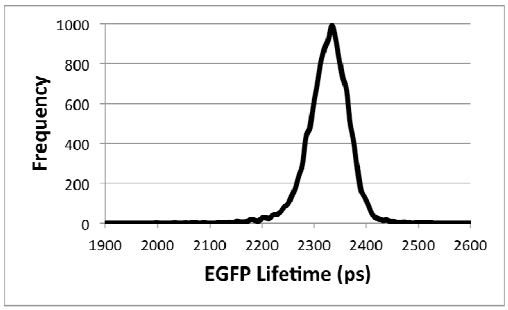
B. EGFP-Nrf2 + mCherry	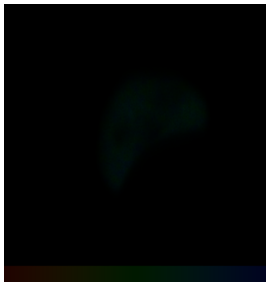 1.9 ns 2.6 ns	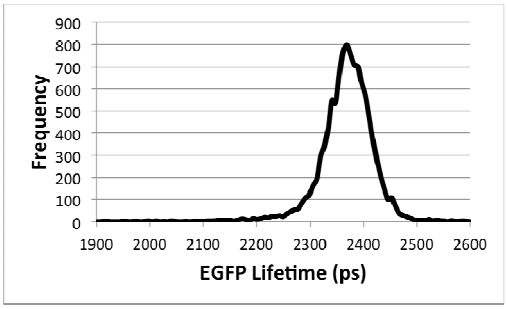
C. EGFP-Nrf2 + Keap1-mCherry	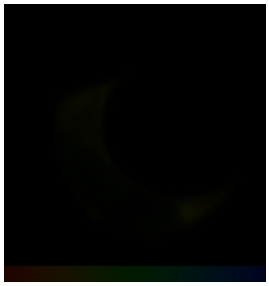 1.9 ns 2.6 ns	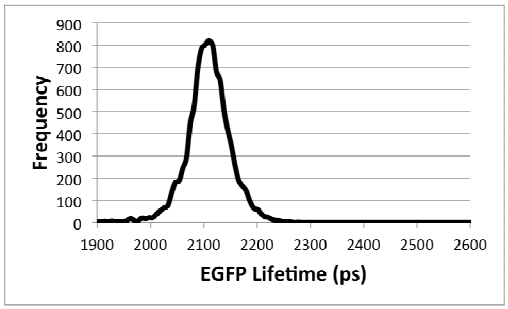
D. EGFP-Nrf2 + Keap1-mCherry	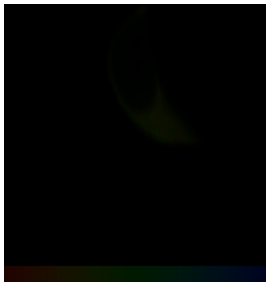 1.9 ns 2.6 ns	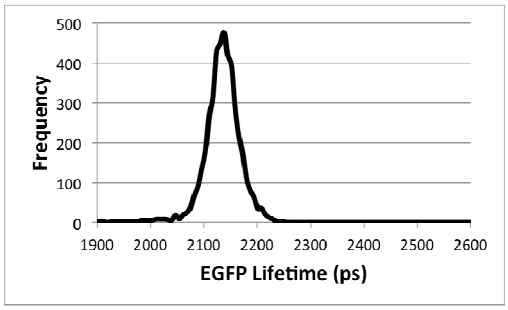

Figure 3.17. Fluorescence lifetime imaging of EGFP-Nrf2 in the presence of the inducer STCA. HEK293 cells were transfected with either EGFP-Nrf2 + mCherry (A, B) or EGFP-Nrf2 + Keap1-mCherry (C, D) and treated with 100μM of the inducer STCA for 1 hour before being imaged. The left column shows the EGFP image from which the lifetime data are derived. The middle column shows a pictorial representation of the EGFP lifetime where the colour of the cell corresponds to the lifetime of EGFP, ranging

from 1.9 ns to 2.6 ns as indicated on the legend below the image. The right column shows the lifetime data from each pixel of the image plotted on a graph, with lifetime on the x-axis and frequency on the y-axis. Graphs A-D clearly show that the lifetime of EGFP-Nrf2 in the presence of mCherry alone (A, B) is significantly longer than in the presence of Keap1-mCherry (C, D) indicating that there is a FRET interaction between the two fusion proteins 1 hour after STCA treatment. This lifetime change is shown in the images in the second column, in which A and B are blue and C and D are yellow, corresponding to a reduced lifetime of EGFP-Nrf2 in the presence of Keap1-mCherry.

Chapter 4: High-resolution analysis of the Keap1-Nrf2 complex in the basal state

Introduction

In addition to being the most accurate method with which to measure FRET interactions, a second advantage of using FLIM is its high resolution, which enables the user to visualise protein complex dynamism in live cells. This is possible as the EGFP lifetime can be used to calculate the FRET efficiency throughout the cell, from which the distance between the fluorophores can be calculated.

Equation 4.1 shows how the FRET efficiency (E) is derived from the fluorescence lifetime data. The constant τ_d is the EGFP lifetime taken from cells transfected with EGFP-Nrf2 + mCherry (**Table 3.2**) and is used for all cells. The variable τ_{da} is calculated on a pixel-by-pixel basis in cells transfected with EGFP-Nrf2 + Keap1-mCherry. Within the SPCImage software, the FRET efficiency is calculated by analysing the lifetime data using a two-component exponential decay model, where the first compenent is free (τ_{da}) and the second is fixed (τ_d) at 2375 ps (**Figure 4.1**and Equation 4.1).

$$E = 1 - (\tau_{da}/\tau_d), \qquad \text{Equation 4.1}$$

Where, E = FRET efficiency
τ_{da} = Lifetime of donor in the presence of acceptor
τ_d = Lifetime of donor alone

This FRET efficiency data can then be used to calculate the distance between the fluorophores, and thus provides data of the physical arrangement of the protein complex in live cells (Equation 4.2). Therefore, a FRET efficiency of 30% does not specify that 30% of the fluorophores are involved in a FRET interaction, but instead refers to the distance between the fluorophores. Thus, the comparison between a FRET efficiency of 30% with that of 20% would indicate that the fluorophores generating the 30% FRET efficiency are closer together.

$r = R_0 \times [(1/E) - 1]^{\frac{1}{6}}$ Equation 4.2

Where, r = Distance between the fluorophores
R_0 = Forster distance at which 50% energy transfer takes place
E = FRET efficiency

[For the EGFP/ mCherry FRET pair the value of R_0 has been calculated as 4.7nm (Lleres et al. 2007)]

Interestingly, it has previously been shown by Lleres et al. 2009 that in the case of fluorescently labelled histones the FRET efficiency distribution can be sub-divided into distinct regions. This means that the distance between the fluorophores is not constant for all FRET interactions, and suggests that the proteins may be found in multiple protein complexes which are each associated with a distinct FRET efficiency.

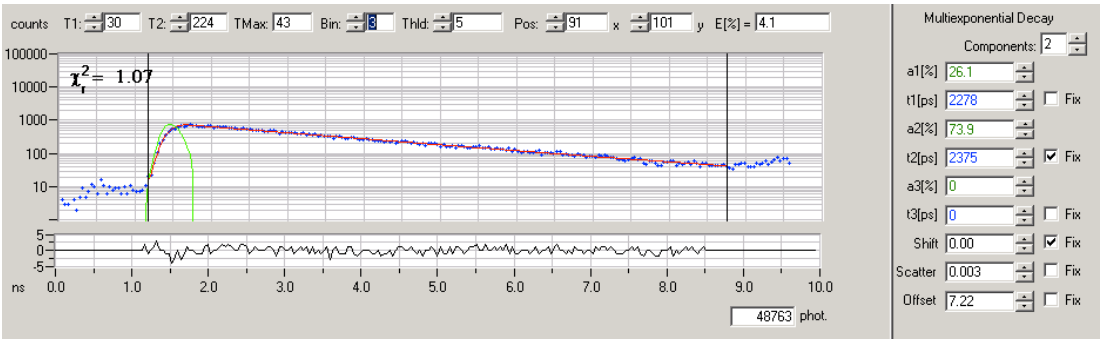

Figure 4.1. FRET efficiency as calculated by SPCImage software. The image above is a screen shot taken from the SPCImage software, which was used to calculate the FRET efficiency from the EGFP lifetime data. In contrast to the lifetime data, the FRET efficiency is calculated using a 2 component multiexponential decay model (box at top right), with the t2 value fixed at 2375 ps (checked box on the right) as calculated from EGFP-Nrf2 + mCherry co-transfected HEK293 cells.

<u>Aim</u>

The aim of this part of the project was to calculate the FRET efficiency of the EGFP-Nrf2/ Keap1-mCherry interaction, and to use these data to probe the dynamics of the protein complex in the basal state.

Results

In addition to observing a significant lifetime difference for EGFP-Nrf2 in the presence and absence of Keap1-mCherry, and thus a FRET interaction between Nrf2 and Keap1, we also wanted to calculate the FRET efficiency to see if the lifetime data contained within it evidence of a dynamic interaction. It has previously been shown by Lleres et al. 2009 that fluorescence lifetime changes can be coupled with changes in the conformation of the protein complexes, and that these complexes can be seen by studying the FRET efficiency (E). Using Equation I, we were able to calculate E for EGFP-Nrf2 in the presence and absence of Keap1-mCherry (**Figure 4.2**). For all of the cells analysed, τ_{da} was the EGFP lifetime specific to each pixel in an individual cell, and τ_d was the average lifetime of EGFP-Nrf2 in the absence of Keap1-mCherry, which was 2375 ps (**Table 3.2**).

Figure 4.2 shows representative FRET efficiency data. The first column shows the EGFP image from which the FRET efficiency is derived. The second column shows the false-colour image of the cell, in which the colour corresponds to the amount of E as defined by the legend below the image (blue = 0%, red = 30% FRET efficiency). The third column shows a graph of the data presented in the FRET efficiency image, in which the value of E from each pixel has been plotted on the x-axis. **Figure4.2A, B** show that in the absence of Keap1-mCherry, the value of E is 0 across almost the entire cell. This corresponds to a blue image in the second column.

As expected (from the lifetime data), in the cytoplasm of EGFP-Nrf2 + Keap1-mCherry co-transfected cells, E > 0.Surprisingly, the data for E revealed the presence of two distinct populations of interacting fluorophores. The graphs in **Figure 4.2C, D** clearly show 2 distinct peaks of FRET efficiency, one centred at 13%and the other at 21%. This pattern was highly reproducible and although the relative areas of the peaks varied among cells, both populations of E were always present. The image data in the second column of **Figure 4.2C, D** show that the distribution of these different populations of E was uniform throughout the cell.The fact that these data showed two different FRET interactions indicates that the Keap1-Nrf2 complex exists in two distinct conformations in cells.

EGFP Image	FRET Efficiency	FRET Efficiency

A. EGFP-Nrf2 + mCherry	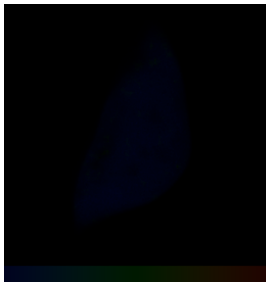 0% 30%	
B. EGFP-Nrf2 + mCherry	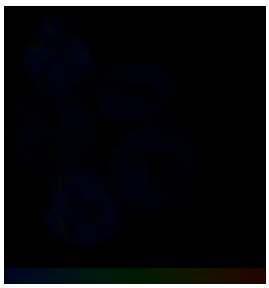 0% 30%	
C. EGFP-Nrf2 + Keap1-mCherry	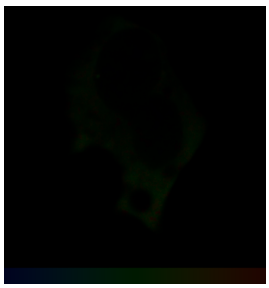 0% 30%	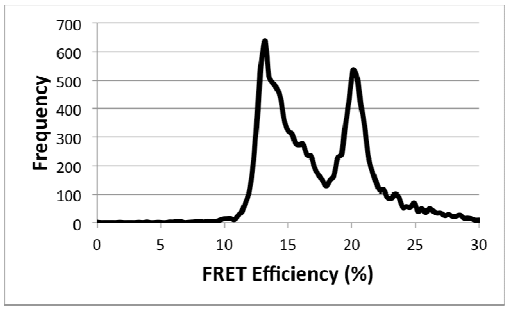
D. EGFP-Nrf2 + Keap1-mCherry	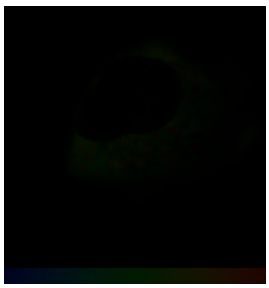 0% 30%	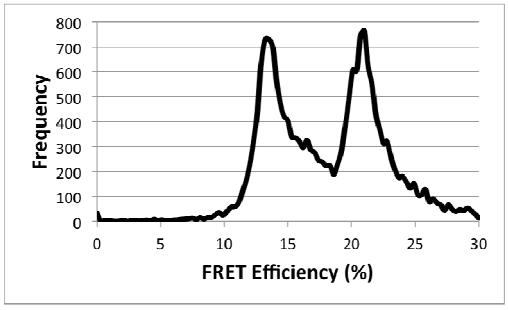

Figure 4.2. FRET efficiency derived from EGFP-Nrf2 lifetime data. HEK293 cells were transfected with either EGFP-Nrf2 + mCherry (A, B) or EGFP-Nrf2 + Keap1-mCherry (C, D) and imaged 24 hours later. The left column shown the EGFP image from which the FRET efficiency data are derived. The middle column shows a pictorial representation of the FRET efficiency where the colour of the cell corresponds to the FRET efficiency, ranging from 0% to 30% as indicated on the legend below the image. The right column shows the FRET efficiency from each pixel of the image plotted on a

graph, with FRET efficiency on the x-axis and frequency on the y-axis. Graphs A-B show that the FRET efficiency in EGFP-Nrf2 and mCherry co-transfected cells is 0%, which corresponds with the blue colour of the cells in A and B. In EGFP-Nrf2 and Keap1-mCherry co-transfected cells (C, D), the FRET efficiency graphs show two distinct peaks, one at 13% and the other at 21% FRET efficiency, suggesting that there are two different FRET interactions between the EGFP and mCherry fluorophores within the Keap1-Nrf2 complex. These different FRET efficiency populations are shown pictorially in the central column of C and D, where the green and yellow colours are distributed evenly across the cells.

This result was unexpected, and suggested that the system may be more dynamic than previously anticipated.

Our first step to determine the identity of the different FRET efficiency populations was to consider what is already known about the interaction between Keap1 and Nrf2. It has been shown that Nrf2 binds to a Keap1 dimer through two distinct motifs; a high affinity ETGE motif, and a low affinity DLG motif (McMahon et al. 2006, Tong et al. 2006a)(**Figure 4.3A**). In the absence of the ETGE motif, Nrf2 does not bind to Keap1, therefore, our first approach was to use a deletion mutant of the DLG motif to see if this has any effect on the FRET efficiency of the interaction (**Figure 4.3B**).

As shown in **Figure 4.4**, EGFP-Nrf2ΔDLG was able to bind to Keap1-mCherry and generate FRET. In the presence of free mCherry alone, the lifetime of EGFP-Nrf2ΔDLG was 2382 ps, whilst when Keap1-mCherry was expressed in place of mCherry the lifetime was significantly reduced to 2227 ps (p= 1.25E-12, **Tables4.1, 4.2**). Interestingly, the loss of the DLG motif increased the lifetime of EGFP relative to wild-type Nrf2 (2155 ps vs. 2227 ps), suggesting that the change in the interaction between Nrf2 and Keap1 in the absence of the DLG motif is coupled to a change in FRET. Although the two proteins still interact giving rise to FRET, the longer lifetime of EGFP in the mutant suggests that the FRET efficiency may also have changed.

When we calculate E for EGFP-Nrf2ΔDLG and Keap1-mCherry co-transfected cells, we can see that the interaction at 13% has been maintained, whilst the 21% FRET efficiency population is lost relative to wild type Nrf2 (compare graphs in **Figure 4.5C,D** with **Figure 4.2C,D**). Together, these data show that when Nrf2 is bound to Keap1 through its ETGE motif alone, it

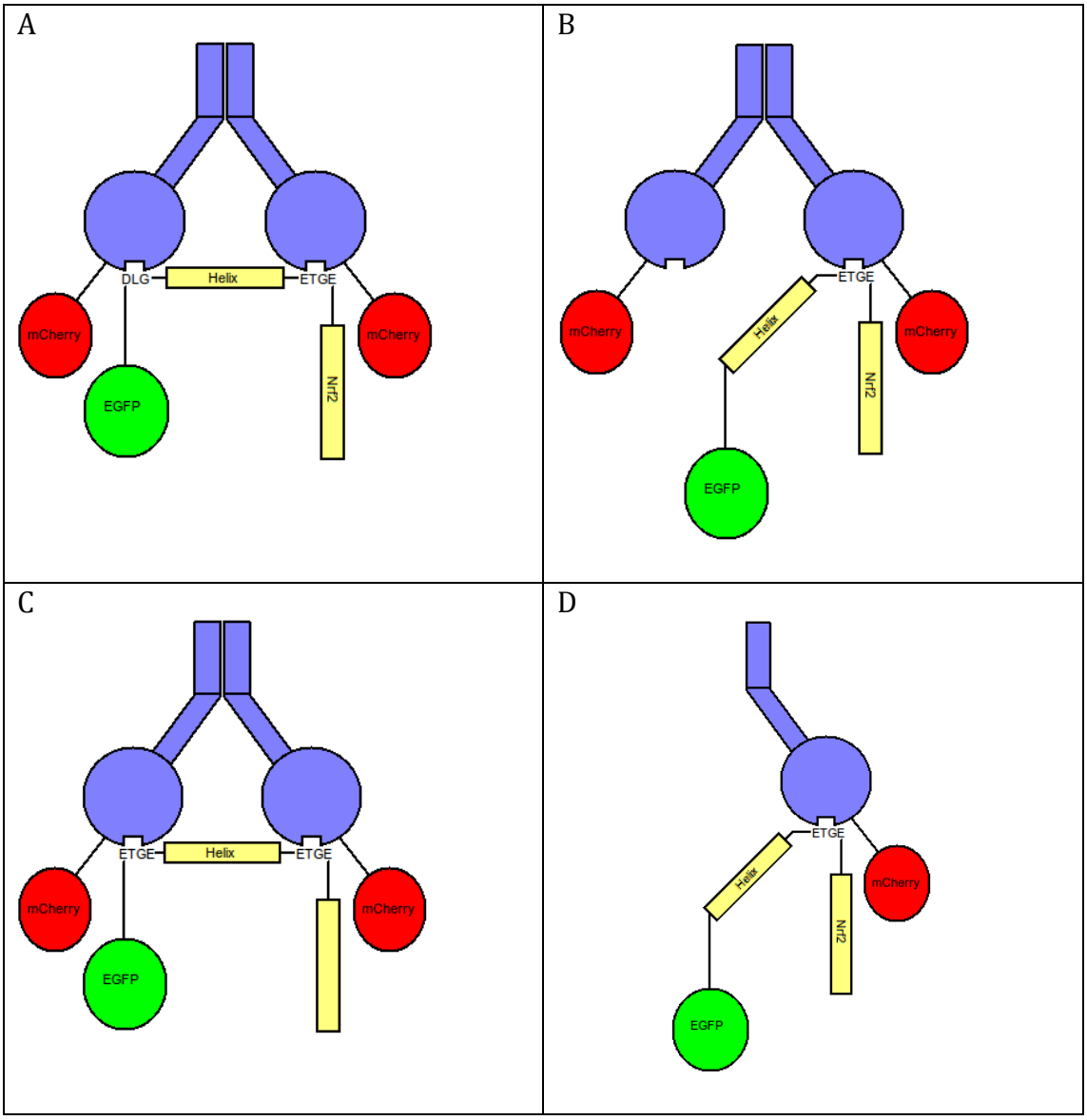

Figure 4.3. Cartoon representations of Keap1-Nrf2 complexes. The different combinations of wild type and mutant Nrf2 and Keap1 proteins used in Chapter 4, and the ways in which they interact, are shown schematically in the cartoons. In all images, Keap1 is shown in blue, mCherry in red, Nrf2 in yellow and EGFP in green. **A.** Shows the interaction of wild-type Nrf2 with Keap1, where Nrf2 is bound to Keap1 through both its high affinity ETGE and low affinity DLG motifs. **B.** Shows the interaction between Nrf2ΔDLG and wild-type Keap1. This mutant of Nrf2 interacts with the Keap1 dimer through only its high affinity ETGE motif.**C.** Shows the interaction between Nrf2-doubleETGE and wild-type Keap1. This mutant interacts with Keap1 through two high affinity ETGE motifs.**D.** Shows the interaction between Nrf2ΔDLG and Keap1-mono-mCherry, a Keap1 mutant which cannot dimerise.

EGFP Image	EGFP Lifetime	EGFP Lifetime
A. EGFP-Nrf2ΔDLG + mCherry	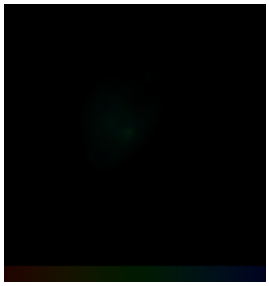 1.9 ns 2.6 ns	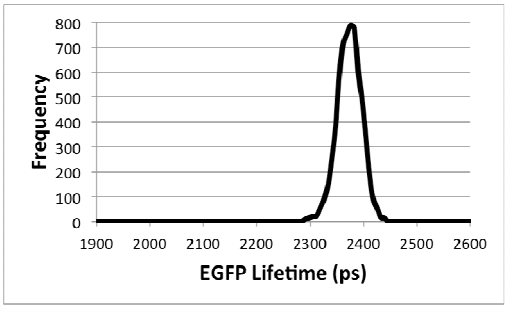
B. EGFP-Nrf2ΔDLG + mCherry	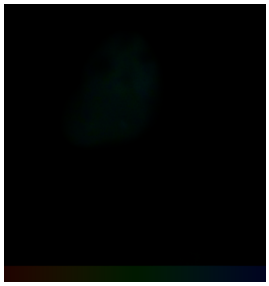 1.9 ns 2.6 ns	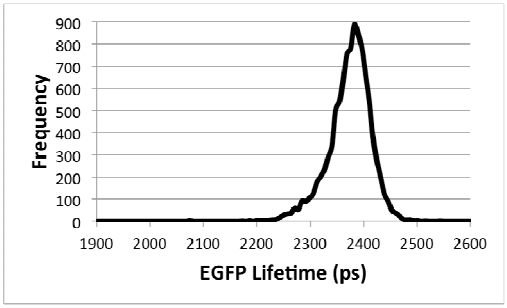
C. EGFP-Nrf2ΔDLG + Keap1-mCherry	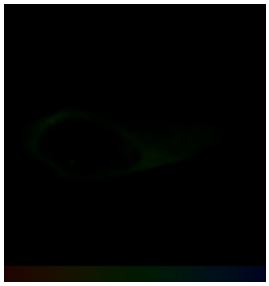 1.9 ns 2.6 ns	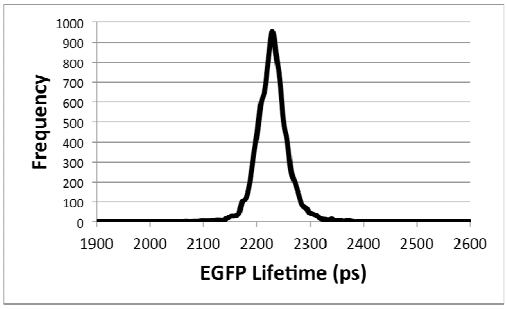
D. EGFP-Nrf2ΔDLG + Keap1-mCherry	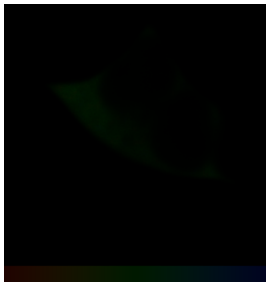 1.9 ns 2.6 ns	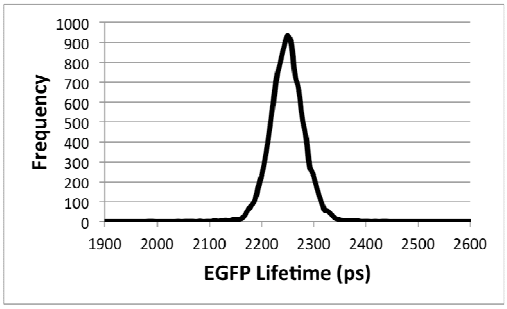

Figure 4.4. Fluorescence lifetime imaging of EGFP-Nrf2ΔDLG. HEK293 cells were transfected with either EGFP- Nrf2ΔDLG + mCherry (A, B) or EGFP- Nrf2ΔDLG + Keap1-mCherry (C, D). The left column shows the EGFP image from which the lifetime data are derived. The middle column shows a pictorial representation of the EGFP lifetime where the colour of the cell corresponds to the lifetime of EGFP, ranging from 1.9 ns to 2.6 ns as indicated on the legend below the image. The right column shows the lifetime data from

each pixel of the image plotted on a graph, with lifetime on the x-axis and frequency on the y-axis. Graphs A-D clearly show that the lifetime of EGFP-Nrf2ΔDLG in the presence of mCherry alone (A, B) is significantly longer than in the presence of Keap1-mCherry (C, D) indicating that there is a FRET interaction between the two fusion proteins. This lifetime change is shown in the images in the second column, in which A and B are blue, and C and D are green, corresponding to a reduced lifetime of EGFP-Nrf2ΔDLG in the presence of Keap1-mCherry.

	Lifetime (ps)	N	SD	T-test
EGFP-Nrf2ΔDLG + mCherry	2382	8	18	
EGFP-Nrf2ΔDLG + Keap1-mCherry	2227	11	19	p = 1.25E-12
EGFP-Nrf2ΔDLG + Keap1-mono-mCherry	2249	8	27	p = 1.30E-8
EGFP-Nrf2-doubleETGE + mCherry	2369	5	21	
EGFP-Nrf2-doubleETGE + Keap1-mCherry	2093	13	18	p = 3.97E-15

Table 4.1. FLIM data for EGFP-Nrf2ΔDLG and EGFP-Nrf2-doubleETGE transfected cells. The table shows the lifetime, number of cells imaged and standard deviation of the lifetime for both EGFP-Nrf2ΔDLG and EGFP-Nrf2-doubleETGE transfected cells. The lifetime of EGFP-Nrf2ΔDLG is significantly reduced by the presence of either Keap1-mCherry (p = 1.25E-12) or Keap1-mono-mCherry (p =1.30E-8) showing that these combinations of fusion proteins generate FRET interactions. The lifetime of EGFP-Nrf2-doubleETGE is also significantly reduced by the presence of Keap1-mCherry (p = 3.97E-15) showing that these fusion proteins generate a FRET interaction.

corresponds to a FRET efficiency of 13%, whilst when the DLG motif is present, and Nrf2 can bind to Keap1 through both its DLG and ETGE motifs simultaneously, the 21% FRET efficiency population can be formed. Interestingly, because both the 13% and the 21% FRET efficiency populations are present in wild type Nrf2 transfected cells, the data suggest that the Keap1-Nrf2 complex forms two distinct conformations, one in which only the ETGE motif of Nrf2 is bound to the Keap1 dimer (represented by the 13% FRET efficiency population) and a second in which both the DLG and ETGE motifs are bound to Keap1 (representing the 21% FRET efficiency population), and that both of these complexes are present within the same cell at the same time in the basal state.

EGFP Image	FRET Efficiency	FRET Efficiency
A. EGFP-Nrf2ΔDLG + mCherry	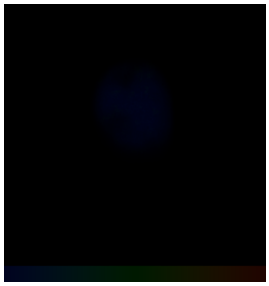 0% 30%	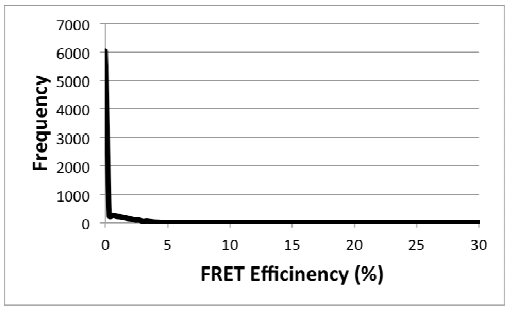
B. EGFP-Nrf2ΔDLG + mCherry	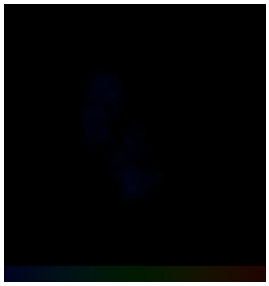 0% 30%	
C. EGFP-Nrf2ΔDLG + Keap1-mCherry	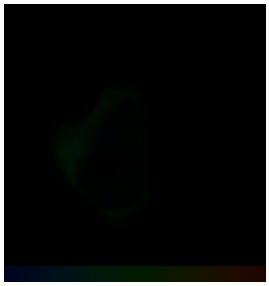 0% 30%	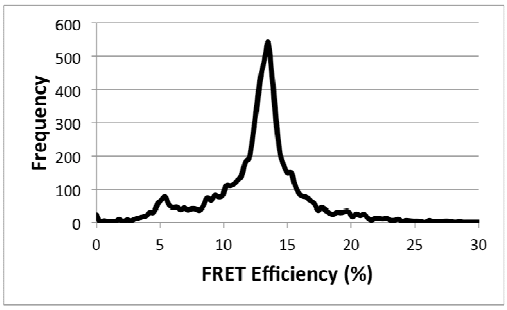
D. EGFP-Nrf2ΔDLG + Keap1-mCherry	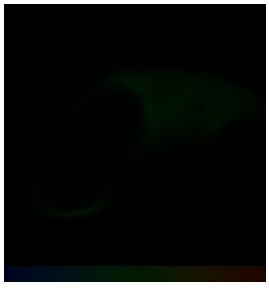 0% 30%	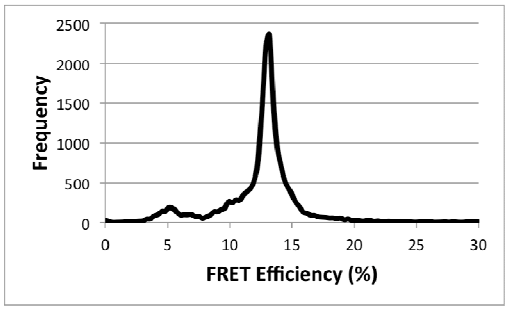

Figure 4.5. FRET efficiency derived from EGFP- Nrf2ΔDLG lifetime data. HEK293 cells were transfected with either EGFP-Nrf2ΔDLG + mCherry (A, B) or EGFP- Nrf2ΔDLG + Keap1-mCherry (C, D) and imaged 24 hours later. The left column shown the EGFP image from which the FRET efficiency data are derived. The middle column shows a pictorial representation of the FRET efficiency where the colour of the cell corresponds to the FRET efficiency, ranging from 0% to 30% as indicated on the legend below the

image. The right column shows the FRET efficiency from each pixel of the image plotted on a graph, with FRET efficiency on the x-axis and frequency on the y-axis. Graphs A-B show that the FRET efficiency in EGFP-Nrf2ΔDLG and mCherry co-transfected cells is 0%, which corresponds with the blue colour of the cells in A and B. In EGFP- Nrf2ΔDLG and Keap1-mCherry co-transfected cells (C, D), the FRET efficiency graphs shows one peak at 13% FRET efficiency, indicating that there is a single FRET interaction between the EGFP and mCherry fluorophores within the Keap1-Nrf2ΔDLG complex. This FRET efficiency population is shown pictorially in the central column of C and D, where the green colour is distributed evenly across the cells.

One caveat to this conclusion is that because the Keap1 dimer contains two mCherry fluorophores, it may be possible for the EGFP-Nrf2 which is bound to Keap1 through both the DLG and ETGE motifs to FRET with both fluorophores simultaneously. Thus a single conformation of the Keap1-Nrf2 complex may be able to give rise to two FRET interactions leading to two different FRET efficiency populations.

In order to test this possibility, we designed a second mutant of Nrf2 which binds to Keap1 more tightly due to the addition of a second ETGE motif in place of the original DLG motif (**Figure 4.3C**). If the two FRET efficiency populations come from a single conformation of the Keap1-Nrf2 complex, then the tighter binding of EGFP-Nrf2-doubleETGE will have no effect on the FRET efficiency when transfected along with Keap1. However, if the two FRET efficiency populations represent two distinct conformations of the Keap1-Nrf2 complex, one in which only the ETGE motif is bound, and the other in which both the ETGE and DLG motifs are bound to a Keap1 dimer, then the addition of a second ETGE motif should lead to an increase in the complex in which both motifs are bound, as the additional ETGE motif will bind more tightly to Keap1 than the endogenous DLG motif.

When EGFP-Nrf2-doubleETGE was transfected along with Keap1-mCherry, we still saw a FRET interaction characterised by a reduction in EGFP lifetime (**Figure 4.6**). Interestingly, the lifetime of this doubleETGE mutant was reduced when compared with wild type Nrf2 (2093 ps vs. 2155 ps), suggesting there was more FRET with this new mutant (**Tables4.1, 4.2**). Interestingly, this reduced lifetime corresponded to an increase in the interaction at 21% FRET efficiency (**Figure 4.7**). Together these data establish that the two FRET

Nrf2	Lifetime
doubleETGE	2054
doubleETGE	2075
doubleETGE	2082
doubleETGE	2082
doubleETGE	2089
doubleETGE	2089
doubleETGE	2096
doubleETGE	2096
doubleETGE	2096
doubleETGE	2103
doubleETGE	2110
WT	2110
doubleETGE	2117
doubleETGE	2117
WT	2138
WT	2138
WT	2138
WT	2152
WT	2152
WT	2152
WT	2152
WT	2159
WT	2166
WT	2173
WT	2173
WT	2180
WT	2187
DLG	2194
DLG	2208
DLG	2208
DLG	2222
DLG	2229
DLG	2229
DLG	2229
DLG	2236
DLG	2236
DLG	2250
DLG	2257

Table 4.2. The combined lifetimes of wild type and mutant EGFP-Nrf2 transfected cells. The table above shows the individual fluorescence lifetimes for all cells co-transfected with Keap1-mCherry and either EGFP-Nrf2 (yellow), EGFP-Nrf2-doubleETGE (red) or EGFP-Nrf2ΔDLG (green). The cells are ordered by EGFP lifetime from shortest to longest. The table clearly shows that cells transfected with EGFP-Nrf2-

doubleETGE (which binds tightly to both members of the Keap1 dimer) have the shortest lifetime, while those transfected with EGFP-Nrf2ΔDLG (which binds to only one member of the Keap1 dimer) have the longest lifetimes. The cells that were transfected with wild type EGFP-Nrf2 have lifetimes between these mutants. These data suggest that in wild type cells, the population of Keap1-Nrf2 complexes is found as a mixture of tight and weak interactions, which when combined and averaged across the cell gives a lifetime between that of the tightly- and weakly-interacting mutants.

efficiency populations are not produced by a single conformation of the Keap1-Nrf2 complex, but instead that this complex is found in two distinct states.

Because Keap1 forms a dimer, our data to this point were limited by the fact that it was not clear with which of the two Keap1-mCherry proteins the EGFP fluorophore was interacting to produce the 13% FRET efficiency signal. The knowledge of which pair of fluorophores were interacting may give us a greater insight into the structure of the Keap1-Nrf2 complex.The 13% FRET efficiency population in EGFP-Nrf2ΔDLG transfected cells could be produced in two different ways (**Figure 4.8**). It could be produced by an interaction between either the Keap1 protein which is bound to the ETGE motif of Nrf2 (FRET in *cis* because the two proteins which generate FRET are directly bound to one another), or to the other member of the Keap1 dimer which is unbound to Nrf2, but which normally binds to the DLG motif when it is present (FRET in *trans*, because this Keap1 and Nrf2 combination are not directly bound together).

In order to determine with which member of the Keap1 dimer EGFP-Nrf2ΔDLG interacts with to generate FRET, we made a mutant of Keap1 which is unable to dimerise, named Keap1-mono-mCherry (**Figure 4.3D**). When plasmids encoding these two proteins were transfected into cells, the lifetime of EGFP was reduced relative to the control, showing that FRET took place (**Figure 4.9A,B, Table 4.1**). Interestingly, when the lifetime data were used to calculate the FRET efficiency, we found that the 13% FRET efficiency interaction was maintained between EGFP-Nrf2ΔDLG and Keap1-mono-mCherry, and that the 21% FRET efficiency population was completely absent, showing that the 13% FRET efficiency population corresponds to FRET between EGFP and the Keap1 protein which binds to the ETGE motif of Nrf2 (**Figure 4.9C,D**).

All of the data presented in **Figures 4.2-4.9** concern the interaction between Nrf2 and Keap1 in the cytoplasm, as this has previously been suggested

EGFP Image	EGFP Lifetime	EGFP Lifetime
A. EGFP-Nrf2-doubleETGE + mCherry	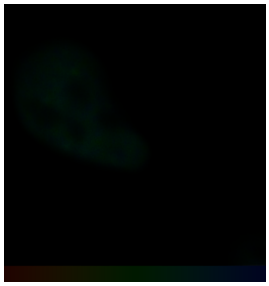 1.9 ns 2.6 ns	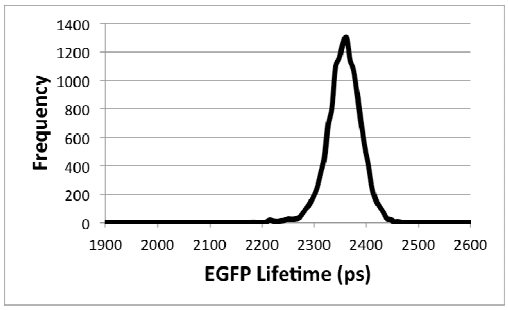
B. EGFP-Nrf2-doubleETGE + mCherry	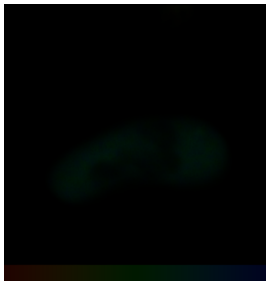 1.9 ns 2.6 ns	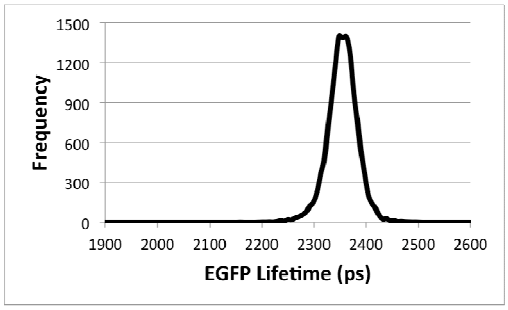
C. EGFP-Nrf2-doubleETGE + Keap1-mCherry	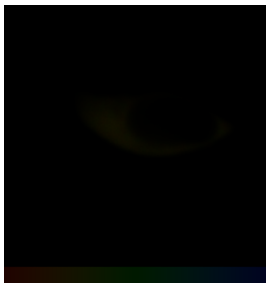 1.9 ns 2.6 ns	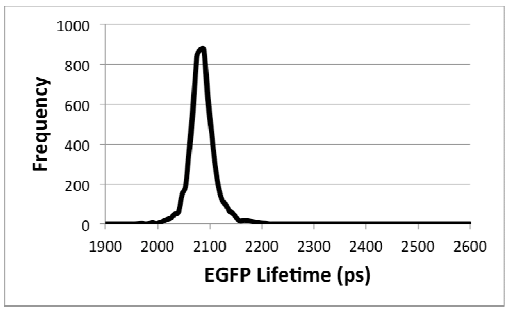
D. EGFP-Nrf2-doubleETGE + Keap1-mCherry	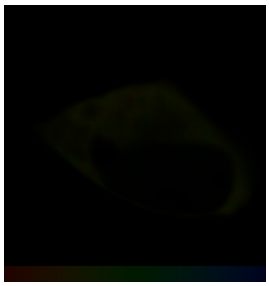 1.9 ns 2.6 ns	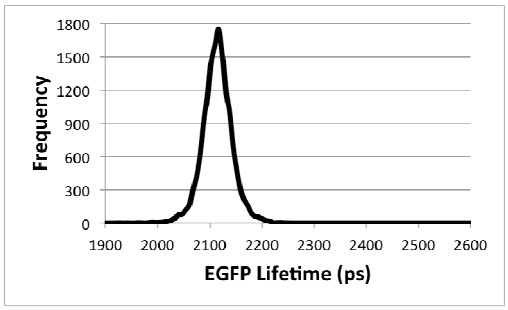

Figure 4.6. Fluorescence lifetime imaging of EGFP-Nrf2-doubleETGE. HEK293 cells were transfected with either EGFP- Nrf2-doubleETGE + mCherry (A, B) or EGFP- Nrf2-

doubleETGE + Keap1-mCherry (C, D). The left column shows the EGFP image from which the lifetime data are derived. The middle column shows a pictorial representation of the EGFP lifetime where the colour of the cell corresponds to the lifetime of EGFP, ranging from 1.9 ns to 2.6 ns as indicated on the legend below the image. The right column shows the lifetime data from each pixel of the image plotted on a graph, with lifetime on the x-axis and frequency on the y-axis. Graphs A-D clearly show that the lifetime of EGFP-Nrf2-doubleETGE in the presence of mCherry alone (A, B) is significantly longer than in the presence of Keap1-mCherry (C, D) indicating that there is a FRET interaction between the two fusion proteins. This lifetime change is shown in the images in the second column, in which A and B are blue, and C and D are yellow, corresponding to a reduced lifetime of EGFP-Nrf2-doubleETGE in the presence of Keap1-mCherry.

to be the main site of the Keap1-Nrf2 interaction (Watai et al. 2007). Interestingly, we also observed a weak EGFP signal in the nucleus (with an intensity 10-fold lower than the cytoplasm) and wished to analyse it to determine whether Nrf2 is also able to bind to Keap1 in the nuclear compartment. In accordance with the literature, we also found a weak nuclear Keap1 signal (as shown in the confocal microscopy images in **Figure 4.10**), highlighting the fact that both proteins are present in the nucleus and thus may be able to interact there (Nguyen et al. 2005, Watai et al. 2007, Sun et al. 2011, Kaspar et al. 2012).

As shown in **Table 4.3**, in the nucleus of EGFP-Nrf2 + Keap1-mCherry co-transfected cells the lifetime of EGFP fluorescence is 2203 ps. This is significantly shorter than in the absence of Keap1 ($p = 1.56E-18$), demonstrating a FRET interaction between EGFP-Nrf2 and Keap1-mCherry in the nucleus. Interestingly, when a comparison is made between the lifetime of EGFP fluorescence in the cytoplasm and nucleus of the same cell, it is clear that in all cases the lifetime in the nucleus is significantly longer (**Table 4.3**, $p = 1.759E-9$).

In order to determine whether the longer lifetime in the nucleus corresponds to a change in the conformation of the Keap1-Nrf2 complex, we calculated the FRET efficiency of the interaction in both the cytoplasm and nucleus of individual cells (**Figure 4.11**). The left column of **Figure 4.11** shows the FRET efficiency image of the cell, the central column shows a graph of the FRET efficiency of the cytoplasm, whilst the right column shows a graph of the FRET efficiency of the nucleus. Strikingly, in contrast to the cytoplasm, the FRET efficiency in the nucleus only contains the interaction at 13% FRET efficiency,

EGFP Image	FRET Efficiency	FRET Efficiency
A. EGFP-Nrf2-doubleETGE + mCherry	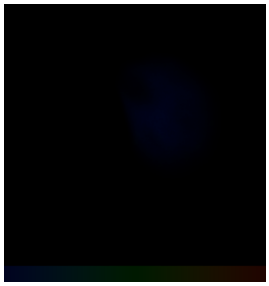 0% 30%	
B. EGFP-Nrf2-doubleETGE + mCherry	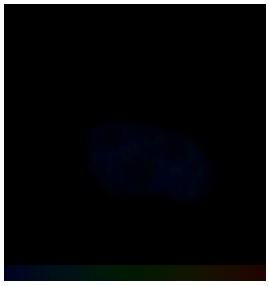 0% 30%	
C. EGFP-Nrf2-doubleETGE + Keap1-mCherry	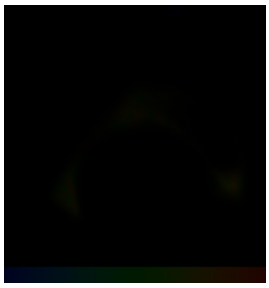 0% 30%	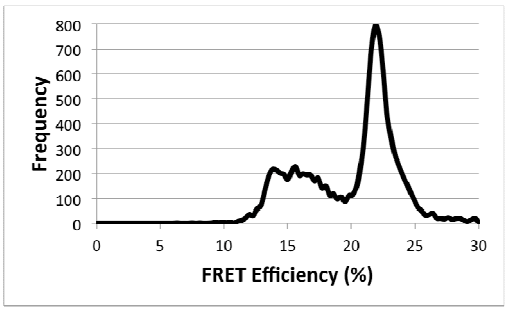
D. EGFP-Nrf2-doubleETGE + Keap1-mCherry	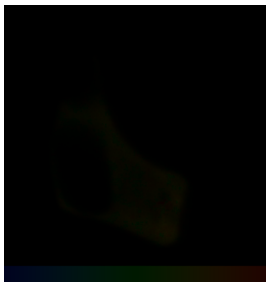 0% 30%	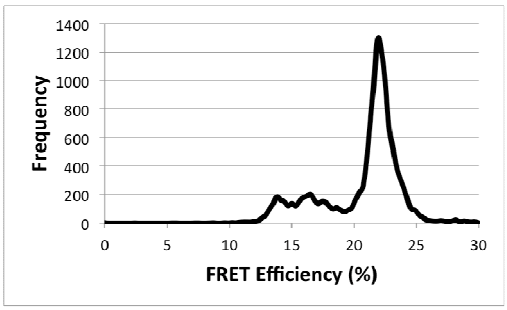

Figure 4.7. FRET efficiency derived from EGFP-Nrf2-doubleETGE lifetime data. HEK293 cells were transfected with either EGFP-Nrf2-doubleETGE + mCherry (A, B) or

EGFP-Nrf2-doubleETGE + Keap1-mCherry (C, D) and imaged 24 hours later. The left column shown the EGFP image from which the FRET efficiency data are derived. The middle column shows a pictorial representation of the FRET efficiency where the colour of the cell corresponds to the FRET efficiency, ranging from 0% to 30% as indicated on the legend below the image. The right column shows the FRET efficiency from each pixel of the image plotted on a graph, with FRET efficiency on the x-axis and frequency on the y-axis. Graphs A-B show that the FRET efficiency in EGFP-Nrf2-doubleETGE and mCherry co-transfected cells is 0%, which corresponds with the blue colour of the cells in A and B. In EGFP-Nrf2-doubleETGE and Keap1-mCherry co-transfected cells (C, D), the FRET efficiency graphs show two distinct peaks, a small one at 13% and a larger one at 21% FRET efficiency, suggesting that there is one major FRET interaction between the EGFP and mCherry fluorophores within the Keap1-Nrf2-doubleETGE complex. The distribution of the two FRET efficiency populations is shown pictorially in the central column of C and D, where the predominant colour is yellow (corresponding to the 21% population), which is distributed evenly throughout the cell, along with a small amount of green (corresponding to the 13% population).

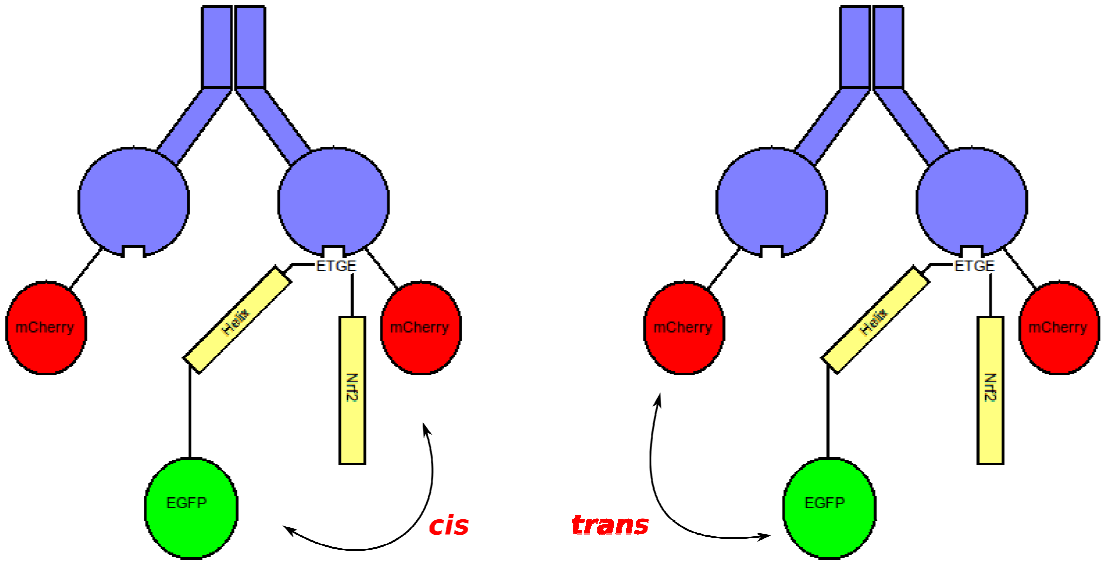

Figure 4.8. The alternate mechanisms through which the 13% FRET efficiency population can be generated. The cartoons show the interaction between EGFP-Nrf2ΔDLG and Keap1-mCherry, where Keap1 is shown in blue, mCherry in red, Nrf2 in yellow and EGFP in green. The FRET interaction which generates the 13% FRET efficiency population could be generated in two different ways: either between the EGFP fluorophore and the mCherry fused to the Keap1 protein which is bound to the ETGE motif (left, FRET in *cis*), or between the EGFP fluorophore and the mCherry fused to the Keap1 protein which is not bound to Nrf2 (right, FRET in *trans*).

suggesting that Nrf2 binds to the Keap1 dimer through only the ETGE motif in the nucleus.

In order to study the nuclear complex more closely, we also calculated the EGFP lifetime and FRET efficiency for the Nrf2 mutants Nrf2ΔDLG and Nrf2-doubleETGE (**Tables 4.4, 4.5, Figures 4.12, 4.13**). In the case of EGFP-Nrf2ΔDLG the lifetime is longer in the nucleus than in the cytoplasm, however the 13% FRET efficiency population is maintained (**Table 4.4, Figure 4.12**). In the case of EGFP-Nrf2-doubleETGE, again the lifetime is increased, and the FRET efficiency changes to include a higher proportion of the interaction at 13% relative to the cytoplasm (**Table 4.5, Figure 4.13**). Interestingly, both Nrf2 mutants only interact with Keap1 through their high affinity ETGE motifs, and yet both show an increased lifetime in the nucleus, and in the case of Nrf2-doubleETGE, a reduction in the interaction at 21% FRET efficiency. Together these data suggest that in the nucleus, the Keap1 dimer binds to the ETGE motif of Nrf2 with a lower affinity, potentially because Keap1 is engaged in binding with another protein or proteins. These other protein(s) appear to be able to completely displace the DLG motif of wild-type Nrf2, and can also compete for binding with the high affinity ETGE motif.

EGFP Image	EGFP Lifetime	EGFP Lifetime

A. EGFP-Nrf2ΔDLG + Keap1-mono-mCherry	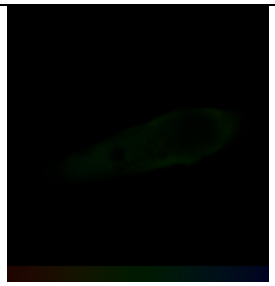 1.9 ns 2.6 ns	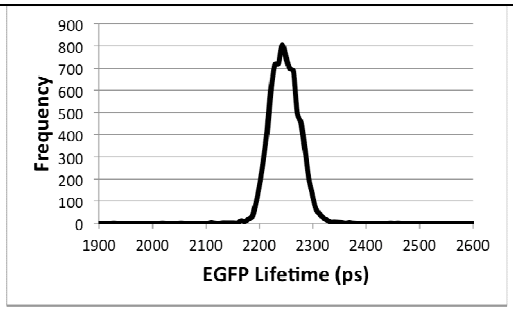
B. EGFP-Nrf2ΔDLG + Keap1-mono-mCherry	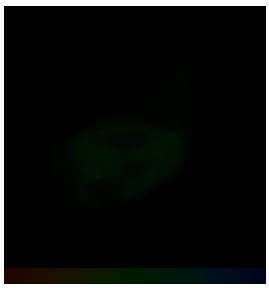 1.9 ns 2.6 ns	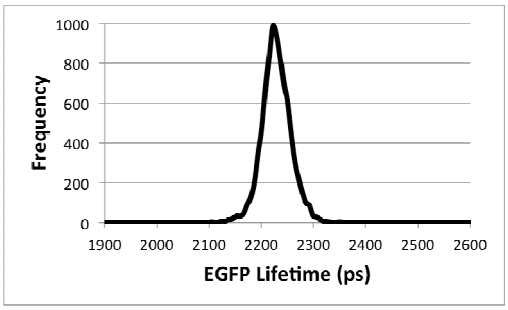
EGFP Image	FRET Efficiency	FRET Efficiency
C. EGFP-Nrf2ΔDLG + Keap1-mono-mCherry	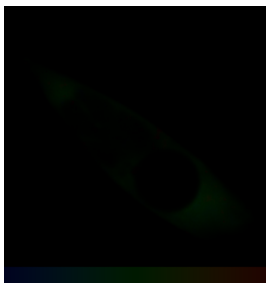 0% 30%	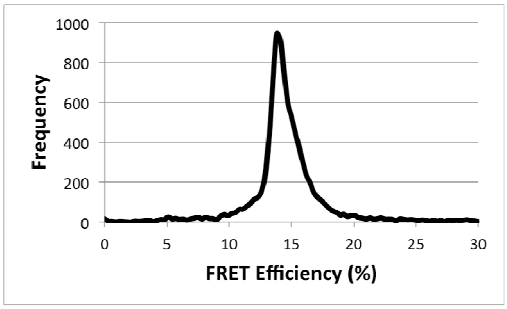
D. EGFP-Nrf2ΔDLG + Keap1-mono-mCherry	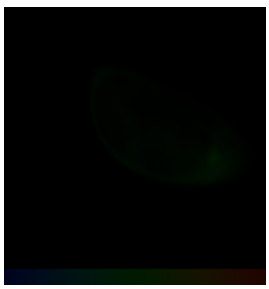 0% 30%	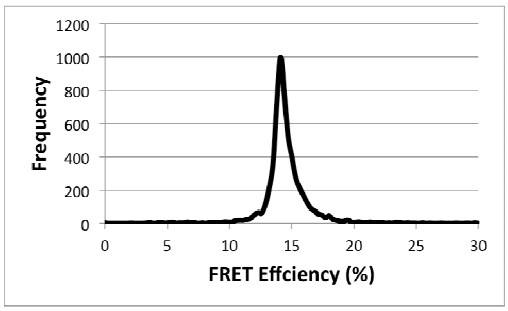

Figure 4.9. FRET efficiency derived from EGFP-Nrf2ΔDLG lifetime data. HEK293 cells were transfected with EGFP-Nrf2ΔDLG + Keap1-mono-mCherry and both the lifetime (A, B) and FRET efficiency (C, D) were calculated. A, B show the fluorescence lifetime data. The left column shows the EGFP image from which the lifetime data are

derived. The middle column shows a pictorial representation of the EGFP lifetime where the colour of the cell corresponds to the lifetime of EGFP, ranging from 1.9 ns to 2.6 ns as indicated on the legend below the image. The right column shows the lifetime data from each pixel of the image plotted on a graph, with lifetime on the x-axis and frequency on the y-axis. Graphs A-B clearly show that the lifetime of EGFP-Nrf2ΔDLG in the presence of Keap1-mono-mCherry is significantly shorter than in the presence of mCherry alone (Figure 4.3 A,B) indicating that there is a FRET interaction between the two fusion proteins. C, D show the FRET efficiency data for EGFP- Nrf2ΔDLG + Keap1-mono-mCherry co-transfected cells.The left column shows the EGFP image from which the FRET efficiency data are derived. The middle column shows a pictorial representation of the FRET efficiency where the colour of the cell corresponds to the FRET efficiency, ranging from 0% to 30% as indicated on the legend below the image. The right column shows the FRET efficiency from each pixel of the image plotted on a graph, with FRET efficiency on the x-axis and frequency on the y-axis. The FRET efficiency graphs (C, D) shows one peak at 13% FRET efficiency, indicating that there is a single FRET interaction between the EGFP and mCherry fluorophores within the Keap1-mono-Nrf2ΔDLG complex. This FRET efficiency population is shown pictorially in the central column of C and D, where the green colour is distributed evenly across the cells.

Keap1-mCherry + EGFP-Nrf2	Cytoplasmic Lifetime (ps)	Nuclear Lifetime (ps)
Cell 1	2152	2201
Cell 2	2173	2215
Cell 3	2152	2194
Cell 4	2173	2222
Cell 5	2138	2180
Cell 6	2138	2187
Cell 7	2152	2187
Cell 8	2159	2180
Cell 9	2110	2145
Cell 10	2138	2173
Cell 11	2166	2236
Cell 12	2187	2236
Cell 13	2152	2215
Cell 14	2166	2243
Cell 15	2145	2215
Cell 16	2152	2215
AVERAGE	2153	2203
SD	18	27
Paired T-test	p = 1.759E-9	

Table 4.3. FLIM data for the cytoplasm and nucleus of EGFP-Nrf2 transfected cells. The table shows the lifetime data for 16 individual cells co-transfected with EGFP-Nrf2 + Keap1-mCherry. The lifetime was separately calculated in the cytoplasm and nucleus of each cell, and a paired T-test was carried out which shows that the lifetime in the nucleus is significantly longer than in the cytoplasm (p = 1.759E-9).

EGFP-Nrf2	Keap1-mCherry

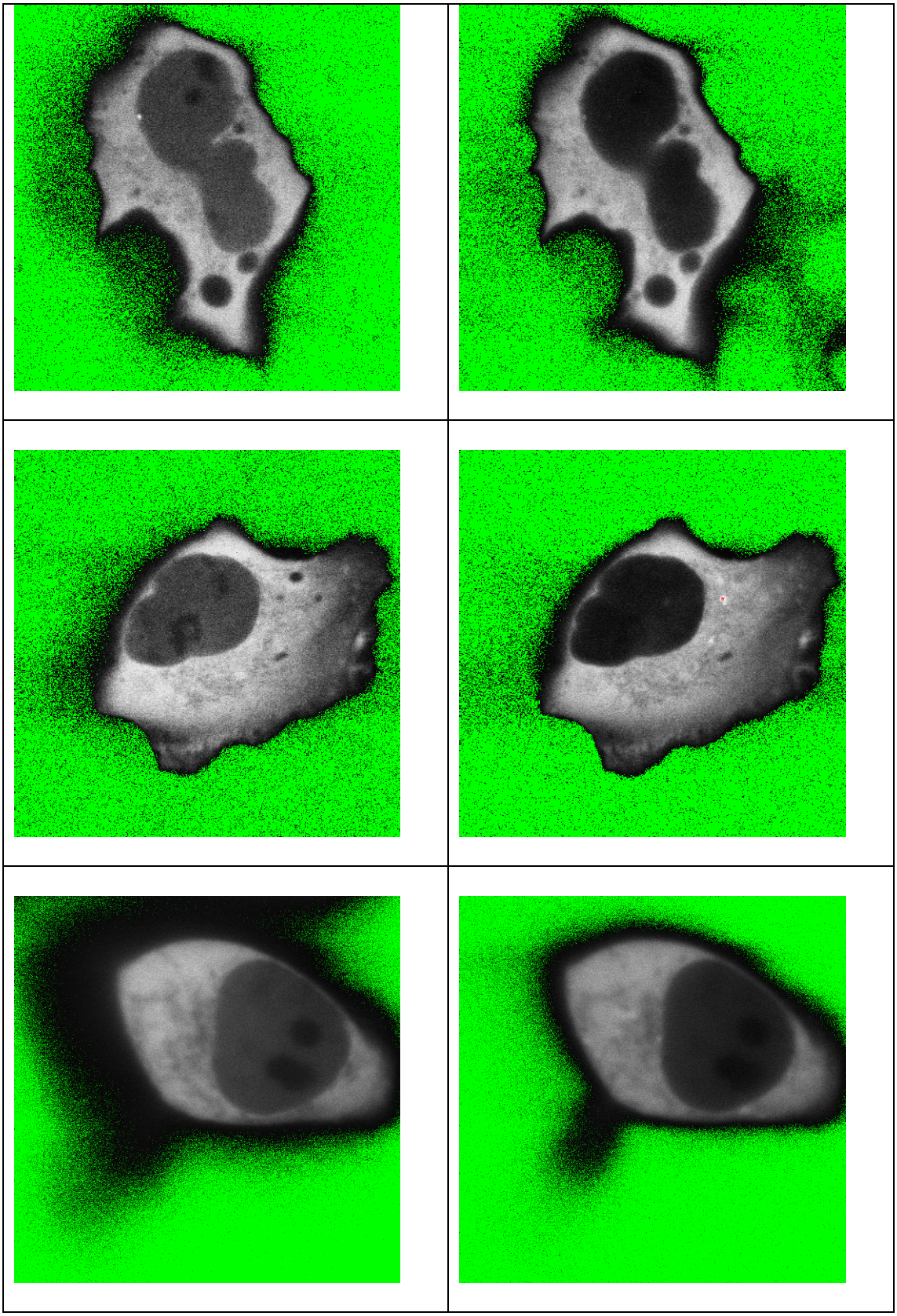

Figure 4.10. Cellular localisation of Nrf2 and Keap1 fusion proteins. HEK293 cells were co-transfected with the EGFP-Nrf2 and Keap1-mCherry expression plasmids and the localisation of the resulting fluorescence was monitored using confocal microscopy. The EGFP channel is shown in the left column, and the mCherry channel in the right

column. In all three cells the distribution of both EGFP-Nrf2 and Keap1-mCherry is similar, with a higher intensity signal for both fusion proteins in the cytoplasm, and a detectable, though weaker signal in the nucleus.

Discussion

The aim of this part of the study was to use the FLIM data to investigate the dynamism of the Keap1-Nrf2 interaction in the basal state, by analysing the FRET efficiency of the interaction. To our knowledge, the only previous example of use of this approach is that of Lleres et al 2009. In this paper, the authors identified 3 distinct FRET efficiency populations in histone labelled chromatin, and found that the relative proportions of these populations changes during mitosis as the chromatin changes its compaction state. In the case of the interaction between EGFP-Nrf2 and Keap1-mCherry, we also saw distinct FRET efficiency populations (**Figure 4.2**). Furthermore, we have advanced the methodology employed in Lleres et al's original study by determining the identity of each of the two distinct FRET populations.

The interaction between Nrf2 and Keap1 is shown schematically in **Figure 4.3A**. The low affinity DLG, and high affinity ETGE motifs of Nrf2 each bind to a member of the Keap1 dimer. This double binding is believed to be required in order to correctly orientate the lysine residues in the helix between the DLG and ETGE motifs for ubiquitination by the Keap1-dependent E3 ubiquitin ligase (McMahon et al. 2006, Tong et al. 2006a). The FRET efficiency of the interaction between wild type EGFP-Nrf2 and Keap1-mCherry is shown with a cartoon of the protein complexes(**Figure 4.14**), and clearly shows 2 distinct populations of FRET efficiency, one at 21% and the other at 13%. Using equation 4.2, these FRET efficiency values can be converted to the physical distances of 56 Å and 64 Å, respectively. This suggests that the protein complex of Keap1 and Nrf2 is found in two distinct conformations, one in which the EGFP and mCherry fluorophores are 56 Å apart, and the other, in which they are 64 Å apart. This idea is initially quite puzzling when considering the current understanding of the interaction in the basal state (**Figure 4.3A**), and suggests that the interaction between Keap1 and Nrf2 is more complex than previously thought.

In order to try to understand what the two FRET efficiency interactions may represent, our first approach was to mutate the low affinity DLG motif in Nrf2, so that Nrf2 can bind to Keap1 through the ETGE motif alone, and test whether this has any impact on the FRET efficiency (**Figure 4.15A**). We found that this interaction generated only the 13% FRET efficiency population,

FRET Efficiency Image	FRET Efficiency: Cytoplasm	FRET Efficiency: Nucleus
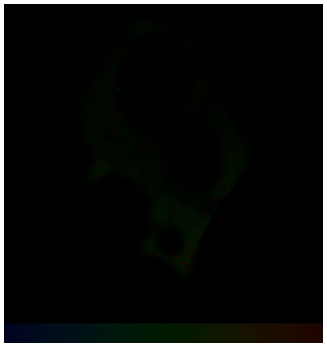 0% 30% A. EGFP-Nrf2 + Keap1-mCherry	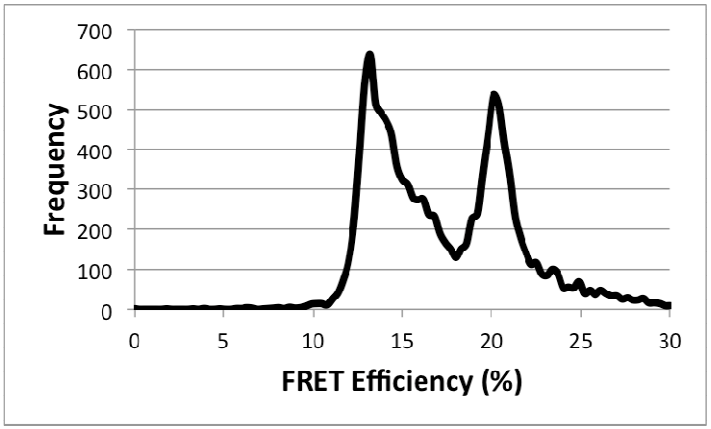	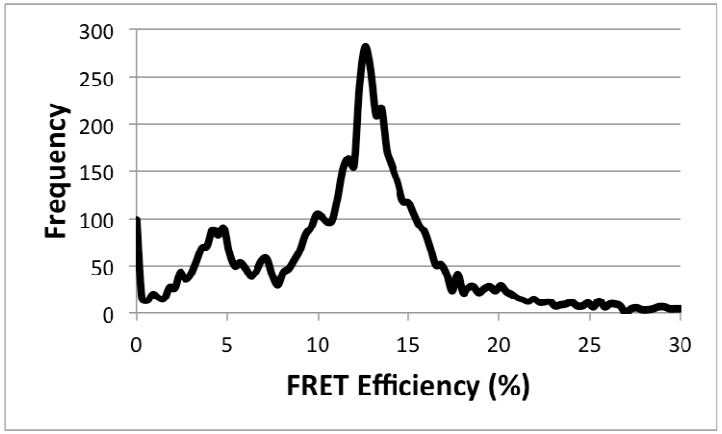
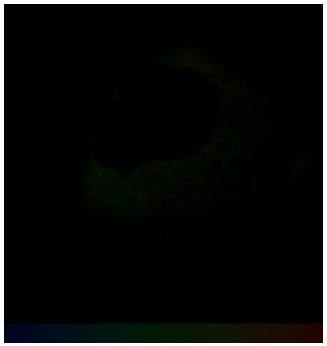 0% 30% B. EGFP-Nrf2 + Keap1-mCherry	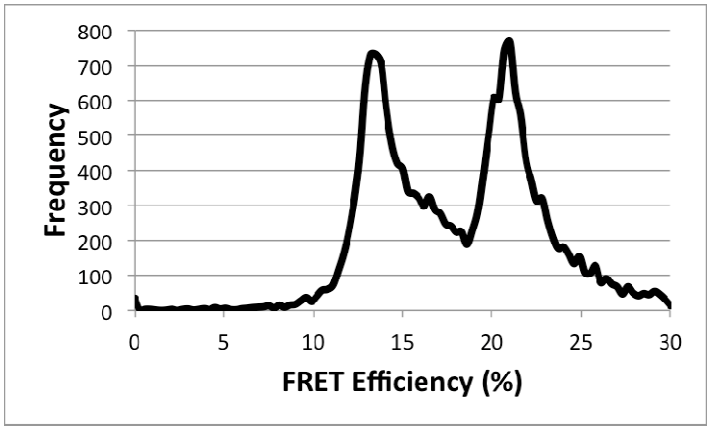	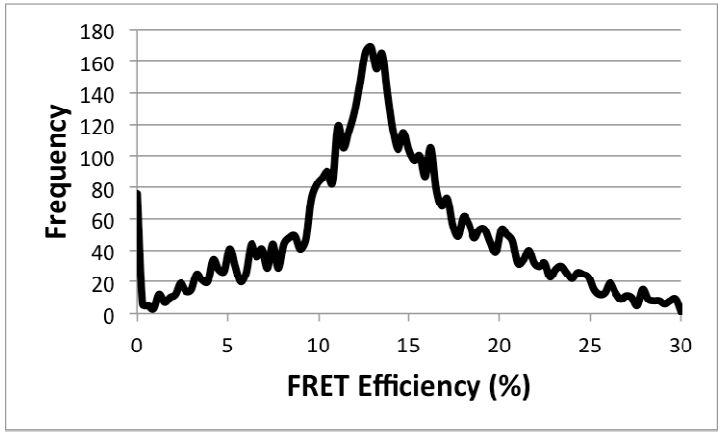

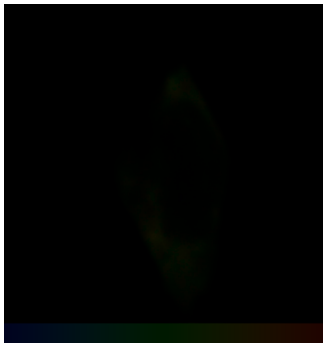

0% 30%

C. EGFP-Nrf2 + Keap1-mCherry

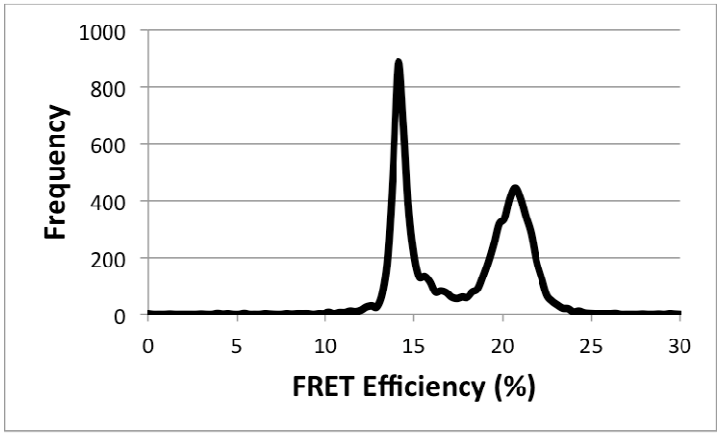

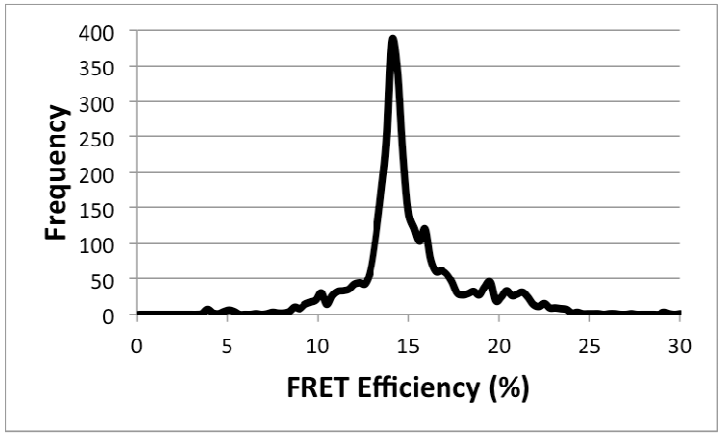

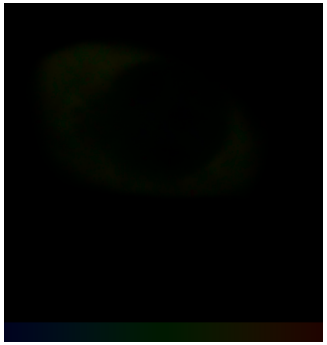

0% 30%

D. EGFP-Nrf2 + Keap1-mCherry

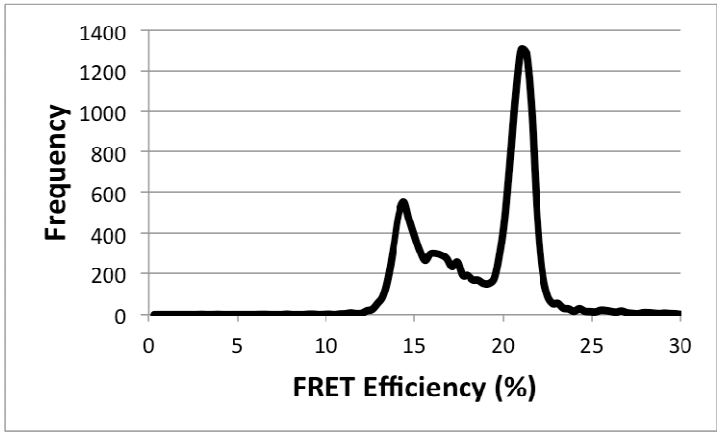

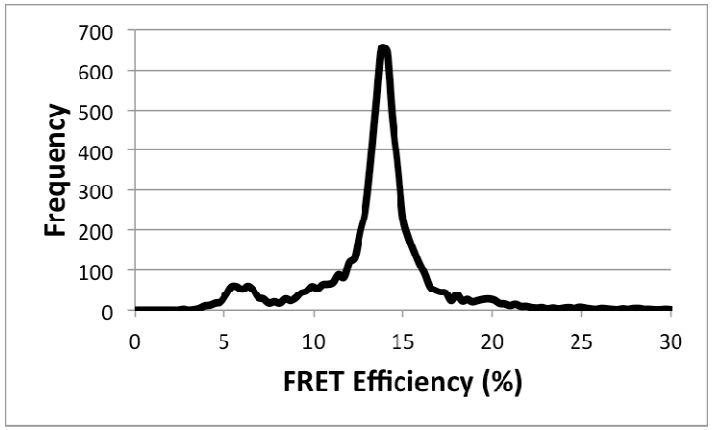

Figure 4.11. FRET efficiency derived from cytoplasmic and nuclear EGFP-Nrf2 lifetime data. HEK293 cells were transfected with EGFP-Nrf2 + Keap1-mCherry and imaged 24 hours later. The left column shows a pictorial representation of the FRET efficiency where the colour of the cell corresponds to the FRET efficiency, ranging from 0% to 30% as indicated on the legend below the image. The central column shows the FRET efficiency from each pixel of the cytoplasm plotted on a graph, with FRET efficiency on the x-axis and frequency on the y-axis. The right column shows the FRET efficiency from each pixel of the nucleus plotted on a graph, with FRET efficiency on the x-axis and frequency on the y-axis. In all cells A-D, the FRET efficiency graphs of the cytoplasmic compartment show two distinct peaks, one at 13% and the other at 21% FRET efficiency, suggesting that there are two different FRET interactions between the EGFP and mCherry fluorophores within the Keap1-Nrf2 complex. In contrast, in all cases A-D the FRET efficiency in the nucleus contains only the FRET efficiency population at 13%, suggesting that in the nucleus there is a single FRET interaction between the EGFP and mCherry fluorophores within the Keap1-Nrf2 complex.

demonstrating that Nrf2 binding to Keap1 though the ETGE motif alone represents the 13% FRET efficiency population. Interestingly, because the DLG mutant Nrf2 never forms the 21% FRET efficiency interaction, it suggests that when Nrf2 is bound to Keap1 by both the ETGE and DLG motifs this must represent the 21% FRET efficiency interaction. In addition, because wild type Nrf2 produces a FRET efficiency distribution with both the 13% and 21%

Keap1-mCherry + EGFP-Nrf2ΔDLG	Cytoplasmic Lifetime (ps)	Nuclear Lifetime (ps)
Cell 1	2236	2250
Cell 2	2229	2236
Cell 3	2208	2222
Cell 4	2194	2257
Cell 5	2208	2243
Cell 6	2236	2299
Cell 7	2250	2285
Cell 8	2229	2264
Cell 9	2222	2257
Cell 10	2229	2268
AVERAGE	2224	2258
SD	17	23
Paired T-test	p = 0.000307	

Table 4.4. FLIM data for the cytoplasm and nucleus of EGFP-Nrf2ΔDLG transfected cells. The table shows the lifetime data for 16 individual cells co-transfected with EGFP-Nrf2ΔDLG + Keap1-mCherry. The lifetime was separately calculated in the cytoplasm and nucleus of each cell, and a paired T-test was carried out which shows that the lifetime in the nucleus is significantly longer than in the cytoplasm (p = 0.000307).

FRET Efficiency Image	FRET Efficiency: Cytoplasm	FRET Efficiency: Nucleus
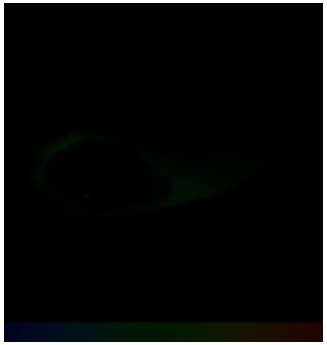 0% 30% A. EGFP-Nrf2**Δ**DLG + Keap1-mCherry	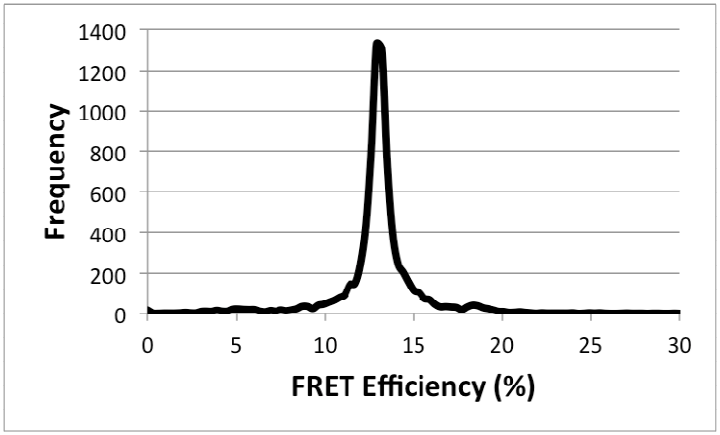	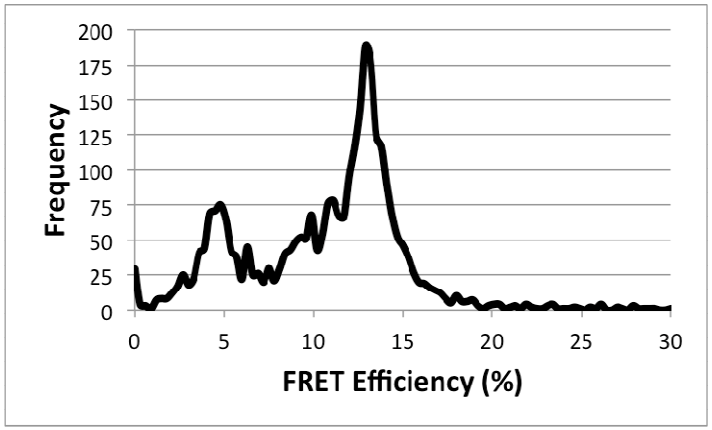
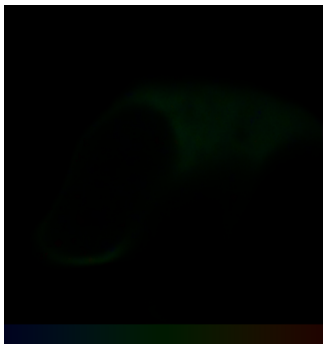 0% 30% B. EGFP-Nrf2 **Δ**DLG + Keap1-mCherry	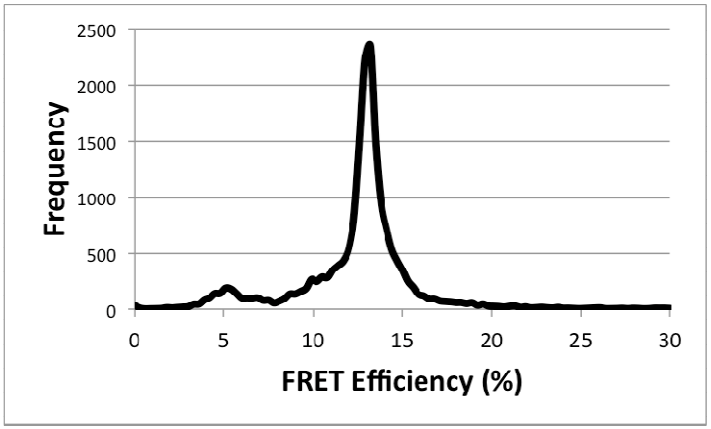	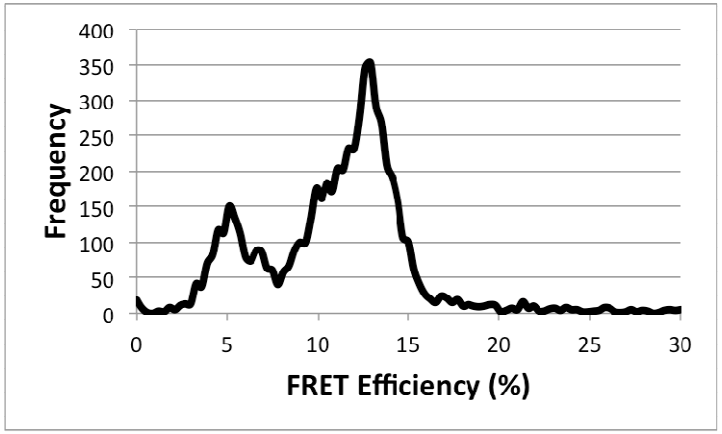

Figure 4.12. FRET efficiency derived from cytoplasmic and nuclear EGFP-Nrf2ΔDLG lifetime data. HEK293 cells were transfected with EGFP-Nrf2ΔDLG + Keap1-mCherry and imaged 24 hours later. The left column shows a pictorial representation of the FRET efficiency where the colour of the cell corresponds to the FRET efficiency, ranging from 0% to 30% as indicated on the legend below the image. The central column shows the FRET efficiency from each pixel of the cytoplasm plotted on a graph, with FRET efficiency on the x-axis and frequency on the y-axis. The right column shows the FRET efficiency from each pixel of the nucleus plotted on a graph, with FRET efficiency on the x-axis and frequency on the y-axis. In all cells, the FRET efficiency graphs of the cytoplasmic compartment show one peak at 13% FRET efficiency, suggesting that there is a single FRET interaction between the EGFP and mCherry fluorophores within the Keap1- Nrf2ΔDLG complex. The FRET efficiency in the nucleus also contains only the FRET efficiency population at 13%, suggesting that, as with the cytoplasm, in the nucleus there is a single FRET interaction between the EGFP and mCherry fluorophores within the Keap1- Nrf2ΔDLG complex.

Keap1-mCherry + EGFP-Nrf2-doubleETGE	Cytoplasmic Lifetime (ps)	Nuclear Lifetime (ps)
Cell 1	2082	2096
Cell 2	2054	2061
Cell 3	2082	2089
Cell 4	2089	2103
Cell 5	2117	2180
Cell 6	2096	2124
Cell 7	2096	2138
Cell 8	2096	2103
Cell 9	2103	2117
Cell 10	2075	2096
Cell 11	2110	2124
Cell 12	2089	2124
Cell 13	2117	2156
AVERAGE	2093	2116
SD	18	31
Paired T-test	p = 0.000326	

Table 4.5. FLIM data for the cytoplasm and nucleus of EGFP-Nrf2-doubleETGE transfected cells. The table shows the lifetime data for 13 individual cells co-transfected with EGFP-Nrf2-doubleETGE + Keap1-mCherry. The lifetime was separately calculated in the cytoplasm and nucleus of each cell, and a paired T-test was carried out which shows that the lifetime in the nucleus is significantly longer than in the cytoplasm ($p = 0.000326$).

FRET Efficiency Image	FRET Efficiency: Cytoplasm	FRET Efficiency: Nucleus
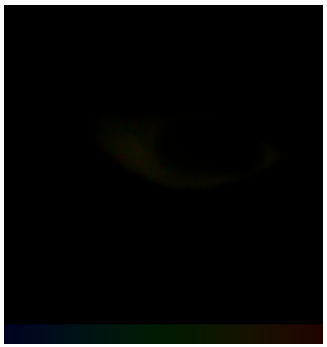 0% 30% A. EGFP-Nrf2-doubleETGE + Keap1-mCherry	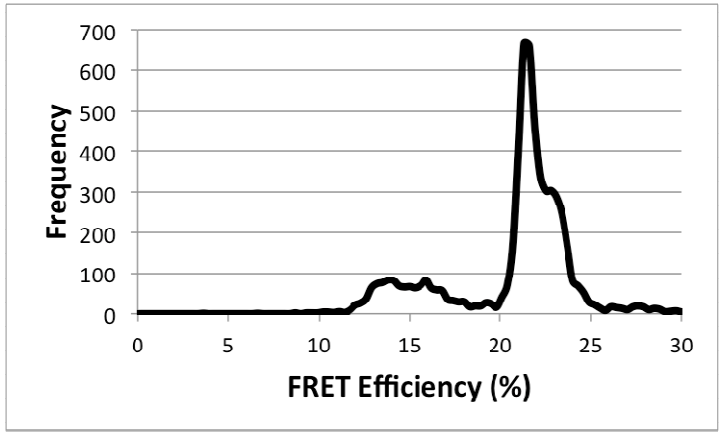	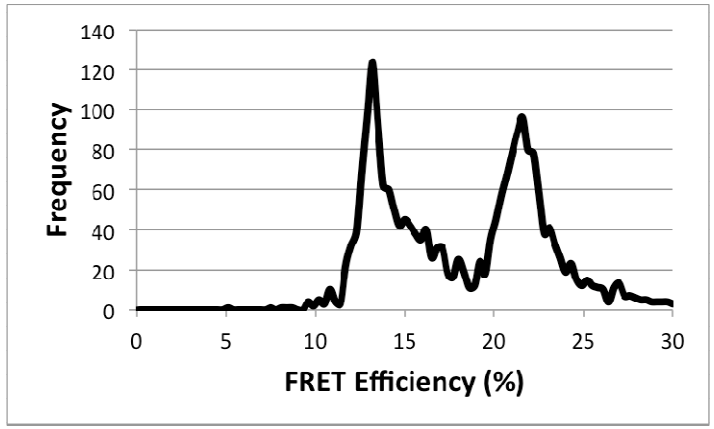
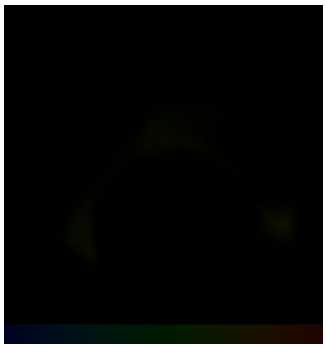 0% 30% B. EGFP-Nrf2-doubleETGE + Keap1-mCherry	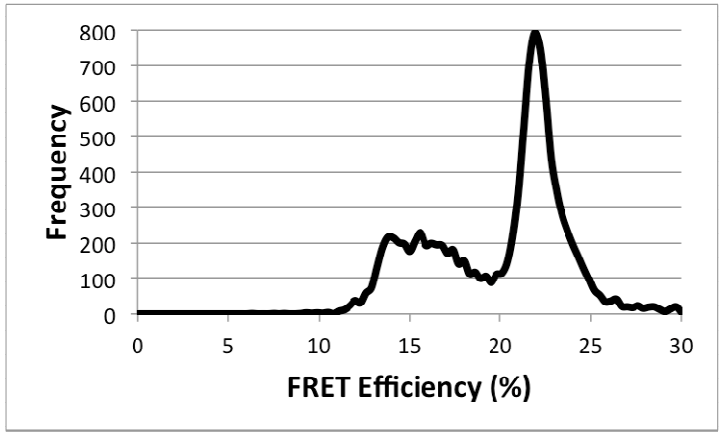	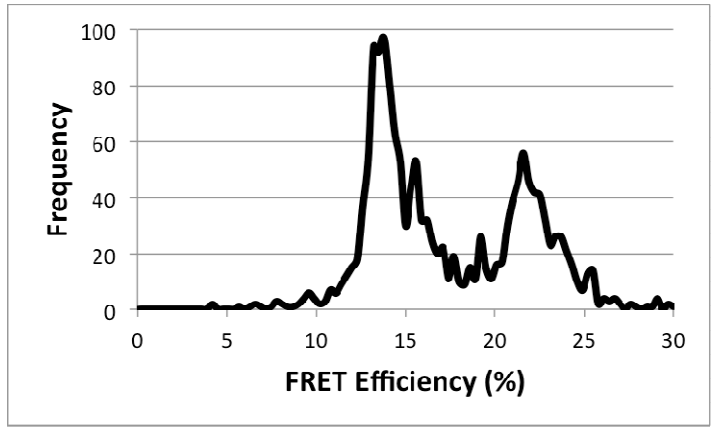

Figure 4.13. FRET efficiency derived from cytoplasmic and nuclear EGFP-Nrf2-doubleETGE lifetime data. HEK293 cells were transfected with EGFP-Nrf2-doubleETGE + Keap1-mCherry and imaged 24 hours later. The left column shows a pictorial representation of the FRET efficiency where the colour of the cell corresponds to the FRET efficiency, ranging from 0% to 30% as indicated on the legend below the image. The central column shows the FRET efficiency from each pixel of the cytoplasm plotted on a graph, with FRET efficiency on the x-axis and frequency on the y-axis. The right column shows the FRET efficiency from each pixel of the nucleus plotted on a graph, with FRET efficiency on the x-axis and frequency on the y-axis. In both A and B, the FRET efficiency graphs of the cytoplasmic compartment show two distinct peaks, a major peak at 21% FRET efficiency and a minor peak at 13% FRET efficiency, suggesting that there is predominantly one FRET interactions between the EGFP and mCherry fluorophores within the Keap1-Nrf2-doubleETGE complex. In contrast, the FRET efficiency in the nucleus contains a more equal distribution between the 21% and 13% FRET efficiency populations, indicating that there are two distinct FRET interactions between the EGFP and mCherry fluorophores within the Keap1-Nrf2-doubleETGE complex in the nucleus.

populations it implies that the Keap1-Nrf2 complex is found in 2 distinct states in cells, one in which the only the ETGE motif is bound to Keap1 (the "open conformation"), and one in which both the DLG and ETGE motifs are bound (the "closed conformation"). The idea that a single Keap1-Nrf2 complex conformation could generate both FRET efficiency interactions was rejected through the use of a mutant Nrf2 with two high affinity ETGE motifs (**Figure 4.15B**). This mutant Nrf2 bound more tightly to Keap1, and increased the abundance of the 21% FRET efficiency population relative to the 13%.

Together these data show that in wild type Nrf2, the presence of the weakly binding DLG motif is required for the formation of the 13% FRET efficiency population (when it is unbound) and for the formation of the 21% FRET efficiency population (when it is bound, **Figure 4.14**). These data suggest that nature has chosen a more elaborate mechanism through which Nrf2 is regulated by Keap1; Nrf2 is not simply bound or unbound, but can also be found in a third, half-bound state, which we call the "open conformation".

Interestingly, the open conformation is the predominant state in which the Keap1-Nrf2 complex is found in the nucleus (**Figure 4.11**). The fact that the DLG motif is never bound to Keap1 in the nucleus suggests that some other protein is able to outcompete it in that compartment. Interestingly, both the Nrf2-doubleETGE and the Nrf2ΔDLG mutants also show a longer lifetime in the nucleus, coupled with reduced FRET efficiency. Together these data suggest that

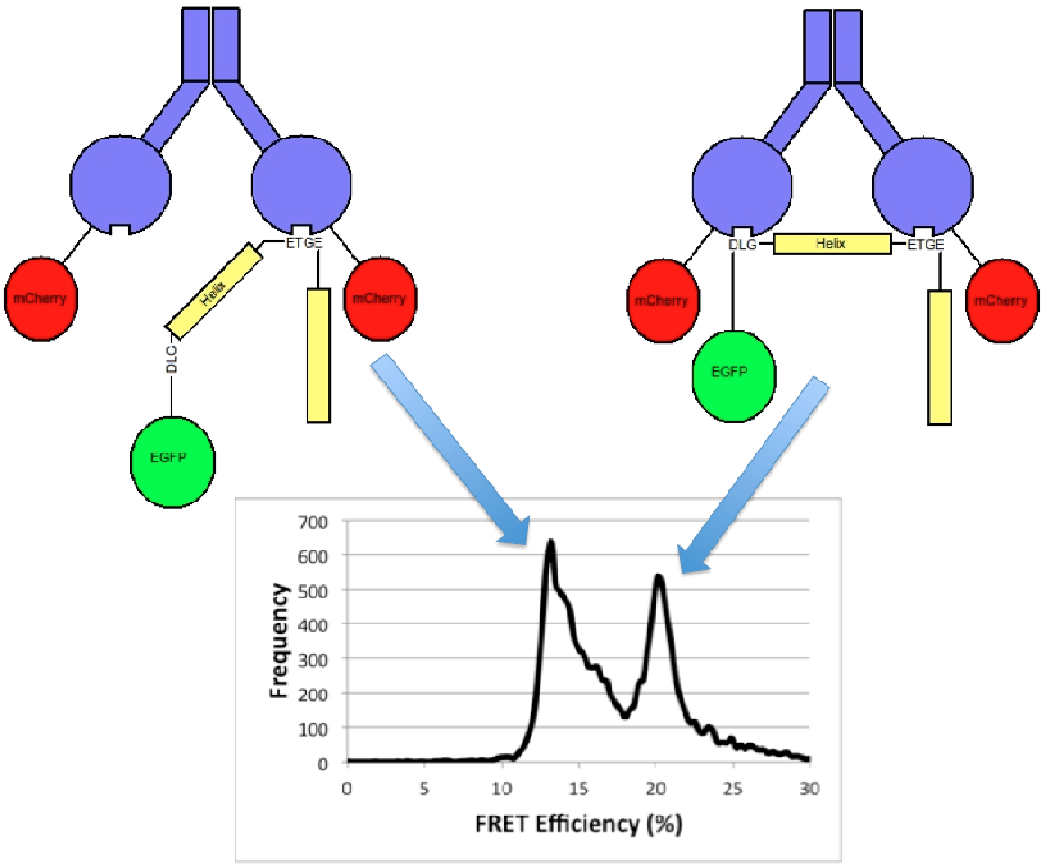

Figure 4.14. The open and closed conformations of the Keap1-Nrf2 complex. The interactions between Keap1 and Nrf2 are shown schematically above the FRET efficiency distribution. In the images, Keap1 is shown in blue, mCherry in red, Nrf2 in yellow and EGFP in green. On the left, the Keap1-Nrf2 complex is shown in the open conformation, in which only the ETGE motif of Nrf2 is bound to the Keap1 dimer. This conformation generates the 13% FRET efficiency population shown in the graph. On the right, the closed conformation is shown, where both the DLG and ETGE motifs of Nrf2 are bound to the Keap1 dimer. This conformation generates the 21% FRET efficiency population shown below in the graph.

the additional nuclear partner of Keap1 is also able to compete with the ETGE motif for binding, as both of these Nrf2 mutants only contain high affinity ETGE motifs, yet both exhibit reduced binding (**Figures 4.11, 4.12, Tables 4.4, 4.5**).

Previous studies have shown that at least some of the cellular pool of Keap1 is able to enter the nucleus (Nguyen et al. 2005, Watai et al. 2007, Sun et al. 2011, Kaspar et al. 2012). Interestingly, in addition to Nrf2, Keap1 has also been shown to bind to two nuclear proteins, Prothymosin-α and Palb2, either of

Cartoon of Keap1-Nrf2 interaction	FRET Efficiency

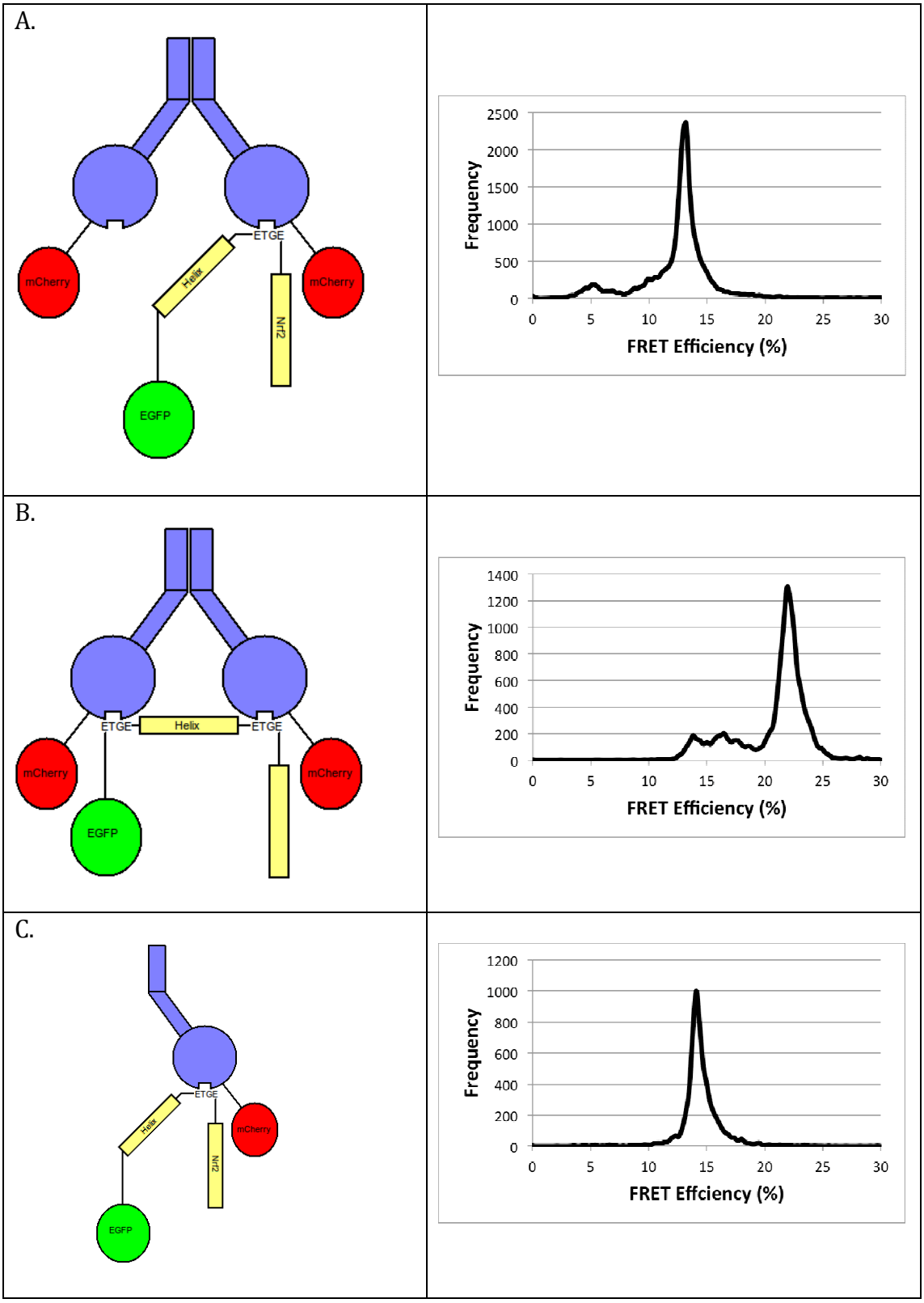

Figure 4.15. Complexes of mutant Nrf2 and Keap1 with corresponding representative FRET efficiency graphs. In the left column the different combinations of mutant Nrf2 and wild type or mutant Keap1 proteins used in Chapter 4, and the ways in which they interact, are shown schematically in the cartoons. In the right column, representative FRET efficiency graphs are shown for the combinations of proteins shown in the adjacent cartoon. In all images, Keap1 is shown in blue, mCherry in red,

Nrf2 in yellow and EGFP in green. **A.** Shows the interaction between Nrf2ΔDLG and wild-type Keap1. This mutant of Nrf2 interacts with the Keap1 dimer through only its high affinity ETGE motif, and generates a single FRET efficiency interaction at 13%. **B.**Shows the interaction between Nrf2-doubleETGE and wild-type Keap1. This mutant interacts with Keap1 through two high affinity ETGE motifs, and generates a FRET efficiency profile with a major peak at 21% and a minor peak at 13% FRET efficiency. **C.** Shows the interaction between Nrf2ΔDLG and Keap1-mono-mCherry. This Keap1 mutant cannot dimerise, and generates a FRET efficiency distribution with one peak at 13% FRET efficiency.

which could be responsible for the displacement of the DLG motif of Nrf2 in the nucleus.

Prothymosin-α is a ubiquitous protein which is involved in cellular proliferation and protection against apoptosis (Karapetian et al. 2005, Niture et al. 2009). The crystal structure of the ENGE motif of Prothymosin-α bound to the Kelch domain of Keap1 has been solved and shows that the proteins bind at the same site as both the ETGE and DLG motifs of Nrf2 (Padmanabhan et al. 2008). Palb2 is a DNA repair protein, and contains a conserved ETGE motif through which it competes for binding of Keap1 with Nrf2 in the nucleus (Ma et al. 2012). Both of these proteins have previously been shown to bind to Keap1 at the same site as the ETGE and DLG motifs of Nrf2, and thus either or both proteins could be responsible for the loss of DLG binding in the nucleus and absence of the Keap1-Nrf2 complex in the closed conformation.

Chapter 5: High-resolution analysis of the Keap1-Nrf2 complex in the induced state

Introduction

In Chapter 4 we presented data which suggested that in the basal state the Keap1-Nrf2 complex is found in two distinct states, the open and closed conformations. The existence of an open conformation has previously been proposed (but never shown) independently by the Yamamoto and Hayes labs (McMahon et al. 2006, Tong et al. 2006a). They suggested that binding of inducers leads to the release of the low affinity DLG motif from the Keap1 dimer, resulting in the inhibition of Nrf2 ubiquitination (**Figure 1.4**). This mechanism is known as the "hinge and latch model" of Nrf2 regulation, and was proposed in order to explain why Nrf2 contains binding motifs with such differing affinities for Keap1 (the DLG motif binds Keap1 with a 100-fold lower affinity than the ETGE motif).

Interestingly, in the hinge and latch model, the position in which the latch is unhooked directly corresponds to the "open conformation" which we observe Keap1 and Nrf2 form in the basal state. The experiments in Chapter 4 are concerned with the interaction between Keap1 and Nrf2 in the basal state, but we also wished to examine whether the relative proportions of the open and closed conformations are affected by the addition of inducers and the activation of the pathway. This will allow us to directly test the hinge and latch model to determine whether it is correct, or whether a new model is required to fully explain the mode by which Keap1 regulates Nrf2 protein levels in response to inducers.

Aim

The aim of this part of the study is to use FLIM-generated FRET efficiency data to investigate how the interaction between Keap1 and Nrf2 changes (if at all) in response to inducers.

Results

In order to determine what effect, if any, inducers have on the conformation of the Keap1-Nrf2 complex, we wished to calculate the FRET efficiency of the interaction in the induced state and compare it to the basal state. Because variation is seen in the FRET efficiency distribution between cells in the basal state (**Figure 4.2**), we wished to image the same cell in both the basal and induced state, to obtain a more accurate picture of the effects of inducers in individual cells.

In response to inducers, Nrf2 accumulates within 1 hour, and thus we reasoned that this would be a good time point at which to study the Keap1-Nrf2 interaction (**Figure 3.2**) (McMahon et al. 2003, Nguyen et al. 2003). Because this experimental approach would involve imaging the same cell twice over a period of 1 hour, it was essential to establish that the EGFP lifetime is stable over this time period independent of the activity of inducers. As shown in **Figure 5.1A,B** and **Table 5.1**, the lifetime of EGFP-Nrf2 was unchanged when imaged twice, one hour apart, in the basal state. Importantly, the FRET efficiency distribution was also unaffected by repeated imaging (**Figure 5.1C,D**), showing that imaging a cell twice affects neither the EGFP lifetime nor the FRET efficiency distribution in EGFP-Nrf2 + Keap1-mCherry co-transfected cells.

We have previously shown that in response to inducers, Nrf2 is not released from Keap1, as the lifetime of EGFP-Nrf2 is still reduced compared with the control when inducers are added (**Chapter 3**). Therefore, we anticipated that inducers may lead to a change in the conformation if the Keap1-Nrf2 complex, but not to the dissociation of the proteins. **Figure 5.2** shows representative data from EGFP-Nrf2 + Keap1-mCherry co-transfected cells, imaged before and 1 hour after 5 μM SFN treatment. In the left column of **Figure 5.2**, the EGFP image is shown from which the lifetime and FRET efficiency data are derived. In the central column, the corresponding false-colour images of the cells are shown depicting either the EGFP lifetime (A, B) or FRET efficiency (C, D), with the colour of the cell corresponding to the legend beneath the image. In the right column, the graph of either the EGFP lifetime (A, B) or FRET efficiency (C, D) is shown, with the lifetime (or FRET efficiency) from each pixel of the cytoplasm plotted on the x-axis, and the frequency on the y-axis. From **Figure 5.2A,B**, it is clear that in

EGFP Image	EGFP Lifetime	EGFP Lifetime

A. Cell 1	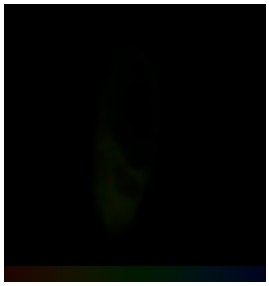 1.9 ns 2.6 ns	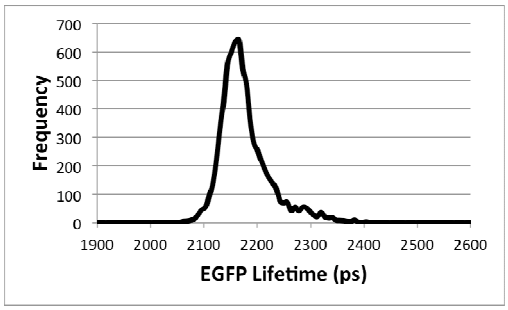
B. Cell 1 + 1 hr	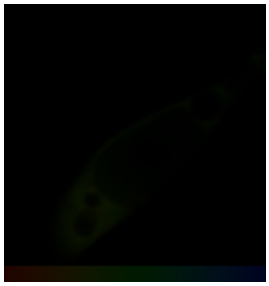 1.9 ns 2.6 ns	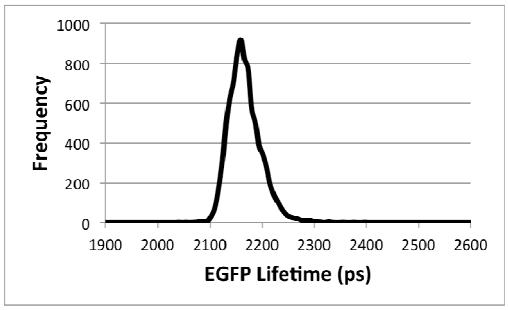
EGFP Image	FRET Efficiency	FRET Efficiency
C. Cell 2	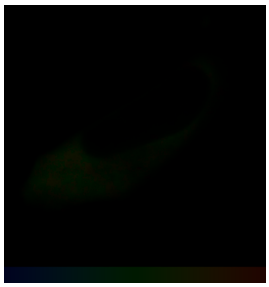 0% 30%	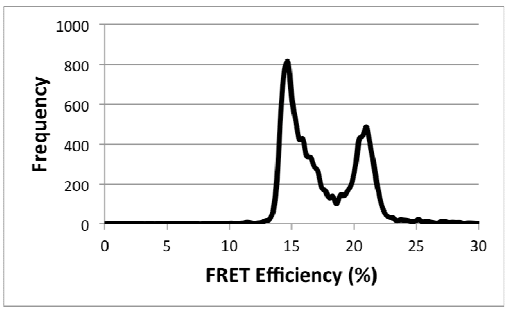
D. Cell 2 + 1 hr	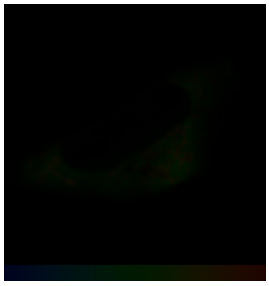 0% 30%	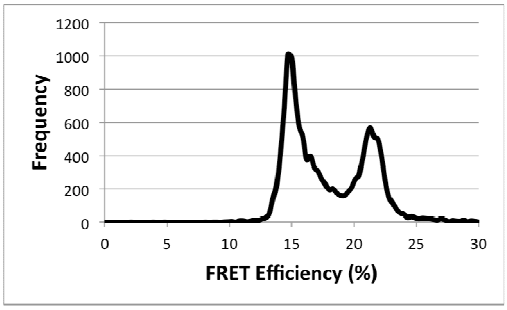

Figure 5.1. The lifetime and FRET efficiency of EGFP-Nrf2 transfected cells imaged twice in an 1 hour period. HEK293 cells were transfected with EGFP-Nrf2 + Keap1-mCherry and both the lifetime (A, B) and FRET efficiency (C, D) were calculated. A, B show the fluorescence lifetime data from a single cell imaged twice, the second image being taken 1 hour after the first. The left column shows the EGFP image from which the lifetime data are derived. The middle column shows a pictorial representation of the EGFP lifetime where the colour of the cell corresponds to the lifetime of EGFP, ranging from 1.9 ns to 2.6 ns as indicated on the legend below the image. The right column

shows the lifetime data from each pixel of the image plotted on a graph, with lifetime on the x-axis and frequency on the y-axis. Graphs A-B clearly show that the lifetime of EGFP-Nrf2 is stable over a 1 hour period in the basal state. C, D show the FRET efficiency data for a single EGFP- Nrf2 + Keap1-mCherry co-transfected cell data which was imaged twice, the second image being taken 1 hour after the first.The left column shown the EGFP image from which the FRET efficiency data are derived. The middle column shows a pictorial representation of the FRET efficiency where the colour of the cell corresponds to the FRET efficiency, ranging from 0% to 30% as indicated on the legend below the image. The right column shows the FRET efficiency from each pixel of the image plotted on a graph, with FRET efficiency on the x-axis and frequency on the y-axis. The FRET efficiency graphs (C, D) show that the FRET efficiency distribution in the basal state is stable over a 1 hour period. The FRET efficiency distributions are shown pictorially in the central column of C and D, where the green and yellow colours are distributed evenly across the cell.

the induced state, the graph of the lifetime of EGFP-Nrf2 in the cytoplasm is shifted to the left compared to the basal state, corresponding to a reduced lifetime in the induced state. This means that the EGFP and mCherry fluorphores are closer together in the induced state, suggesting that there is a tighter interaction between Keap1 and Nrf2, and more FRET upon the addition of SFN. Interestingly, **Table 5.2** shows that this effect is very reproducible and that the reduction in EGFP-Nrf2 lifetime after 1 hour treatment with 5 μM SFN treatment is statistically significant ($p = 0.009$).

	T_1 Lifetime (ps)	T_1 + 1 hr Lifetime (ps)
Cell 1	2138	2131
Cell 2	2117	2117
Cell 3	2166	2159
Cell 4	2145	2138
Cell 5	2103	2103
Cell 6	2152	2152
AVERAGE	2136.8	2133.3

Table 5.1. Lifetime of EGFP-Nrf2 in individual cells imaged twice, 1 hour apart. HEK293 cells were co-transfected with EGFP-Nrf2 and Keap1-mCherry and imaged 24 hours later. The table shows the lifetime of EGFP fluorescence in cells imaged twice in the basal state, with 1 hour between images. The table shows that the EGFP-Nrf2 lifetime is very stable over a 1 hour time period and is unaffected by multiple imaging ($p > 0.05$).

EGFP Image	EGFP Lifetime	EGFP Lifetime

A. Cell 1	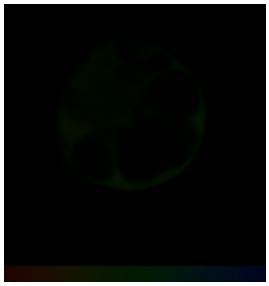 1.9 ns 2.6 ns	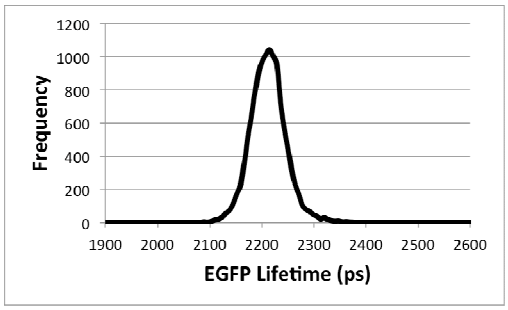
B. Cell 1 + 1 hr SFN	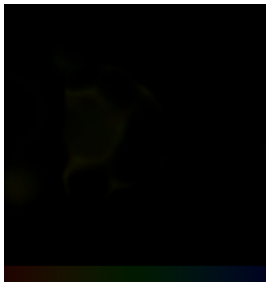 1.9 ns 2.6 ns	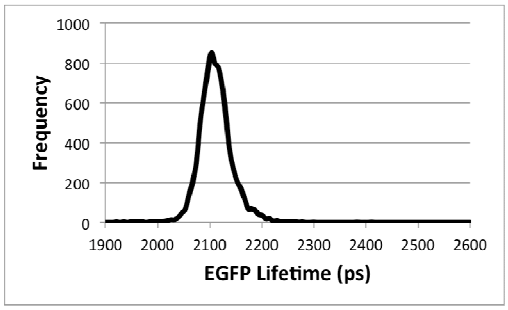
EGFP Image	FRET Efficiency	FRET Efficiency
C. Cell 2	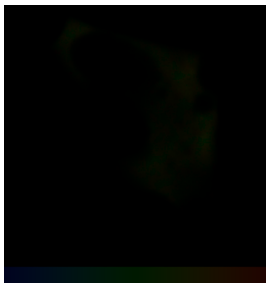 0% 30%	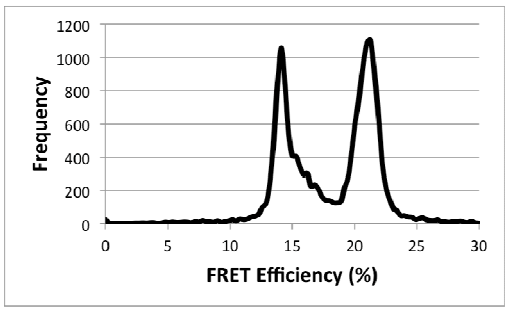
D. Cell 2 + 1 hr SFN	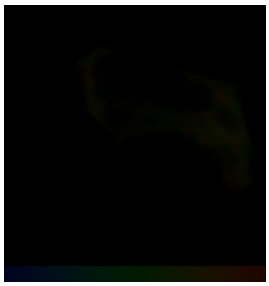 0% 30%	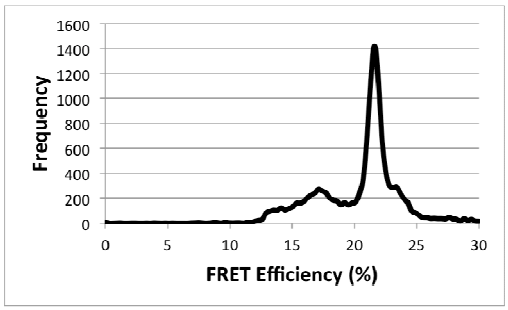

EGFP Image	FRET Efficiency	FRET Efficiency

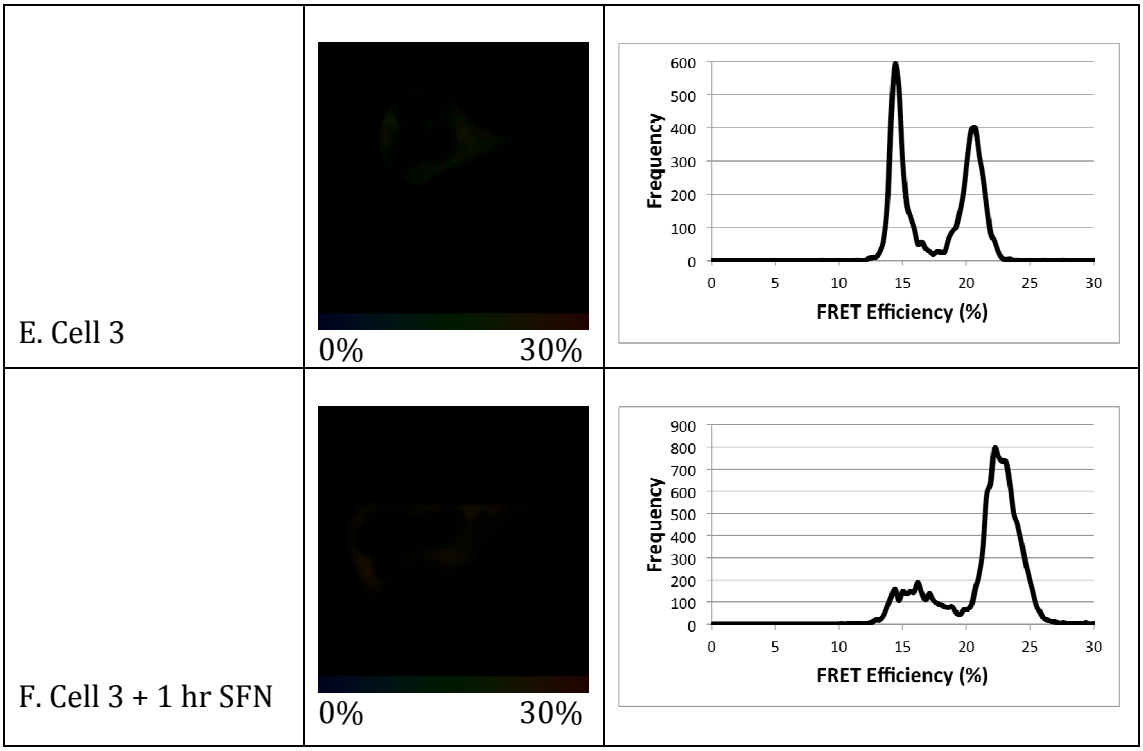

Figure 5.2. The lifetime and FRET efficiency in the cytoplasm of EGFP-Nrf2 transfected cells imaged before and after treatment with SFN. HEK293 cells were transfected with EGFP-Nrf2 + Keap1-mCherry, and both the lifetime (A, B) and FRET efficiency (C-F) in the cytoplasmic compartment were calculated. A, B show the fluorescence lifetime data from a single cell imaged twice, once in the basal state (A) and once after 1 hour treatment with 5μM SFN (B). The left column shows the EGFP image from which the lifetime data are derived. The middle column shows a pictorial representation of the EGFP lifetime where the colour of the cell corresponds to the lifetime of EGFP, ranging from 1.9 ns to 2.6 ns as indicated on the legend below the image. The right column shows the lifetime data from each pixel of the image plotted on a graph, with lifetime on the x-axis and frequency on the y-axis. Graphs A-B clearly show that the lifetime of EGFP-Nrf2 is reduced after treatment with SFN for 1 hour. C-F show the FRET efficiency data for individual EGFP-Nrf2 + Keap1-mCherry co-transfected cells which were imaged twice, once in the basal state (C, E) and once after 1 hour treatment with 5μM SFN (D, F)**.** The left column shown the EGFP image from which the FRET efficiency data are derived. The middle column shows a pictorial representation of the FRET efficiency where the colour of the cell corresponds to the FRET efficiency, ranging from 0% to 30% as indicated on the legend below the image. The right column shows the FRET efficiency from each pixel of the image plotted on a graph, with FRET efficiency on the x-axis and frequency on the y-axis. The FRET efficiency graphs (C-F) show that the FRET efficiency distribution is altered by SFN, which leads to an increase in the interaction at 21% FRET efficiency. The FRET efficiency distributions are shown pictorially in the central column of C-F, where an increase in the amount of yellow relative to green can be seen in response to SFN.

Gratifyingly, this reduction in lifetime upon SFN treatment is coupled with a change in the FRET efficiency. As shown in **Figure 5.2C** and **5.2E**, in the basal

state the cytoplasmic Keap1-Nrf2 complex was found equally distributed in the open (13% FRET efficiency population) and closed conformations (21% FRET efficiency population). However, after treatment with SFN, the FRET efficiency dramatically shifts to favour the closed conformation (**Figure 5.2D,F**).

This result was not specific to the Cys-151 targeting inducer SFN, as STCA, which targets Cys-273 and Cys-288 of Keap1, produced comparable results. After 1 hour treatment with 10 μM STCA, the lifetime of EGFP-Nrf2 in the cytoplasm was significantly reduced (**Figure 5.4A,B, Table 5.3**), and the FRET efficiency distribution was shifted to favour the 21% FRET efficiency population, corresponding to the closed conformation (**Figure 5.4C,D**).

Interestingly, the effect of inducers on the lifetime of EGFP-Nrf2 and the conformation of the Keap1-Nrf2 complex was not restricted to the cytoplasm. SFN treatment lead to a significant decrease in EGFP-Nrf2 lifetime in the nucleus, which was correlated with a modest increase in the proportion of the Keap1-Nrf2 complex in the closed conformation (**Table 5.2, Figure 5.3**).

Keap1-mCherry + EGFP-Nrf2	Basal Cytoplasmic Lifetime (ps)	SFN Induced Cytoplasmic Lifetime (ps)		Basal Nuclear Lifetime (ps)	SFN Induced Nuclear Lifetime (ps)
Cell 1	2215	2103		2264	2124
Cell 2	2138	2089		2180	2138
Cell 3	2152	2110		2194	2159
Cell 4	2198	2173		2271	2257
Cell 5	2166	2117		2208	2124
Cell 6	2131	2096		2187	2117
AVERAGE	2167	2115		2217	2153
SD	34	30		40	53
Paired T-test	p = 0.009			p = 0.017	

Table 5.2. Lifetime of EGFP-Nrf2 in individual cells imaged before and after SFN treatment. HEK293 cells were co-transfected with EGFP-Nrf2 and Keap1-mCherry and imaged 24 hours later. The table shows the lifetime of EGFP fluorescence in the cytoplasm and nucleus of cells imaged in the basal state, and again after 1 hour treatment with 5 μM SFN. The table shows that treatment with SFN leads to a significant reduction in the EGFP-Nrf2 lifetime in both the cytoplasmic and nuclear compartments.

EGFP Image	FRET Efficiency	FRET Efficiency

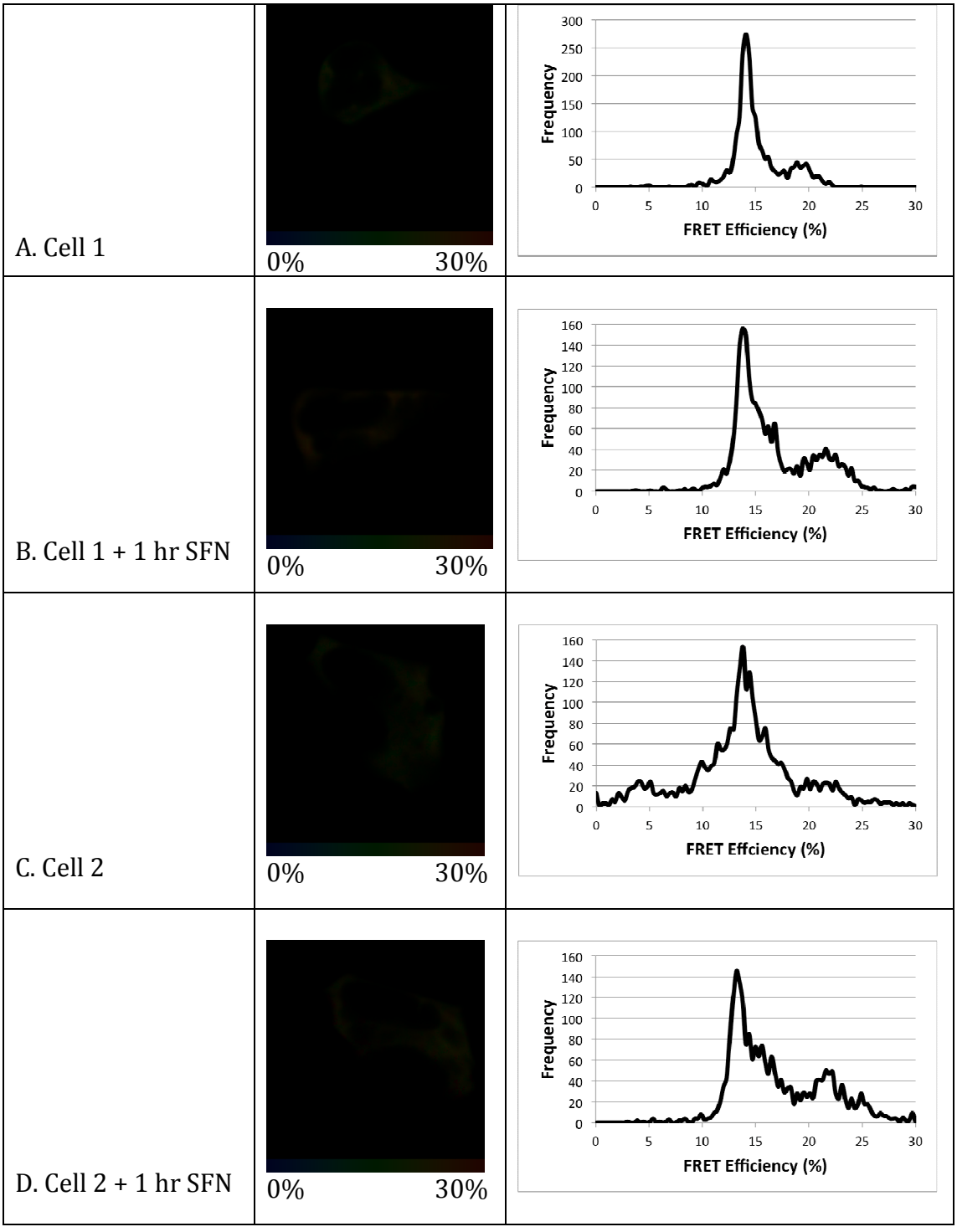

Figure 5.3. The nuclear FRET efficiency of EGFP-Nrf2 transfected cells imaged before and after treatment with SFN. HEK293 cells were transfected with EGFP-Nrf2 + Keap1-mCherry, from which the FRET efficiency of the interaction between these fusion proteins in the nucleus was calculated. A-D show the FRET efficiency data for individual EGFP-Nrf2 + Keap1-mCherry co-transfected cells which were imaged twice, once in the basal state (A, C) and once after 1 hour treatment with 5μM SFN (B, D). The left column shown the EGFP image from which the FRET efficiency data are derived. The middle column shows a pictorial representation of the FRET efficiency where the colour of the cell corresponds to the FRET efficiency, ranging from 0% to 30% as indicated on the legend below the image. The right column shows the FRET efficiency from each pixel

of the image plotted on a graph, with FRET efficiency on the x-axis and frequency on the y-axis. The FRET efficiency graphs (A-D) show that the FRET efficiency distribution is altered by SFN, which leads to a modest increase in the interaction at 21% FRET efficiency.

Together, these data suggest that inducers function by promoting the formation of the closed conformation of the Keap1-Nrf2 complex. In order to gain an alternate perspective on how the two complexes relate to each other, and to understand how the two conformations can be interconverted, we wished to manipulate the Keap1-Nrf2 pathway with a chemical which does not bind directly to Keap1, and thus does not directly influence the Keap1-Nrf2 complex. As Nrf2 is targeted by Keap1 for degradation by the proteasome, we decided to inhibit this degradation through use of the proteasomal inhibitor MG132.

When used to treat EGFP-Nrf2 + mCherry transfected cells, 10 μM MG132 had no effect on the lifetime of EGFP, demonstrating that it doesn't have any FRET-independent effects on the EGFP fluorophore (**Table 5.4**). Unexpectedly, treatment of EFP-Nrf2 + Keap1-mCherry co-transfected cells with 10 μM MG132

Keap1-mCherry + EGFP-Nrf2	Basal Cytoplasmic Lifetime (ps)	STCA Induced Cytoplasmic Lifetime (ps)		Basal Nuclear Lifetime (ps)	STCA Induced Nuclear Lifetime (ps)
Cell 1	2152	2089		no data	2131
Cell 2	2138	2103		2236	2145
Cell 3	2117	2096		no data	2124
Cell 4	2117	2075		no data	no data
AVERAGE	2131	2091		N/A	2133
SD	17	12		N/A	11
Paired T-test	p = 0.019				

Table 5.3. Lifetime of EGFP-Nrf2 in individual cells imaged before and after STCA treatment. HEK293 cells were co-transfected with EGFP-Nrf2 and Keap1-mCherry and imaged 24 hours later. The table shows the lifetime of EGFP fluorescence in the cytoplasm and nucleus of cells imaged in the basal state, and again after 1 hour treatment with 10 μM STCA. The table shows that treatment with STCA leads to a significant reduction in the EGFP-Nrf2 lifetime in the cytoplasm (p = 0.019).

EGFP Image	EGFP Lifetime	EGFP Lifetime

A. Cell 1	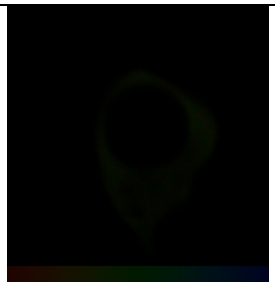 1.9 ns 2.6 ns	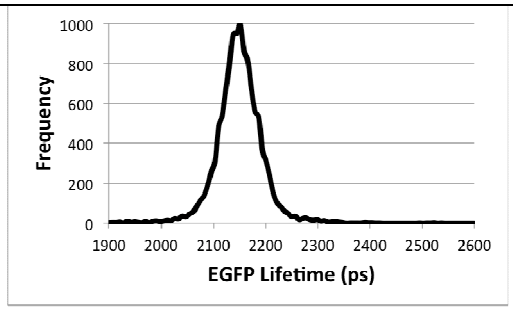
B. Cell 1 + 1 hr STCA	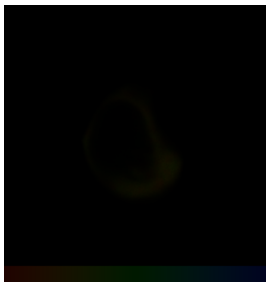 1.9 ns 2.6 ns	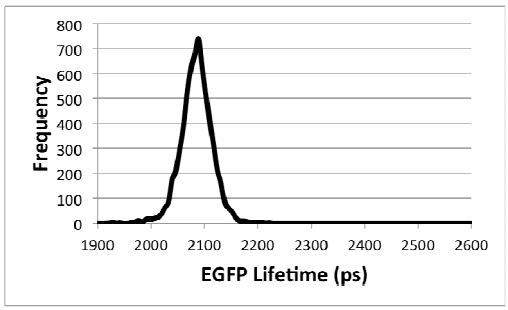
EGFP Image	FRET Efficiency	FRET Efficiency
C. Cell 2	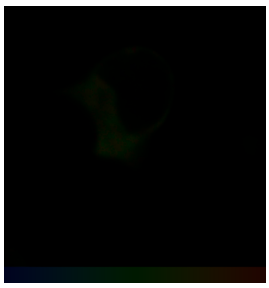 0% 30%	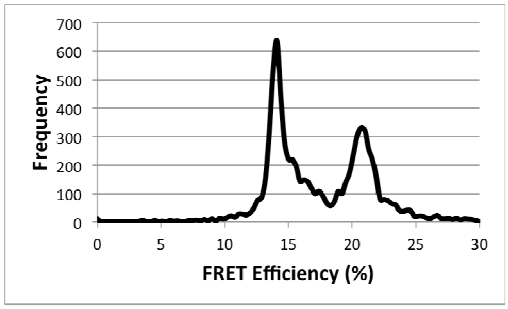
D. Cell 2 + 1 hr STCA	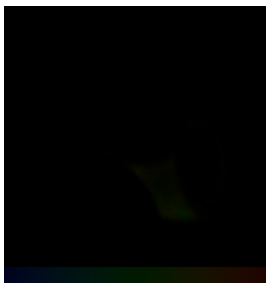 0% 30%	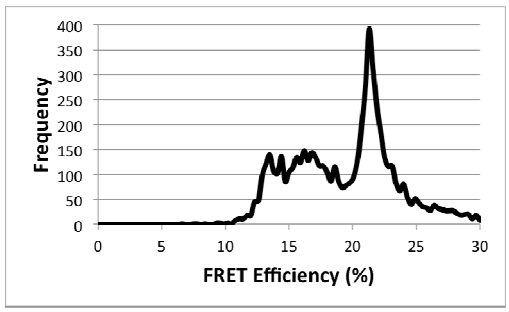

Figure 5.4. The lifetime and FRET efficiency in the cytoplasm of EGFP-Nrf2 transfected cells imaged before and after treatment with STCA. HEK293 cells were transfected with EGFP-Nrf2 + Keap1-mCherry, and both the lifetime (A, B) and FRET efficiency (C-D) in the cytoplasmic compartment were calculated. A, B show the fluorescence lifetime data from a single cell imaged twice, once in the basal state (A) and once after 1 hour treatment with 10μM STCA (B). The left column shows the EGFP image from which the lifetime data are derived. The middle column shows a pictorial representation of the EGFP lifetime where the colour of the cell corresponds to the

lifetime of EGFP, ranging from 1.9 ns to 2.6 ns as indicated on the legend below the image. The right column shows the lifetime data from each pixel of the image plotted on a graph, with lifetime on the x-axis and frequency on the y-axis. Graphs A-B clearly show that the lifetime of EGFP-Nrf2 is reduced after treatment with STCA for 1 hour. C-D show the FRET efficiency data for a single EGFP-Nrf2 + Keap1-mCherry co-transfected cell which was imaged twice, once in the basal state (C) and once after 1 hour treatment with 10μM STCA (D)**.** The left column shows the EGFP image from which the FRET efficiency data are derived. The middle column shows a pictorial representation of the FRET efficiency where the colour of the cell corresponds to the FRET efficiency, ranging from 0% to 30% as indicated on the legend below the image. The right column shows the FRET efficiency from each pixel of the image plotted on a graph, with FRET efficiency on the x-axis and frequency on the y-axis. The FRET efficiency graphs (C,D) show that the FRET efficiency distribution is altered by STCA, which leads to an increase in the interaction at 21% FRET efficiency. The FRET efficiency distributions are shown pictorially in the central column of C,D, where an increase in the amount of yellow relative to green can be seen in response to STCA.

lead to a reduction in the cytoplasmic EGFP-Nrf2 lifetime and the accumulation of the complex in the closed conformation (**Table 5.5, Figure 5.5, 5.6**). Interestingly, even in cells in which in the basal state the majority of the Keap1-Nrf2 complex is found in the open conformation, MG132 treatment was still able to promote the formation of the closed conformation (**Figure 5.6C,D**). It is interesting to note that MG132 was also able to reduce the lifetime of EGFP-Nrf2 in the nucleus, where it can promote the formation of the closed conformation, independent of any known direct modification of Keap1 (**Table 5.5, Figure 5.7**).

Discussion

In order to gain a thorough understanding of the mechanism through which Nrf2 is regulated by Keap1, we wished to study this interaction in both the basal (Chapter 4) and induced states (Chapter 5). We wanted to extend our single cell FLIM-based approach to examine the effects of inducers in individual cells, and importantly, we wished to study the interaction between Keap1 and Nrf2 in the same cell both in the basal and induced state. We believe that this approach is best suited to study the effects of inducers as it minimises the consequences of cellular heterogeneity caused by transient transfection of the fusion proteins. The validity of this approach is predicated on the idea that the lifetime and FRET efficiency are constant within a cell over a 1 hour period, so that any effects observed after the treatment with inducers for 1 hour were dependent on the activity of the inducer on Keap1, and not on the time that the image was taken, or the fact that the cell had already been imaged previously. Thankfully, both the lifetime of EGFP-Nrf2 and the FRET efficiency distribution were constant over a 1 hour time period, thus our multiple imaging approach could be used to assay the effects of inducers on the Keap1-Nrf2 complex (**Figure 5.1, Table 5.1**).

Interestingly, we found that both SFN and STCA led to a significant decrease in the EGFP-Nrf2 lifetime (**Table 5.2, 5.4**). A lower EGFP lifetime means that EGFP and mCherry fluorphores are closer together, which suggests that the Keap1-Nrf2 complex undergoes a conformational change in response to inducers such that the distance between the fluorophores is reduced, allowing more FRET to occur. Importantly, this lifetime decrease correlated with a change in FRET efficiency, and this change in FRET efficiency corresponded to a change in the relative abundances of the complexes identified in the basal state, and not the formation of a different Keap1-Nrf2 complex. In the cytoplasm, both SFN and STCA changed the FRET efficiency distributions. In the basal state the Keap1-Nrf2 complex was found equally in the open and closed conformations, whilst in cells treated with inducers, this changed so that the closed conformation was the dominant complex in which the Keap1 and Nrf2 were found (**Figure 5.2, 5.4**). The fact that different inducers which target different cysteine residues of Keap1 (SFN binds to Cys-151, STCA bind to Cys-273 and -288) both function in the

EGFP Image	EGFP Lifetime	EGFP Lifetime

A. EGFP-Nrf2 + mCherry + MG132	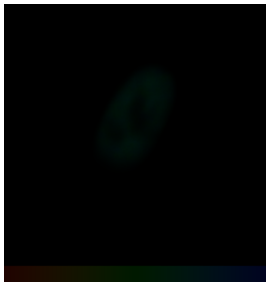 1.9 ns 2.6 ns	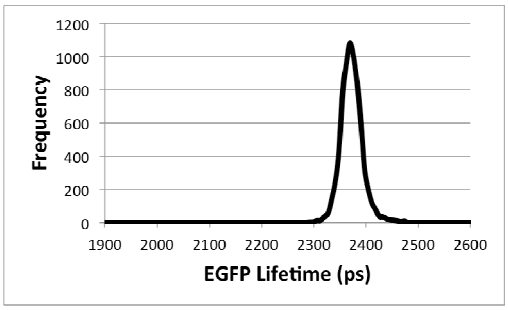
B. EGFP-Nrf2 + mCherry + MG132	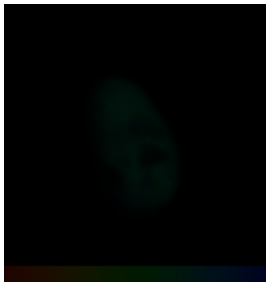 1.9 ns 2.6 ns	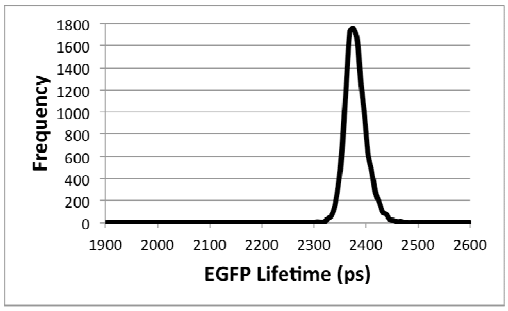
C. EGFP-Nrf2 + Keap1-mCherry	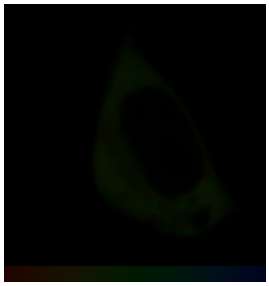 1.9 ns 2.6 ns	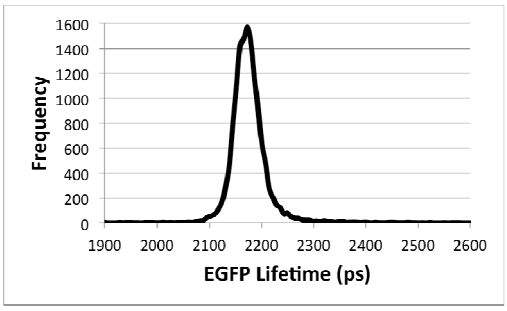
D. EGFP-Nrf2 + Keap1-mCherry + 1hr MG132	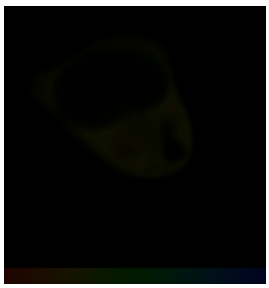 1.9 ns 2.6 ns	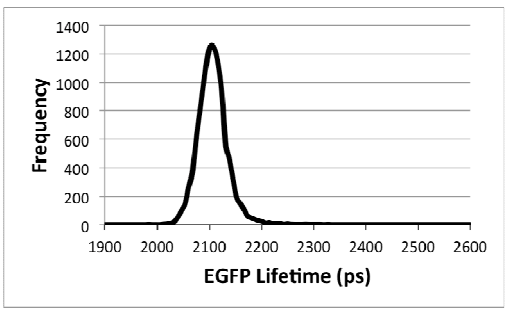

Figure 5.5. The cytoplasmic lifetime in EGFP-Nrf2 transfected cells imaged before and after treatment with MG132. HEK293 cells were transfected with either EGFP-Nrf2 + mCherry (A,B), or EGFP-Nrf2 + Keap1-mCherry (C,D), and the lifetime of EGFP fluorescence was calculated. A,B show the fluorescence lifetime data of cells imaged in the presence of MG132 and absence of Keap1-mCherry. C,D show the fluorescence lifetime data from a single cell imaged twice, once in the basal state (C) and once after 1

hour treatment with 10μM MG132 (D). The left column shows the EGFP image from which the lifetime data are derived. The middle column shows a pictorial representation of the EGFP lifetime where the colour of the cell corresponds to the lifetime of EGFP, ranging from 1.9 ns to 2.6 ns as indicated on the legend below the image. The right column shows the lifetime data from each pixel of the image plotted on a graph, with lifetime on the x-axis and frequency on the y-axis. Graphs A,B show that in the absence of FRET, MG132 has no effect on the lifetime of EGFP-Nrf2. Graphs C-D clearly show that the lifetime of EGFP-Nrf2 is reduced after treatment with MG132 for 1 hour.

same way suggest that the phenomenon which we observed is not inducer or cysteine specific, and may point to a general mechanism though which inducers stabilise Nrf2 (**Figure 5.8**).

Interestingly, we found that in the nucleus SFN also leads to a decrease in EGFP lifetime and a modest increase in formation of the closed conformation (**Table 5.3, Figure 5.4**). We were unable to determine the effect of STCA on the lifetime of EGFP-Nrf2 in the nucleus due to the challenges presented in working with nuclear lifetime data. In the basal state, EGFP-Nrf2 in predominantly found in the cytoplasm (**Figure 4.9**), and thus the imaging conditions were optimised for data collection in the cytoplasmic compartment. On average, the signal is 10-fold lower in the nucleus, which makes analysing the data more difficult as the contribution of noise to the overall signal is much greater when the intensity of the signal is lower. The intensity of signal required to calculate the FRET efficiency is even greater than that required for the lifetime, as the FRET efficiency is calculated using a two-component analysis which requires more

	Inducer	Lifetime (ps)	N	SD	T-test
EGFP-Nrf2 + mCherry	None	2375	13	12	
EGFP-Nrf2 + mCherry	10 μM MG132	2379	5	18	$p > 0.05$

Table 5.4. FLIM data for EGFP-Nrf2 transfected cells treated with MG132 in the absence of Keap1-mCherry. The table shows the lifetime, number of cells imaged and standard deviation of the lifetime for EGFP-Nrf2 + mCherry co-transfected HEK293 cells in the presence and absence of 10 μM MG132. The data clearly show that the treatment of cells with MG132 for 1 hour has no effect on the lifetime of EGFP-Nrf2.

EGFP Image	FRET Efficiency	FRET Efficiency

A. Cell 1	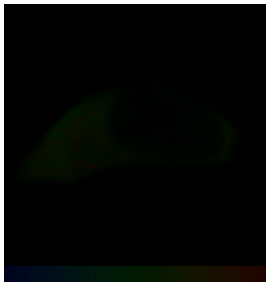 0% 30%	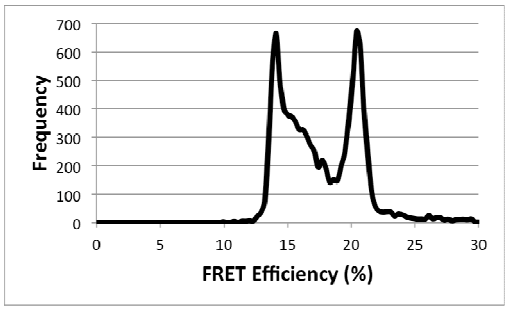
B. Cell 1 + 1 hr MG132	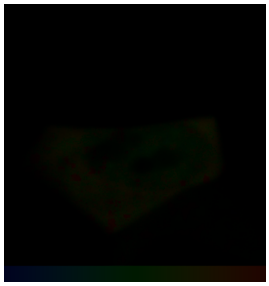 0% 30%	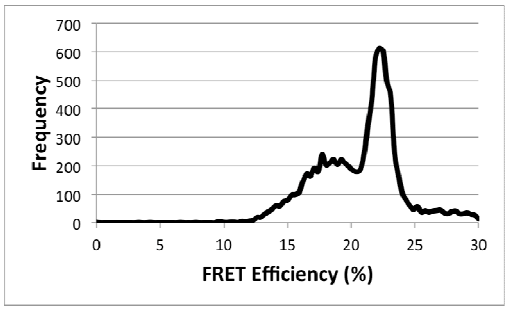
C. Cell 2	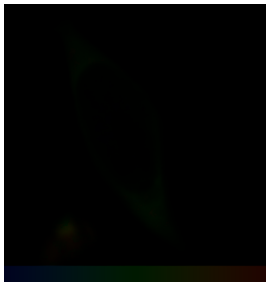 0% 30%	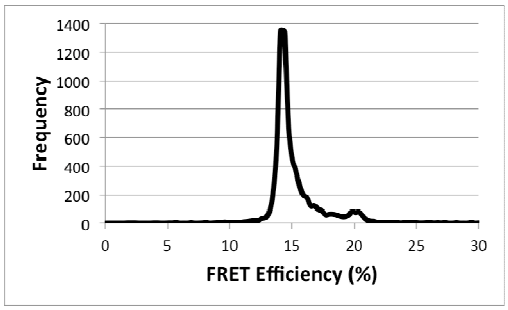
D. Cell 2 + 1 hr MG132	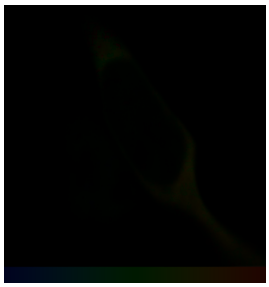 0% 30%	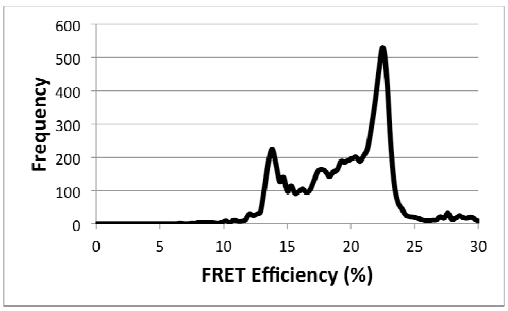

Figure 5.6. The FRET efficiency in the cytoplasm of EGFP-Nrf2 transfected cells imaged before and after treatment with MG132. HEK293 cells were transfected with EGFP-Nrf2 + Keap1-mCherry, from which the FRET efficiency in the cytoplasmic compartment were calculated. A-D show the FRET efficiency data for individual EGFP-Nrf2 + Keap1-mCherry co-transfected cells which were imaged twice, once in the basal state (A, C) and once after 1 hour treatment with 10μM MG132 (B, D)**.** The left column shows the EGFP image from which the FRET efficiency data are derived. The middle column shows a pictorial representation of the FRET efficiency where the colour of the cell corresponds to the FRET efficiency, ranging from 0% to 30% as indicated on the

legend below the image. The right column shows the FRET efficiency from each pixel of the image plotted on a graph, with FRET efficiency on the x-axis and frequency on the y-axis. The FRET efficiency graphs (A-D) show that the FRET efficiency distribution is altered by MG132, which leads to a profound increase in the interaction at 21% FRET efficiency. The FRET efficiency distributions are shown pictorially in the central column of A-D, where an increase in the amount of yellow relative to green can be seen in response to MG132.

data. This may in part explain why the reduction in lifetime of EGFP-Nrf2 in the nucleus in response to inducers is coupled with a modest change in the FRET efficiency, whilst similar reductions in cytoplasmic lifetime are coupled with more significant changes to the FRET efficiency distributions (compare **Figure 5.2** with **Figure 5.3**).

Whilst in most cases it was possible to calculate the EGFP-lifetime and FRET efficiency distribution in the nucleus, it could not be done universally. Thus, from the cells imaged prior to STCA treatment, a reliable nuclear lifetime could not be established and thus the effect of the inducer in the nucleus could not be determined (**Table 5.3**). We may note however, that in the basal state, the

Keap1-mCherry + EGFP-Nrf2	Basal Cytoplasmic Lifetime (ps)	MG132 Treated Cytoplasmic Lifetime (ps)		Basal Nuclear Lifetime (ps)	MG132 Treated Nuclear Lifetime (ps)
Cell 1	2180	2103		2250	2208
Cell 2	2145	2117		2201	2180
Cell 3	2173	2124		N/A	N/A
Cell 4	2145	2068		2187	N/A
Cell 5	2166	2089		2215	2152
Cell 6	2152	2138		2222	2215
Cell 7	2173	2103		2236	2180
AVERAGE	2162	2106		2219	2187
SD	14	21		23	25
Paired T-test	p = 0.000324			p = 0.0229	

Table 5.5. Lifetime of EGFP-Nrf2 in individual cells imaged before and after MG132 treatment. HEK293 cells were co-transfected with EGFP-Nrf2 and Keap1-mCherry and imaged 24 hours later. The table shows the lifetime of EGFP fluorescence in the cytoplasm and nucleus of cells imaged in the basal state, and again after 1 hour treatment with 10 μM MG132. The table shows that treatment with MG132 leads to a significant reduction in the EGFP-Nrf2 lifetime in both the cytoplasmic and nuclear compartments.

EGFP Image	FRET Efficiency	FRET Efficiency

A. Cell 1	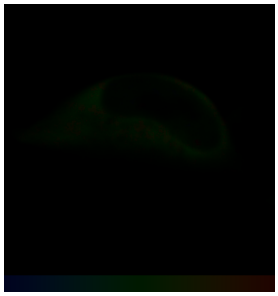 0% 30%	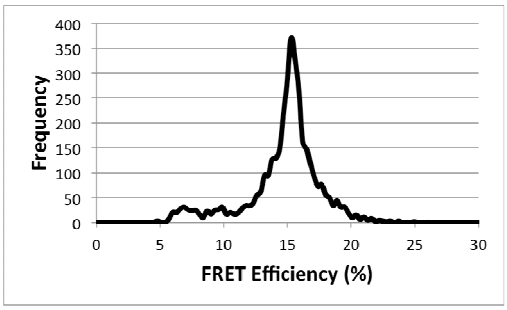
B. Cell 1 + 1 hr MG132	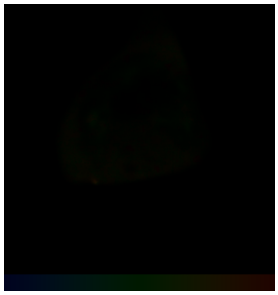 0% 30%	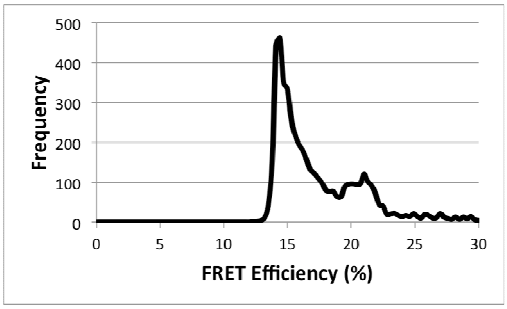
C. Cell 2	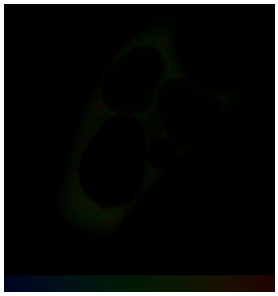 0% 30%	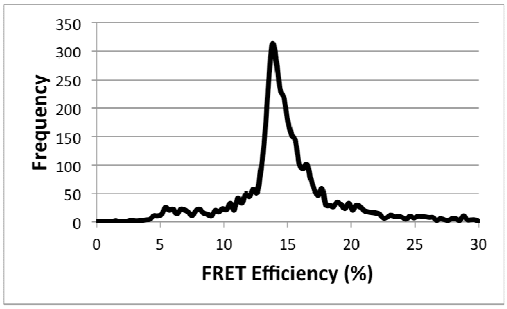
D. Cell 2 + 1 hr MG132	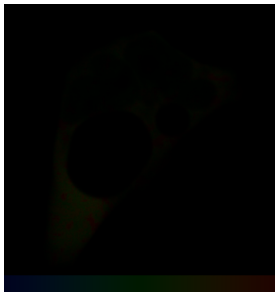 0% 30%	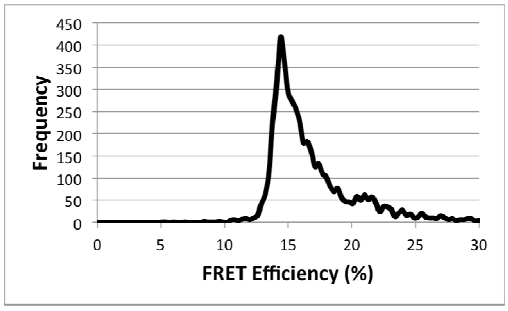

Figure 5.7. The nuclear FRET efficiency of EGFP-Nrf2 transfected cells imaged before and after treatment with MG132. HEK293 cells were transfected with EGFP-Nrf2 + Keap1-mCherry, from which the FRET efficiency of the interaction between these fusion proteins in the nucleus was calculated. A-D show the FRET efficiency data for individual EGFP-Nrf2 + Keap1-mCherry co-transfected cells which were imaged twice, once in the basal state (A, C) and once after 1 hour treatment with 10μM MG132 (B, D). The left column shows the EGFP image from which the FRET efficiency data are derived. The middle column shows a pictorial representation of the FRET efficiency where the

colour of the cell corresponds to the FRET efficiency, ranging from 0% to 30% as indicated on the legend below the image. The right column shows the FRET efficiency from each pixel of the image plotted on a graph, with FRET efficiency on the x-axis and frequency on the y-axis. The FRET efficiency graphs (A-D) show that the FRET efficiency distribution is altered by MG132, which leads to a modest increase in the interaction at 21% FRET efficiency.

average nuclear lifetime of EGFP-Nrf2 was 2203 ps (**Table 4.2**), and in the 3 cells in which it was possible to calculate the nuclear lifetime after the addition of STCA, it was 2133 ps (**Table 5.3**). This suggests that the trend of inducer activity leading to a decrease in the EGFP-Nrf2 lifetime may also be true in the nucleus of cells treated with STCA.

Together these results present a stark contrast to the existing models of Nrf2 regulation, particularly to the widely accepted hinge and latch model. The hinge and latch model was proposed when the second binding site of Nrf2 was discovered (McMahon et al. 2006, Tong et al. 2006a). It was noted that the DLG motif binds with a 100-fold lower affinity than the ETGE motif, and yet this motif is absolutely required for the physiological regulation of Nrf2 by Keap1. In the absence of the DLG motif, through either targeted deletion by researchers or by point mutations in cancer, Nrf2 is no longer ubiquitinated by the Keap1-dependent E3-ubiquitin ligase (McMahon et al. 2006, Shibata et al. 2008a). Together, the fact that the DLG motif shows weaker binding to Keap1, coupled with the idea that loss of DLG binding to Keap1 results in Nrf2 stabilisation, led to the formulation of the hinge and latch model (**Figure 1.4**). The hinge and latch model was proposed despite the fact that there was no experimental evidence to support the existence of the "open latch" conformation of the Keap1-Nrf2 complex in the induced state (Tong et al. 2006a, Tong et al. 2006b). Our FRET efficiency data can directly visualise this complex as it corresponds exactly to the 13% FRET efficiency population. However, in contrast to the hinge and latch model, our data clearly show no accumulation of the Keap1-Nrf2 complex in the 13% FRET efficiency population. Instead our data suggest that inducers function by promoting the formation of the 21% FRET efficiency population, which represents the closed conformation, and thus that inducers lead to the DLG motif

Open Conformation	Closed Conformation	FRET efficiency
A. 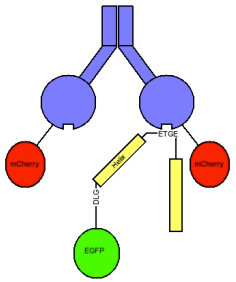	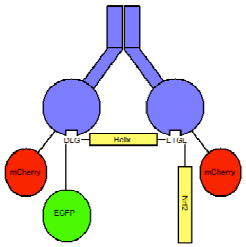	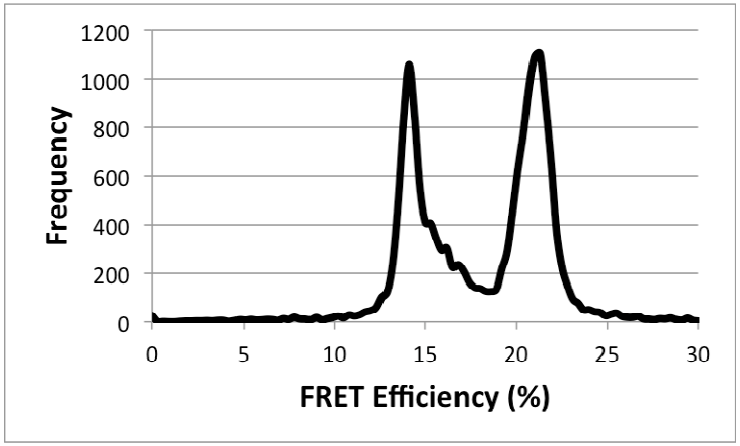
B. 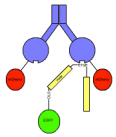	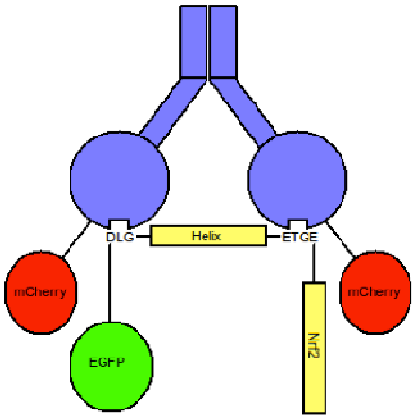	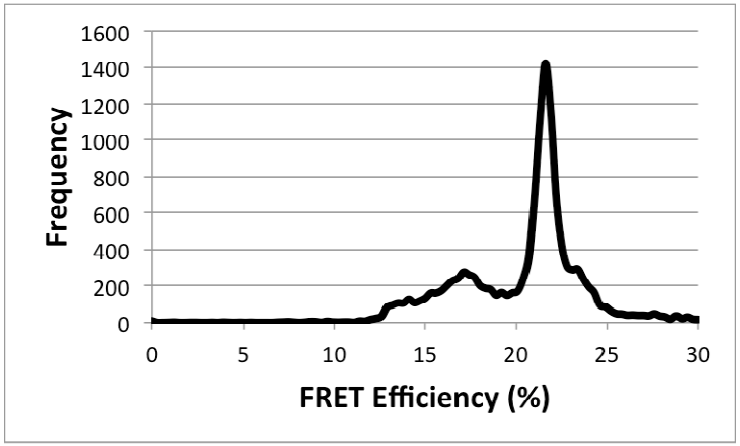

Figure 5.8. The impact of inducers and proteasomal inhibition on the conformation of the Keap1-Nrf2 complex. Row **A** depicts, in cartoon form, the Keap1-Nrf2 complex in the basal state. Our data show that in the basal state, the Keap-Nrf2 complex is distributed equally in the open and closed conformations. **A** FRET efficiency distribution corresponding to this is shown on the left. **B** shows how the distribution between the two conformations is altered by inducers and the proteasomal inhibitor MG132. Under these conditions, the complex shifts to favour the closed conformation (shown by a relative increase in size of the closed conformation relative to the open conformation). This shift is reflected in the FRET efficiency distribution, which shows a much greater interaction at 21% FRET efficiency corresponding to the closed conformation.

of Nrf2 binding more tightly to Keap1, not less, as postulated by the hinge and latch model.

As shown in Chapter 4, in the basal state, the Keap1-Nrf2 complex is found in both an open and closed conformation. From these data alone it is unclear whether these two states existed in equilibrium with one another, with both states being required for ubiquitination of Nrf2, or as two points in a cycle, where one conformation is formed and then progresses to the second conformation to allow the ubiquitination process. The inducer data showed that inducers promote the formation of the closed conformation, however this stabilisation could occur by either a change in the equilibrium dynamics, or an alteration in the binding cycle, both of which could manifest themselves as an increase in the interaction at 21% FRET efficiency. For this reason we chose to stabilise Nrf2 using the proteasomal inhibitor MG132, which does not bind directly to Keap1, yet stabilises Nrf2 by blockings its degradation by the proteasome. This allowed us to investigate how the two conformations of the Keap1-Nrf2 complex relate to one another. If MG132 has no effect on the Keap1-Nrf2 complex, it will suggest that the two conformations are in equilibrium with one another. However, if the two states of the complex represent two points on a cycle, then blocking the cycle by inhibiting Nrf2's degradation will lead to the accumulation of the complex at the later point of the cycle.

When we treated cells with MG132, we saw a reduction in the lifetime of EGFP-Nrf2 coupled with an increase in the FRET efficiency distribution at the 21% interaction (**Table 5.5, Figure 5.5, 5.6**). Interestingly, in cells in which the Keap1-Nrf2 complex is almost exclusively in the open conformation in the basal

state, inhibition of the proteasome leads to a dramatic shift in the FRET efficiency distribution, from mostly 13% to mostly 21% (**Figure 5.6C,D**), suggesting that the interaction between Keap1 and Nrf2 forms a cycle, in which the 21% FRET efficiency population (closed conformation) is the later point in the cycle, and thus the 13% population (open conformation) represents the initial position of the cycle. As inducers also lead to the accumulation of the Keap1-Nrf2 complex in the closed conformation, our data suggest that they too function to inhibit the cycle of Nrf2 ubiquitination by Keap1.

We observed that even in the nucleus, MG132 is able to reduce the lifetime of EGFP-Nrf2 and increase the abundance of the closed conformation (**Table 5.5, Figure 5,7**). As MG132 only increases the amount of Nrf2 in the nucleus, and doesn't directly modify Keap1, these data suggest that the Keap1-Nrf2 complex is able to form the closed conformation in the nucleus. The main reason that this does not occur in the basal state is most likely because of the low levels of Nrf2 which mean that it is outcompeted for binding to Keap1 by other nuclear protein such as Prothymosin-α or Palb2 (Padmanabhan et al. 2008, Ma et al. 2012). This suggests that the function of the other Keap1-binding proteins in the nucleus is to compete with the DLG motif of Nrf2, and thus reduce the efficiency of Keap1 in the nucleus relative to the cytoplasm to allow basal level expression of Nrf2-target genes.

Chapter 6: Establishment of a FRAP-based assay to study the Cul3-Keap1-Nrf2 complex

Introduction

In addition to studying the interaction between Keap1 and Nrf2 using FRET/ FLIM, we also wished to use an independent single cell analysis method that would support or dispute our FRET results. The method we chose was the microscopy-based technique fluorescence recovery after photobleaching (FRAP). This method measures the rate of diffusion of proteins, and allows the determination of dynamic changes within the complex in which a protein is found as conditions within the cell change (Reits et al 2001). The principal behind FRAP is shown in cartoon form in **Figure 6.1**. The cells are first transfected with an expression plasmid of the protein of interest fused to GFP, so that the protein's localisation and movement can be visualised. Next, a laser is used to photo-bleach a small area in the cell resulting in the loss or reduction of fluorescence in the bleached region. Due to the natural diffusion of the proteins within the cell, this bleached region will recover its fluorescence as the proteins from the surrounding regions diffuse into the bleached spot. As such this method measures the diffusion rate of the fusion protein. Interestingly, if the protein of interest is found within a complex, FRAP allows the user to evaluate the status of this complex as the cellular conditions change. This is due to the properties of diffusion, whereby smaller proteins diffuse faster than larger proteins or protein complexes. Thus if the activity of a drug leads to the dissociation of a protein complex, this can be measured by FRAP as the individual members of the dissociated complex will diffuse faster in the presence of the drug. FRAP has been used to study a wide variety of cellular processes, from the localisation changes of the transcription factor β-catenin, to the mechanism of RNA splicing (Krieghoff et al. 2006, Lleres et al. 2010).

In addition to using FRAP to study the interaction between Nrf2 and Keap1, this technique is also well suited to test one of the other models of Nrf2 activation, that of the dissociation of Keap1 from Cullin-3 (**Figure 1.3**). This technique will allow us to complement the existing biochemical data with a live cell imaging approach to test whether inducers function to dissociate the Keap1-dependent E3-ubiquitin ligase.

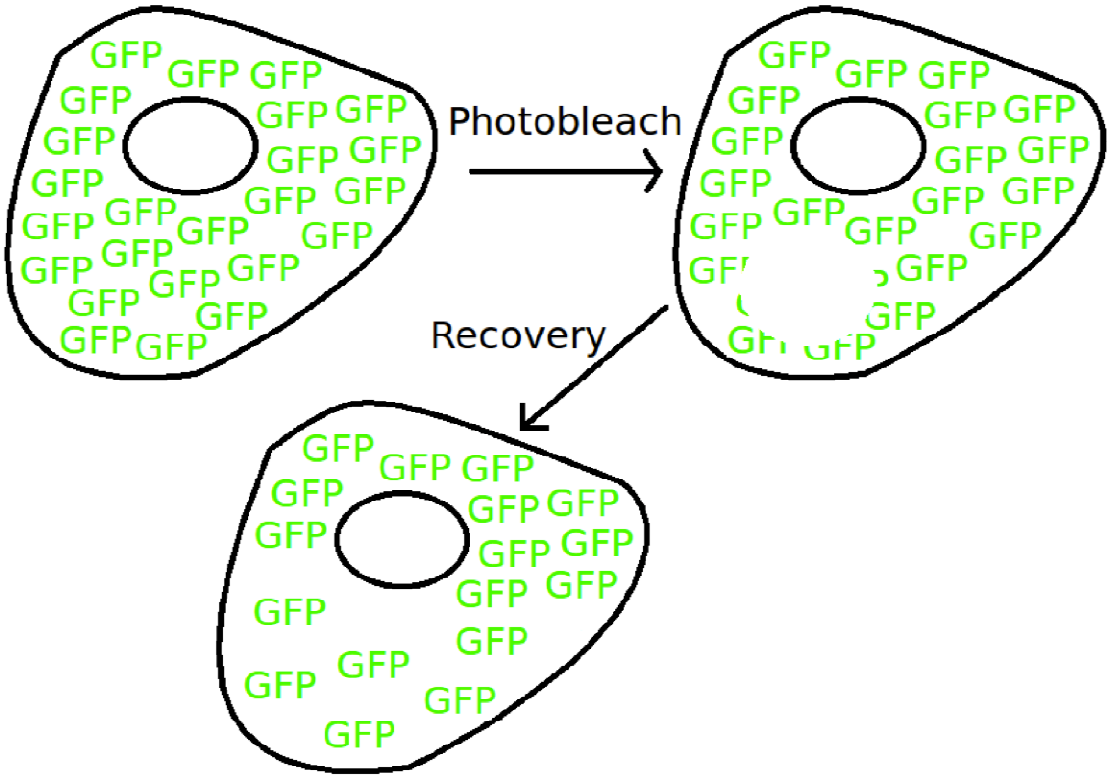

Figure 6.1. Fluorescence recovery after photobleaching (FRAP). This microscopy technique measures the rate at which fluorescently labelled proteins are able to diffuse in live cells. This is shown in cartoon form above, where a cell is transfected with an expression plasmid for GFP the expression of which is distributed evenly across the cytoplasm. A laser is then used to photobleach a small area in the cell. The cell is then rapidly imaged after the bleach event, during which time the surrounding GFP diffuses into the bleached area and the fluorescence signal is recovered. This allows the user to study the diffusion dynamics of the protein to which GFP is fused. If the fusion protein is found in a protein complex which can dissociate upon the addition of a drug, this can be measured using FRAP, as once dissociated, the fusion protein will diffuse more rapidly.

Aim

The aim of this part of the project was to use FRAP to study the impact of inducers on the interactions between Keap1-Nrf2 and Keap1-Cul3.

Results

Our first aim was to validate this technique by ectopically expressing Nrf2-EGFP and Keap1-mCherry in HEK293 cells (at exactly the same experimental conditions as those used for the FRET experiments), and then exposing the cells to an inducer to measure whether there was any dissociation of Keap1 and Nrf2. Our previous FRET data had suggested that there is no dissociation of Keap1 and Nrf2 in response to inducers, and we expected to see a similar result with the FRAP experiments.

As shown in **Figure 6.2A-C**, cells were imaged before the bleach event, during the bleach event and after the recovery of fluorescence in the bleached spot. **Figure 6.2D,E** shows the localisation of Nrf2-EGFP and Keap1-mCherry, which is largely cytoplasmic, and consequently all bleach events were carried out in the cytoplasm also. **Figure 6.2F** shows the fluorescent recovery plotted against time within the bleached spot. It shows that before the bleaching, the fluorescence was 1.0 (or 100%), it was then bleached to 60% of its original intensity before quickly recovering to 85% of its original intensity as surrounding Nrf2-EGFP diffused into the bleached area. From this recovery graph, we can extract the value of T½, the time taken for the fluorescence intensity to recover to half of its maximum recovery intensity, and this T½value can be used to compare different cells with different starting EGFP intensities.

Figure 6.2A-F shows an example of a cell imaged in the basal state, whilst **Figure 6.2G-L** is a representative of cells which have been exposed to 0.1 μM CDDO for 1 hr. **Table 6.1** shows the summary of the FRAP data for this experiment. In the basal state, the T½ recovery time was 0.592s, and in the presence of 0.1 μM CDDO it was 0.681s ($p>0.05$). Thus there was no significant difference between the rate at which Nrf2-EGFP was able to diffuse into the bleached spot in the absence or the presence of the inducer, indicating that Nrf2's ability to diffuse is not altered in the induced state, and thus that it is not released from Keap1.

We then wished to determine whether inducers lead to the dissociation of the Keap1-dependent E3-ubiquitin ligase, which consists of Keap1, Cullin-3 (Cul3) and Rbx1. In order to accomplish this goal, we generated fusion proteins

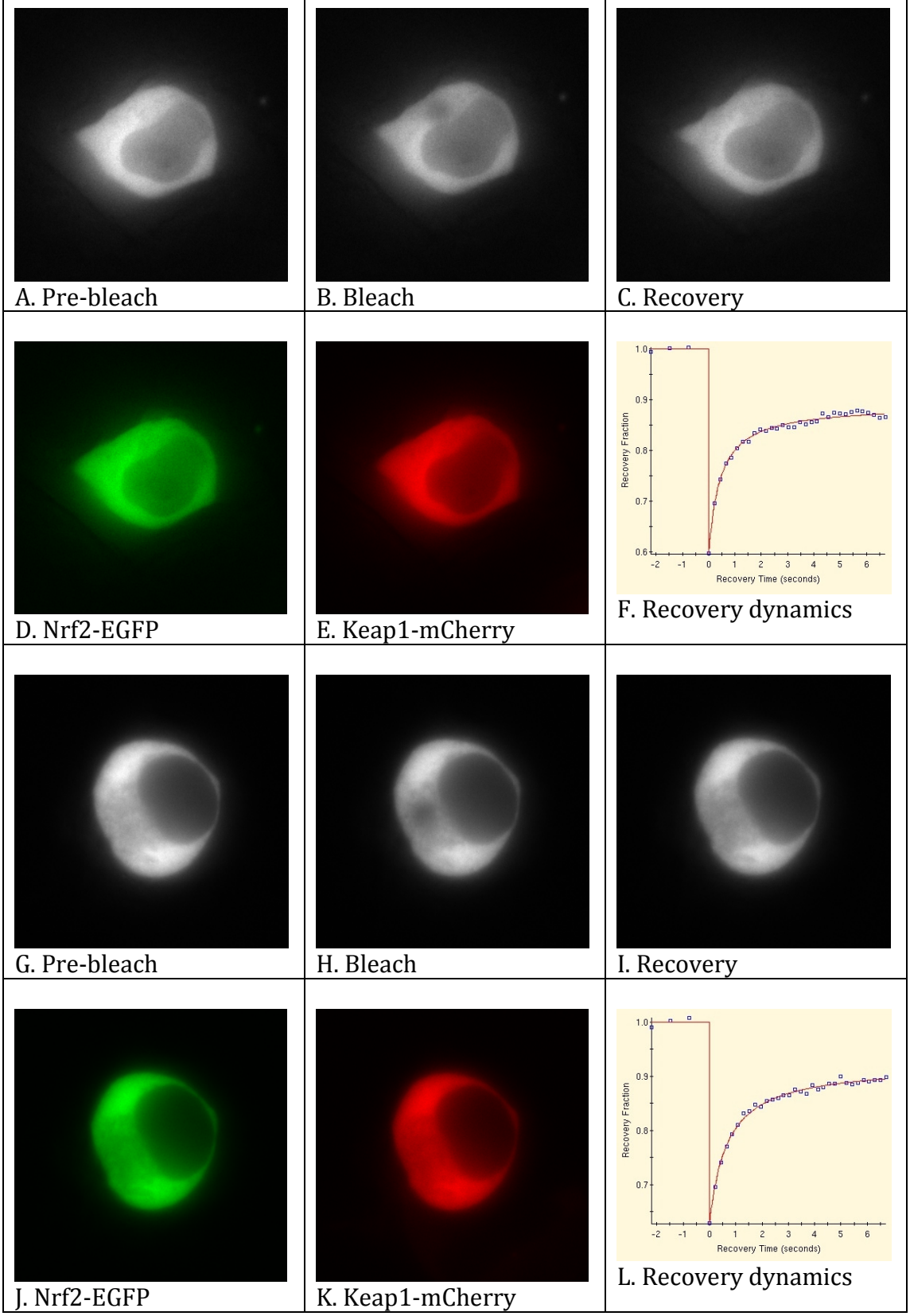

Figure 6.2. FRAP experiments to study the interaction between Keap1 and Nrf2. HEK293 cells were transfected with Nrf2-EGFP + mCherry-Keap1, and imaged 24 hours later. Six images in the panel above display the data from a single experiment, with A-F showing a representative example of data in the basal state, and G-L showing

representative data for cells treated with 0.1 μM CDDO for 1 hour. Each cell was imaged three times pre-bleach (A), and 30 times post bleach (B) to capture the recovery of EGFP fluorescence (C). D and E show the localisation of EGFP-Nrf2 and mCherry-Keap1, whilst the recovery dynamics are plotted in the graph shown in F. From this graph, the T½ value was calculated as the amount of time required for half of the maximal intensity of fluorescence to be recovered.

of Keap1-EGFP and mCherry-Cul3 and transfected them in HEK293 cells to examine their diffusion dynamics using FRAP.

Importantly, before this was done we needed to determine whether Keap1-EGFP and mCherry-Cul3 interact in cells. In order to do this, we expressed the Keap1 fusion protein in either the presence or the absence of mCherry-Cul3. If Keap1-EGFP is able to interact with mCherry-Cul3, then its diffusion time should be slower when mCherry-Cul3 is present compared to when it is absent. Representative cells from these experiments are shown in **Figure 6.3**, where in A-F data are shown from Keap1-EGFP and mCherry co-transfected cells, whilst in the example shown in G-L the cells were co-transfected with Keap1-EGFP and mCherry-Cul3. By comparing 3E and 3K it is clear that the fusion of Cul3 to mCherry changes the localisation of the fluorophore from whole cell to cytoplasmic. Due to the co-localisation of Keap1 and Cul3 (**Figure 6.3J, K**), all of the bleach spots were produced in the cytoplasm. As shown in **Table 6.2**, in the absence of Cul3, the T½value of Keap1-EGFP was 0.29 s, and when mCherry-Cul3 was co-transfected the T½was increased to 0.347. This difference was statistically significant ($p = 0.022$) showing that, when expressed, Keap1-EGFP and mCherry-Cul3 do bind to one another in live cells.

	Inducer	**T½ (s)**	**N**	**SD**	**T-test**
Nrf2-EGFP + Keap1-mCherry	None	0.592	23	0.178	
Nrf2-EGFP + Keap1-mCherry	0.1 μM CDDO	0.681	28	0.224	$p > 0.05$

Table 6.1. FRAP data for Nrf2-EGFP transfected cells. The table shows the recovery time (T½), number of cells imaged and standard deviation of the recovery time for Nrf2-EGFP + Keap1-mCherry co-transfected HEK293 cells in the basal state and after 1 hour treatment with the inducer CDDO (0.1 μM). The recovery time of Nrf2-EGFP is unaffected by addition of the inducer ($p > 0.05$) showing that the Keap1-Nrf2 complex does not dissociate in response to CDDO.

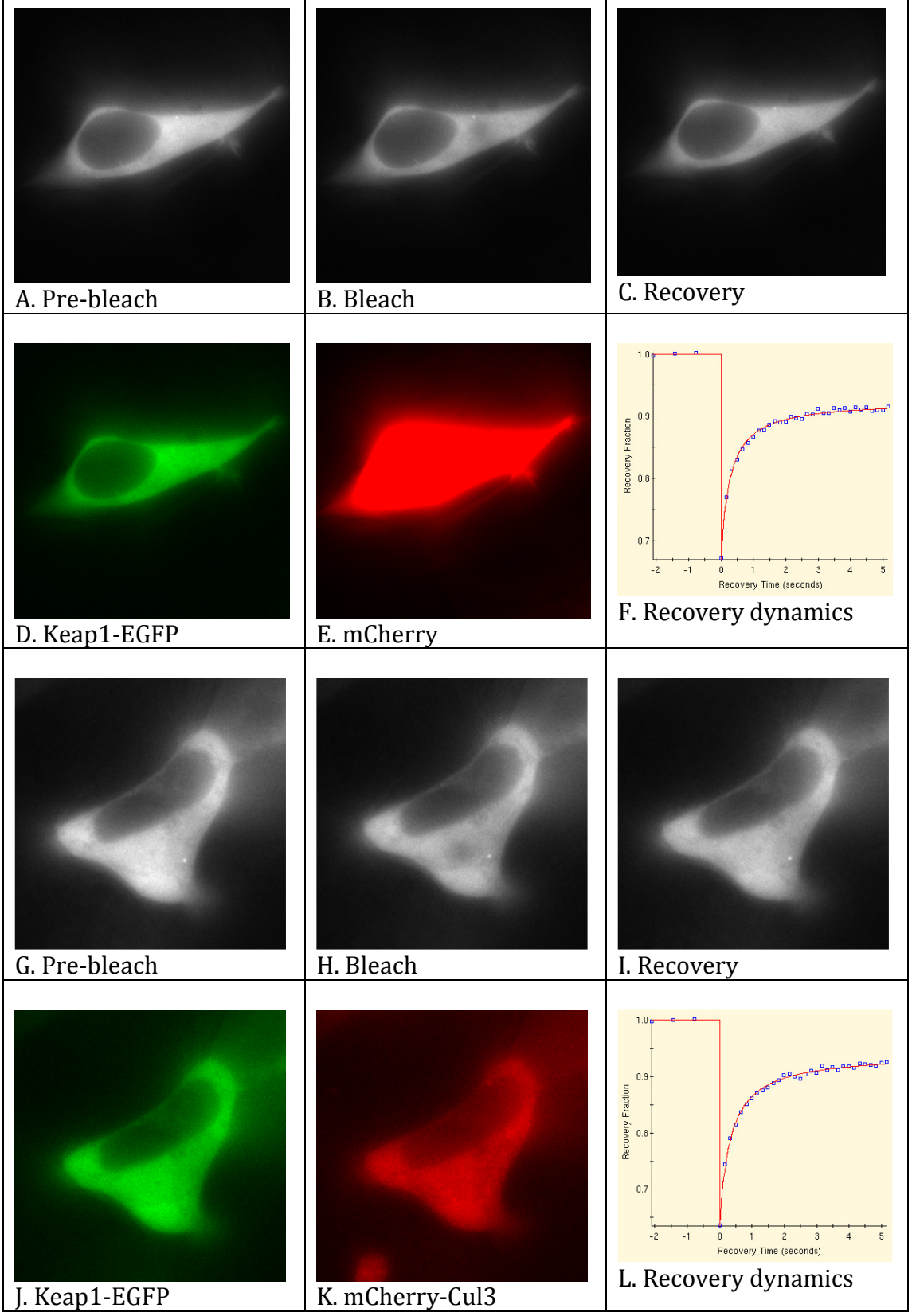

Figure 6.3. FRAP experiments to demonstrate that Keap1-EGFP and mCherry-Cul3 interact in live cells. HEK293 cells were transfected with either Keap1-EGFP + mCherry (A-F) or Keap1-EGFP + mCherry-Cul3 (G-L) and imaged 24 hours later. Six

images in the panel above display the data from a single experiment. Each cell was imaged three times pre-bleach (A), and 30 times post bleach (B) to capture the recovery of EGFP fluorescence (C). D and E show the localisation of Keap1-EGFP and free mCherry, whilst the recovery dynamics are plotted in the graph shown in F. From this graph, the T½ value was calculated as the amount of time required for half of the maximal intensity of fluorescence to be recovered. A comparison of E and K shows that the fusion of Cul3 to mCherry changes its localisation from whole cell to mainly cytoplasmic.

We then wished to determine whether inducers lead to the dissociation of Keap1 from Cul3. If inducers function through the dissociation of the Keap1-dependent E3-ubiquitin ligase, then we would expect to see a decrease in the T½value after inducer treatment. Firstly we imaged cells in the basal state, and then we added the inducers to the cell culture medium, incubated the cells for 1 hour and imaged the same dish again. Representative images are shown in **Figure 6.4** and **6.5** and the data are summarised in **Table 6.2**. We found that the T½value was unaffected by the inducers SFN, STCA, CDDO and H_2O_2, suggesting that

	Inducer	**T½ (s)**	**N**	**SD**	**T-test**
Keap1-EGFP + mCherry	None	0.290	41	0.073	
Keap1-EGFP + mCherry-Cul3	None	0.347	15	0.098	p = 0.022
Keap1-EGFP + mCherry-Cul3	None	0.320	20	0.075	
Keap1-EGFP + mCherry-Cul3	5 µM SFN	0.334	22	0.053	p > 0.05
Keap1-EGFP + mCherry-Cul3	None	0.347	15	0.098	
Keap1-EGFP + mCherry-Cul3	10 µM STCA	0.367	27	0.090	p > 0.05
Keap1-EGFP + mCherry-Cul3	None	0.374	18	0.085	
Keap1-EGFP + mCherry-Cul3	0.1 µM CDDO	0.372	30	0.096	p > 0.05
Keap1-EGFP + mCherry-Cul3	None	0.416	29	0.087	
Keap1-EGFP + mCherry-Cul3	400 µM H_2O_2	0.385	20	0.061	p > 0.05

Table 6.2. FRAP data for Keap1-EGFP transfected cells. The table shows the recovery time (T½), number of cells imaged and standard deviation of the recovery time for Keap1-EGFP + mCherry, and Keap1-EGFP + mCherry-Cul3 co-transfected HEK293 cells. In the basal state, the recovery time of Keap1-EGFP is lower in the presence of free mCherry than in the presence of mCherry-Cul3 (p = 0.022), demonstrating that Keap1-EGFP interacts with mCherry-Cul3 in cells. In Keap1-EGFP + mCherry-Cul3 co-transfected cells, the addition of the inducers SFN, STCA, CDDO and H_2O_2 has no effect on

the recovery time, suggesting that the Keap1-Cul3 complex is not dissociated after 1 hour treatment with these inducers.

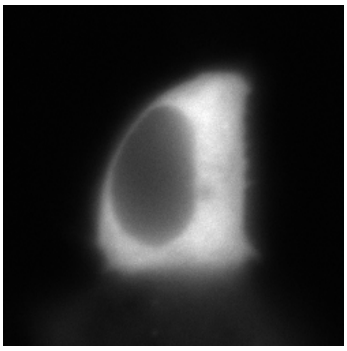

A. Pre-bleach

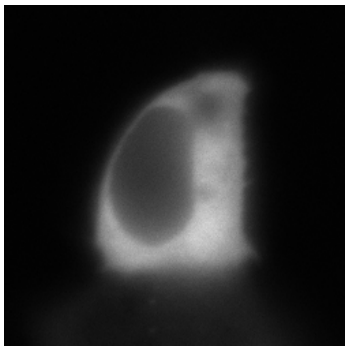

B. Bleach

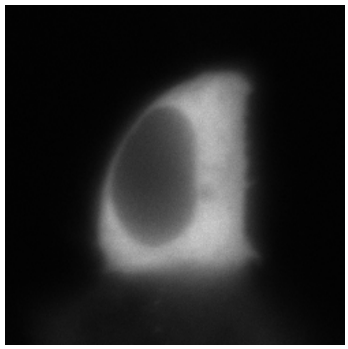

C. Recovery

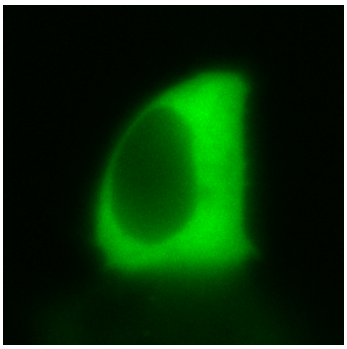

D. Keap1-EGFP

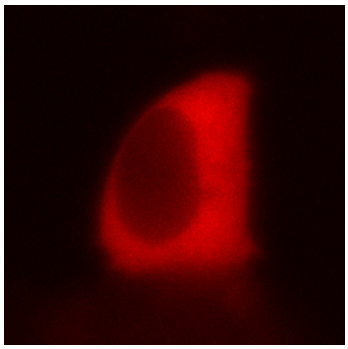

E. mCherry-Cul3

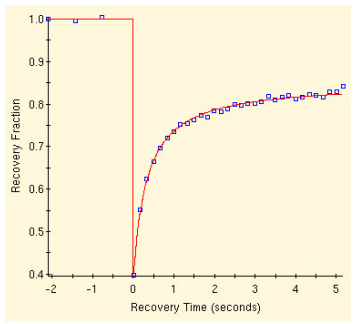

F. Recovery dynamics

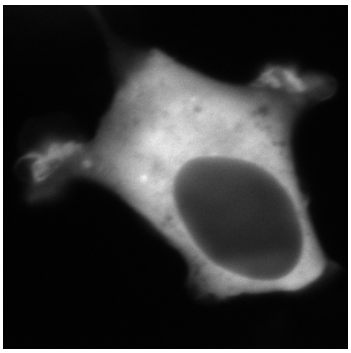

G. Pre-bleach

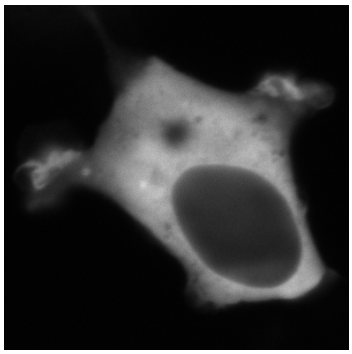

H. Bleach

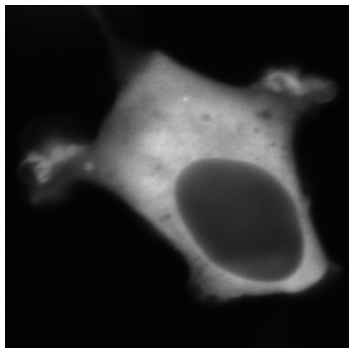

I. Recovery

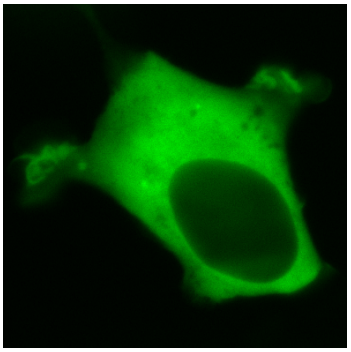

J. Keap1-EGFP

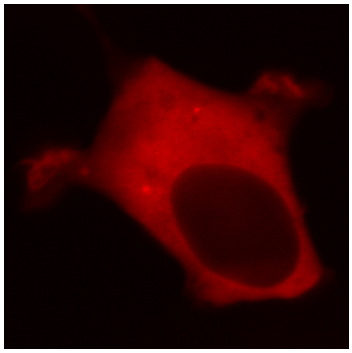

K. mCherry-Cul3

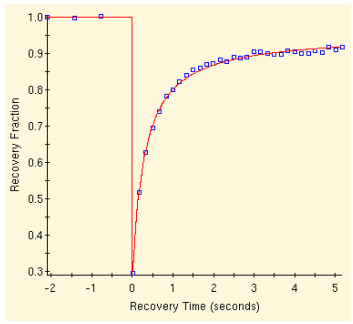

L. Recovery dynamics

Figure 6.4. FRAP experiments to study the interaction between Keap1 and Cul3. HEK293 cells were transfected with Keap1-EGFP + mCherry-Cul3, and imaged 24 hours later. Six images in the panel above display the data from a single experiment, with A-F showing a representative example of data in the basal state, and G-L showing representative data for cells treated with 400 μM H_2O_2 for up to 1 hour. Each cell was imaged three times pre-bleach (A), and 30 times post bleach (B) to capture the recovery of EGFP fluorescence (C). D and E show the localisation of Keap1-EGFP and mCherry-Cul3, whilst the recovery dynamics are plotted in the graph shown in F. From this graph, the T½ value was calculated as the amount of time required for half of the maximal intensity of fluorescence to be recovered.

inducers of different types do not function through the dissociation of the Keap1-dependent E3-ubiquitin ligase during the first 1 hour after inducer treatment.

Discussion

The aim of the FRAP experiments were two-fold. Firstly we wished to use a complementary method to FRET/ FLIM to study the dynamics of the Nrf2-Keap1 interaction in response to inducers, and secondly we wished to study how inducers impact the Keap1-dependent E3-ubiquitin ligase complex.

There were a number of experimental differences between the FRAP and FLIM experiments, despite the fact that the overall experimental design was similar. In the FLIM experiments, the length of time of the image acquisition step was very long at 90 s. This contrasts sharply with FRAP, which requires numerous images at regular intervals. As a result, the FRAP exposure times per image were very short (50 ms) which means that a much brighter image is required for FRAP than FLIM, where long exposure times are sympathetic to weakly fluorescent cells. In the case of Nrf2-EGFP expression, the exposure time is crucial, as Nrf2 is targeted for degradation by Keap1, and thus is present at low levels, even when ectopically expressed. The short exposure time required for FRAP combined with the low level of Nrf2-EGFP expression meant that carrying out the FRAP experiments with Nrf2-EGFP and Keap1-mCherry was very difficult, and because of this the only inducer which was analysed was CDDO.

A second difference between the FLIM and FRAP experiments was the way we imaged the cells pre- and post-induction. For the FLIM data, we wanted to image the same cell before and after the inducer was added to see how the FRET efficiency changed. This method is not compatible for use in FRAP experiments, because the photo-bleaching is a destructive event which reduces the total fluorescence signal from the cell, and this fluorescence reduction would influence a second measurement if the same cell was to be imaged both before and after inducer treatment. For this reason, cells were not imaged both before and after the inducers were added, and instead those cells which were imaged in the basal state were avoided post-induction.

In good agreement with the FLIM data, the FRAP data of EGFP-Nrf2 and Keap1-mCherry co-transfected cells showed that the two proteins do not dissociate after 1 hour of treatment with CDDO (**Table 6.1**). Together these

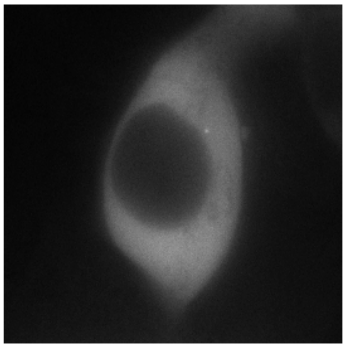

A. Pre-bleach

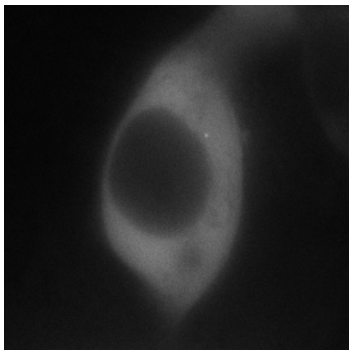

B. Bleach

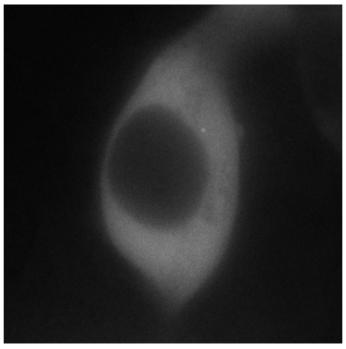

C. Recovery

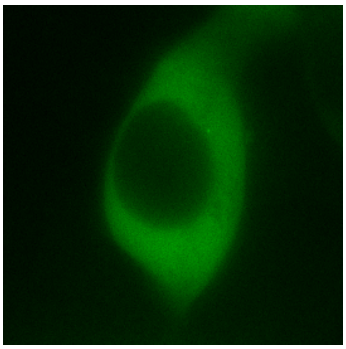

D. Keap1-EGFP

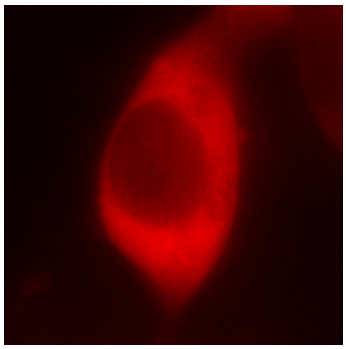

E. mCherry-Cul3

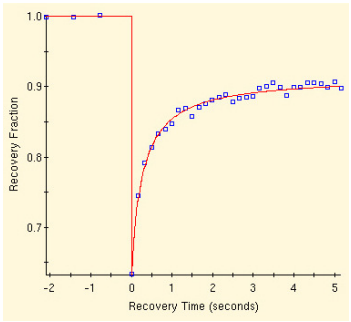

F. Recovery dynamics

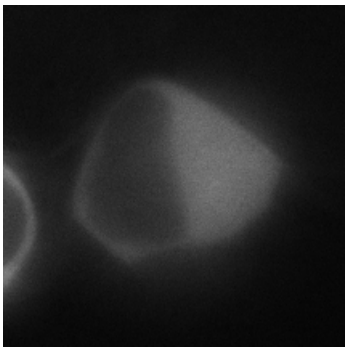

G. Pre-bleach

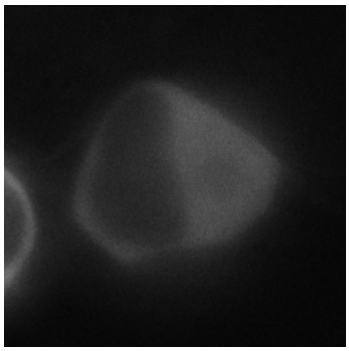

H. Bleach

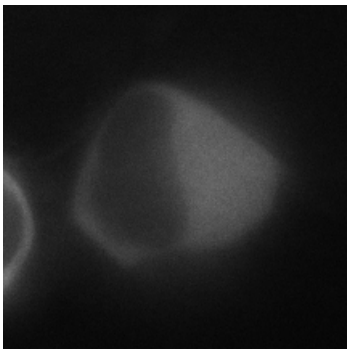

I. Recovery

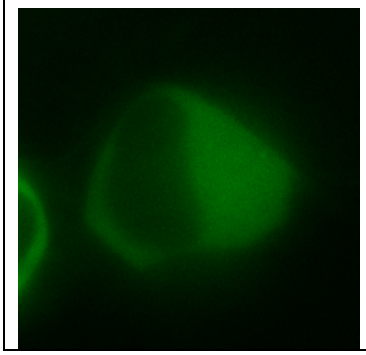

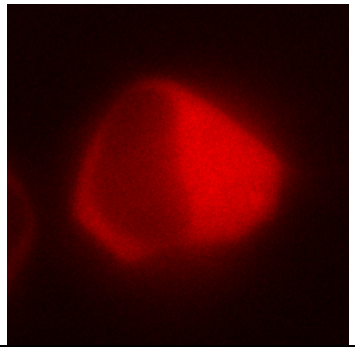

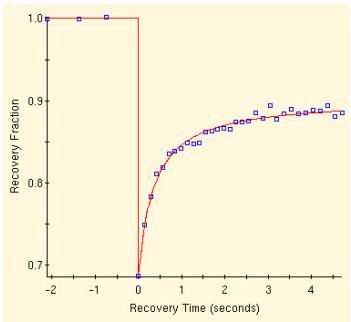

J. Keap1-EGFP	K. mCherry-Cul3	L. Recovery dynamics

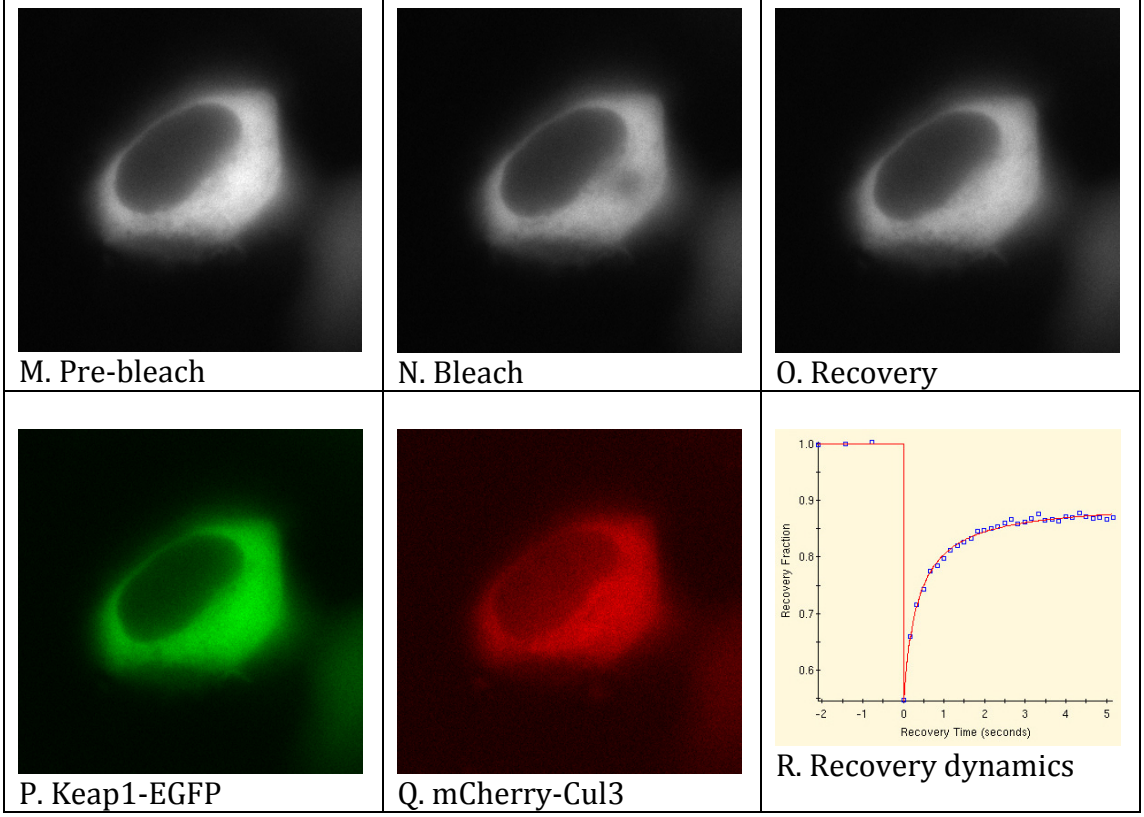

Figure 6.5. FRAP experiments to study the interaction between Keap1 and Cul3. HEK293 cells were transfected with Keap1-EGFP + mCherry-Cul3, and imaged 24 hours later. Six images in the panel above display the data from a single experiment, with A-F showing a representative example of data for cells treated with 10 μM STCA for 1 hour, G-L showing representative data for cells treated with 0.1 μM CDDO for 1 hour, and M-R showing data for cells treated with 5 μM SFN for 1 hour. Each cell was imaged three times pre-bleach (A), and 30 times post bleach (B) to capture the recovery of EGFP fluorescence (C). D and E show the localisation of Keap1-EGFP and mCherry-Cul3, whilst the recovery dynamics are plotted in the graph shown in F. From this graph, the T½ value was calculated as the amount of time required for half of the maximal intensity of fluorescence to be recovered.

results correlate well with previously published data, in which the interaction between Nrf2 and Keap1 has been shown to be maintained in response to a variety of inducers (Zhang et al. 2004, Eggler et al. 2005), which shows that the regulation of Nrf2 by Keap1 is more complex than the simple sequestration-release model (**Figure 1.2**) of Nrf2 by Keap1 in the cytoplasm.

It has previously been proposed that inducers function through the direct dissociation of Keap1-dependent E3-ubiquitin ligase (**Figure 1.3**) (Zhang et al. 2004, Gao et al. 2007, Rachakonda et al. 2008, Hur et al. 2010), particularly those inducers which target C-151 of Keap1. As there is currently no crystal structure of either the full-length Keap1 protein, or the Cul3-BTB domain interface, it is difficult so say with any certainty where the C151 residue is located. However, based on the published structures of the BTB-domain protein PLZF and the Cul-1 interacting protein Skp1, it has been suggested thatβ-strand-3 and α-helix-5 within the BTB domain are both important for BTB-Cul-3 interactions (Ahmad et al. 1998, Zheng et al. 2002, Zipper and Mulcahy 2002, Xu et al. 2003). Interestingly, C151 is located either within or adjacent to α-helix-5, which suggests that, based on its location, modification of C151 may disrupt Keap1-Cul3 binding.

As this model of Nrf2 regulation was not tested in our FRET experiments, we decided to test it using FRAP. Due to the increased stability of Keap1-EGFP compared with Nrf2-EGFP, Keap1-EGFP gave a much brighter image, and therefore inducers of several different types could be tested for their ability to dissociate Keap1 and Cul3. Because we wished to determine whether the dissociation of Keap1 from Cul3 caused the stabilisation of Nrf2, we chose the physiologically relevant time point of 1 hr after which to study the effects of inducers. Interestingly, we found that none of the inducers tested produced a change in the T½value of Keap1-EGFP (**Table 6.2**). Therefore, in contrast to previously published data, we must conclude from the FRAP experiments that none of the 4 inducers tested lead to the dissociation of Keap1 from Cul-3 after 1 hour of treatment.

The previously published data that led to the model of Keap1-Cul3 dissociation is based on co-IP experiments, where inducers were found to cause a modest reduction in the intensity of the pulled-down protein when either Keap1 or Cul-3 are used as the bait (Zhang et al. 2004, Gao et al. 2007, Rachakonda et al. 2008, Hur et al. 2010). Interestingly, although a range of inducers have been used to show this reduction in binding, the occurrence of dissociation has never been rigorously established. If inducers function primarily to dissociate the Keap1-Cul3 complex, then this dissociation should precede Nrf2

stabilisation. If true, this causality should be demonstrated experimentally, where the co-IP experiment showing reduced binding of Keap1 to Cul3 should be done at a time point prior to Nrf2 stabilisation. To date this has not been done. The published co-IP experiments show reduced binding between Keap1 and Cul3 at 2 hours for oxidised n-3 fatty acids, 2 hours for IAB and 5 hours for tBHQ and SFN (Zhang et al. 2004, Gao et al. 2007, Rachakonda et al. 2008, Hur et al. 2010). In contrast, inducers stabilise Nrf2 within 30 minutes (McMahon et al. 2003, Nguyen et al. 2003), and thus the published data do not adequately show that dissociation of the Keap1-Cul3 complex leads to stabilisation of Nrf2 as causality has not been demonstrated. We therefore conclude that, at least during the initial phase of Nrf2 stabilisation, inducers function to inactivate Keap1, and not by dissociating the Keap1-dependent E3 ubiquitin ligase.

Even though inducers did not alter the T½value in Keap1/Cul3 co-transfected cells, there was a degree of variability among experiments. Thus, **Table 6.2** shows that in the basal state, the T½value of Keap1-EGFP + mCherry-Cul3 varies from 0.320 to 0.416 s. This difference can be explained by differences in the microscope set-up. Before each experiment, the laser must be correctly aligned so that the bleach spot is as circular as possible to maximise the effectiveness of the bleaching. This alignment is performed manually and is responsible for the differences in bleaching seen among cells from different experiments. For example, in the experiment shown in **Figure 6.4H,L** the bleach reduced the intensity to 30% of the pre-bleach level, whilst in **Figure 6.5H,L** the bleached spot is at 70% of the pre-bleach level. Every effort was made to minimise these differences, but due to the fact that the alignment is carried out by hand, variations are inevitable. For this reason and in order to reduce the variation within a single experimental set, the basal controls were always imaged at the same time and with the same laser alignment as the induced samples.

In order to study the interaction between Keap1 and Cullin-3 using FRAP we had to tag both proteins with fluorphores. In the case of Keap1, the addition of a fluorophore at the C-terminus has been shown to have a minimal effect on the proteins function (Chapter 3). In the case of Cullin-3, the addition of any tag to either the N- or C-terminus inhibits the activity of the protein due to the location of the tag within the E3 ligase complex. Whilst it would be preferable

that the Cullin-3 fusion protein was functional, it does not change the conclusion drawn from these experiments. The aim of the Keap1 FRAP experiments was to determine whether the interaction between Keap1 and Cullin-3 changes in response to inducers. We have shown that the Keap1 and Cullin-3 fusion proteins are able to bind to one another in cells, and that this interaction in not altered by the addition of inducers (**Table 6.2**). The fact that our Cullin-3 fusion does not form a functional E3 ligase is unfortunate, but is not essential for these experiments, as the aim of the experiment was not to test the functionality of the E3 ligase complex but the interaction between Keap1 and Cullin-3.

Chapter 7

General Discussion

The overall aim of this project was to investigate the spatio-temporal dynamics of the regulation of the Keap1-Nrf2 interactions in individual cells by use of microscopy-based techniques. By analysing cellular processes at the single-cell level, the investigator can make discoveries which could be otherwise masked by cellular heterogeneity if tackled at the cell population level (Spiller et al. 2010). For example, single-cell analysis has revealed that the activation of the NF-κB pathway leads to a change in localisation of the transcription factor RelA, such that it oscillates between the cytoplasic and nuclear compartments due to the formation of a negative feedback loop between NF-κB and its negative regulator IκB (Nelson et al. 2004, Ashall et al. 2009). As these oscillations are asynchronous, this process can only be studied at the single cell level. Similarly, single cell analysis has been used to study the dynamics of the p53 response in the basal and induced state (Loewer et al. 2010). The authors found that in response to DNA damage, the p53 level followed a regular pulse-like pattern, with ~5 peaks over a 24-hour period. Interestingly, it was shown that in the absence of stressors, the p53 level also followed a pulse-like pattern, but with 1-2 pulses per 24 hours. As in the case of NF-κB, because these pulses of p53 stability are asynchronous between cells, they can only be detected in individual cells.

It has previously been suggested that the interaction between Keap1 and Nrf2 may be dynamic, and that this dynamism may be modulated by inducers (**Figures 1.2-1.7**). For this reason we decided to establish a single cell FLIM/ FRET system in which to study the interaction between Keap1 and Nrf2 in both the basal and induced state (**Chapter 3**). We found that in the basal state, Keap1 is able to bind to Nrf2, and that this interaction is maintained in the induced state (**Tables 3.2, 3.3**). We used FRAP to study the Keap1-Cul3 interaction (which together with Rbx1 form the E3-ubiquitin ligase responsible for targeting Nrf2

for ubiquitination), and found that the Keap1-Cul3 complex is not dissociated by inducers prior to Nrf2 stabilisation (**Chapter 6**).

Due to the high resolution of the FLIM/ FRET data, coupled with the use of various mutant forms of Nrf2 and Keap1, we were able to show that the Keap1-Nrf2 complex exists in two distinct conformations in the basal state, an open conformation, corresponding to Nrf2 bound to a single member of the Keap1 dimer, and a closed conformation, in which Nrf2 is bound to both members of the Keap1 dimer (**Chapter 4**). Interestingly, we found that inducers shift the balance in favour of the closed conformation (**Figures 5.2, 5.4**). In order to gain a deeper understanding of the relationship between the two conformations, we also inhibited the degradation of Nrf2 though use of the proteasomal inhibitor MG132. As with the inducers, MG132 causes accumulation of the Keap1-Nrf2 complex in the closed conformation, despite the fact that, to our knowledge, MG132 does not bind directly to Keap1 (**Figure 5.6**). These data suggest to us that the interaction between Keap1 and Nrf2 follows a cycle, whose function is to maintain Nrf2 at a low level in the basal state, but has the ability to rapidly stabilise Nrf2 when its cytoprotective properties are required, and allows for multiple forms of regulation (see below).

Our new cyclical model of Nrf2 regulation by Keap1 is shown schematically in **Figure 7.1A**. Newly translated Nrf2 (in yellow) binds first through its high affinity ETGE motif to one member of a free Keap1 dimer (in blue) to form the open conformation. It has previously been shown that when the ETGE motif alone is bound to the Keap1, Nrf2 is not targeted for ubiquitination by the E3-ubiquitin ligase (McMahon et al. 2006), and therefore whilst in the open conformation, Nrf2 is not ubiquitinated. After a period of time in the open conformation, Nrf2 progresses to form the closed conformation through the binding of the low affinity DLG motif to the other member of the Keap1 dimer. The formation of the closed conformation aligns Nrf2's lysine residues, located in the α-helix between the DLD and ETGE motifs, in such a way as to make ubiquitination possible. Thus, in the closed conformation, Nrf2 is polyubiquitinated, and subsequently released for degradation by the proteasome. The free Keap1 dimer is then able to bind to newly synthesized Nrf2 and the cycle begins again.

This model is supported experimentally by the data from cells treated with MG132 (**Figure 5.6A**). If the open and closed states were in equilibrium with one another, then blocking the destruction of Nrf2 by the proteasome should have no impact on the equilibrium of the complexes, and thus no changes

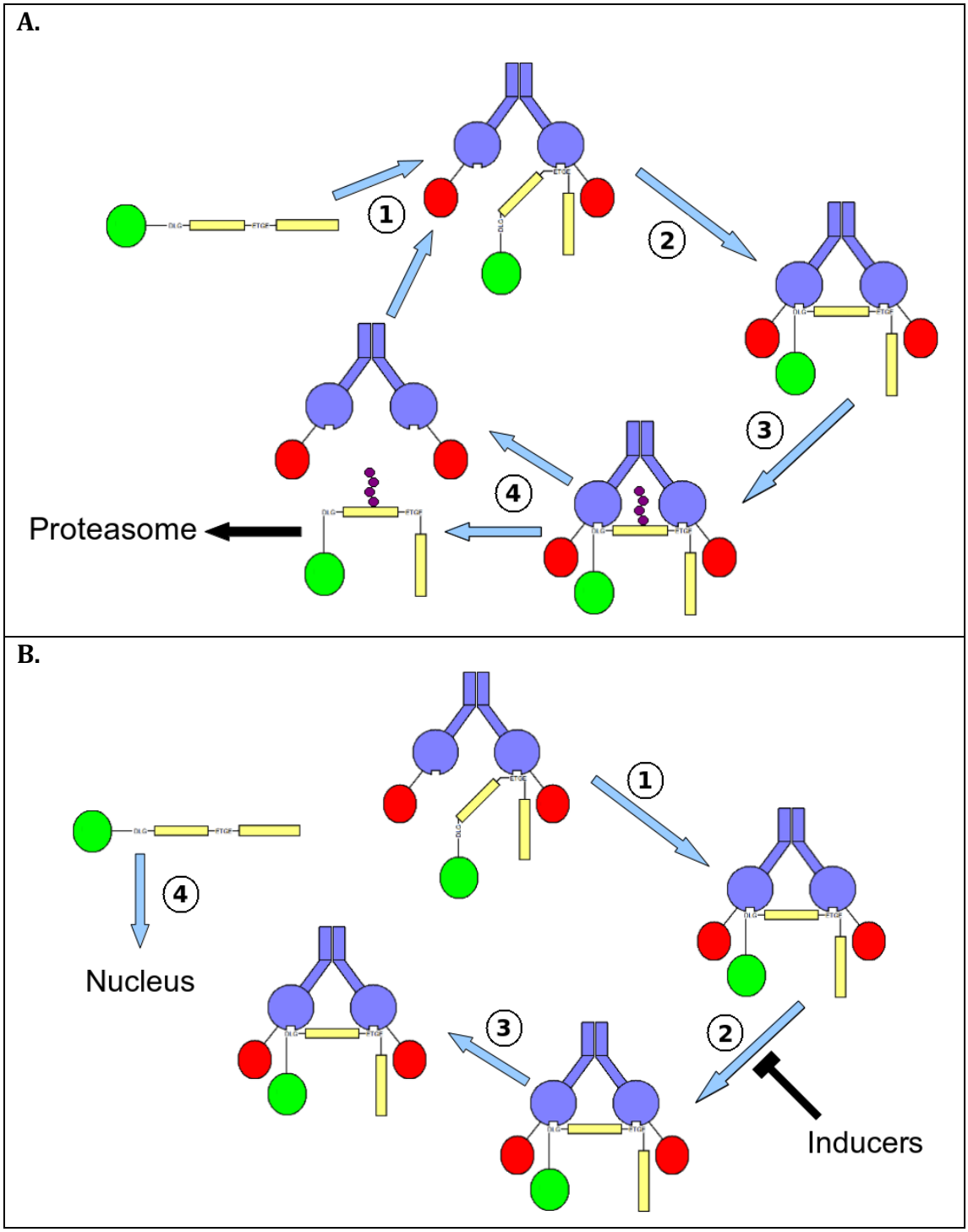

Figure 7.1. Cyclical model of the ubiquitination of Nrf2. A. In the basal state, newly translated Nrf2 (in yellow) binds to a free Keap1 dimer (in blue) through its ETGE motif

to form the open conformation (1). After a period of time in the open conformation, the DLG motif binds to the second member of the Keap1 dimer to form the closed conformation (2). Once in the closed conformation, Nrf2 can be targeted for ubiquitination by the Keap1-dependent E3-ubiquitin ligase (3). Once ubiquitinated, Nrf2 is released from Keap1 and degraded by the proteasome. The free Keap1 dimer is then able to bind to newly translate Nrf2 and the cycle begins again (4). **B.** Inducers function to uncouple the formation of the closed conformation from ubiquitination (2). This means that Nrf2 is not released from Keap1 (3), free Keap1 is not regenerated, and newly translated Nrf2 is able to translocate to the nucleus and turn on the expression of cytoprotective genes (4).

would be observed in either the lifetime of EGFP or the FRET efficiency of the interaction. As the MG132 treatment leads to an accumulation in the closed conformation, the data suggest that the different conformations are not in equilibrium, but that instead, they represent two distinct phases of a cycle. Inhibition of the proteasomal degradation of Nrf2 blocks the cycle, which leads to the accumulation of the Keap1-Nrf2 complex in the later stage of the cycle – in the closed conformation.

Inducers function to inhibit the ubiquitination of Nrf2 (Zhang et al. 2004, Kobayashi et al. 2006). Our data show that, at first glance paradoxically, this is coupled with the formation of the closed conformation of the Keap1-Nrf2 complex (**Figures 5.2, 5.4**), the same conformation that in the basal state is associated with the ubiquitination of Nrf2 (**Figure 7.1A**). This raises an important question: how can these two seemingly contradictory facts be reconciled?

We would suggest that the closed conformation in the basal and induced states are not identical, or more accurately, they are identical with respect to the relationship between the Kelch domain of Keap1 and Nrf2, but not with respect to Nrf2 with the rest of the Keap1-dependent E3-uqibuitin ligase (**Figure 7.2**). In the basal state, the closed conformation orientates the lysine residues of Nrf2 so that they can be ubiquitinated by the E2 ubiquitin-conjugating enzyme that is bound to the E3. The direct binding of inducers to reactive cysteine residues of Keap1 leads to conformational changes in Keap1 (Dinkova-Kostova et al. 2005a) such that, whilst Nrf2 is still bound to Keap1 through both its ETGE and DLG motifs, it is no longer correctly aligned with the E2 ubiquitin-conjugating enzyme, and thus ubiquitination does not occur. This results in the Keap1-Nrf2

complex accumulating in the closed conformation (**Figure 7.1B**), where, without ubiquitination, Nrf2 is effectively "trapped", and cannot be released by the Keap1 dimer. An interesting corollary of our model is that ubiquitination not only marks Nrf2 for proteasomal degradation, but also for release from Keap1.

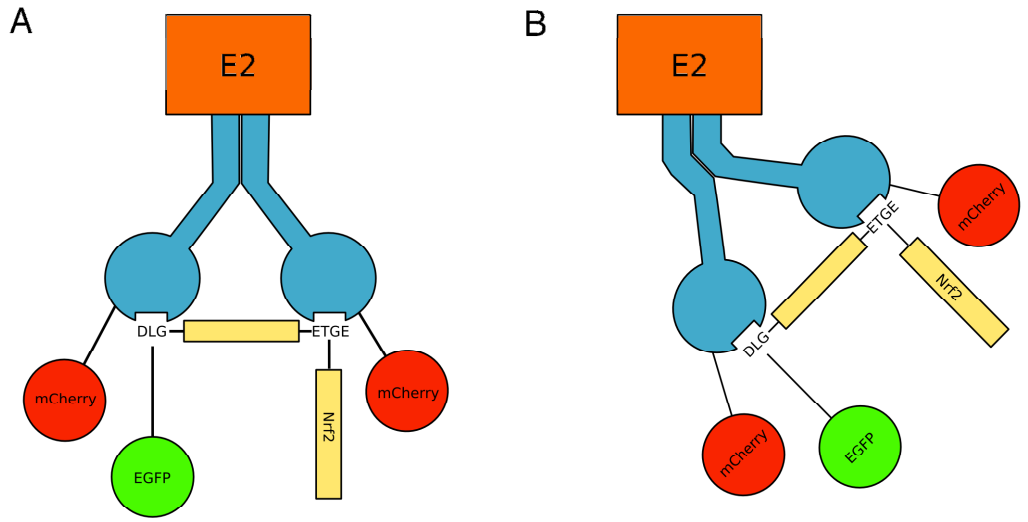

Figure 7.2 A comparison between the closed conformations in the basal and induced states. The cartoons above show a comparison between the closed conformations in the basal (A) and induced (B) state. In the images, Keap1 is shown in blue, mCherry in red, Nrf2 in yellow, EGFP in green and the E2 ubiquitin-conjugating enzyme in orange. **A.** The closed conformation in shown in the basal state, where Nrf2 is correctly aligned for ubiquitin transfer from the E2 to the lysine residues in the helix located between the DLG and ETGE motifs. **B.** The closed conformation in the induced state. Inducers bind directly to Keap1, leading to a conformational change in Keap1 and the misalignment of Nrf2 relative to the E2 enzyme. As a result of this misalignment, Nrf2 is not ubiquitinated by the E2 ubiquitin-conjugating enzyme, free Keap1 cannot be regenerated, and the newly synthesized Nrf2 is stabilised in the cell.

One prediction that can be made based on this model is that in the absence of new translation, inducers will have no effect on Nrf2 stabilisation. This has been shown to be the true by multiple groups, suggesting that de novo translation of Nrf2 is required for cytoprotection (Sekhar et al. 2000, Kobayashi et al. 2006, Shay et al. 2012). In tumour samples, gain-of-function mutations have been found in both the ETGE and DLG motifs, emphasising the importance of the two-site binding of Nrf2 to Keap1 (Shibata et al. 2008a). This correlates well with our model, where the loss of either motif will lead to stabilisation of Nrf2, due to the inability of the complex to form the closed conformation and allow the cycle to proceed.

One interesting feature of our model is the existence of the open conformation in the basal state. For what reason may this state exist, and why is the closed conformation not formed immediately upon Nrf2 binding to Keap1 through the high affinity ETGE motif? Analysis of the sequence of the Nrf2

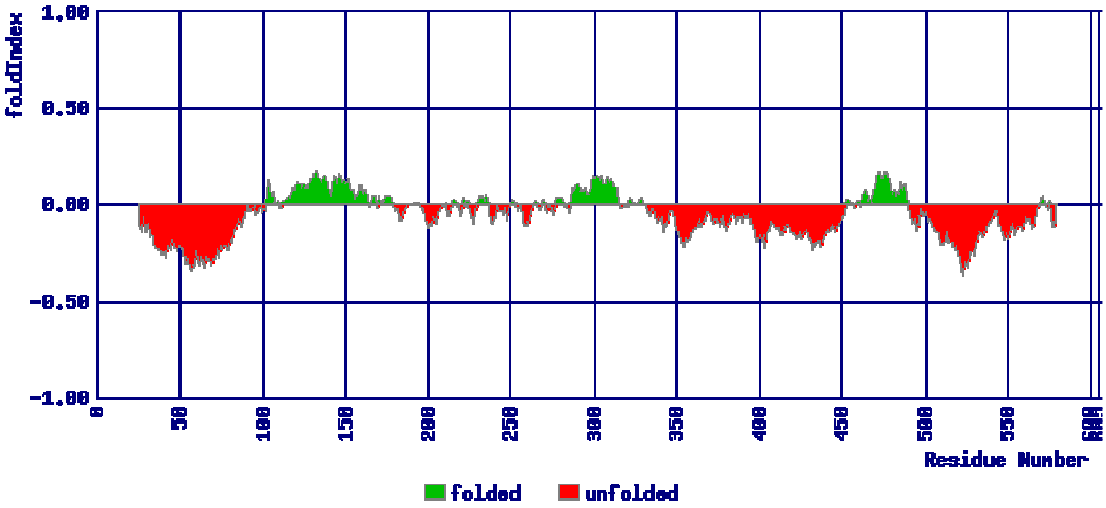

Figure 7.3.Folding status of human Nrf2 protein. The protein sequence of full-length human Nrf2 was analysed using the FoldIndex software (Prilusky et al. 2005). The image shows the Nrf2 sequence on the x-axis and the foldIndex value on the y-axis, where positive values (in green) indicate a folded region, and negative values (in red) indicate an unfolded region of the protein. The DLG and ETGE motifs of Nrf2 are located in the first 100 amino acids of the protein, and are thus in an unfolded region.

protein suggests that the Neh2 domain (which contains both the ETGE and DLG motifs) may be unfolded in the native state, and thus it may take time for the DLG motif to form the correct β-hairpin conformation required to bind to Keap1 (**Figure 7.3**)(Tong et al. 2007). Alternatively, the open conformation may be formed due to other proteins competing with the DLG motif of Nrf2 for Keap1 binding in the basal state (see below). Either way, it appears that the formation of the open conformation is an important feature of the Keap1-Nrf2 complex.

We believe that the existence of the open conformation provides the cell with advantages, as it allows Nrf2 activity to be regulated by other signalling pathways (**Figure 7.4**). It has recently been shown that both p21 (in the case of p53 activation) and p62 (in the case of autophagy inhibition) are also able to regulate Nrf2 activity. They do this by directly binding to regions of the Keap1-Nrf2 complex that are exposed in the open conformation, but may be hidden in the closed conformation: p21 binds to the DLG motif of Nrf2, and p62 competes

with the DLG motif for binding to the Kelch domain of Keap1 (Chen et al. 2009,Komatsu et al. 2010). In both cases, p21 and p62 inhibit the formation of the closed conformation, leading to the stabilisation of Nrf2. Thus, we believe that the

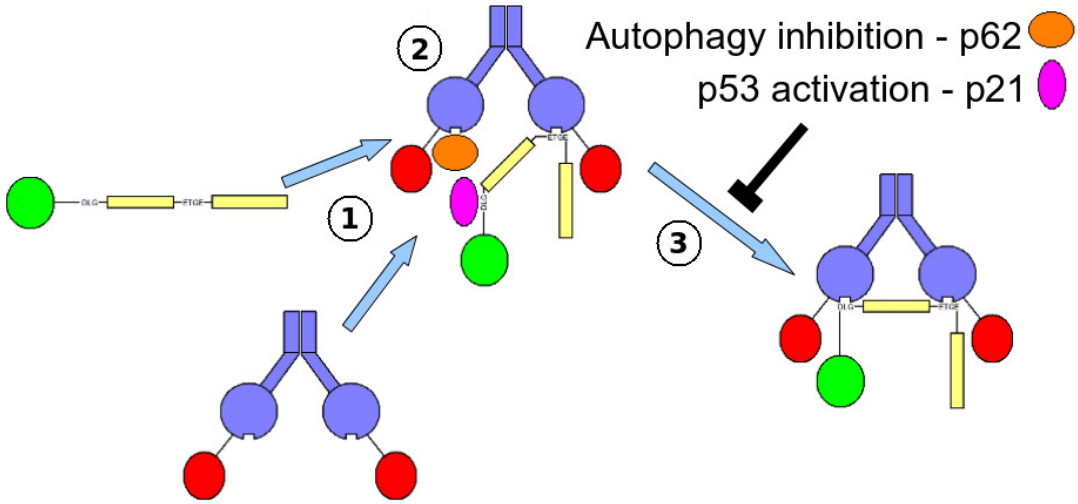

Figure 7.4. Regulation of Nrf2 by p21 and p62. In the basal state, newly translated Nrf2 (in yellow) binds to a free Keap1 dimer (in blue) through its ETGE motif to form the open conformation (1). In the case of either autophagy inhibition, p62 (in orange) or in the case of p53 activation, p21 (in purple) bind to motifs in the Keap1-Nrf2 complex which are exposed in the open conformation (2). This means that Nrf2 cannot form the closed conformation, and thus cannot be targeted for ubiquitination by Keap1, which disrupts the cycle and results in the stabilisation of Nrf2 (3).

Keap1-Nrf2 complex forms the open conformation to allow the cell to regulate cytoprotective gene expression through multiple pathways.

We believe that the responsiveness of the Keap1-Nrf2 pathway is fine tuned by the relative levels of Keap1 and Nrf2 proteins within the cell. The cycle of Nrf2 ubiquitination may be balanced such that the Keap1-dependent E3-ubiquitin ligase is functioning at its maximal capability in the basal state, and that the amount of newly-translated Nrf2 exactly matches the capacity of the E3 ligase to target it for degradation. This “tipping point” state and lack of buffering capacity allows the pathway to respond exceedingly quickly to the cellular environment and allows the cell to rapidly upregulate cytoprotective genes.

The idea that the cycle is finely balanced is well supported by existing data. In pancreatic cancer, a modest (less than 2-fold) K-Ras-dependent increase in transcription of Nrf2 leads an increase in Nrf2 protein levels and transcription

of cytoprotective genes (DeNicola et al. 2011). This suggests that in the basal state, the Nrf2 cycle operates at a level close to saturation, and that any increase in the transcription or translation of Nrf2 overloads Keap1, which in turn allows newly translated Nrf2 to translocate to the nucleus and turn on expression of target genes. Conversely, a reduction in the level of Keap1 also leads to an increase in Nrf2 protein levels (Taguchi et al. 2010), which reinforces the idea that the system has little spare capacity, presumably to allow for rapid upregulation of Nrf2-dependent genes when required by the cell.

The proposition that the binding of Nrf2 to Keap1, and the subsequent ubiquitination of Nrf2, follows a cycle is not without precedent. It has previously been suggested that the formation and dissociation of E3-ubiquitin ligases follows a cyclical pattern regulated by the ubiquitin-like protein Nedd8 (Cope and Deshaies 2003). This suggests that regulatory cycles might be a common mechanistic theme in protein ubiquitination and degradation.

Interestingly, the weak EGFP-Nrf2 signal in the nucleus could, in most cases, also be analysed. Here we found that in the basal state, the Keap1-Nrf2 complex exists exclusively in the open conformation (**Figure 4.11**). Both inducers and inhibition of the proteasome were able to promote the formation of the closed complex in the nucleus (**Figures 5.3, 5.7**), suggesting that although the closed conformation can be formed there, under normal circumstances it does not, presumably as other proteins such as Prothymosin-α or Palb2 compete with the DLG motif of Nrf2 for binding to Keap1. The absence of the closed conformation in the nucleus at basal state suggests that in this compartment, Nrf2 is not targeted for ubiquitination by Keap1. This makes biological sense, as Nrf2-dependent transcription does occur in the basal state (McMahon et al. 2001), and if Keap1 was too efficient then this basal transcription would not have been possible.

Future work

From the model presented in **Figure 7.1**, a number of testable predictions can be made which would either support or refute our model. Firstly, if the binding of Nrf2 to Keap1 follows a cycle, then inhibiting the entry of newly

synthesised Nrf2 into the cycle should lead a reduction in the amount of the complex in the open conformation relative to the closed conformation. When these experiments were carried out using cycloheximide to inhibit the translation of Nrf2, we observed an increase in interaction in the closed conformation, as would be predicted from our model. In addition, from **Figure 7.4** it is suggested that competition for binding to Keap1 with the DLG motif of Nrf2 will lead to an increase in the Keap1-Nrf2 complex bound in the open conformation. In order to test this, we used the small molecule HB229, which binds directly to the Kelch domain of Keap1, to compete with the DLG motif of Nrf2 for Keap1 binding, and in these experiments we observed an increased EGFP-Nrf2 lifetime, and an increase in the interaction in the open conformation. This suggests that by competing for binding of Keap1 with the DLG motif of Nrf2, small molecules, or proteins such as p21 or p62 inhibit the formation of the closed conformation and thus inhibit the ubiquitination of Nrf2.

In order to improve upon and support our model of the interaction between Keap1 and Nrf2, future experiments should be carried out using an independent methodology to validate our FLIM results. One powerful method that has the potential to complement our FRET data is fluorescence cross-correlation spectroscopy (FCCS), another microscopy-based single cell analysis technique which could be used to study the Keap1-Nrf2 complex.

FCCS involves imaging a small volume (1 pixel of a confocal image) within a cell over a short period of time, and measuring the fluctuations of the fluorescence signal through the volume (Bacia and Schwille 2007). As fluorescent proteins diffuse into and out of the imaged region, the intensity of the signal fluctuates about a mean value, and thus FCCS allows the user to determine the average level of fluorescence in the cell, and by extension, the concentration of any fusion protein which is fluorescently labelled. Interestingly, FCCS allows the user to track two fluorescent channels at once, which allows the user to study the binding kinetics within a protein complex. This is because FCCS measures three variables, the diffusion of the two different coloured fluorophores (eg EGFP and mCherry), and the co-diffusion of EGFP and mCherry together. If co-diffusion is observed (that is, if a fluctuation in the green channel occurs at exactly the same time at the red channel), it suggests that the fusion proteins are diffusing

together through the imaged volume as a complex. Because the data generated from FCCS are numerical it can be used to study the binding kinetics of protein complexes in live cells (for an example see equation 7.1). FCCS has been used to study a variety of cellular processes, including signal transduction through the MAP Kinase pathway (Maeder et al. 2007, Slaughter et al. 2007).

$$K_d = \frac{[Green][Red]}{[Bound]} \quad \text{Equation 7.1}$$

where: K_d = dissociation constant of the green and red protein complex

[Green] = concentration of green labelled proteins not in a complex with red labelled proteins

[Red] = concentration of red labelled proteins not in a complex with green labelled proteins

[Bound] = concentration of the complex between green and red labelled proteins

Because FCCS measures fluctuations in the fluorescence signals, a low fluorescence intensity provides the best data, as when the signal is weak a small fluctuation in the intensity has a larger effect on the measured signal. For example, if each EGFP protein gives an intensity value of 1 and, on average, only 5 EGFP proteins are present in a given pixel, then the diffusion of a single protein out of this pixel will reduce the intensity by 20%. However, if the overall intensity of the EGFP signal in the cell is high, and on average 100 EGFP proteins are present in each pixel, then the diffusion of a single protein out of the imaged pixel will reduce the intensity by only 1%, thus greatly reducing the sensitivity of the technique.

For this reason, FCCS would not only complement the existing FLIM data, but would also improve upon one of the flaws of the model as it is currently presented: the fact that the current data are derived from an overexpression system.

To extend the current project, and to better understand the physiological interaction between Keap1 and Nrf2, EGFP and mCherry fusion proteins of

Keap1 and Nrf2 would be knocked into the endogenous Keap1 and Nrf2 loci in a well characterised cell line which responds well to inducers, such as Hepa1c1c7 cells. This would mean that the level of the fusion proteins would be tightly regulated by endogenous transcriptions factors, and would accurately model the physiological response to inducers and stress.

In this system, we would knock-into the Nrf2 locus both wild type Nrf2 and the two binding mutants used in the FRET experiments. We would expect the 2xETGE mutant to bind most tightly to Keap1 (and thus have the lowest K_d), the ΔDLG to bind weakly to Keap1 (and thus have the highest K_d), and for wild type Nrf2 to have a K_d value between the two mutants, showing that both the open and closed conformations are present in the basal state. We could then use this basal data as a reference point to study the interaction between Keap1 and Nrf2 in response to inducers. If the FCCS data supported the FLIM data, we would expect to see that the accumulation of the Keap1-Nrf2 complex in the closed conformation in the induced state corresponds with a reduced K_d in the FCCS measurements.

References

Abbas T, Dutta A (2009) p21 in cancer: intricate networks and multiple activities. Nat Rev Cancer 9:400-414

Ahmad KF, Engel CK, Prive GG (1998) Crystal structure of the BTB domain from PLZF. Proc Natl Acad Sci USA 95:12123-12128

Ahn YH, Hwang Y, Liu H, Wang XJ, Zhang Y, Stephenson KK, Boronina TN, Cole RN, Dinkova-Kostova AT, Talalay P, Cole PA (2010) Electrophilic tuning of the chemoprotective natural product sulforaphane. Proc Natl Acad Sci USA 107:9590-9595

Akao M, Kuroda K (1990) Inhibitory effect of fumaric acid on hepatocarcinogenesis by thioacetamide in mice. Chem Pharm Bull (Tokyo) 38:2012-2014

Alam J, Wicks C, Stewart D, Gong P, Touchard C, Otterbein S, Choi AM, Burow ME, Tou J (2000) Mechanism of heme oxygenase-1 gene activation by cadmium in MCF-7 mammary epithelial cells. Role of p38 kinase and Nrf2 transcription factor. J Biol Chem 275:27694-27702

An JH, Blackwell TK (2003) SKN-1 links C. elegans mesendodermal specification to a conserved oxidative stress response. Genes Dev 2003 17:1882-1893

Ansell PJ, Lo SC, Newton LG, Espinosa-Nicholas C, Zhang DD, Liu JH, Hannink M, Lubahn DB. (2005) Repression of cancer protective genes by 17beta-estradiol: ligand-dependent interaction between human Nrf2 and estrogen receptor alpha. Mol Cell Endocrinol 243:27-34

Aoki Y, Sato H, Nishimura N, Takahashi S, Itoh K, Yamamoto M (2001) Accelerated DNA adduct formation in the lung of the Nrf2 knockout mouse exposed to diesel exhaust. Toxicol Appl Pharmacol 173:154-160

Aoki Y, Hashimoto AH, Amanuma K, Matsumoto M, Hiyoshi K, Takano H, Masumura K, Itoh K, Nohmi T, Yamamoto M (2007) Enhanced spontaneous and benzo(a)pyrene-induced mutations in the lung of Nrf2-deficient gpt delta mice. Cancer Res 67:5643-5648

Arai R, Ueda H, Kitayama A, Kamiya N, Nagamune T (2001) Design of the linkers which effectively separate domains of a bifunctional fusion protein. Protein Eng 14:529-532

Ashall L, Horton CA, Nelson DE, Paszek P, Harper CV, Sillitoe K, Ryan S, Spiller DG, Unitt JF, Broomhead DS, Kell DB, Rand DA, See V, White MRH (2009) Pulsatile stimulation determines timing and specificity of NF-κB-dependent transcription. Science 324:242-246

Asher G, Lotem J, Cohen B, Sachs L, Shaul Y. Regulation of p53 stability and p53-dependent apoptosis by NADH quinone oxidoreductase 1 (2001) Proc Natl Acad Sci USA 98:1188-1193

Asher G, Lotem J, Sachs L, Kahana C, Shaul Y (2002) Mdm-2 and ubiquitin-independent p53 proteasomal degradation regulated by NQO1. Proc Natl Acad Sci USA 99:13125-13130

Bacia K, Schwille P (2007) Practical guidelines for dual-color fluorescence cross-correlation spectroscopy. Nat Protocol 2: 2842-2856

Bae I, Fan S, Meng Q, Rih JK, Kim HJ, Kang HJ, Xu J, Goldberg ID, Jaiswal AK, Rosen EM (2004) BRCA1 induces antioxidant gene expression and resistance to oxidative stress. Cancer Res 64:7893-7909

Baeuerle PA, Baltimore D (1988) I□B: a specific inhibitor of the NF-□B transcription factor. Science 242:540-546

Baird L, Dinkova-Kostova AT (2011) The cytoprotective role of the Keap1-Nrf2 pathway. Arch Toxicol 85: 241-272

Bakin AV, Stourman NV, Sekhar KR, Rinehart C, Yan X, Meredith MJ, Arteaga CL, Freeman ML (2005) Smad3-ATF3 signaling mediates TGF-beta suppression of genes encoding Phase II detoxifying proteins. Free Radic Biol Med 38:375-387

Bannai S, Ishii T (1982) Transport of cystine and cysteine and cell growth in cultured human diploid fibroblasts: effect of glutamate and homocysteate. J Cell Physiol 112:265-272

Bashir T, Dorrello NV, Amador V, Guardavaccaro D, Pagano M (2004) Control of the SCF(Skp2-Cks1) ubiquitin ligase by the APC/C(Cdh1) ubiquitin ligase. Nature 428:190-193

Becks L, Prince M, Burson H, Christophe C, Broadway M, Itoh K, Yamamoto M, Mathis M, Orchard E, Shi R, McLarty J, Pruitt K, Zhang S, Kleiner-Hancock HE (2010) Aggressive mammary carcinoma progression in Nrf2 knockout mice treated with 7,12-dimethylbenz[a]anthracene. BMC Cancer 10:540

Bensasson RV, Zoete V, Dinkova-Kostova AT, Talalay P (2008) Two-step mechanism of induction of the gene expression of a prototypic cancer-protective enzyme by diphenols. Chem Res Toxicol 21:805-812

Bensasson RV, Zoete V, Berthier G, Talalay P, Dinkova-Kostova AT (2010) Potency ranking of triterpenoids as inducers of a cytoprotective enzyme and as inhibitors of a cellular inflammatory response via their electron affinity and their electrophilicity index. Chem Biol Interact 186:118-126

Benson AM, Batzinger RP, Ou SY, Bueding E, Cha YN, Talalay P (1978) Elevation of hepatic glutathione *S*-transferase activities and protection against mutagenic metabolites of benzo(*a*)pyrene by dietary antioxidants. Cancer Res 38:4486-4495

Benson AM, Cha YN, Bueding E, Heine HS, Talalay P (1979) Elevation of extrahepatic glutathione S-transferase and epoxide hydratase activities by 2(3)-tert-butyl-4-hydroxyanisole. Cancer Res 39:2971-2977

Benson AM, Hunkeler MJ, Talalay P (1980) Increase of NAD(P)H:quinone reductase by dietary antioxidants: possible role in protection against carcinogenesis and toxicity. Proc Natl Acad Sci USA 77:5216-5220

Beyer TA, Xu W, Teupser D, auf dem Keller U, Bugnon P, Hildt E, Thiery J, Kan YW, Werner S (2008) Impaired liver regeneration in Nrf2 knockout mice: role of ROS-mediated insulin/IGF-1 resistance. EMBO J 27:212-223

Bhattacharya A, Li Y, Wade KL, Paonessa JD, Fahey JW, Zhang Y (2010) Allyl Isothiocyanate-rich mustard seed powder inhibits bladder cancer growth and muscle invasion. Carcinogenesis in press

Biteau B, Labarre J, Toledano MB (2003) ATP-dependent reduction of cysteine-sulphinic acid by S. cerevisiae sulphiredoxin. Nature 425:980-984

Bloom DA, Jaiswal AK (2003) Phosphorylation of Nrf2 at Ser40 by protein kinase C in response to antioxidants leads to the release of Nrf2 from INrf2, but is not required for Nrf2 stabilization/accumulation in the nucleus and

transcriptional activation of antioxidant response element-mediated NAD(P)H:quinone oxidoreductase-1 gene expression. J Biol Chem 278:44675-44682

Borst P, Evers R, Kool M, Wijnholds J (2000) A family of drug transporters: the multidrug resistance-associated proteins. J Natl Cancer Inst 92:1295-1302

Brown SL, Sekhar KR, Rachakonda G, Sasi S, Freeman ML (2008) Activating transcription factor 3 is a novel repressor of the nuclear factor erythroid-derived 2-related factor 2 (Nrf2)-regulated stress pathway. Cancer Res 68:364-368

Burczynski ME, Lin HK, Penning TM (1999) Isoform-specific induction of a human aldo-keto reductase by polycyclic aromatic hydrocarbons (PAHs), electrophiles, and oxidative stress: implications for the alternative pathway of PAH activation catalysed by human dihydrodiol dehydrogenase. Cancer Res 59:607-614

Calkins MJ, Jakel RJ, Johnson DA, Chan K, Kan YW, Johnson JA (2005) Protection from mitochondrial complex II inhibition in vitro and in vivo by Nrf2-mediated transcription. Proc Natl Acad Sci USA 102:244-249

Chambers KF, Bacon JR, Kemsley EK, Mills RD, Ball RY, Mithen RF, Traka MH (2009) Gene expression profile of primary prostate epithelial and stromal cells in response to sulforaphane or iberin exposure. Prostate 69:1411-1421

Chan K, Kan YW (1999) Nrf2 is essential for protection against acute pulmonary injury in mice. Proc Natl Acad Sci USA 96:12731-12736

Chanas SA, Jiang Q, McMahon M, McWalter GK, McLellan LI, Elcombe CR, Henderson CJ, Wolf CR, Moffat GJ, Itoh K, Yamamoto M, Hayes JD (2002) Loss of the Nrf2 transcription factor causes a marked reduction in constitutive and inducible expression of the glutathione S-transferase Gsta1, Gsta2, Gstm1, Gstm2, Gstm3 and Gstm4 genes in the livers of male and female mice. Biochem J 365:405-416

Chang LC, Gerhäuser C, Song L, Farnsworth NR, Pezzuto JM, Kinghorn AD (1997) Activity-guided isolation of constituents of *Tephrosia purpurea* with the

potential to induce the phase II enzyme, quinone reductase. J Nat Prod 60:869-873

Chen W, Sun Z, Wang XJ, Jiang T, Huang Z, Fang D, Zhang DD (2009) Direct interaction between Nrf2 and p21(Cip1/WAF1) upregulates the Nrf2-mediated antioxidant response. Mol Cell 34:663-673

Cho HY, Reddy SP, Debiase A, Yamamoto M, Kleeberger SR (2005) Gene expression profiling of NRF2-mediated protection against oxidative injury. Free Radic Biol Med 38:325-343

Chowdhry S, Zhang Y, McMahon M, Sutherland C, Cuadrado A, Hayes JD (2012) Nrf2 is controlled by two distinct β-TrCP recognition motifs in its Neh6 domain, one of which can be modulated by GSK-3 activity. Oncogene, in press

Chung FL, Conaway CC, Rao CV, Reddy BS (2000) Chemoprevention of colonic aberrant crypt foci in Fischer rats by sulforaphane and phenethyl isothiocyanate. Carcinogenesis 21:2287-2291

Conaway CC, Wang CX, Pittman B, Yang YM, Schwartz JE, Tian D, McIntee EJ, Hecht SS, Chung FL (2005) Phenethyl isothiocyanate and sulforaphane and their N-acetylcysteine conjugates inhibit malignant progression of lung adenomas induced by tobacco carcinogens in A/J mice. Cancer Res 65:8548-8557

Cope GA, Deshaies RJ (2003) COP9 Signalosome: A multifunctional regulator of SCF and other Cullin-based ubiquitin ligases. Cell 114:663-671

Coulouarn C, Factor VM, Thorgeirsson SS (2008) Transforming growth factor-beta gene expression signature in mouse hepatocytes predicts clinical outcome in human cancer. Hepatology 47:2059-2067

Cullinan SB, Zhang D, Hannink M, Arvisais E, Kaufman RJ, Diehl JA (2003) Nrf2 is a direct PERK substrate and effector of PERK-dependent cell survival. Mol Cell Biol 23:7198-7209

Cullinan SB, Diehl JA (2004) PERK-dependent activation of Nrf2 contributes to redox homeostasis and cell survival following endoplasmic reticulum stress. J Biol Chem 279:20108-20117

Cullinan SB, Gordan JD, Jin J, Harper JW, Diehl JA (2004) The Keap1-BTB protein is an adaptor that bridges Nrf2 to a Cul3-based E3 ligase: oxidative stress sensing by a Cul3-Keap1 ligase. Mol Cell Biol 24:8477-8486

Dash PK, Zhao J, Orsi SA, Zhang M, Moore AN (2009) Sulforaphane improves cognitive function administered following traumatic brain injury. Neurosci Lett 460:103-107

Delaunay A, Isnard AD, Toledano MB (2000) H_2O_2 sensing through oxidation of the Yap1 transcription factor. EMBO J 19:5157-5166

De Long MJ, Prochaska HJ, Talalay P (1985) Tissue-specific induction patterns of cancer-protective enzymes in mice by tert-butyl-4-hydroxyanisole and related substituted phenols. Cancer Res 45:546-551

DeNicola GM, Karreth FA, Humpton TJ, Gopinathan A, Wei C, Frese K, Mangal D, Yu KH, Yeo CJ, Calhoun ES, Scrimieri F, Winter JM, Hruban RH, Iacobuzio-Donahue C, Kern SE, Blair IA, Tuveson DA (2011) Oncogene-induced Nrf2 transcription promotes ROS detoxification and tumorigenesis. Nature 475:106-109

Derynck R, Akhurst RJ, Balmain A (2001) TGF-beta signaling in tumor suppression and cancer progression. Nat Genet 29:117-129

Desaint S, Luriau S, Aude JC, Rousselet G, Toledano MB (2004) Mammalian antioxidant defences are not inducible by H_2O_2. J Biol Chem 279:31157-31163

Devling TW, Lindsay CD, McLellan LI, McMahon M, Hayes JD (2005) Utility of siRNA against Keap1 as a strategy to stimulate a cancer chemopreventive phenotype. Proc Natl Acad Sci USA 102:7280-7285

Dhakshinamoorthy S, Jain AK, Bloom DA, Jaiswal AK (2005) Bach1 competes with Nrf2 leading to negative regulation of the antioxidant response element (ARE)-mediated NAD(P)H:quinone oxidoreductase 1 gene expression and induction in response to antioxidants. J Biol Chem 280:16891-1900

DiDonato JA, Hayakawa M, Rothwarf DM, Zandi E, Karin M (1997) A cytokine-responsive I□B kinase that activates the transcription factor NF-□B. Nature 388:548-554

Dinkova-Kostova AT, Abeygunawardana C, Talalay P (1998) Chemoprotective properties of phenylpropenoids, bis(benzylidene)cycloalkanones, and related Michael reaction acceptors: correlation of potencies as phase 2 enzyme inducers and radical scavengers. J Med Chem 41:5287-5296

Dinkova-Kostova AT, Talalay P (1999) Relation of structure of curcumin analogs to their potencies as inducers of Phase 2 detoxification enzymes. Carcinogenesis 20:911-914

Dinkova-Kostova AT, Massiah MA, Bozak RE, Hicks RJ, Talalay P (2001) Potency of Michael reaction acceptors as inducers of enzymes that protect against carcinogenesis depends on their reactivity with sulfhydryl groups. Proc Natl Acad Sci USA 98:3404-3409

Dinkova-Kostova AT, Holtzclaw WD, Cole RN, Itoh K, Wakabayashi N, Katoh Y, Yamamoto M, Talalay P (2002) Direct evidence that sulfhydryl groups of Keap1 are the sensors regulating induction of phase 2 enzymes that protect against carcinogens and oxidants. Proc Natl Acad Sci USA 99:11908-11913

Dinkova-Kostova AT, Holtzclaw WD, Wakabayashi N (2005a) Keap1, the sensor for electrophiles and oxidants that regulates the phase 2 response, is a zinc metalloprotein. Biochemistry 44:6889-6899

Dinkova-Kostova AT, Liby KT, Stephenson KK, Holtzclaw WD, Gao X, Suh N, Williams C, Risingsong R, Honda T, Gribble GW, Sporn MB, Talalay P (2005b) Extremely potent triterpenoid inducers of the phase 2 response: correlations of protection against oxidant and inflammatory stress. Proc Natl Acad Sci USA 102:4584-4589

Dinkova-Kostova AT, Jenkins SN, Fahey JW, Ye L, Wehage SL, Liby KT, Stephenson KK, Wade KL, Talalay P (2006) Protection against UV-light-induced skin carcinogenesis in SKH-1 high-risk mice by sulforaphane-containing broccoli sprout extracts. Cancer Lett 240:243-252

Dinkova-Kostova AT, Jenkins SN, Wehage SL, Huso DL, Benedict AL, Stephenson KK, Fahey JW, Liu H, Liby KT, Honda T, Gribble GW, Sporn MB, Talalay P (2008) A dicyanotriterpenoid induces cytoprotective enzymes and reduces multiplicity of skin tumors in UV-irradiated mice. Biochem Biophys Res Commun 367:859-865

Dinkova-Kostova AT, Talalay P (2010) NAD(P)H:quinone acceptor oxidoreductase 1 (NQO1), a multifunctional antioxidant enzyme and exceptionally versatile cytoprotector. Arch Biochem Biophys 501:116-123

Dinkova-Kostova AT, Talalay P, Sharkey J, Zhang Y, Holtzclaw WD, Wang XJ, David E, Schiavoni KH, Finlayson S, Mierke DF, Honda T (2010) An exceptionally potent inducer of cytoprotective enzymes: elucidation of the structural features that determine inducer potency and reactivity with Keap1. J Biol Chem 285:33747-33755

Dumont M, Wille E, Calingasan NY, Tampellini D, Williams C, Gouras GK, Liby K, Sporn M, Nathan C, Flint Beal M, Lin MT (2009) Triterpenoid CDDO-methylamide improves memory and decreases amyloid plaques in a transgenic mouse model of Alzheimer's disease. J Neurochem 109:502-512

Eggler AL, Liu G, Pezzuto JM, van Breemen RB, Mesecar AD (2005) Modifying specific cysteines of the electrophile-sensing human Keap1 protein is insufficient to disrupt binding to the Nrf2 domain Neh2. Proc Natl Acad Sci USA 102:10070-10075

Eggler AL, Small E, Hannink M, Mesecar AD (2009) Cul3-mediated Nrf2 ubiquitination and antioxidant response element (ARE) activation are dependent on the partial molar volume at position 151 of Keap1. Biochem J 422:171-180

Enomoto A, Itoh K, Nagayoshi E, Haruta J, Kimura T, O'Connor T, Harada T, Yamamoto M (2001) High sensitivity of Nrf2 knockout mice to acetaminophen hepatotoxicity associated with decreased expression of ARE-regulated drug metabolizing enzymes and antioxidant genes. Toxicol Sci 59:169-177

Esposito F, Cuccovillo F, Russo L, Casella F, Russo T, Cimino F (1998) A new p21waf1/cip1 isoform is an early event of cell response to oxidative stress. Cell Death Differ 5:940-945

Fagerholm R, Hofstetter B, Tommiska J, Aaltonen K, Vrtel R, Syrjäkoski K, Kallioniemi A, Kilpivaara O, Mannermaa A, Kosma VM, Uusitupa M, Eskelinen M, Kataja V, Aittomäki K, von Smitten K, Heikkilä P, Lukas J,

Holli K, Bartkova J, Blomqvist C, Bartek J, Nevanlinna H (2008) NAD(P)H:quinone oxidoreductase 1 NQO1*2 genotype (P187S) is a strong prognostic and predictive factor in breast cancer. Nat Genet 40:844-853

Fahey JW, Zhang Y, Talalay P (1997) Broccoli sprouts: an exceptionally rich source of inducers of enzymes that protect against chemical carcinogens. Proc Natl Acad Sci USA 94:10367-10372

Fahey JW, Zalcmann AT, Talalay P (2001) The chemical diversity and distribution of glucosinolates and isothiocyanates among plants. Phytochemistry 56:5-51

Fahey JW, Haristoy X, Dolan PM, Kensler TW, Scholtus I, Stephenson KK, Talalay P, Lozniewski A (2002) Sulforaphane inhibits extracellular, intracellular, and antibiotic-resistant strains of Helicobacter pylori and prevents benzo[*a*]pyrene-induced stomach tumors. Proc Natl Acad Sci USA 99:7610-7615

Fahey JW, Dinkova-Kostova AT, Stephenson KK, Talalay P (2004) The "Prochaska" microtiter plate bioassay for inducers of NQO1. Methods Enzymol 382:243-258

Faraonio R, Vergara P, Di Marzo D, Pierantoni MG, Napolitano M, Russo T, Cimino F (2006) p53 suppresses the Nrf2-dependent transcription of antioxidant response genes. J Biol Chem 281:39776-39784

Fourquet S, Guerois R, Biard D, Toledano MB (2010) Activation of NRF2 by nitrosative agents and H2O2 involves KEAP1 disulfide formation. J Biol Chem 285:8463-8471

Friling RS, Bensimon A, Tichauer Y, Daniel V (1990) Xenobiotic-inducible expression of murine glutathione S-transferase Ya subunit gene is controlled by an electrophile-responsive element. Proc Natl Acad Sci USA 87:6258-6262

Frohlich DA, McCabe MT, Arnold RS, Day ML (2008) The role of Nrf2 in increased reactive oxygen species and DNA damage in prostate tumorigenesis. Oncogene 27:4353-4362

Furukawa M, He YJ, Borchers C, Xiong Y (2003) Targeting of protein ubiquitination by BTB-Cullin 3-Roc1 ubiquitin ligases. Nat Cell Biol 5:1001-1007

Furukawa M, Xiong Y (2005) BTB protein Keap1 targets antioxidant transcription factor Nrf2 for ubiquitination by the Cullin 3-Roc1 ligase. Mol Cell Biol 25:162-171

Galan JM, Peter M (1999) Ubiquitin-dependent degradation of multiple F-box proteins by an autocatalytic mechanism. Proc Natl Acad Sci USA 96:9124-9129

Gao L, Wang J, Sekhar KR, Yin H, Yared NF, Schneider SN, Sasi S, Dalton TP, Anderson ME, Chan JY, Morrow JD, Freeman ML (2007) Novel n-3 fatty acid oxidation products activate Nrf2 by destabilizing the association between Keap1 and Cullin3. J Biol Chem 282:2529-2537

Gartel AL, Tyner AL (2002) The role of the cyclin-dependent kinase inhibitor p21 in apoptosis. Mol Cancer Ther 1:639-649

Gasper AV, Traka M, Bacon JR, Smith JA, Taylor MA, Hawkey CJ, Barrett DA, Mithen RF (2007) Consuming broccoli does not induce genes associated with xenobiotic metabolism and cell cycle control in human gastric mucosa. J Nutr 137:1718-1724

Geyer R, Wee S, Anderson S, Yates J, Wolf DA (2003) BTB/POZ domain proteins are putative substrate adaptors for cullin 3 ubiquitin ligases. Mol Cell 12:783-790

Gibbs A, Schwartzman J, Deng V, Alumkal J (2009) Sulforaphane destabilizes the androgen receptor in prostate cancer cells by inactivating histone deacetylase 6. Proc Natl Acad Sci USA 106:16663-16668

Gills JJ, Jeffery EH, Matusheski NV, Moon RC, Lantvit DD, Pezzuto JM (2006) Sulforaphane prevents mouse skin tumorigenesis during the stage of promotion. Cancer Lett 236:72-79

Gong P, Stewart D, Hu B, Vinson C, Alam J (2002) Multiple basic-leucine zipper proteins regulate induction of the mouse heme oxygenase-1 gene by arsenite. Arch Biochem Biophys 405:265-274

Gu JQ, Park EJ, Vigo JS, Graham JG, Fong HH, Pezzuto JM, Kinghorn AD (2002) Activity-guided isolation of constituents of Renealmia nicolaioides with

the potential to induce the phase II enzyme quinone reductase. J Nat Prod 65:1616-1620

Guo Z, Kozlov S, Lavin MF, Person MD, Paull TT (2010) ATM activation by oxidative stress. Science 330:517-521

Gupta GP, Massagué J (2006) Cancer metastasis: building a framework. Cell 127:679-695

Halkier BA, Gershenzon J (2006) Biology and biochemistry of glucosinolates. Annu Rev Plant Biol 57:303-333

Hall A, Nelson K, Poole L, Karplus PA (2010) Structure-based insights into the catalytic power and conformational dexterity of peroxiredoxins. Antioxid Redox Signal, in press

Hatcher H, Planalp R, Cho J, Torti FM, Torti SV (2008) Curcumin: from ancient medicine to current clinical trials. Cell Mol Life Sci 65:1631-1652

Hayashi A, Suzuki H, Itoh K, Yamamoto M, Sugiyama Y (2003) Transcription factor Nrf2 is required for the constitutive and inducible expression of multidrug resistance-associated protein 1 in mouse embryo fibroblasts. Biochem Biophys Res Commun 310:824-829

Hayes JD, Flanagan JU, Jowsey IR (2005) Glutathione transferases. Annu Rev Pharmacol Toxicol 45:51-88

Hayes JD, McMahon M, Chowdhry S, Dinkova-Kostova AT (2010) Cancer chemoprevention mechanisms mediated through the Keap1-Nrf2 pathway. Antioxid Redox Signal 13:1713-1748

He CH, Gong P, Hu B, Stewart D, Choi ME, Choi AM, Alam J (2001) Identification of activating transcription factor 4 (ATF4) as an Nrf2-interacting protein. Implication for heme oxygenase-1 gene regulation. J Biol Chem 276:20858-20865

He X, Chen MG, Lin GX, Ma Q (2006) Arsenic induces NAD(P)H-quinone oxidoreductase I by disrupting the Nrf2 x Keap1 x Cul3 complex and recruiting Nrf2 x Maf to the antioxidant response element enhancer. J Biol Chem 281:23620-23631

He X, Lin GX, Chen MG, Zhang JX, Ma Q (2007) Protection against chromium (VI)-induced oxidative stress and apoptosis by Nrf2. Recruiting Nrf2 into the

nucleus and disrupting the nuclear Nrf2/Keap1 association. Toxicol Sci 98:298-309

He X, Chen MG, Ma Q (2008) Activation of Nrf2 in defense against cadmium-induced oxidative stress. Chem Res Toxicol 21:1375-1383

He X, Ma Q (2009) NRF2 cysteine residues are critical for oxidant/electrophile-sensing, Kelch-like ECH-associated protein-1-dependent ubiquitination-proteasomal degradation, and transcription activation. Mol Pharmacol 76:1265-1278

Healy ZR, Lee NH, Gao X, Goldring MB, Talalay P, Kensler TW, Konstantopoulos K (2005) Divergent responses of chondrocytes and endothelial cells to shear stress: cross-talk among COX-2, the phase 2 response, and apoptosis. Proc Natl Acad Sci USA 102:14010-14015

Henkel G, Krebs B (2004) Metallothioneins: zinc, cadmium, mercury, and copper thiolates and selenolates mimicking protein active site features--structural aspects and biological implications. Chem Rev 104:801-824

Holland R, Fishbein JC (2010) Chemistry of the cysteine sensors in Kelch-like ECH-associated protein 1. Antioxid Redox Signal 13:1749-1761

Holmgren A, Lu J (2010) Thioredoxin and thioredoxin reductase: current research with special reference to human disease. Biochem Biophys Res Commun 396:120-124

Homma S, Ishii Y, Morishima Y, Yamadori T, Matsuno Y, Haraguchi N, Kikuchi N, Satoh H, Sakamoto T, Hizawa N, Itoh K, Yamamoto M (2009) Nrf2 enhances cell proliferation and resistance to anticancer drugs in human lung cancer. Clin Cancer Res 15:3423-3432

Hong F, Sekhar KR, Freeman ML, Liebler DC (2005) Specific patterns of electrophile adduction trigger Keap1 ubiquitination and Nrf2 activation. J Biol Chem 280:31768-31775

Hoshino H, Kobayashi A, Yoshida M, Kudo N, Oyake T, Motohashi H, Hayashi N, Yamamoto M, Igarashi K (2000) Oxidative stress abolishes leptomycin B-sensitive nuclear export of transcription repressor Bach2 that counteracts activation of Maf recognition element. J Biol Chem 275:15370-15376

Hu R, Khor TO, Shen G, Jeong WS, Hebbar V, Chen C, Xu C, Reddy B, Chada K, Kong AN (2006) Cancer chemoprevention of intestinal polyposis in ApcMin/+ mice by sulforaphane, a natural product derived from cruciferous vegetable. Carcinogenesis 27:2038-2046

Huang HC, Nguyen T, Pickett CB (2000) Regulation of the antioxidant response element by protein kinase C-mediated phosphorylation of NF-E2-related factor 2. Proc Natl Acad Sci USA 97:12475-12480

Huang HC, Nguyen T, Pickett CB (2002) Phosphorylation of Nrf2 at Ser-40 by protein kinase C regulates antioxidant response element-mediated transcription. J Biol Chem 277:42769-42774

Huang LE, Arany Z, Livingston DM, Bunn HF (1996) Activation of hypoxia-inducible transcription factor depends primarily upon redox-sensitive stabilization of its alpha subunit. J Biol Chem 271:32253-32259

Hur W, Sun Z, Jiang T, Mason DE, Peters EC, Zhang DD, Luesch H, Schultz PG, Gray NS (2010) A small-molecule inducer of the antioxidant response element. Chem Biol 17:537-547

Hurst R, Bao Y, Jemth P, Mannervik B, Williamson G (1998) Phospholipid hydroperoxide glutathione peroxidase activity of human glutathione transferases. Biochem J 332:97-100

Iida K, Itoh K, Kumagai Y, Oyasu R, Hattori K, Kawai K, Shimazui T, Akaza H, Yamamoto M (2004) Nrf2 is essential for the chemopreventive efficacy of oltipraz against urinary bladder carcinogenesis. Cancer Res 64:6424-6431

Iida K, Itoh K, Maher JM, Kumagai Y, Oyasu R, Mori Y, Shimazui T, Akaza H, Yamamoto M (2007) Nrf2 and p53 cooperatively protect against BBN-induced urinary bladder carcinogenesis. Carcinogenesis 28:2398-2403

Ikeda Y, Sugawara A, Taniyama Y, Uruno A, Igarashi K, Arima S, Ito S, Takeuchi K (2000) Suppression of rat thromboxane synthase gene transcription by peroxisome proliferator-activated receptor gamma in macrophages via an interaction with NRF2. J Biol Chem 275:33142-33150

Innamorato NG, Rojo AI, García-Yagüe AJ, Yamamoto M, de Ceballos ML, Cuadrado A (2008) The transcription factor Nrf2 is a therapeutic target against brain inflammation. J Immunol 181:680-689

Ishii T, Itoh K, Takahashi S, Sato H, Yanagawa T, Katoh Y, Bannai S, Yamamoto M (2000) Transcription factor Nrf2 coordinately regulates a group of oxidative stress-inducible genes in macrophages. J Biol Chem 275:16023-16029

Itoh K, Igarashi K, Hayashi N, Nishizawa M, Yamamoto M (1995) Cloning and characterization of a novel erythroid cell-derived CNC family transcription factor heterodimerizing with the small Maf family proteins. Mol Cell Biol 15:4184-4193

Itoh K, Chiba T, Takahashi S, Ishii T, Igarashi K, Katoh Y, Oyake T, Hayashi N, Satoh K, Hatayama I, Yamamoto M, Nabeshima Y (1997) An Nrf2/small Maf heterodimer mediates the induction of phase II detoxifying enzyme genes through antioxidant response elements. Biochem Biophys Res Commun 236:313-322

Itoh K, Wakabayashi N, Katoh Y, Ishii T, Igarashi K, Engel JD, Yamamoto M (1999) Keap1 represses nuclear activation of antioxidant responsive elements by Nrf2 through binding to the amino-terminal Neh2 domain. Genes Dev 13:76-86

Itoh K, Wakabayashi N, Katoh Y, Ishii T, O'Connor T, Yamamoto M (2003) Keap1 regulates both cytoplasmic-nuclear shuttling and degradation of Nrf2 in response to electrophiles. Genes Cells 8:379-391

Iwasaki K, Hailemariam K, Tsuji Y (2007) PIAS3 interacts with ATF1 and regulates the human ferritin H gene through an antioxidant-responsive element. J Biol Chem 282:22335-22343

Jain AK, Bloom DA, Jaiswal AK (2005) Nuclear import and export signals in control of Nrf2. J Biol Chem 280:29158-29168

Jain AK, Jaiswal AK (2006) Phosphorylation of tyrosine 568 controls nuclear export of Nrf2. J Biol Chem 281:12132-12142

Jain AK, Jaiswal AK (2007) GSK-3 acts upstream of Fyn kinase in regulation of nuclear export and degradation of NF-E2 related factor 2. J Biol Chem 282:16502-16510

Jain A, Lamark T, Sjøttem E, Larsen KB, Awuh JA, Øvervatn A, McMahon M, Hayes JD, Johansen T (2010) p62/SQSTM1 is a target gene for transcription factor NRF2 and creates a positive feedback loop by inducing

antioxidant response element-driven gene transcription. J Biol Chem 285:22576-22591

Jiang T, Chen N, Zhao F, Wang XJ, Kong B, Zheng W, Zhang DD (2010) High levels of Nrf2 determine chemoresistance in type II endometrial cancer. Cancer Res 70:5486-5496

Jin Y, Penning TM (2007) Aldo-keto reductases and bioactivation/detoxication. Annu Rev Pharmacol Toxicol 47:263-292

Johnsen O, Murphy P, Prydz H, Kolsto AB (1998) Interaction of the CNC-bZIP factor TCF11/LCR-F1/Nrf1 with MafG: binding-site selection and regulation of transcription. Nucleic Acids Res 26:512-520

Jung K, Park J, Maeng PJ, Kim H (2005) Fluorescence quenching of green fluorescence protein during denaturation by guanidine. Bull Korean Chem Soc 26:413-417

Kaidery NA, Banerjee R, Yang L, Smirnova NA, Hushpulian DM, Liby KT, Williams CR, Yamamoto M, Kensler TW, Ratan RR, Sporm MB, Beal MF, Gazaryan IG, Thomas B (2012) Antioxid Redox Signal, in press

Kamura T, Koepp DM, Conrad MN, Skowyra D, Moreland RJ, Iliopoulos O, Lane WS, Kaelin WG Jr, Elledge SJ, Conaway RC, Harper JW, Conaway JW (1999) Rbx1, a component of the VHL tumor suppressor complex and SCF ubiquitin ligase. Science 284:657-661

Kan Z, Jaiswal BS, Stinson J, Janakiraman V, Bhatt D, Stern HM, Yue P, Haverty PM, Bourgon R, Zheng J, Moorhead M, Chaudhuri S, Tomsho LP, Peters BA, Pujara K, Cordes S, Davis DP, Carlton VE, Yuan W, Li L, Wang W, Eigenbrot C, Kaminker JS, Eberhard DA, Waring P, Schuster SC, Modrusan Z, Zhang Z, Stokoe D, de Sauvage FJ, Faham M, Seshagiri S. Diverse somatic mutation patterns and pathway alterations in human cancers. Nature 466:869-873

Kang JG, Paget MS, Seok YJ, Hahn MY, Bae JB, Hahn JS, Kleanthous C, Buttner MJ, Roe JH (1999) σ^R, an anti-sigma factor regulated by redox change. EMBO J 18:4292-4298

Kang KW, Cho MK, Lee CH, Kim SG (2001) Activation of phosphatidylinositol 3-kinase and Akt by tert-butylhydroquinone is responsible for antioxidant

response element-mediated rGSTA2 induction in H4IIE cells. Mol Pharmacol 59:1147-1156

Kang MI, Kobayashi A, Wakabayashi N, Kim SG, Yamamoto M (2004) Scaffolding of Keap1 to the actin cytoskeleton controls the function of Nrf2 as key regulator of cytoprotective phase 2 genes. Proc Natl Acad Sci USA 101:2046-2051

Kappos L, Gold R, Miller DH, Macmanus DG, Havrdova E, Limmroth V, Polman CH, Schmierer K, Yousry TA, Yang M, Eraksoy M, Meluzinova E, Rektor I, Dawson KT, Sandrock AW, O'Neill GN (2008) Efficacy and safety of oral fumarate in patients with relapsing-remitting multiple sclerosis: a multicentre, randomised, double-blind, placebo-controlled phase IIb study. Lancet 372:1463-1472

Karapetian RN, Evstafieva AG, Abaeva IS, Chichkova NV, Filonov GS, Rubtsov YP, Sukhacheva EA, Melnikov SV, Schneider U, Wanker EE, Vartapetian AB (2005) Nuclear oncoprotein prothymosin alpha is a partner of Keap1: implications for expression of oxidative stress-protecting genes. Mol Cell Biol 25:1089-1099

Karin M (1995) The regulation of AP-1 activity by mitogen-activated protein kinases. J Biol Chem 270:16483-16486

Karin M, Hunter T (1995) Transcriptional control by protein phosphorylation: signal transmission from the cell surface to the nucleus. Curr Biol 5:747-757

Kaspar JW, Niture SK, Jaiswal AK (2012) Antioxidant-induced INrf2 (Keap1) tyrosine 85 phosphorylation controls the nuclear export and degradation of the INrf2-Cul3-Rbx1 complex to allow normal Nrf2 activation and repression. J Cell Sci 125:1027-1038

Katoh Y, Itoh K, Yoshida E, Miyagishi M, Fukamizu A, Yamamoto M (2001) Two domains of Nrf2 cooperatively bind CBP, a CREB binding protein, and synergistically activate transcription. Genes Cells 6:857-868

Katoh Y, Iida K, Kang MI, Kobayashi A, Mizukami M, Tong KI, McMahon M, Hayes JD, Itoh K, Yamamoto M (2005) Evolutionary conserved N-terminal domain of Nrf2 is essential for the Keap1-mediated degradation of the protein by proteasome. Arch Biochem Biophys 433:342-350

Katsuoka F, Motohashi H, Ishii T, Aburatani H, Engel JD, Yamamoto M (2005) Genetic evidence that small Maf proteins are essential for the activation of antioxidant response element-dependent genes. Mol Cell Biol 25:8044-8051

Kensler TW, Chen JG, Egner PA, Fahey JW, Jacobson LP, Stephenson KK, Ye L, Coady JL, Wang JB, Wu Y, Sun Y, Zhang QN, Zhang BC, Zhu YR, Qian GS, Carmella SG, Hecht SS, Benning L, Gange SJ, Groopman JD, Talalay P (2005) Effects of glucosinolate-rich broccoli sprouts on urinary levels of aflatoxin-DNA adducts and phenanthrene tetraols in a randomized clinical trial in He Zuo township, Qidong, People's Republic of China. Cancer Epidemiol. Biomarkers Prev 14:2605-2613

Kerppola TK (2006) Visualization of molecular interactions by fluorescence complementation. Nat Rev Cell Biol 7:449-456

Khor TO, Huang MT, Kwon KH, Chan JY, Reddy BS, Kong AN (2006) Nrf2-deficient mice have an increased susceptibility to dextran sulfate sodium-induced colitis. Cancer Res 66:11580-11584

Khor TO, Huang MT, Prawan A, Liu Y, Hao X, Yu S, Cheung WK, Chan JY, Reddy BS, Yang CS, Kong AN (2008) Increased susceptibility of Nrf2 knockout mice to colitis-associated colorectal cancer. Cancer Prev Res (Phila) 1:187-191

Ki SH, Cho IJ, Choi DW, Kim SG (2005) Glucocorticoid receptor (GR)-associated SMRT binding to C/EBPbeta TAD and Nrf2 Neh4/5: role of SMRT recruited to GR in GSTA2 gene repression. Mol Cell Biol 25:4150-4165

Kim JE, You DJ, Lee C, Ahn C, Seong JY, Hwang JI (2010) Suppression of NF-□B signaling by KEAP1 regulation of IKK□ activity through autophagic degradation and inhibition of phosphorylation. Cell Signal 22:1645-1654

Kim YC, Masutani H, Yamaguchi Y, Itoh K, Yamamoto M, Yodoi J (2001) Hemin-induced activation of the thioredoxin gene by Nrf2. A differential regulation of the antioxidant responsive element by a switch of its binding factors. J Biol Chem 276:18399-18406

Kobayashi A, Kang MI, Okawa H, Ohtsuji M, Zenke Y, Chiba T, Igarashi K, Yamamoto M (2004) Oxidative stress sensor Keap1 functions as an

adaptor for Cul3-based E3 ligase to regulate proteasomal degradation of Nrf2. Mol Cell Biol 24:7130-7139

Kobayashi A, Kang MI, Watai Y, Tong KI, Shibata T, Uchida K, Yamamoto M (2006) Oxidative and electrophilic stresses activate Nrf2 through inhibition of ubiquitination activity of Keap1. Mol Cell Biol 26:221-229

Kobayashi M, Itoh K, Suzuki T, Osanai H, Nishikawa K, Katoh Y, Takagi Y, Yamamoto M. (2002) Identification of the interactive interface and phylogenic conservation of the Nrf2-Keap1 system. Genes Cells 7:807-820

Kobayashi M, Li L, Iwamoto N, Nakajima-Takagi Y, Kaneko H, Nakayama Y, Eguchi M, Wada Y, Kumagai Y, Yamamoto M (2009) The antioxidant defense system Keap1-Nrf2 comprises a multiple sensing mechanism for responding to a wide range of chemical compounds. Mol Cell Biol 29:493-502

Komatsu M, Kurokawa H, Waguri S, Taguchi K, Kobayashi A, Ichimura Y, Sou YS, Ueno I, Sakamoto A, Tong KI, Kim M, Nishito Y, Iemura S, Natsume T, Ueno T, Kominami E, Motohashi H, Tanaka K, Yamamoto M (2010) The selective autophagy substrate p62 activates the stress responsive transcription factor Nrf2 through inactivation of Keap1. Nat Cell Biol 12:213-223

Konishi H, Tanaka M, Takemura Y, Matsuzaki H, Ono Y, Kikkawa U, Nishizuka Y (1997) Activation of protein kinase C by tyrosine phosphorylation in response to H_2O_2. Proc Natl Acad Sci USA 94:11233-11237

Konishi H, Yamauchi E, Taniguchi H, Yamamoto T, Matsuzaki H, Takemura Y, Ohmae K, Kikkawa U, Nishizuka Y (2001) Phosphorylation sites of protein kinase C delta in H2O2-treated cells and its activation by tyrosine kinase in vitro. Proc Natl Acad Sci USA 98:6587-6592

Krieghoff E, Behrens J, Mayr B (2006) Nucleo-cytoplasmic distribution of β-catenin in regulated by retention. J Cell Sci 119:1453-1463

Kuge S, Jones N, Nomoto A (1997) Regulation of yAP-1 nuclear localization in response to oxidative stress. EMBO J 16:1710-1720

Kuge S, Arita M, Murayama A, Maeta K, Izawa S, Inoue Y, Nomoto A (2001) Regulation of the yeast Yap1p nuclear export signal is mediated by redox

signal-induced reversible disulfide bond formation. Mol Cell Biol 21:6139-6150

Kuroda K, Akao M (1989) Inhibitory effect of fumaric acid on 3'-methyl-4-(dimethylamino)azobenzene-induced hepatocarcinogenesis in rats. Chem Pharm Bull (Tokyo) 37:1345-1346

Kuroda K, Kanisawa M, Akao M (1982) Inhibitory effect of fumaric acid on forestomach and lung carcinogenesis by a 5-nitrofuran naphthyridine derivative in mice. J Natl Cancer Inst 69:1317-1320

Kuroda K, Terao K, Akao M (1983) Inhibitory effect of fumaric acid on 3-methyl-4'-(dimethylamino)-azobenzene-induced hepatocarcinogenesis in rats. J Natl Cancer Inst 71:855-857

Kuroda K, Terao K, Akao M (1987) Inhibitory effect of fumaric acid on hepatocarcinogenesis by thioacetamide in rats. J Natl Cancer Inst 79:1047-1051

Kuroiwa Y, Nishikawa A, Kitamura Y, Kanki K, Ishii Y, Umemura T, Hirose M (2006) Protective effects of benzyl isothiocyanate and sulforaphane but not resveratrol against initiation of pancreatic carcinogenesis in hamsters. Cancer Lett 241:275-280

Kwak MK, Itoh K, Yamamoto M, Sutter TR, Kensler TW (2001) Role of transcription factor Nrf2 in the induction of hepatic phase 2 and antioxidative enzymes *in vivo* by the cancer chemoprotective agent, 3H-1, 2-dimethiole-3-thione. Mol Med 7:135-145

Kwak MK, Itoh K, Yamamoto M, Kensler TW (2002) Enhanced expression of the transcription factor Nrf2 by cancer chemopreventive agents: role of antioxidant response element-like sequences in the nrf2 promoter. Mol Cell Biol 22:2883-2892

Kwak MK, Wakabayashi N, Itoh K, Motohashi H, Yamamoto M, Kensler TW (2003) Modulation of gene expression by cancer chemopreventive dithiolethiones through the Keap1-Nrf2 pathway. Identification of novel gene clusters for cell survival. J Biol Chem 278:8135-8145

Lau A, Wang XJ, Zhao F, Villeneuve NF, Wu T, Jiang T, Sun Z, White E, Zhang DD (2010) A noncanonical mechanism of Nrf2 activation by autophagy

deficiency: direct interaction between Keap1 and p62. Mol Cell Biol 30:3275-3285

Lee DF, Kuo HP, Liu M, Chou CK, Xia W, Du Y, Shen J, Chen CT, Huo L, Hsu MC, Li CW, Ding Q, Liao TL, Lai CC, Lin AC, Chang YH, Tsai SF, Li LY, Hung MC (2009) KEAP1 E3 ligase-mediated downregulation of NF-□B signaling by targeting IKK□. Mol Cell 36:131-140

Lee JM, Hanson JM, Chu WA, Johnson JA (2001) Phosphatidylinositol 3-kinase, not extracellular signal-regulated kinase, regulates activation of the antioxidant-responsive element in IMR-32 human neuroblastoma cells. J Biol Chem 2001 276:20011-20016

Levonen AL, Landar A, Ramachandran A, Ceaser EK, Dickinson DA, Zanoni G, Morrow JD, Darley-Usmar VM (2004) Cellular mechanisms of redox cell signalling: role of cysteine modification in controlling antioxidant defences in response to electrophilic lipid oxidation products. Biochem J 378:373-382

Levy S, Jaiswal AK, Forman HJ (2009) The role of c-Jun phosphorylation in EpRE activation of phase II genes. Free Radic Biol Med 47:1172-1179

Li B, Wang X, Rasheed N, Hu Y, Boast S, Ishii T, Nakayama K, Nakayama KI, Goff SP (2004) Distinct roles of c-Abl and Atm in oxidative stress response are mediated by protein kinase C delta. Genes Dev 18:1824-1837

Li J, Stein TD, Johnson JA (2004) Genetic dissection of systemic autoimmune disease in Nrf2-deficient mice. Physiol Genomics 18:261-272

Li W, Jain MR, Chen C, Yue X, Hebbar V, Zhou R, Kong AN (2005) Nrf2 Possesses a redox-insensitive nuclear export signal overlapping with the leucine zipper motif. J Biol Chem 280:28430-28438

Li W, Yu SW, Kong AN (2006) Nrf2 possesses a redox-sensitive nuclear exporting signal in the Neh5 transactivation domain. J Biol Chem 281:27251-27263

Li W, Yu S, Liu T, Kim JH, Blank V, Li H, Kong AN (2008) Heterodimerization with small Maf proteins enhances nuclear retention of Nrf2 via masking the NESzip motif. Biochim Biophys Acta 1783:1847-1856

Li W, Thakor N, Xu EY, Huang Y, Chen C, Yu R, Holcik M, Kong AN (2010) An internal ribosomal entry site mediates redox-sensitive translation of Nrf2. Nucleic Acids Res 38:778-788

Li X, Zhang D, Hannink M, Beamer LJ (2004) Crystal structure of the Kelch domain of human Keap1. J Biol Chem 279:54750-54758

Liby K, Honda T, Williams CR, Risingsong R, Royce DB, Suh N, Dinkova-Kostova AT, Stephenson KK, Talalay P, Sundararajan C, Gribble GW, Sporn MB (2007a) Novel semisynthetic analogues of betulinic acid with diverse cytoprotective, antiproliferative, and proapoptotic activities. Mol Cancer Ther 6:2113-2119

Liby K, Royce DB, Williams CR, Risingsong R, Yore MM, Honda T, Gribble GW, Dmitrovsky E, Sporn TA, Sporn MB (2007b) The synthetic triterpenoids CDDO-methyl ester and CDDO-ethyl amide prevent lung cancer induced by vinyl carbamate in A/J mice. Cancer Res 67:2414-2419

Liby K, Yore MM, Roebuck BD, Baumgartner KJ, Honda T, Sundararajan C, Yoshizawa H, Gribble GW, Williams CR, Risingsong R, Royce DB, Dinkova-Kostova AT, Stephenson KK, Egner PA, Yates MS, Groopman JD, Kensler TW, Sporn MB (2008a) A novel acetylenic tricyclic bis-(cyano enone) potently induces phase 2 cytoprotective pathways and blocks liver carcinogenesis induced by aflatoxin. Cancer Res 68:6727-6733

Liby K, Black CC, Royce DB, Williams CR, Risingsong R, Yore MM, Liu X, Honda T, Gribble GW, Lamph WW, Sporn TA, Dmitrovsky E, Sporn MB (2008b) The rexinoid LG100268 and the synthetic triterpenoid CDDO-methyl amide are more potent than erlotinib for prevention of mouse lung carcinogenesis. Mol Cancer Ther 7:1251-1257

Liby K, Risingsong R, Royce DB, Williams CR, Yore MM, Honda T, Gribble GW, Lamph WW, Vannini N, Sogno I, Albini A, Sporn MB (2008c) Prevention and treatment of experimental estrogen receptor-negative mammary carcinogenesis by the synthetic triterpenoid CDDO-methyl Ester and the rexinoid LG100268. Clin Cancer Res 14:4556-4563

Liby K, Risingsong R, Royce DB, Williams CR, Ma T, Yore MM, Sporn MB (2009) Triterpenoids CDDO-methyl ester or CDDO-ethyl amide and rexinoids

LG100268 or NRX194204 for prevention and treatment of lung cancer in mice. Cancer Prev Res (Phila) 2:1050-1058

Liby KT, Royce DB, Risingsong R, Williams CR, Maitra A, Hruban RH, Sporn MB (2010) Synthetic triterpenoids prolong survival in a transgenic mouse model of pancreatic cancer. Cancer Prev Res (Phila) in press

Lipton SA (2007) Pathologically activated therapeutics for neuroprotection. Nat Rev Neurosci 8:803-808

Liu H, Dinkova-Kostova AT, Talalay P (2008) Coordinate regulation of enzyme markers for inflammation and for protection against oxidants and electrophiles. Proc Natl Acad Sci USA 105:15926-15931

Lleres D, Swift S, Lamond AI (2007) Detecting protein-protein interactions in vivo with FRET using multiphoton fluorescence lifetime imaging microscopy (FLIM). Curr Protoc Cytom 12:Unit12.10

Lleres D, James J, Swift S, Norman DG, Lamond AI (2009) Quantitative analysis of chromatin compaction in living cells using FLIM-FRET. J Cell Biol 16:481-496

Lleres D, Denegri M, Biggiogera M, Ajuh P, Lamond AI (2010) Direct interaction between hnRNP-M and CDC5L/ PLRG1 proteins affects alternative splice site choice. EMBO Rep 11: 445-451

Lo SC, Hannink M (2006a) PGAM5, a Bcl-XL-interacting protein, is a novel substrate for the redox-regulated Keap1-dependent ubiquitin ligase complex. J Biol Chem 281:37893-37903

Lo SC, Hannink M (2006b) CAND1-mediated substrate adaptor recycling is required for efficient repression of Nrf2 by Keap1. Mol Cell Biol 26:1235-1244

Lo SC, Li X, Henzl MT, Beamer LJ, Hannink M (2006) Structure of the Keap1:Nrf2 interface provides mechanistic insight into Nrf2 signaling. EMBO J 25:3605-3617

Lo SC, Hannink M (2008) PGAM5 tethers a ternary complex containing Keap1 and Nrf2 to mitochondria. Exp Cell Res 314:1789-1803

Loewer A, Batchelor E, Gaglia G, Lahav G (2010) Basal dynamics of p53 reveal transcriptionally attenuated pulses in cycling cells. Cell 142:1-12

Loignon M, Miao W, Hu L, Bier A, Bismar TA, Scrivens PJ, Mann K, Basik M, Bouchard A, Fiset PO, Batist Z, Batist G (2009) Cul3 overexpression depletes Nrf2 in breast cancer and is associated with sensitivity to carcinogens, to oxidative stress, and to chemotherapy. Mol Cancer Ther 8:2432-2440

Lubos E, Loscalzo J, Handy DE (2010) Glutathione peroxidase-1 in health and disease: from molecular mechanisms to therapeutic opportunities. Antioxid Redox Signal, in press

Ma J, Cai H, Wu T, Sobhian B, Huo Y, Alcivar A, Mehta M, Cheung KL, Ganesan S, Kong AT, Zhang DD, Xia B (2012) Palb2 interacts with Keap1 to promote Nrf2 nuclear accumulation and function. Mol Cell Biol 32:1506-1517

MacCallum PR, Jack SC, Egan PA, McDermott BT, Elliott RM, Chan SW (2006) Cap-dependent and hepatitis C virus internal ribosome entry site-mediated translation are modulated by phosphorylation of eIF2alpha under oxidative stress. J Gen Virol 87:3251-3262

MacLeod AK, McMahon M, Plummer SM, Higgins LG, Penning TM, Igarashi K, Hayes JD (2009) Characterization of the cancer chemopreventive NRF2-dependent gene battery in human keratinocytes: demonstration that the KEAP1-NRF2 pathway, and not the BACH1-NRF2 pathway, controls cytoprotection against electrophiles as well as redox-cycling compounds. Carcinogenesis 30:1571-1580

Maeder CI, Hink MA, Kinkhabwala A, Mayr R, Bastiaens PI, Knop M (2007) Spatial regulation of Fus3 MAP kinase activity through a reaction-diffusion mechanism in yeast pheromone signalling. Nat Cell Biol 9: 1319-1326

Mahaffey CM, Zhang H, Rinna A, Holland W, Mack PC, Forman HJ (2009) Multidrug-resistant protein-3 gene regulation by the transcription factor Nrf2 in human bronchial epithelial and non-small-cell lung carcinoma. Free Radic Biol Med 46:1650-1657

Maher JM, Dieter MZ, Aleksunes LM, Slitt AL, Guo G, Tanaka Y, Scheffer GL, Chan JY, Manautou JE, Chen Y, Dalton TP, Yamamoto M, Klaassen CD (2007) Oxidative and electrophilic stress induces multidrug resistance-associated protein transporters via the nuclear factor-E2-related factor-2 transcriptional pathway. Hepatology 46:1597-1610

Malhotra D, Portales-Casamar E, Singh A, Srivastava S, Arenillas D, Happel C, Shyr C, Wakabayashi N, Kensler TW, Wasserman WW, Biswal S (2010) Global mapping of binding sites for Nrf2 identifies novel targets in cell survival response through ChIP-Seq profiling and network analysis. Nucleic Acids Res 38:5718-5734

Mannervik B, Board PG, Hayes JD, Listowsky I, Pearson WR (2005) Nomenclature for mammalian soluble glutathione transferases. Methods Enzymol 401:1-8

Marini MG, Chan K, Casula L, Kan YW, Cao A, Moi P (1997) hMAF, a small human transcription factor that heterodimerizes specifically with Nrf1 and Nrf2. J Biol Chem 272:16490-16497

Maxwell PH, Wiesener MS, Chang GW, Clifford SC, Vaux EC, Cockman ME, Wykoff CC, Pugh CW, Maher ER, Ratcliffe PJ (1999) The tumour suppressor protein VHL targets hypoxia-inducible factors for oxygen-dependent proteolysis. Nature 399:271-275

McMahon M, Itoh K, Yamamoto M, Chanas SA, Henderson CJ, McLellan LI, Wolf CR, Cavin C, Hayes JD (2001) The Cap'n'Collar basic leucine zipper transcription factor Nrf2 (NF-E2 p45-related factor 2) controls both constitutive and inducible expression of intestinal detoxification and glutathione biosynthetic enzymes. Cancer Res 61:3299-3307

McMahon M, Itoh K, Yamamoto M, Hayes JD (2003) Keap1-dependent proteasomal degradation of transcription factor Nrf2 contributes to the negative regulation of antioxidant response element-driven gene expression. J Biol Chem 278:21592-21600

McMahon M, Thomas N, Itoh K, Yamamoto M, Hayes JD (2004) Redox-regulated turnover of Nrf2 is determined by at least two separate protein domains, the redox-sensitive Neh2 degron and the redox-insensitive Neh6 degron. J Biol Chem 279:31556-31567

McMahon M, Thomas N, Itoh K, Yamamoto M, Hayes JD (2006) Dimerization of substrate adaptors can facilitate cullin-mediated ubiquitylation of proteins by a "tethering" mechanism: a two-site interaction model for the Nrf2-Keap1 complex. J Biol Chem 281:24756-24768

McMahon M, Lamont DJ, Beattie KA, Hayes JD (2010) Keap1 perceives stress via three sensors for the endogenous signaling molecules nitric oxide, zinc, and alkenals. Proc Natl Acad Sci USA 107:18838-18843

Misico RI, Song LL, Veleiro AS, Cirigliano AM, Tettamanzi MC, Burton G, Bonetto GM, Nicotra VE, Silva GL, Gil RR, Oberti JC, Kinghorn AD, Pezzuto JM. (2002) Induction of quinone reductase by withanolides. J Nat Prod 65:677-680

Miyawaki A (2011) Development of probes for cellular functions using fluorescent proteins and fluorescence resonance energy transfer. Annu Rev Biochem 80:357-373

Moi P, Chan K, Asunis I, Cao A, Kan YW (1994) Isolation of NF-E2-related factor 2 (Nrf2), a NF-E2-like basic leucine zipper transcriptional activator that binds to the tandem NF-E2/AP1 repeat of the b-globin locus control region. Proc Natl Acad Sci USA 91:9926-9930

Morris JR, Boutell C, Keppler M, Densham R, Weeked D, Alamshah A, Butler L, Galanty Y, Pangon L, Kiuchi T, Ng T, Solomon E (2009) The SUMO modificationpathway is involved in the BRCA1 response to genotoxic stress. Nature 462:886-890

Morse MA, Amin SG, Hecht SS, Chung FL (1989a) Effects of aromatic isothiocyanates on tumorigenicity, O6-methylguanine formation, and metabolism of the tobacco-specific nitrosamine 4-(methylnitrosamino)-1-(3-pyridyl)-1-butanone in A/J mouse lung. Cancer Res 49:2894-2897

Morse MA, Wang CX, Stoner GD, Mandal S, Conran PB, Amin SG, Hecht SS, Chung FL (1989b) Inhibition of 4-(methylnitrosamino)-1-(3-pyridyl)-1-butanone-induced DNA adduct formation and tumorigenicity in the lung of F344 rats by dietary phenethyl isothiocyanate. Cancer Res 49:549-553

Morse MA, Eklind KI, Hecht SS, Jordan KG, Choi CI, Desai DH, Amin SG, Chung FL (1991) Structure-activity relationships for inhibition of 4-(methylnitrosamino)-1-(3-pyridyl)-1-butanone lung tumorigenesis by arylalkyl isothiocyanates in A/J mice. Cancer Res 51:1846-1850

Motohashi H, O'Connor T, Katsuoka F, Engel JD, Yamamoto M (2002) Integration and diversity of the regulatory network composed of Maf and CNC families of transcription factors. Gene 294:1-12

Mukherjee S, Gangopadhyay H, Das DK (2008) Broccoli: a unique vegetable that protects mammalian hearts through the redox cycling of the thioredoxin superfamily. J Agric Food Chem 56:609-617

Mukherjee S, Lekli I, Ray D, Gangopadhyay H, Raychaudhuri U, Das DK (2010) Comparison of the protective effects of steamed and cooked broccolis on ischaemia-reperfusion-induced cardiac injury. Br J Nutr 103:815-823

Munday R, Mhawech-Fauceglia P, Munday CM, Paonessa JD, Tang L, Munday JS, Lister C, Wilson P, Fahey JW, Davis W, Zhang Y (2008) Inhibition of urinary bladder carcinogenesis by broccoli sprouts. Cancer Res 68:1593-1600

Mustacich D, Powis G (2000) Thioredoxin reductase. Biochem J 346:1-8

Muto A, Tashiro S, Tsuchiya H, Kume A, Kanno M, Ito E, Yamamoto M, Igarashi K (2002) Activation of Maf/AP-1 repressor Bach2 by oxidative stress promotes apoptosis and its interaction with promyelocytic leukemia nuclear bodies. J Biol Chem 277:20724-20733

Myzak MC, Karplus PA, Chung FL, Dashwood RH (2004) A novel mechanism of chemoprotection by sulforaphane: inhibition of histone deacetylase. Cancer Res 64:5767-5774

Myzak MC, Dashwood WM, Orner GA, Ho E, Dashwood RH (2006) Sulforaphane inhibits histone deacetylase in vivo and suppresses tumorigenesis in Apc-minus mice. FASEB J 20:506-508

Nelson DE, Ihekwaba AEC, Elliott M, Johnson JR, Gibney CA, Foreman BE, Nelson G, See V, Horton CA, Spiller DG, Edwards SW, McDowell HP, Unitt JF, Sullivan E, Grimley R, Benson N, Broomhead D, Kell DB, White MRH (2004) Oscillations in NF-κB signalling control the dynamics of gene expression. Science 306: 704-708

Ng T, Squire A, Hansra G, Bornancin F, Prevostel C, Hanby A, Harris W, Barned D, Schmidt S, Mellor H, Bastiaens PIH, Parker PJ (1999) Imaging protein kinase Cα activation in cells. Science 283:2085-2089

Nguyen T, Sherratt PJ, Huang HC, Yang CS, Pickett CB (2003) Increased protein stability as a mechanism that enhances Nrf2-mediated transcriptional activation of the antioxidant response element. Degradation of Nrf2 by the 26 S proteasome. J Biol Chem 278:4536-4541

Nguyen T, Sherratt PJ, Nioi P, Yang CS, Pickett CB (2005) Nrf2 controls constitutive and inducible expression of ARE-driven genes through a dynamic pathway involving nucleocytoplasmic shuttling by Keap1. J Biol Chem 280:32485-32492

Nioi P, Nguyen T, Sherratt PJ, Pickett CB (2005) The carboxy-terminal Neh3 domain of Nrf2 is required for transcriptional activation. Mol Cell Biol 25:10895-10906

Nioi P, Nguyen T (2007) A mutation of Keap1 found in breast cancer impairs its ability to repress Nrf2 activity. Biochem Biophys Res Commun 362:816-21

Niture SK, Jaiswal AK (2009) Prothymosin-□ mediates nuclear import of the INrf2/Cul3 Rbx1 complex to degrade nuclear Nrf2. J Biol Chem 284:13856-13868

Niture SK, Jain AK, Jaiswal AK (2009) Antioxidant-induced modification of INrf2 cysteine 151 and PKC-delta-mediated phosphorylation of Nrf2 serine 40 are both required for stabilization and nuclear translocation of Nrf2 and increased drug resistance. J Cell Sci 122:4452-4464

Noyan-Ashraf MH, Wu L, Wang R, Juurlink BH (2006) Dietary approaches to positively influence fetal determinants of adult health. FASEB J 20:371-373

Ogura T, Tong KI, Mio K, Maruyama Y, Kurokawa H, Sato C, Yamamoto M (2010) Keap1 is a forked-stem dimer structure with two large spheres enclosing the intervening, double glycine repeat, and C-terminal domains. Proc Natl Acad Sci USA 107:2842-2847

Ohta T, Iijima K, Miyamoto M, Nakahara I, Tanaka H, Ohtsuji M, Suzuki T, Kobayashi A, Yokota J, Sakiyama T, Shibata T, Yamamoto M, Hirohashi S (2008) Loss of Keap1 function activates Nrf2 and provides advantages for lung cancer cell growth. Cancer Res 68:1303-1309

Padmanabhan B, Scharlock M, Tong KI, Nakamura Y, Kang MI, Kobayashi A, Matsumoto T, Tanaka A, Yamamoto M, Yokoyama S. (2005) Purification, crystallization and preliminary X-ray diffraction analysis of the Kelch-like motif region of mouse Keap1. Acta Crystallogr Sect F Struct Biol Cryst Commun 61:153-155

Padmanabhan B, Tong KI, Ohta T, Nakamura Y, Scharlock M, Ohtsuji M, Kang MI, Kobayashi A, Yokoyama S, Yamamoto M (2006) Structural basis for defects of Keap1 activity provoked by its point mutations in lung cancer. Mol Cell 21:689-700

Padmanabhan B, Tong KI, Kobayashi A, Yamamoto M, Yokoyama S (2008a) Structural insights into the similar modes of Nrf2 transcription factor recognition by the cytoplasmic repressor Keap1. J Synchrotron Radiat 15:273-276

Padmanabhan B, Nakamura Y, Yokoyama S (2008b) Structural analysis of the complex of Keap1 with a prothymosin α peptide. Acta Crystallogr Sect F Struct Biol Cryst Commun 64:233-238

Paget MS, Kang JG, Roe JH, Buttner MJ (1998) σ^R, an RNA polymerase sigma factor that modulates expression of the thioredoxin system in response to oxidative stress in *Streptomyces coelicolor* A3(2). EMBO J 17:5776-5782

Pause A, Lee S, Worrell RA, Chen DY, Burgess WH, Linehan WM, Klausner RD (1997) The von Hippel-Lindau tumor-suppressor gene product forms a stable complex with human CUL-2, a member of the Cdc53 family of proteins. Proc Natl Acad Sci USA 94:2156-2161

Perkins ND (2004) NF-kappaB: tumor promoter or suppressor? Trends Cell Biol 14:64-69

Perl AK, Wilgenbus P, Dahl U, Semb H, Christofori G (1998) A causal role for E-cadherin in the transition from adenoma to carcinoma. Nature 392:190-193

Pi J, Bai Y, Reece JM, Williams J, Liu D, Freeman ML, Fahl WE, Shugar D, Liu J, Qu W, Collins S, Waalkes MP (2007) Molecular mechanism of human Nrf2 activation and degradation: role of sequential phosphorylation by protein kinase CK2. Free Radic Biol Med 2007 42:1797-1806

Pietsch EC, Chan JY, Torti FM, Torti SV (2003) Nrf2 mediates the induction of ferritin H in response to xenobiotics and cancer chemopreventive dithiolethiones. J Biol Chem 278:2361-2369

Ping Z, Liu W, Kang Z, Cai J, Wang Q, Cheng N, Wang S, Wang S, Zhang JH, Sun X (2010) Sulforaphane protects brains against hypoxic-ischemic injury through induction of Nrf2-dependent phase 2 enzyme. Brain Res 1343:178-185

Pintard L, Willis JH, Willems A, Johnson JL, Srayko M, Kurz T, Glaser S, Mains PE, Tyers M, Bowerman B, Peter M (2003) The BTB protein MEL-26 is a substrate-specific adaptor of the CUL-3 ubiquitin-ligase. Nature 425:311-316

Posner GH, Cho CG, Green JV, Zhang Y, Talalay P (1994) Design and synthesis of bifunctional isothiocyanate analogs of sulforaphane: correlation between structure and potency as inducers of anticarcinogenic detoxication enzymes. J Med Chem 37:170-176

Powis G, Montfort WR (2001) Properties and biological activities of thioredoxins. Annu Rev Pharmacol Toxicol 41:261-295

Prestera T, Talalay P, Alam J, Ahn YI, Lee PJ, Choi AM (1995) Parallel induction of heme oxygenase-1 and chemoprotective phase 2 enzymes by electrophiles and antioxidants: regulation by upstream antioxidant-responsive elements (ARE). Mol Med 1:827-837

Prilusky J, Felder CE, Zeev-Ben-Mordehai T, Rydberg EH, Man O, Beckmann JS, Silman I, Sussman JL (2005) FoldIndex: a simple tool to predict whether a given protein sequence is intrinsically unfolded. Bioinformatics 21:3435-3438

Prochaska HJ, Bregman HS, De Long MJ, Talalay P (1985a) Specificity of induction of cancer protective enzymes by analogues of tert-butyl-4-hydroxyanisole (BHA). Biochem Pharmacol 34:3909-3914

Prochaska HJ, De Long MJ, Talalay P. (1985b) On the mechanisms of induction of cancer-protective enzymes: a unifying proposal. Proc Natl Acad Sci USA 82:8232-8236

Prochaska HJ, Talalay P, Sies H (1987) Direct protective effect of NAD(P)H:quinone reductase against menadione-induced

chemiluminescence of postmitochondrial fractions of mouse liver. J Biol Chem 262:1931-1934

Prochaska HJ, Santamaria AB (1988) Direct measurement of NAD(P)H:quinone reductase from cells cultured in microtiter wells: a screening assay for anticarcinogenic enzyme inducers. Anal Biochem 169:328-336

Purdom-Dickinson SE, Sheveleva EV, Sun H, Chen QM (2007) Translational control of nrf2 protein in activation of antioxidant response by oxidants. Mol Pharmacol 72:1074-1081

Rachakonda G, Xiong Y, Sekhar KR, Stamer SL, Liebler DC, Freeman ML (2008) Covalent modification at Cys151 dissociates the electrophile sensor Keap1 from the ubiquitin ligase CUL3. Chem Res Toxicol 21:705-710

Rachakonda G, Sekhar KR, Jowhar D, Samson PC, Wikswo JP, Beauchamp RD, Datta PK, Freeman ML (2010) Increased cell migration and plasticity in Nrf2-deficient cancer cell lines. Oncogene 29:3703-3714

Rada P, Rojo AI, Chowdhry S, McMahon M, Hayes JD, Cuadrado A. (2011) SCF/ β-TrCP promotes glycogen synthase kinase 3-dependent degradation of the Nrf2 transcription factor in a Keap1-independent manner. Mol Cell Biol 31:1121-1133

Rada P, Rojo AL, Evrard-Todeschi N, Innamorato NG, Cotte A, Jaworski T, Tobon-Velasco JC, Divijver H, Garcia-Mayoral MF, Van Leuven F, Hayes JD, Bertho G, Cuadrado A (2012) Structural and functional characterization of Nrf2 degradation by glycogen synthase kinase 3/ β-TrCP axis. Mol Cell Biol 32:3486-3499

Ramos-Gomez M, Kwak MK, Dolan PM, Itoh K, Yamamoto M, Talalay P, Kensler TW (2001) Sensitivity to carcinogenesis is increased and chemoprotective efficacy of enzyme inducers is lost in nrf2 transcription factor-deficient mice. Proc Natl Acad Sci USA 98:3410-3415

Rangasamy T, Cho CY, Thimmulappa RK, Zhen L, Srisuma SS, Kensler TW, Yamamoto M, Petrache I, Tuder RM, Biswal S (2004) Genetic ablation of Nrf2 enhances susceptibility to cigarette smoke-induced emphysema in mice. J Clin Invest 114:1248-1259

Reddy NM, Kleeberger SR, Bream JH, Fallon PG, Kensler TW, Yamamoto M, Reddy SP (2008) Genetic disruption of the Nrf2 compromises cell-cycle

progression by impairing GSH-induced redox signaling. Oncogene 27:5821-5832

Reid G, Wielinga P, Zelcer N, van der Heijden I, Kuil A, de Haas M, Wijnholds J, Borst P (2003) The human multidrug resistance protein MRP4 functions as a prostaglandin efflux transporter and is inhibited by nonsteroidal antiinflammatory drugs. Proc Natl Acad Sci USA 100:9244-9249

Reits EAJ, Neefjes JJ (2001) From fixed to FRAP: measuring protein mobility and activity in living cells. Nat Cell Biol 3:E145-E147

Rhee SG, Jeong W, Chang TS, Woo HA (2007) Sulfiredoxin, the cysteine sulfinic acid reductase specific to 2-Cys peroxiredoxin: its discovery, mechanism of action, and biological significance. Kidney Int Suppl:S3-S8

Robbins DJ, Nybakken KE, Kobayashi R, Sisson JC, Bishop JM, Thérond PP (1997) Hedgehog elicits signal transduction by means of a large complex containing the kinesin-related protein costal2. Cell 90:225-234

Robinson DN, Cooley L (1997) Drosophila kelch is an oligomeric ring canal actin organizer. J Cell Biol 138:799-810

Rocks O, Peyker A, Kahms M, Verveer PJ, Koerner C, Lumbierres M, Kuhlmann J, Waldmann H, Wittinghofer A, Basyiaens PIH (2005) An acylation cycle regulates localization and activity of palmitoylated Ras isoforms. Science 307:1746-1752

Ross D, Zhou H (2010) Relationships between metabolic and non-metabolic susceptibility factors in benzene toxicity. Chem Biol Interact 184:222-228

Rushmore TH, Pickett CB (1990) Transcriptional regulation of the rat glutathione S-transferase Ya subunit gene. Characterization of a xenobiotic-responsive element controlling inducible expression by phenolic antioxidants. J Biol Chem 265:14648-14653

Rushmore TH, Morton MR, Pickett CB (1991) The antioxidant responsive element. Activation by oxidative stress and identification of the DNA consensus sequence required for functional activity. J Biol Chem 266:11632-11639

Rushworth SA, MacEwan DJ (2008) HO-1 underlies resistance of AML cells to TNF-induced apoptosis. Blood 111:3793-3801

Rybin VO, Guo J, Sabri A, Elouardighi H, Schaefer E, Steinberg SF (2004) Stimulus-specific differences in protein kinase C delta localization and activation mechanisms in cardiomyocytes. J Biol Chem 279:19350-19361

Ryter SW, Choi AM (2010) Heme oxygenase-1/carbon monoxide: novel therapeutic strategies in critical care medicine. Curr Drug Targets 11:1485-1494

Salazar M, Rojo AI, Velasco D, de Sagarra RM, Cuadrado A (2006) Glycogen synthase kinase-3beta inhibits the xenobiotic and antioxidant cell response by direct phosphorylation and nuclear exclusion of the transcription factor Nrf2. J Biol Chem 281:14841-14851

Sankaranarayanan K, Jaiswal AK (2004) Nrf3 negatively regulates antioxidant-response element-mediated expression and antioxidant induction of NAD(P)H:quinone oxidoreductase1 gene. J Biol Chem 279:50810-50817

Schimrigk S, Brune N, Hellwig K, Lukas C, Bellenberg B, Rieks M, Hoffmann V, Pöhlau D, Przuntek H (2006) Oral fumaric acid esters for the treatment of active multiple sclerosis: an open-label, baseline-controlled pilot study. Eur J Neurol 13:604-610

Sekhar KR, Soltaninassab SR, Borrelli MJ, Xu ZQ, Meredith MJ, Domann FE, Freeman ML (2000) Inhibition of the 26S proteasome induces expression of GLCLC, the catalytic subunit for gamma-glutamylcysteine synthetase. Biochem Biophys Res Commun 270:311-317

Sekhar KR, Rachakonda G, Freeman ML (2010) Cysteine-based regulation of the CUL3 adaptor protein Keap1. Toxicol Appl Pharmacol 244:21-26

Semenza GL (2003) Targeting HIF-1 for cancer therapy. Nat Rev Cancer 3:721-732

Shapiro TA, Fahey JW, Dinkova-Kostova AT, Holtzclaw WD, Stephenson KK, Wade KL, Ye L, Talalay P (2006) Safety, tolerance, and metabolism of broccoli sprout glucosinolates and isothiocyanates: a clinical phase I study. Nutr. Cancer 55:53-62

Shay KP, Michels AJ, Li W, Kong AN, Hagen TM (2012) Cap-independent Nrf2 translation is part of a lipoic acid-stimulated detoxification stress response. Biochim Biophys Acta 1823:1102-1109

Shen G, Khor TO, Hu R, Yu S, Nair S, Ho CT, Reddy BS, Huang MT, Newmark HL, Kong AN (2007) Chemoprevention of familial adenomatous polyposis by natural dietary compounds sulforaphane and dibenzoylmethane alone and in combination in ApcMin/+ mouse. Cancer Res 67:9937-9944

Shibata T, Ohta T, Tong KI, Kokubu A, Odogawa R, Tsuta K, Asamura H, Yamamoto M, Hirohashi S (2008a) Cancer related mutations in NRF2 impair its recognition by Keap1-Cul3 E3 ligase and promote malignancy. Proc Natl Acad Sci USA 105:13568-13573

Shibata T, Kokubu A, Gotoh M, Ojima H, Ohta T, Yamamoto M, Hirohashi S (2008b) Genetic alteration of Keap1 confers constitutive Nrf2 activation and resistance to chemotherapy in gallbladder cancer. Gastroenterology 135:1358-1368, 1368.e1-4

Shibata T, Saito S, Kokubu A, Suzuki T, Yamamoto M, Hirohashi S (2010) Global Downstream Pathway Analysis Reveals a Dependence of Oncogenic NF-E2-Related Factor 2 Mutation on the mTOR Growth Signaling Pathway. Cancer Res 70:9095-9105

Shimomura O, Johnson FH, Saiga Y (1962) Extraction, purification and properties of aequorin, a bioluminescent protein from the luminous hydromedusan, Aequorea. J Cell Comp Physiol 59:223-239

Sidransky H, Ito N, Verney E (1966) Influence of a-naphthyl-isothiocyanate on liver tumorigenesis in rats ingesting ethionine and N-2-fluorenylacetamide.J Natl Cancer Inst 37:677-686

Siebenlist U, Franzoso G, Brown K (1994) Structure, regulation and function of NF-kappa B. Annu Rev Cell Biol 10:405-455

Siegel D, Gustafson DL, Dehn DL, Han JY, Boonchoong P, Berliner LJ, Ross D (2004) NAD(P)H:quinone oxidoreductase 1: role as a superoxide scavenger. Mol Pharmacol 65:1238-1247

Siglin JC, Barch DH, Stoner GD (1995) Effects of dietary phenethyl isothiocyanate, ellagic acid, sulindac and calcium on the induction and progression of N-nitrosomethylbenzylamine-induced esophageal carcinogenesis in rats. Carcinogenesis 16:1101-1106

Singh A, Misra V, Thimmulappa RK, Lee H, Ames S, Hoque MO, Herman JG, Baylin SB, Sidransky D, Gabrielson E, Brock MV, Biswal S (2006) Dysfunctional KEAP1-NRF2 interaction in non-small-cell lung cancer. PLoS Med 3:e420

Singh A, Ling G, Suhasini AN, Zhang P, Yamamoto M, Navas-Acien A, Cosgrove G, Tuder RM, Kensler TW, Watson WH, Biswal S (2009) Nrf2-dependent sulfiredoxin-1 expression protects against cigarette smoke-induced oxidative stress in lungs. Free Radic Biol Med 46:376-386

Sisson JC, Ho KS, Suyama K, Scott MP (1997) Costal2, a novel kinesin-related protein in the Hedgehog signaling pathway. Cell 90:235-245

Sjöblom T, Jones S, Wood LD, Parsons DW, Lin J, Barber TD, Mandelker D, Leary RJ, Ptak J, Silliman N, Szabo S, Buckhaults P, Farrell C, Meeh P, Markowitz SD, Willis J, Dawson D, Willson JK, Gazdar AF, Hartigan J, Wu L, Liu C, Parmigiani G, Park BH, Bachman KE, Papadopoulos N, Vogelstein B, Kinzler KW, Velculescu VE (2006) The consensus coding sequences of human breast and colorectal cancers. Science 314:268-274

Slaughter BD, Schwartz JW, Li R (2007) Mapping dynamic protein interactions in MAP kinase signalling using live-cell fluorescence fluctuation spectroscopy and imaging. Proc Natl Acad Sci USA. 104: 20320-20325

Smith MT, Wang Y, Skibola CF, Slater DJ, Lo Nigro L, Nowell PC, Lange BJ, Felix CA (2002) Low NAD(P)H:quinone oxidoreductase activity is associated with increased risk of leukemia with MLL translocations in infants and children. Blood 100:4590-4593

Snyder GH, Cennerazzo MJ, Karalis AJ, Field D (1981) Electrostatic influence of local cysteine environments on disulfide exchange kinetics. Biochemistry 20:6509-6519

Spencer SR, Xue LA, Klenz EM, Talalay P (1991) The potency of inducers of NAD(P)H:(quinone-acceptor) oxidoreductase parallels their efficiency as substrates for glutathione transferases. Structural and electronic correlations. Biochem J 273:711-717

Spiller DG, Wood CD, Rand DA, White MRH (2010) Measurement of single-cell dynamics. Nature 465:736-745

Stack C, Ho D, Wille E, Calingasan NY, Williams C, Liby K, Sporn M, Dumont M, Beal MF (2010) Triterpenoids CDDO-ethyl amide and CDDO-

trifluoroethyl amide improve the behavioral phenotype and brain pathology in a transgenic mouse model of Huntington's disease. Free Radic Biol Med 49:147-158

Stacy DR, Ely K, Massion PP, Yarbrough WG, Hallahan DE, Sekhar KR, Freeman ML (2006) Increased expression of nuclear factor E2 p45-related factor 2 (NRF2) in head and neck squamous cell carcinomas. Head Neck 28:813-818

Stanley EL, Hume R, Coughtrie MW (2005) Expression profiling of human fetal cytosolic sulfotransferases involved in steroid and thyroid hormone metabolism and in detoxification. Mol Cell Endocrinol 240:32-42

Stewart D, Killeen E, Naquin R, Alam S, Alam J (2003) Degradation of transcription factor Nrf2 via the ubiquitin-proteasome pathway and stabilization by cadmium. J Biol Chem 278:2396-2402

Stoner GD, Adams C, Kresty LA, Amin SG, Desai D, Hecht SS, Murphy SE, Morse MA (1998) Inhibition of N'-nitrosonornicotine-induced esophageal tumorigenesis by 3-phenylpropyl isothiocyanate. Carcinogenesis 19:2139-2143

Sun Z, Zhang S, Chan JY, Zhang DD (2007) Keap1 controls postinduction repression of the Nrf2-mediated antioxidant response by escorting nuclear export of Nrf2. Mol Cell Biol 27:6334-6349

Sun Z, Huang Z, Zhang DD (2009) Phosphorylation of Nrf2 at multiple sites by MAP kinases has a limited contribution in modulating the Nrf2-dependent antioxidant response. PLoS One 4:e6588

Sun Z, Wu T, Zhao F, Lau A, Birch CM, Zhang DD (2011) KPNA6 (importin α7)-mediated nuclear import of Keap1 represses the Nrf2-dependent antioxidant response. Mol Cell Biol 31:1800-1811

Surh YJ, Chun KS (2007) Cancer chemopreventive effects of curcumin. Adv Exp Med Biol 595:149-172

Suzuki T, Maher J, Yamamoto M (2011) Select heterozygous Keap1 mutations have a dominant-negative effect on wild-type Keap1 *in vivo*. Cancer Res 71:1700-1709

Sykiotis GP, Bohmann D (2008) Keap1/Nrf2 signaling regulates oxidative stress tolerance and lifespan in Drosophila. Dev Cell 14:76-85

Taguchi K, Maher JM, Suzuki T, Kawatani Y, Motohashi H, Yamamoto M (2010) Genetic analysis of cytoprotective functions supported by graded expression of Keap1. Mol Cell Biol 30:3016-3026

Talalay P, De Long MJ, Prochaska HJ (1988) Identification of a common chemical signal regulating the induction of enzymes that protect against chemical carcinogenesis. Proc Natl Acad Sci USA 85:8261-8265

Talalay P, Fahey JW, Holtzclaw WD, Prestera T, Zhang Y (1995) Chemoprotection against cancer by phase 2 enzyme induction. Toxicol Lett 82-83:173-179

Talalay P, Fahey JW, Healy ZR, Wehage SL, Benedict AL, Min C, Dinkova-Kostova AT (2007) Sulforaphane mobilizes cellular defenses that protect skin against damage by UV radiation. Proc Natl Acad Sci USA 104:17500-17505

Thimmulappa RK, Mai KH, Srisuma S, Kensler TW, Yamamoto M, Biswal S (2002) Identification of Nrf2-regulated genes induced by the chemopreventive agent sulforaphane by oligonucleotide microarray. Cancer Res 62:5196-5203

Tong KI, Katoh Y, Kusunoki H, Itoh K, Tanaka T, Yamamoto M (2006a) Keap1 recruits Neh2 through binding to ETGE and DLG motifs: characterization of the two-site molecular recognition model. Mol Cell Biol 26:2887-2900

Tong KI, Kobayashi A, Katsuoka F, Yamamoto M (2006b) Two-site substrate recognition model for the Keap1-Nrf2 system: a hinge and latch mechanism. Biol Chem 387:1311-1320

Tong KI, Padmanabhan B, Kobayashi A, Shang C, Hirotsu Y, Yokoyama S, Yamamoto M (2007) Different electrostatic potentials define ETGE and DLG motifs as hinge and latch in oxidative stress response. Mol Cell Biol 27:7511-7521

Tsien RY (1998) The green fluorescent protein. Annu Rev Biochem 67:509-544

Tsuji Y (2005) JunD activates transcription of the human ferritin H gene through an antioxidant response element during oxidative stress. Oncogene 24:7567-7578

Traka M, Gasper AV, Melchini A, Bacon JR, Needs PW, Frost V, Chantry A, Jones AM, Ortori CA, Barrett DA, Ball RY, Mills RD, Mithen RF (2008) Broccoli

consumption interacts with GSTM1 to perturb oncogenic signalling pathways in the prostate. PLoS One 3:e2568

Velichkova M, Hasson T (2005) Keap1 regulates the oxidation-sensitive shuttling of Nrf2 into and out of the nucleus via a Crm1-dependent nuclear export mechanism. Mol Cell Biol 25:4501-4513

Venugopal R, Jaiswal AK (1996) Nrf1 and Nrf2 positively and c-Fos and Fra1 negatively regulate the human antioxidant response element-mediated expression of NAD(P)H:quinone oxidoreductase1 gene. Proc Natl Acad Sci USA 93:14960-14965

Wakabayashi N, Itoh K, Wakabayashi J, Motohashi H, Noda S, Takahashi S, Imakado S, Kotsuji T, Otsuka F, Roop DR, Harada T, Engel JD, Yamamoto M (2003) Keap1-null mutation leads to postnatal lethality due to constitutive Nrf2 activation. Nat Genet 35:238-245

Wakabayashi N, Dinkova-Kostova AT, Holtzclaw WD, Kang MI, Kobayashi A, Yamamoto M, Kensler TW, Talalay P (2004) Protection against electrophile and oxidant stress by induction of the phase 2 response: fate of cysteines of the Keap1 sensor modified by inducers. Proc Natl Acad Sci USA 101:2040-2045

Wakabayashi N, Slocum SL, Skoko JJ, Shin S, Kensler TW (2010a) When NRF2 talks, who's listening? Antioxid Redox Signal 13:1649-1663

Wakabayashi N, Shin S, Slocum SL, Agoston ES, Wakabayashi J, Kwak MK, Misra V, Biswal S, Yamamoto M, Kensler TW (2010b) Regulation of notch1 signaling by nrf2: implications for tissue regeneration. Sci Signal 3:ra52

Wang XJ, Hayes JD, Wolf CR (2006) Generation of a stable antioxidant response element-driven reporter gene cell line and its use to show redox-dependent activation of nrf2 by cancer chemotherapeutic agents. Cancer Res 66:10983-94

Wang XJ, Hayes JD, Henderson CJ, Wolf CR (2007) Identification of retinoic acid as an inhibitor of transcription factor Nrf2 through activation of retinoic acid receptor alpha. Proc Natl Acad Sci USA 104:19589-19594

Wang XJ, Sun Z, Chen W, Li Y, Villeneuve NF, Zhang DD (2008a) Activation of Nrf2 by arsenite and monomethylarsonous acid is independent of Keap1-

C151: enhanced Keap1-Cul3 interaction. Toxicol Appl Pharmacol 230:383-389

Wang XJ, Sun Z, Villeneuve NF, Zhang S, Zhao F, Li Y, Chen W, Yi X, Zheng W, Wondrak GT, Wong PK, Zhang DD (2008b) Nrf2 enhances resistance of cancer cells to chemotherapeutic drugs, the dark side of Nrf2. Carcinogenesis 29:1235-1243

Wang XJ, Hayes JD, Higgins LG, Wolf CR, Dinkova-Kostova AT (2010) Activation of the NRF2 signaling pathway by copper-mediated redox cycling of *para*- and *ortho*-hydroquinones. Chem Biol 17:75-85

Wasserman WW, Fahl WE (1997) Comprehensive analysis of proteins which interact with the antioxidant responsive element: correlation of ARE-BP-1 with the chemoprotective induction response. Arch Biochem Biophys 344:387-396

Watai Y, Kobayashi A, Nagase H, Mizukami M, McEvoy J, Singer JD, Itoh K, Yamamoto M (2007) Subcellular localization and cytoplasmic complex status of endogenous Keap1. Genes Cells 12:1163-1178

Wattenberg LW (1977) Inhibition of carcinogenic effects of polycyclic hydrocarbons by benzyl isothiocyanate and related compounds. J Natl Cancer Inst 58:395-398

Wattenberg LW (1981) Inhibition of carcinogen-induced neoplasia by sodium cyanate, tert-butyl isocyanate, and benzyl isothiocyanate administered subsequent to carcinogen exposure. Cancer Res 41:2991-2994

Wattenberg LW (1983) Inhibition of neoplasia by minor dietary constituents. Cancer Res 43:2448s-2453s

Wattenberg LW (1985) Chemoprevention of cancer Cancer Res 45:1-8

Wattenberg LW (1987) Inhibitory effects of benzyl isothiocyanate administered shortly before diethylnitrosamine or benzo[*a*]pyrene on pulmonary and forestomach neoplasia in A/J mice. Carcinogenesis 8:1971-1973

Wei W, Ayad NG, Wan Y, Zhang GJ, Kirschner MW, Kaelin WG Jr (2004) Degradation of the SCF component Skp2 in cell-cycle phase G1 by the anaphase-promoting complex. Nature 428:194-198

Welsh SJ, Bellamy WT, Briehl MM, Powis G (2002) The redox protein thioredoxin-1 (Trx-1) increases hypoxia-inducible factor 1alpha protein

expression: Trx-1 overexpression results in increased vascular endothelial growth factor production and enhanced tumor angiogenesis. Cancer Res 62:5089-5095

Wild AC, Moinova HR, Mulcahy RT (1999) Regulation of gamma-glutamylcysteine synthetase subunit gene expression by the transcription factor Nrf2. J Biol Chem 274:33627-33636

Woo HA, Jeong W, Chang TS, Park KJ, Park SJ, Yang JS, Rhee SG (2005) Reduction of cysteine sulfinic acid by sulfiredoxin is specific to 2-cys peroxiredoxins. J Biol Chem 280:3125-3128

Wu L, Noyan-Ashraf MH, Facci M, Wang R, Paterson PG, Ferrie A, Juurlink BH (2004) Dietary approach to attenuate oxidative stress, hypertension, and inflammation in the cardiovascular system. Proc Natl Acad Sci USA 101:7094-7099

Xu C, Huang MT, Shen G, Yuan X, Lin W, Khor TO, Conney AH, Kong AN (2006) Inhibition of 7,12-dimethylbenz(a)anthracene-induced skin tumorigenesis in C57BL/6 mice by sulforaphane is mediated by nuclear factor E2-related factor 2. Cancer Res 66:8293-8296

Xu L, Wei Y, Reboul J, Vaglio P, Shin TH, Vidal M, Elledge SJ, Harper JW (2003) BTB proteins are substrate-specific adaptors in an SCF-like modular ubiquitin ligase containing CUL-3. Nature 425:316-321

Xue F, Cooley L (1993) *kelch* encodes a component of intercellular bridges in Drosophila egg chambers. Cell 1993 72:681-693

Yamamoto T, Suzuki T, Kobayashi A, Wakabayashi J, Maher J, Motohashi H, Yamamoto M (2008) Physiological significance of reactive cysteine residues of Keap1 in determining Nrf2 activity. Mol Cell Biol 28:2758-2770

Yan C, Lee LH, Davis LI (1998) Crm1p mediates regulated nuclear export of a yeast AP-1-like transcription factor. EMBO J 17:7416-7429

Yanaka A, Fahey JW, Fukumoto A, Nakayama M, Inoue S, Zhang S, Tauchi M, Suzuki H, Hyodo I, Yamamoto M (2009) Dietary sulforaphane-rich broccoli sprouts reduce colonization and attenuate gastritis in *Helicobacter pylori*-infected mice and humans. Cancer Prev Res (Phila) 2:353-360

Yang L, Calingasan NY, Thomas B, Chaturvedi RK, Kiaei M, Wille EJ, Liby KT, Williams C, Royce D, Risingsong R, Musiek ES, Morrow JD, Sporn M, Beal MF (2009) Neuroprotective effects of the triterpenoid, CDDO methyl amide, a potent inducer of Nrf2-mediated transcription. PLoS One 4:e5757

Yaron A, Hatzubai A, Davis M, Lavon I, Amit S, Manning AM, Andersen JS, Mann M, Mercurio F, Ben-Neriah Y (1998) Identification of the receptor component of the I□B□-ubiquitin ligase. Nature 396:590-594

Yates MS, Kwak MK, Egner PA, Groopman JD, Bodreddigari S, Sutter TR, Baumgartner KJ, Roebuck BD, Liby KT, Yore MM, Honda T, Gribble GW, Sporn MB, Kensler TW (2006) Potent protection against aflatoxin-induced tumorigenesis through induction of Nrf2-regulated pathways by the triterpenoid 1-[2-cyano-3-,12-dioxooleana-1,9(11)-dien-28-oyl]imidazole. Cancer Res 66:2488-2494

Yates MS, Tran QT, Dolan PM, Osburn WO, Shin S, McCulloch CC, Silkworth JB, Taguchi K, Yamamoto M, Williams CR, Liby KT, Sporn MB, Sutter TR, Kensler TW (2009) Genetic versus chemoprotective activation of Nrf2 signaling: overlapping yet distinct gene expression profiles between Keap1 knockout and triterpenoid-treated mice. Carcinogenesis 30:1024-1031

Ye L, Zhang Y (2001) Total intracellular accumulation levels of dietary isothiocyanates determine their activity in elevation of cellular glutathione and induction of Phase 2 detoxification enzymes. Carcinogenesis 22:1987-1992

Yu R, Lei W, Mandlekar S, Weber MJ, Der CJ, Wu J, Kong AN (1999) Role of a mitogen-activated protein kinase pathway in the induction of phase II detoxifying enzymes by chemicals. J Biol Chem 274:27545-27552

Yu R, Mandlekar S, Lei W, Fahl WE, Tan TH, Kong AN (2000) p38 mitogen-activated protein kinase negatively regulates the induction of phase II drug-metabolizing enzymes that detoxify carcinogens. J Biol Chem 275:2322-2327

Zhang DD, Hannink M (2003) Distinct cysteine residues in Keap1 are required for Keap1-dependent ubiquitination of Nrf2 and for stabilization of Nrf2

by chemopreventive agents and oxidative stress. Mol Cell Biol 23:8137-8151

Zhang DD, Lo SC, Cross JV, Templeton DJ, Hannink M (2004) Keap1 is a redox-regulated substrate adaptor protein for a Cul3-dependent ubiquitin ligase complex. Mol Cell Biol 24:10941-10953

Zhang DD, Lo SC, Sun Z, Habib GM, Lieberman MW, Hannink M (2005) Ubiquitination of Keap1, a BTB-Kelch substrate adaptor protein for Cul3, targets Keap1 for degradation by a proteasome-independent pathway. J Biol Chem 280:30091-30099

Zhang J, Ohta T, Maruyama A, Hosoya T, Nishikawa K, Maher JM, Shibahara S, Itoh K, Yamamoto M (2006) BRG1 interacts with Nrf2 to selectively mediate HO-1 induction in response to oxidative stress. Mol Cell Biol 26:7942-7952

Zhang Y, Talalay P, Cho CG, Posner GH (1992) A major inducer of anticarcinogenic protective enzymes from broccoli: isolation and elucidation of structure. Proc Natl Acad Sci USA 89:2399-2403

Zhang Y, Kensler TW, Cho CG, Posner GH, Talalay P (1994) Anticarcinogenic activities of sulforaphane and structurally related synthetic norbornyl isothiocyanates. Proc Natl Acad Sci USA 91:3147-3150

Zhang Y, Talalay P (1998) Mechanism of differential potencies of isothiocyanates as inducers of anticarcinogenic Phase 2 enzymes. Cancer Res 58:4632-4639

Zhang Y (2000) Role of glutathione in the accumulation of anticarcinogenic isothiocyanates and their glutathione conjugates by murine hepatoma cells. Carcinogenesis 21:1175-1182

Zhang Y, Callaway EC (2002) High cellular accumulation of sulphoraphane, a dietary anticarcinogen, is followed by rapid transporter-mediated export as a glutathione conjugate. Biochem J 364:301-307

Zhao J, Moore AN, Clifton GL, Dash PK (2005) Sulforaphane enhances aquaporin-4 expression and decreases cerebral edema following traumatic brain injury. J Neurosci Res 82:499-506

Zhao J, Kobori N, Aronowski J, Dash PK (2006) Sulforaphane reduces infarct volume following focal cerebral ischemia in rodents. Neurosci Lett 393:108-112

Zhao J, Moore AN, Redell JB, Dash PK (2007a) Enhancing expression of Nrf2-driven genes protects the blood brain barrier after brain injury. J Neurosci 27:10240-10248

Zhao X, Sun G, Zhang J, Strong R, Dash PK, Kan YW, Grotta JC, Aronowski J (2007b) Transcription factor Nrf2 protects the brain from damage produced by intracerebral hemorrhage. Stroke 38:3280-3286

Zheng N, Schulman BA, Song L, Miller JJ, Jeffrey PD, Wang P, Chu C, Koepp DM, Elledge SJ, Pagano M, Conaway RC, Conaway JW, Harper JW, Pavletich NP (2002) Structure of the Cul1-Rbx1-Skp1-F boxSkp2 SCF ubiquitin ligase complex. Nature 416:703-709

Zhou P, Howley PM (1998) Ubiquitination and degradation of the substrate recognition subunits of SCF ubiquitin-protein ligases. Mol Cell 2:571-580

Zhou W, Edelman GM, Mauro VP (2001) Transcript leader regions of two Saccharomyces cerevisiae mRNAs contain internal ribosome entry sites that function in living cells. Proc Natl Acad Sci USA 98:1531-1536

Zhou W, Lo SC, Liu JH, Hannink M, Lubahn DB (2007) ERRbeta: a potent inhibitor of Nrf2 transcriptional activity. Mol Cell Endocrinol 278:52-62

Zipper LM, Mulcahy RT (2002) The Keap1 BTB/POZ dimerization function is required to sequester Nrf2 in cytoplasm. J Biol Chem 277:36544-36552